A thesis entitled

Characterisation of a novel PDE4 and the modification of PDE4 function by phosphorylation and protein-protein interaction

Presented by

Derek A. Wallace

to

University of Glasgow

for the degree of

Doctor of Philosophy

September 2006

Division of Biochemistry and Molecular Biology
Institute of Biomedical and Life Sciences
University of Glasgow

ProQuest LLC.
789 East Eisenhower Parkway
P.O. Box 1346
Ann Arbor, MI 48106 – 1346

This thesis is dedicated to my parents

Acknowledgements

I would like to express my appreciation to Professor Miles D. Houslay, Gardiner Chair of Biochemistry, for providing me with the opportunity to undertake my PhD studies within his laboratory. I have benefited enormously from his knowledge and enthusiasm towards the research presented in this thesis. I must also acknowledge Dr. Richard G. Knowles, Director of Disease Systems and Clinical Biology, and Dr. Robin A. Smith, at GlaxoSmithKline, for sponsoring my PhD and for helpful discussions to advance this work. I hope I have repaid their faith in me with my commitment to the research presented in this thesis. Finally, I would like to thank the Biotechnology and Biological Sciences Research Council and GlaxoSmithKline for the funding, without which this work would not have been possible.

It would be remiss of me not to recognise the crucial role of the research scientists within the Houslay Laboratory who have all, at some point, provided assistance to me during the development of this work.

I would like to thank my family, who have consistently supported me throughout the duration of my PhD. I would especially like to thank my mum and dad, who have provided me with constant encouragement, not to mention financial support. They will never know how much I truly appreciate it.

Finally, to my fiancée, Jen. You have been so understanding of the amount of effort and commitment required to successfully complete this PhD. For that I am truly indebted, I love you.

Summary

cAMP participates in cell signal transduction and influences biological responses such as muscle contraction, learning and memory, inflammatory cytokine production, and cell growth, differentiation and apoptosis. The sole means of cAMP degradation is by PDE enzymes. The PDE4 family represents the major cAMP-hydrolysing activity in many cells. Four genes encode the PDE4 isoforms and over twenty have now been characterised. Each isoform differs by virtue of a unique N-terminal intra-cellular targeting region, and by differential inclusion of regulatory UCR domains via 5' mRNA splicing. The plethora of PDE4 isoforms underpins compartmentalisation of cAMP signalling, facilitating the generation of cAMP domains or gradients.

Work in this thesis characterises a novel PDE4A long isoform, namely PDE4A11. It is expressed with a species-conserved, unique 81 amino acid N-terminal region encoded by a single 5' exon. Transcript analysis of human cells and tissues alludes to tissue-specific and developmental changes in expression. PDE4A11 is targeted to the perinuclear region and membrane ruffles of COS7 cells. Sequence analysis identifies putative PIP3-mediated membrane targeting. PDE4A11 is kinetically comparable to the other PDE4A long isoforms and is inhibited by conventional PDE4 inhibitors. It is insensitive to conformational changes detected by altered rolipram inhibition, a likely consequence of reduced LR2 and/or enhanced N-terminal interactions with Lyn-SH3. Soluble and particulate forms exhibit distinct rates of thermal inactivation. PDE4A11 is activated by PKA phosphorylation at Ser-119 within UCR1. N-terminal phosphorylation by ERK1/2 should be pursued. PDE4A11 couples β-arrestin and is the second PDE4 isoform to interact with XAP2.

Phosphorylation of PDE4 isoforms confers activity and protein interaction regulation. All PDE4 long isoforms are activated by PKA phosphorylation within UCR1. Phosphorylation of the catalytic unit by ERK1/2 occurs in all PDE4 isoforms, except PDE4A, and activates short form PDE4s

and inhibits long forms. Activation of the PI-3K pathway also facilitates PDE4 activation. The identification of PDE4A5 as an authentic substrate for MAPKAPK2 is described, and the functional effects are investigated. This novel phosphorylation occurs at a serine residue, distinct from the PKA site, within UCR1. The kinase and target residue is identified in COS1 cells expressing PDE4A5, following treatment with anisomycin, the p38 MAPK inhibitor, SB203580, and siRNA-mediated knockdown of MAPKAPK2, together with N-terminal truncation of PDE4A5 and Ser-147-Ala mutation. Phosphorylation of PDE4A5 by MAPKAPK2 has no effect on catalytic activity but delays the onset and amplitude of PKA-mediated activation. The interaction of PDE4A5 with XAP2, but not β-arrestin, is attenuated by MAPKAPK2 phosphorylation. Phosphorylation does not affect PDE4A5 intra-cellular targeting or its susceptibility to caspase-3 cleavage. Enzyme conformational change with a Ser-147-Asp phospho-mimetic is not observed.

PDE4 inhibition reduces the production of ROS in many immune and inflammatory cells, consequential of the immuno-suppressive and anti-inflammatory effects of cAMP. Oxidative stress is implicated in the pathogenesis of disease states such as COPD and cardiac hypertrophy. The final chapter of this thesis strives to unravel the role of PDE4 inhibition in the attenuation of ROS production in cardiac myocytes. Angiotensin II promotes the delivery of p47-*phox*, an integral component of the active NADPH oxidase enzyme, to the membrane. Elevation of intra-cellular cAMP concentrations using forskolin and rolipram prevents p47-*phox* translocation, an effect that is partially rescued with the PKA inhibitor, H89. PKA directly phosphorylates p47-*phox* and six putative sites are identified within the C-terminal region. PDE4A4B is able to interact directly with p47-*phox* and p67-*phox*, whereas PDE4A10 only interacts with p47-*phox*, indicating specificity in the PDE4 control of the PKA phosphorylation state of *phox* proteins.

In summary, the work in this thesis contributes further to our understanding of the PDE4 regulation of intra-cellular cAMP concentrations in cells, and the specific response mediated through the multitude of isoforms and modification of function by both phosphorylation and protein interactions.

Contents

List of Figures

Chapter 1

Chapter 3

Chapter 4

Chapter 5

List of Tables

Chapter 1

Chapter 2

Chapter 3

Chapter 4

List of Abbreviations

5-HT	five hydroxytryptamine
7-TM	seven transmembrane-spanning receptors
AC	adenylyl cyclase
ACE	angiotensin converting enzyme
AhR	aryl hydrocarbon (dioxin) receptor
AIP	aryl hydrocarbon receptor-interacting protein
AKAP	A-kinase anchoring protein
AMP	adenosine mono-phosphate
AMPA	α-amino-5-hydroxy-3-methyl-4-isoxazole propionic acid
APC	antigen-presenting cell
ARE	AU-rich elements
Arp	actin-related protein
ASK	apoptosis signal-regulating kinase
ATF	activating transcription factor
ATP	adenosine tri-phosphate
BAL	bronchoalveolar lavage
bp	base pair(s)
BSA	bovine serum albumin
Ca^{2+}/CaM	calcium/calmodulin
CaMK	calcium/calmodulin-dependent kinase
cAMP	3', 5' cyclic adenosine mono-phosphate
cDNA	complementary DNA
CFTR	cystic fibrosis transmembrane conductance regulator
CGD	chronic granulomatous disease
cGMP	3', 5' cyclic guanosine mono-phosphate
CHO	chinese hamster ovary
CK	casein kinase
CLFR	common long form region
COPD	chronic obstructive pulmonary disease
COX	cyclo-oxygenase

CRE	cAMP response element
CBP	CREB binding protein
CNG	cyclic nucleotide-gated
CNS	central nervous system
CREB	cAMP response element binding protein
CREM	CRE modulator
DEP	Dishevelled, Egl-10, Pleckstrin
DISC1	disrupted in schizophrenia 1
dNTP	deoxynucleotide tri-phosphate
DMEM	Dulbecco's modified Eagle's medium
DMSO	di-methyl sulphoxide
DNA	deoxyribonucleic acid
DTT	dithiolthreitol
ECL	enhanced chemiluminescence
E.coli	Escherichia coli
EDTA	ethylenediaminetetraacetic acid
EGTA	ethyleneglycolbis-2-aminoethylether N, N', N'', n'-tetraacetic acid
EHNA	erythro-9-(2-hydroxy-3-nonyl)-adenine
EPAC	guanine nucleotide exchange protein activated by cAMP
ERK	extra-cellular signal-regulated kinase
EST	expressed sequence tag
FCS	foetal calf serum
fMLP	N-formyl-methionine-leucine-phenylalanine
FQF	phenylalanine glutamine phenylalanine
FRET	fluorescence resonance energy transfer
GAF	GTPase activating factor
GDP	guanosine di-phosphate
GEF	guanine nucleotide exchange factor
GFP	green fluorescent protein
G_i	G-protein – inhibitory
GM-CSF	granulocyte macrophage-colony stimulating factor
GPCR	G-protein coupled receptor
GRK	G-protein receptor kinase
G_s	G-protein – stimulatory

GSK-3	glycogen synthase kinase-3
GST	glutathione-S-transferase
GTP	guanosine tri-phosphate
HARBS	high affinity rolipram binding state
HEK	human embryonic kidney
HEPES	N-2-hydroxyethylpiperazine-N'-2-ethanesulphonic acid
hnRNP A0	heterogeneous nuclear ribonucleoprotein A0
HRP	horseradish peroxidase
HSP	heat-shock protein
IBMX	3-isobutyl-1-methylxanthine
IC_{50}	concentration required to inhibit 50% of enzyme activity
IFN	interferon
IgG	immunoglobulin G
IL	interleukin
IPTG	isopropyl-β-D-thiogalactopyranoside
iNOS	inducible nitric oxide synthase
IP_3	inositol 1,4,5 tri-phosphate
JAK	Janus kinase
JNK	c-Jun N-terminal kinase
kDa	kilo Dalton
KHEM	potassium (K), HEPES, EGTA, magnesium (Mg)
KIM	kinase interaction motif
KLH	keyhole limpet haemocyanin
K_m	Michaelis-Menten constant
LARBS	low affinity rolipram binding state
LPC	lysophosphatidylcholine
LPS	lipopolysaccharide
LT	leukotriene
MAP1A-LC2	microtubule-associated protein 1A, light chain 2
MAPK	mitogen-activated protein kinase
MAPKAPK2	MAPK-activated protein kinase 2
MBP	maltose binding protein
MNK	MAPK signal-integrating kinase
mRNA	messenger RNA

mTOR	mammalian target of rapamycin
MW	molecular weight
NADPH	nicotinamide adenine di-nucleotide phosphate (reduced form)
NF-κB	nuclear factor-κB
NMDA	N-methyl-D-aspartic acid
OD	optical density
ORF	open reading frame
PA	phosphatidic acid
PAF	platelet-activating factor
PAS	per-ARNT-sim
PB	phox and Bem1
PBL	polymorphonuclear blood leukocyte
PBS	phosphate buffered saline
PCR	polymerase chain reaction
PDE	cyclic nucleotide phosphodiesterase
PG	prostaglandin
PH	pleckstrin homology
PI	phospho-inositides
PI-3K	phosphatidylinositol-3 kinase
PKA	cAMP-dependent protein kinase or protein kinase A
PKB/Akt	protein kinase B
PKC	protein kinase C
PKG	protein kinase G
PKI	inhibitors of PKA
PKN	protein kinase N
PL	phospholipase
PMA	phorbal 12-myristate 13-acetate
PP	protein phosphatase
PPAR	peroxisome proliferator-activated receptor
PSD	post-synaptic density
PX	phox
RACK	receptor for activated C-kinase
RAID1	RACK1 interaction domain
RD1	ratdnc-1

REM	Ras exchange motif
rEPAC	related to EPAC
RNA	ribonucleic acid
ROS	reactive oxygen species
rpm	revolutions per minute
RT-PCR	reverse transcriptase polymerase chain reaction
RTK	receptor tyrosine kinase
SAP	synapse-associated protein
SAPK	stress-activated protein kinase
SDS	sodium dodecyl sulphate
SDS-PAGE	SDS-polyacrylamide gel electrophoresis
SH3	Src homology 3 domain
siRNA	small interfering RNA
SOD	super-oxide dismutase
Sp1	stimulating protein 1
STAT	signal transducer and activator of transcription
TAE	tris, acetic acid, EDTA
TAF	TBP- associated factor
TAPAS-1	tryptophan anchoring PA selective binding domain-1
TBP	TATA-box binding protein
TBST	tris buffered saline, 0.1% (v/v) tween20
TCR	T-cell receptor
TEMED	N, N, N', N'-tetramethylethylenediamine
Th	T helper
TNF	tumour necrosis factor
TPR	tetratricopeptide repeat
TSH	thyroid stimulating hormone
TTP	tristetraprolin
WAVE-1	Wiskott-Aldrich syndrome protein verprolin homologous-1
XAP2	hepatitis B virus X-associated protein

Chapter 1 Introduction

1.1 General Signal Transduction

The majority of endogenous biological mediators or first messengers, such as peptide hormones, neurotransmitters, cytokines and growth factors cannot penetrate the cell membrane. Therefore, they must elicit their specific biological action through a signal transduction cascade emanating from the cell surface plasma membrane. Such signal transduction is defined as the process of converting a biological signal, represented by the activation of a cell-surface receptor, to an intra-cellular response. Initiation of this response can occur through receptors that contain intrinsic enzymatic activity, receptors that function as ion channels and receptors linked to G-proteins. In many instances the activation of such receptors generates second messenger molecules that are responsible for translating the extra-cellular biological signal to the desired intra-cellular response.

1.2 cAMP as a Second Messenger

The concept of the second messenger was formulated from studies on the 3', 5' cyclic adenosine mono-phosphate (cAMP) signalling system [Beavo and Brunton, 2002]. cAMP is an intra-cellular second messenger molecule that connects, and ultimately regulates, events emanating from the cell surface plasma membrane to nuclear events, such as gene transcription [Montminy, 1997 and Daniel et al., 1998]. cAMP has fundamental roles in metabolic processes, muscle contraction, secretion events, learning and memory, ion channel conductance, pro-inflammatory cytokine production, and cell growth, differentiation and apoptosis [Houslay and Milligan, 1997, Beavo and Brunton, 2002 and Taskén and Aandahl, 2004].

1.3 G-Protein Coupled Receptors

G-protein coupled receptors (GPCRs) are membrane-bound receptors that are coupled to intra-cellular signalling systems via various G-proteins. The binding of ligands, e.g. biogenic amines or peptides, to these receptors induces a conformational change that allows the coupling and activation of G-proteins and the subsequent regulation of intra-cellular cell signalling events through the modulation of enzyme activity, leading to alterations in protein kinases, ion channel conductance and gene expression [Rashid et al., 2004, Strock and Diversé-Pierluissi, 2004 and Hollmann et al., 2005]. The importance of GPCRs in mammalian cell signalling is acknowledged by the fact that approximately 2-5% of the mammalian genome codes for these types of receptors [Yin et al., 2004 and Hollmann et al., 2005]. Examples of GPCRs include the α- and β-adrenergic receptors, the muscarinic acetylcholine receptor, the dopamine receptors, the 5-hydroxytryptamine (5-HT) receptors and the opiate receptors [Rashid et al., 2004].

GPCRs are composed of seven trans-membrane α-helices and are sometimes referred to as 7-transmembrane-spanning receptors (7-TMs). A schematic of the GPCR and G-protein interactions are shown in Figure 1.1. The N-terminal region of the GPCR is located in the extra-cellular space and is hyper-variable. It can vary in length from four to fifty amino acid residues and can be subject to N-linked glycosylation [Yin et al., 2004, Milligan, 2004 and Hollmann et al., 2005]. Seven transmembrane-spanning regions, of approximately twenty to twenty-seven amino acids, cross the lipid bi-layer of the plasma membrane and are linked by alternate intra- and extra-cellular loops. The third transmembrane region contains a critical amino acid residue that confers ligand specificity [Yin et al., 2004 and Hollmann et al., 2005]. This residue is located immediately after a conserved cysteine and if basic the ligand is liable to be a peptide, e.g. vasopressin, and if acidic then it is more probable that the ligand is a biogenic amine, e.g. adrenaline or 5-HT. The C-terminal region is approximately fifty amino acids in length and is relatively conserved throughout all GPCRs. Together with the second and third

cytoplasmic loop, the C-terminal region confers G-protein specificity of binding [Yin et al., 2004 and Hollmann et al., 2005]. GPCRs are now accepted to exist as dimers or even oligomers and this state is a functional requirement [Mercier et al., 2002, Breitwieser, 2004, Milligan, 2004 and Javitch, 2004]. Indeed, without the formation of dimers the promotion and insertion of the GPCR to the plasma membrane appears to be attenuated [Milligan, 2004].

Continuous exposure of a GPCR to a ligand, in many instances, results in profound and rapid attenuation of the intra-cellular signalling processes [Kohout and Lefkowitz, 2003]. This rapid desensitisation process occurs as a result of phosphorylation of the C-terminal domain of the GPCR by G-protein receptor kinase (GRK), the activity of which is regulated by both protein kinase A (PKA) and extra-cellular signal-regulated kinase (ERK) phosphorylation [Lefkowitz et al., 2002, Rapacciuolo et al., 2003, Li et al., 2006 and Vaughan et al., 2006]. Additional desensitisation through A-kinase anchoring protein (AKAP)-recruited PKA phosphorylation of the GPCR may also occur [Tao et al., 2003]. GRK phosphorylation events disrupt GPCR coupling interactions because they allow for the recruitment of cytosolic β-arrestins that bind to the GPCR and physically interdict its coupling to the G-protein [Kohout and Lefkowitz, 2003]. Long-term desensitisation can also arise upon loss of cell surface receptors by receptor internalisation as a consequence of these phosphorylation events. Indeed, GRK phosphorylation of the receptor in recruiting β-arrestin allows transfer to clathrin-coated vesicles, through β-arrestin interactions with clathrin and AP-2, and results in receptor endocytosis [Lefkowitz and Shenoy, 2005 and Vaughan et al., 2006]. Similarly, PKA phosphorylation can also result in receptor endocytosis via caveolae [Rapacciuolo et al., 2003]. Following desensitisation and internalisation the receptors are de-phosphorylated, through protein phosphatase 2 (PP2), in the early endosomes and subsequently recycled and returned to the plasma membrane to participate in further cell signalling events [Oakley et al., 1999, Tao et al., 2003 and Simaan et al., 2005].

The C-terminal region of the GPCR is also the site for other post-translational modifications such as palmitoylation, which can cause insertion

of part of the C-terminal region into the lipid bi-layer thereby forming a fourth intra-cellular loop, ubiquitination, and the interaction with other scaffold protein targets [Yin et al., 2004, Milligan, 2004 and Hollmann et al., 2005]. Ubiquitination of GPCRs prevents receptor recycling and targets it for proteasomal degradation [Penela et al., 2003].

G-proteins are a class of guanine nucleotide binding proteins that interact with the second and third intra-cellular loops and the C-terminal region of the GPCR. There are four major classes of G-proteins, G_s, $G_{i/o}$, $G_{q/11}$ and $G_{12/13}$. Each class of G-protein demonstrates a particular affinity for any given GPCR. However, the other classes of G-proteins are able to bind with reduced affinity, or gain increased affinity, through post-translational modifications, such as phosphorylation or palmitoylation. For example, phosphorylation of the β_2-adrenoceptor by PKA reduces the GPCRs affinity for G_s and increases its affinity for $G_{i/o}$, known as G_s to $G_{i/o}$ switching [Baillie et al., 2003].

Each G-protein is a heterotrimeric protein complex composed of three subunits, α (40-46kDa), β (35kDa), and γ (8kDa) [Hollmann et al., 2005]. In its inactive state the G-protein α-subunit is bound to guanosine di-phosphate (GDP) and this facilitates the interaction between the α-subunit and the βγ-subunits. The βγ-subunits are responsible for the interaction of the inactive heterotrimeric complex with the plasma membrane [Hollmann et al., 2005]. Activation of the GPCR is accompanied by a conformational change within the intra-cellular looped structures. This facilitates the activation of the G-protein heterotrimeric complex via a guanine nucleotide exchange factor (GEF), which slowly substitutes the GDP for guanosine tri-phosphate (GTP) in the α-subunit. This induces both dissociation of the unstable GTP-bound α-subunit with the βγ-subunits and consequently dissociation of all three subunits from the GPCR. This dissociation results in a reduction of agonist binding to the extra-cellular sites of the GPCR. Both the GTP-bound α-subunit and the βγ-subunits can initiate a plethora of intra-cellular downstream cell signalling events, such as the modulation of enzyme activities or ion channels [Cooper, 2003, Strock and Diversé-Pierluissi, 2004, and Li et al., 2006]. An example of

G-protein regulation of enzymes is the adenylyl cyclase isoforms and these are described in Table 1.1. The termination of the signalling occurs through a GTPase activating factor (GAF), whereby GTP is hydrolysed to GDP and the GDP-bound α-subunit and the βγ-subunits re-associate. The heterotrimeric complex returns to its membrane-bound state and is now ready to regulate further intra-cellular signalling processes.

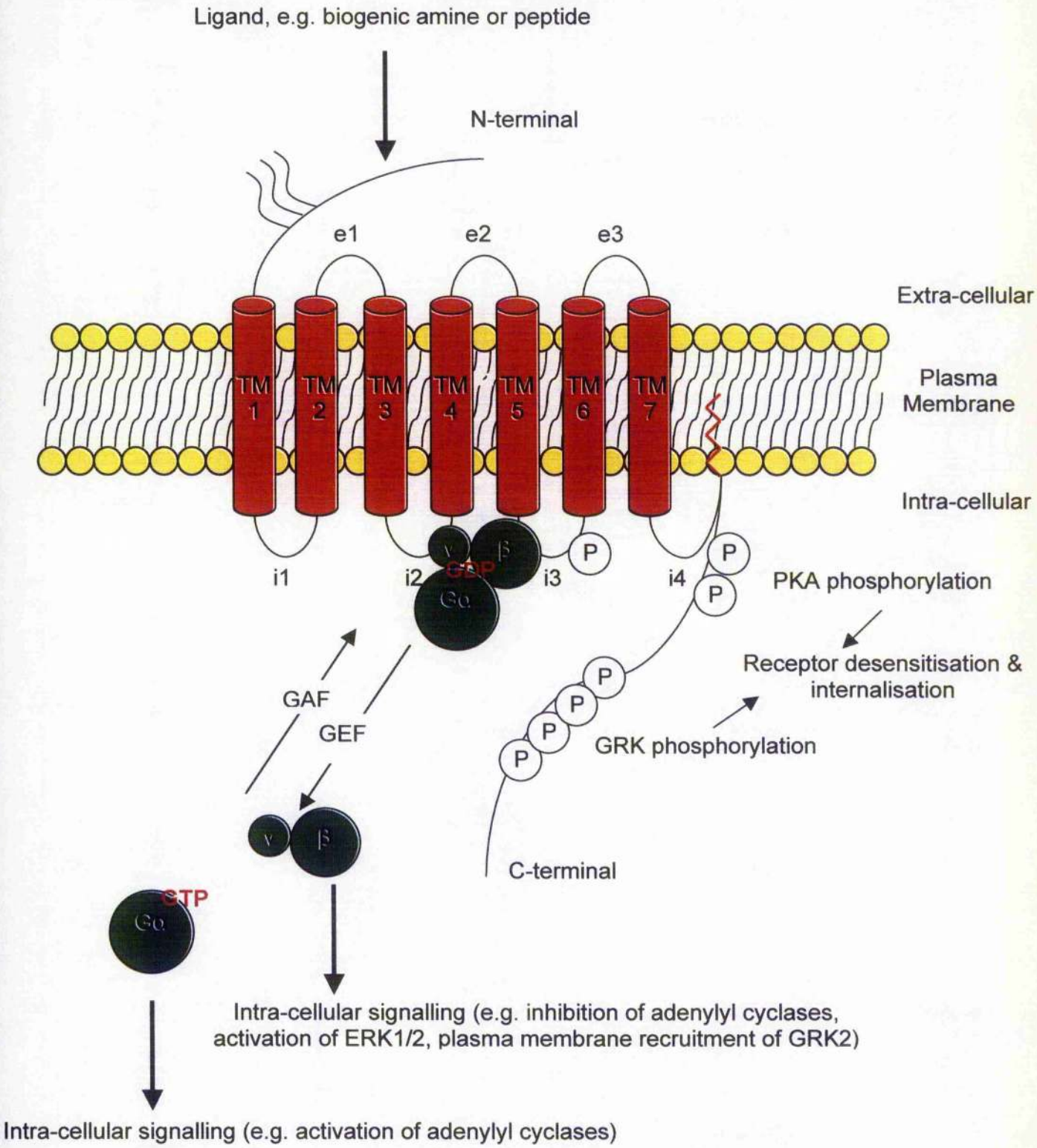

Figure 1.1 – Schematic representation of the G-protein coupled receptor.

1.4 Adenylyl Cyclase

Adenylyl cyclases (ACs) (EC 4.6.1.1) are membrane-associated glycoprotein enzymes that convert adenosine tri-phosphate (ATP) into cAMP, as shown in Figure 1.2 [Taskén and Aandahl, 2004]. AC isoforms show distinct structural homology to DNA polymerase [Cooper, 2003]. There are currently ten known isoforms of ACs, nine of which are membrane associated and the other is a Mn^{2+}-dependent soluble form located within the cytosolic compartment of the cell [Bundey and Insel, 2004]. These isoforms are summarised in Table 1.1, which describes their individual tissue distribution and their specific means of regulation. The membrane-bound isoforms of AC, located at the plasma membrane in lipid rafts [Bundey and Insel, 2004], have two trans-membrane helical regions that facilitate membrane targeting, and two cytosolic domains, known as cyclase homology domains, which are critical for the assembly and function of the catalytic machinery. The intra-molecular interactions of the two cytosolic domains must be in the correct orientation to form an active AC module. Modulation of this interaction may result in an AC conformation that has enhanced or attenuated catalytic activity. The binding of Mg^{2+} ions to two metal ion-binding sites, co-ordinated by two aspartic acid residues, also plays a significant role in regulating AC isoform activity [Cooper, 2003]. Regulation of activity occurs through the binding of free metal ions, through the interaction with various G-protein sub-types and by direct phosphorylation, as discussed in more detail below [Hurley, 1999 and Sunahara and Taussig, 2002].

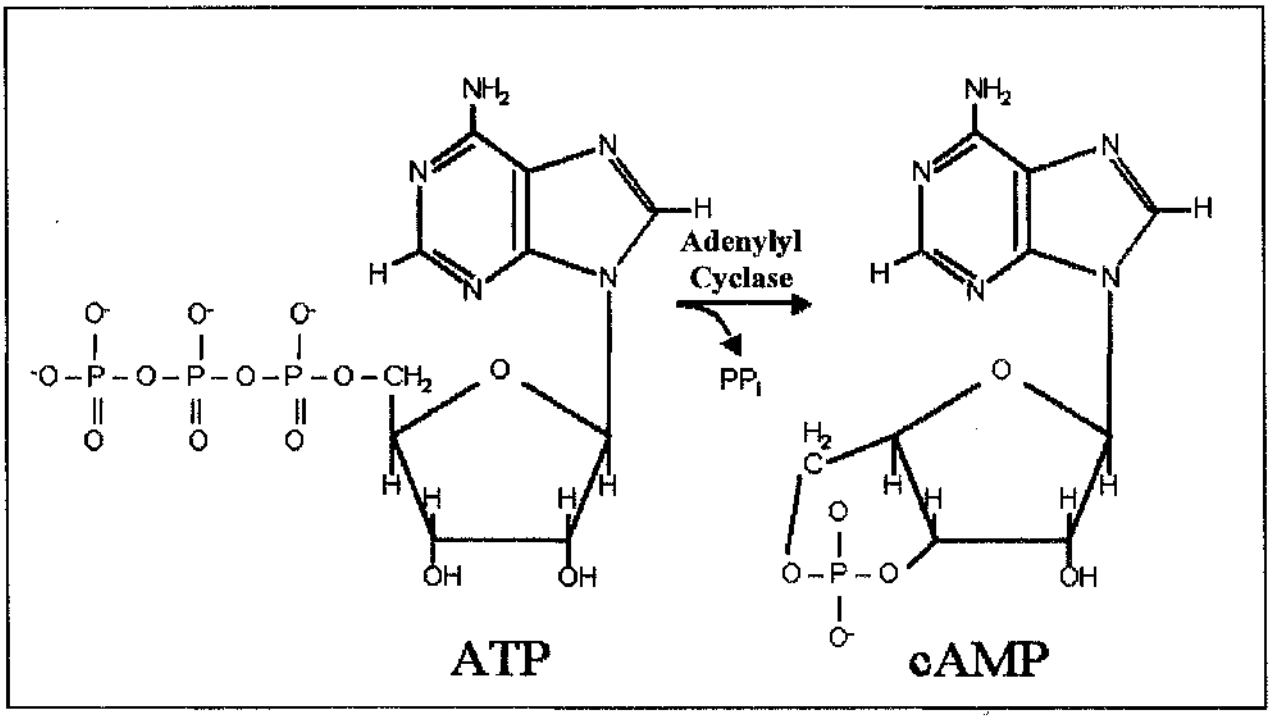

Figure 1.2 – Catalysis of cAMP from ATP by adenylyl cyclase.

The effect of Ca^{2+} binding is isoform-specific and is likely to occur through displacement of the bound Mg^{2+} ions. Interestingly, Ca^{2+} released from intra-cellular locations, e.g. the sarcoplasmic reticulum, has no effect on Ca^{2+} sensitive AC isoforms, whereas the flux of Ca^{2+} ions through L-type Ca^{2+} channels is able to bind and significantly modulate activity [Sunahara and Taussig, 2002]. This is indicative of compartmentalisation of AC isoforms, and their localisation in caveolae or lipid rafts may underlie this effect [Bundey and Insel, 2004]. Intra-cellular Ca^{2+} concentrations between 10-25μM inhibit all AC isoforms, but concentrations in the range of 0.2-0.6μM inhibit AC5 and AC6 but stimulate AC1, AC3 and AC8 [Cooper, 2003 and Beazely and Watts, 2006]. Indeed, Ca^{2+}/calmodulin can stimulate AC1 and AC8 isoforms as well as cAMP-specific phosphodiesterases to generate rapid and dynamic changes in cAMP concentrations [Willoughby and Cooper, 2005]. Soluble AC is uniquely activated by bicarbonate ions (HCO_3^-) [Sun et al., 2002] and it has been recently demonstrated in neutrophils that it can also be activated by TNF-induced increases in intra-cellular Ca^{2+} concentrations [Han et al., 2005].

Forskolin is a synthetic activator of all membrane-bound AC isoforms, except AC9, by augmenting the interaction between the two cytosolic domains that make up the core catalytic unit [Hurley, 1999]. Forskolin acts co-operatively with the G-protein subunit $G\alpha_s$. The activation of ACs by GTP-bound $G\alpha_s$ proteins occurs through a similar mechanism to that of forskolin, and it is postulated that this occurs concomitantly with an activating conformational change in the catalytic unit. Conversely, the GTP-bound G-protein $G\alpha_i$ results in an inhibition of AC5 and AC6 isoforms through direct interaction with the catalytic regions, and a conformational change of equal magnitude but opposite orientation. The binding of $G\alpha_i$ does not occur at the same site as $G\alpha_s$ but at a site on the opposite side, hence the inverse conformational shift. The binding of Gβγ subunits also causes an isoform-specific activation or inhibition respectively. The consensus motif required for Gβγ subunit binding is Gln-Xaa-Xaa-Glu-Arg [Sunahara and Taussig, 2002]. Indeed Gβγ subunits have been shown to regulate ion channel function [Strock and Diversé-Pierluissi, 2004], GPCR kinases [Li et al., 2006] and mitogen-activated protein kinases (MAPKs) [Pearson et al., 2001]. Re-

association of the GDP-bound Gα subunit with the Gβγ subunits terminates the AC signalling event. Whether there is a functional role for $G\alpha_q$ remains to be elucidated [Sunahara and Taussig, 2002].

Post-translational modifications such as phosphorylation, glycosylation and S-nitrosylation can also regulate AC activity [Beazely and Watts, 2006]. Protein kinase C (PKC) is the major protein kinase to regulate AC activity. AC1, AC2, AC3, AC5 and AC7 stimulated activity is enhanced by PKC phosphorylation, whereas AC4 and AC6 phosphorylation by PKC results in down-regulation of stimulated activity. Protein kinase A (PKA) initiates an inhibitory effect on AC5 and AC6, and similarly Ca^{2+}-calmodulin-dependent kinase (CaMK) II and IV phosphorylation of AC3 and AC1 respectively. Furthermore, direct interaction and phosphorylation of the AC2, AC5 and AC6 by c-Raf kinase can also regulate the activity of these isoforms [Ding et al., 2004 and Beazely and Watts, 2006]. N-linked glycosylation has also been established as important for both AC activity and intra-cellular membrane targeting.

Isoform	Distribution	Regulation		
		G-protein	Calcium	Protein Kinases
1	Brain	$G\alpha_s$ stimulation $G\beta\gamma$ inhibition $G\alpha_o$ inhibition	Ca^{2+}/CaM stimulation	PKC weak stimulation CaMK IV inhibition
2	Brain, skeletal muscle, lung & heart	$G\alpha_s$ stimulation $G\beta\gamma$ stimulation	No effect	PKC stimulation c-Raf activation
3	Brain, olfactory epithelium & pancreas	$G\alpha_s$ stimulation	Ca^{2+}/CaM stimulation	PKC weak stimulation CaMK II inhibition
4	Brain, heart, kidney, liver, lung, adipose tissue & uterus	$G\alpha_s$ stimulation $G\beta\gamma$ stimulation	No effect	PKC inhibition
5	Brain, heart, kidney, liver, lung, adipose tissue & uterus	$G\alpha_s$ stimulation $G\beta\gamma$ inhibition $G\alpha_i$ inhibition	Ca^{2+} inhibition	PKA inhibition PKCα/ζ stimulation c-Raf activation
6	Ubiquitous (heart & kidney)	$G\alpha_s$ stimulation $G\beta\gamma$ inhibition $G\alpha_i$ inhibition	Ca^{2+} inhibition	PKA & PKC inhibition c-Raf activation
7	Ubiquitous (brain)	$G\alpha_s$ stimulation $G\beta\gamma$ stimulation	No effect	PKC stimulation
8	Brain, lung & pancreas	$G\alpha_s$ stimulation $G\beta\gamma$ inhibition	Ca^{2+}/CaM stimulation	No effect
9	Brain & skeletal muscle	$G\alpha_s$ stimulation	Ca^{2+}/calcinuerin inhibition	No effect
*Soluble	Ubiquitous (testis)	No effect	Ca^{2+} stimulation	No effect

Table 1.1 – The mammalian adenylyl cyclase enzyme isoforms and their regulatory properties.

The tissue distribution shown in parentheses indicates the most abundant tissue expression of the ubiquitously expressed isoforms.

1.5 cAMP Signalling

1.5.1 cAMP

Earl W. Sutherland established cAMP as a second messenger molecule, shaping the intra-cellular response to the hormone adrenaline [Sutherland and Rall, 1958 and Beavo and Brunton, 2002]. This influential work, undertaken in the late 1950s, was recognised by a Nobel Prize award to Sutherland in 1971. The importance of this cell signalling cascade is reflected in the awards of further Nobel Prizes, to Alfred Gilman and Martin Rodbell for their discovery of G-proteins, to Arvid Carlsson, Paul Greengard and Eric Kandel for their work on the central nervous system (CNS) and the functional role of cAMP and cGMP, and to Richard Axel and Linda Buck for their work on odorant GPCRs and the organisation of the olfactory system.

cAMP is not uniformly distributed within the cell but compartmentalised in functionally distinct pools [Houslay and Milligan, 1997, Zaccolo and Pozzan, 2002, Houslay and Adams, 2003 and Brunton, 2003]. cAMP is produced at a basal concentration of approximately 1μM. These concentrations are able to rise to greater than 10-20μM and fall to basal concentrations in milli-seconds. Such dynamic modulation of intra-cellular cAMP concentrations occurs as a result of alterations in the activation state of adenylyl cyclases and cAMP-specific phosphodiesterases [Houslay and Milligan, 1997 and McConnachie et al., 2006]. It is likely that an uncontrolled increase in cAMP concentration will eventually result in the loss of cAMP compartmentalisation and complete uniform distribution. This is likely to cause aberrant signalling pathways to occur coupled with an inappropriate cell response. Therefore, it is important to retain cAMP in the correct spatial orientation and at the appropriate concentration. This implies the use of scaffold, anchoring and adapter proteins to co-ordinate the assembly and localisation of cAMP signalling complexes, providing efficiency and specificity in signal transduction. cAMP binding proteins include cAMP-specific phosphodiesterases (cAMP-PDEs), cAMP-dependent protein kinase or PKA and their associated AKAPs, guanine

nucleotide exchange proteins activated by cAMP (EPAC), and cAMP-gated ion channels [Beavo and Brunton, 2002].

1.5.2 cAMP-dependent Protein Kinase

cAMP-dependent protein kinase, or PKA, is a broad-spectrum protein kinase that phosphorylates a plethora of target proteins, including receptors, enzymes, ion channels, and the transcription factor CREB. The consensus motif for phosphorylation by PKA is Arg-Arg-Xaa-[Ser/Thr]. It is a tetrameric protein kinase consisting of two catalytic (C) subunits, the activities of which are controlled through the interaction with two regulatory (R) subunits. All subunits are differentially expressed on a cell-type specific basis. There are three genes encoding the catalytic subunits, Cα, Cβ, and Cγ. Splice variants of the catalytic subunits have been reported. Similarly, there are four genes encoding the regulatory subunits, RIα, RIβ, RIIα, and RIIβ, and their associated splice variants. In its tetrameric form PKA is inactive. cAMP co-operatively binds to the R subunits, up to two cAMP molecules per subunit, and facilitates the dissociation of the activated C subunits, both from each other, and the dimeric R subunits [Daniel et al., 1998 and Taskén and Aandahl, 2004].

The RI subunit is generally considered to have a cytosolic sub-cellular localisation [McConnachie et al., 2006]. The RII subunit is thought to be responsible for mediating AKAP interactions [Dodge et al., 2001, Taskén et al., 2001 and McCahill et al., 2005], allowing it to be localised at distinct sub-cellular sites, such as the plasma membrane, and to intra-cellular organelles to provide signalling complexes. The differences in the N-terminal regions of the RI and RII subunits are believed to underlie the disparity for AKAP binding.

Three distinct genes produce three catalytic isoforms, α, β, and γ, each of which is subject to interactions with isoforms of the endogenous inhibitor,

PKI. The N-terminal regions of all PKI isoforms bind to the catalytic subunits and serve as a pseudo-substrate thereby abolishing PKA activity.

1.5.2.1 A-Kinase Anchoring Proteins

AKAPs are expressed on a cell-type specific basis and have distinct patterns of intra-cellular localisation [Taskén and Aandahl, 2004, and Langeberg and Scott, 2005]. AKAPs sequester PKA to promote the close proximity to the wide range of substrates that it phosphorylates [Murphy and Scott, 1998]. Over fifty AKAPs have been identified and there is modest homology between them. However, most AKAPs do conform to a generalised structure, whereby one region facilitates PKA binding, a second region intra-cellular targeting, and several distinct regions for interactions with other signalling molecules [Wong and Scott, 2004]. Some AKAPs promote the delivery of PKA to the plasma membrane through direct interaction with a basic region, found towards the N-terminal of the AKAP, and the phosphatidyl-inositol 4,5 bisphosphate, myristoyl or palmitoyl components of the plasma membrane. And conversely, for example, the C-terminal region of AKAP6 binds the PKA holo-enzyme. Site-directed mutagenesis of a residue in AKAP6 prevents the binding and subsequent recruitment of PKA to the desired cellular location [Carlisle Michel et al., 2004]. AKAPs interact with the PKA RII regulatory subunit at the dimerisation interface of the R subunits [Newlon et al., 1999, Colledge and Scott, 1999 and Newlon et al., 2001]. However, certain AKAPs have also been shown to interact with the PKA RI subunit. Thus, sequestration of PKA RI and RII subunits may be dependent upon the R subunit availability in a particular cell type and the AKAP expression pattern.

AKAP1 interacts with the RIα subunit with a K_d of 185nM whereas the RIIα subunit binds with a K_d of 2nM. AKAP interactions with PKA can be disrupted using a peptide (Ht31) based upon AKAP13 [Klussmann et al., 2001]. Furthermore, AKAPs themselves can be directly phosphorylated by PKA [Tao et al., 2003 and Bajpai et al., 2006]. AKAPs can also integrate a plethora of cell signalling pathways through their interaction with receptors,

e.g. β-adrenoceptors and AMPA/NMDA receptors [Fraser et al., 2000, Oliveria et al., 2003], enzymes including phosphodiesterase-4 (PDE4) [Baillie et al., 2005], other kinases, e.g. PKC, PPs, e.g. PP1 and PP2, and channels, e.g. ion channels and aquaporin-2 [Henn et al., 2004, Hoshi et al., 2005, and Chen and Kass, 2005]. AKAPs can also influence the structural organisation of the cell cytoskeleton through interactions with the actin microfilaments and the microtubules. AKAPs are likely to play a fundamental role in regulating cell cycle progression through interactions with centrosomes, chromatin condensation and de-condensation, and nuclear envelope dis-assembly and re-assembly [Taskén et al., 2001 and Taskén and Aandahl, 2004].

AKAP Gene	Alternative Nomenclature	Protein Interactions
1	S-AKAP84/D-AKAP1/AKAP121/AKAP149	Lamin B, PP1, PDE4A
2	AKAP-KL	
3	AKAP110	$G_{13}\alpha$, PDE4A
4	AKAP82/FSC1	
5	AKAP75/79/150	PKC, PP2B, β-adrenoceptor, SAP97, PSD-95, AMPA & NMDA receptors, L-type Ca^{2+} channels, aquaporin-2 water channel
6	m-AKAP	PDE4D3, PP2A, ERK5, EPAC1
7	AKAP15/18 (α, β, γ, δ)	Na^{+} & L-type Ca^{2+} channels, aquaporin-2 water channel
8	AKAP95	Eg7/condensing, PDE4A
9	AKAP450/AKAP350/Yotiao/CG-NAP/Hyperion	PDE4D3, PP1, PP2A, PKN, PKCε, CK1, NMDA receptor
10	D-AKAP2	
11	AKAP220/hAKAP220	PP1
12	AKAP250/Gravin	PKC, β-adrenoceptor, actin
13	AKAP-Lbc/Ht31/Rt31	

Table 1.2 – The A-kinase anchoring proteins and gene nomenclature.

Many other proteins have been assigned AKAP function to date including Microtubule-associated protein 2B (MAP2B), Ezrin/AKAP78/T-AKAP80, Pericentrin, WAVE-1/Scar, Myosin VIIA, PBR-associated protein 7 (PAP7), Neurobeachin, AKAP28, Myeloid translocation gene (MTG) 8/16b [Asirvatham et al., 2004], AKAP140, AKAP85, Brefeldin A-inhibited guanine nucleotide-exchange protein 2 (BIG2) [Li et al., 2003], and Rab32 but have yet to be given designated gene nomenclature. Table and information adapted from Taskén and Aandahl, 2004, Wong and Scott, 2004 and McConnachie et al., 2006.

1.5.2.2 Gene Transcription

The intra-cellular levels of cAMP have a profound effect at the level of gene transcription [Montminy, 1997 and Zambon et al., 2005]. For gene expression to be regulated by cAMP the promoter region must contain a cAMP response element (CRE), which conforms to the general DNA consensus motif 5'-TGACGTCA-3' [Daniel et al., 1998 and Shaywitz and Greenberg, 1999]. The CRE motif is typically located approximately 100 nucleotides from a TATA box sequence. Genes containing the CRE motif include those encoding certain cAMP-specific PDE4 isoforms [Vicini and Conti, 1997 and Le Jeune et al., 2002], the gluco-corticoid receptor, the aryl aromatic hydrocarbon receptor, insulin, tyrosine hydroxylase, inducible nitric oxide synthase (iNOS) and angiotensinogen, to name but a few [Mayr and Montminy, 2001 and Beavo and Brunton, 2002]. As described in Section 1.5.2 above, cAMP binding to the PKA holoenzyme releases the active C subunits of PKA from their R subunits. Without such dissociation of the holoenzyme, PKA is unable to traverse the nuclear membrane because it is simply too large. The active C subunits cross the nuclear membrane through passive diffusion and directly phosphorylate and activate a number of transcription factors such as cAMP response element binding protein (CREB), cAMP response element modulator (CREM), activating transcription factor-1 (ATF-1) and nuclear factor-κB (NF-κB) [Daniel et al., 1998 and Houslay and Kolch, 2000]. The phosphorylation of CREB is widely accepted as a measurable read-out of PKA activation [MacKenzie and Houslay, 2000, Staples et al., 2001 and Rangarajan et al., 2003]. CREB is phosphorylated by PKA at Ser-133 within the consensus sequence Arg-Arg-Pro-Ser-Tyr [Montminy, 1997 and Houslay and Kolch, 2000]. CREB can also be phosphorylated at additional sites by other kinases including PKC, CaMKs, ERK1/2 via MAPKAPK1/pp90^{rsk}, MAPKAPK2 and casein kinase-2 (CK-2). Indeed, PKA serves as the priming kinase for glycogen synthase kinase-3 (GSK-3) phosphorylation at Ser-129, the activity of which is subject to PKA regulation [Daniel et al., 1998, Fang et al., 2000 and Doble and Woodgett, 2003]. The interaction of phosphorylated CREB dimers with the CRE motif occurs through a basic C-terminal leucine zipper motif (bZIP). The bZIP motif

of CREB also contains the nuclear localisation signal. The subsequent interaction of CREB binding protein (CBP), or its homologue p300, initiates target gene expression through intrinsic histone acetyl-transferase activity and the recruitment of RNA polymerase II [Shaywitz and Greenberg, 1999 and Mayr and Montminy, 2001]. Furthermore, the recruitment to the nearby TATA box of the TATA-binding protein (TBP) and a multitude of TBP-associated factors (TAFs), forming the TFIID multi-protein complex, are crucial components of the transcriptional machinery, with TFIIB bridging the interaction between TFIID and RNA polymerase II. Termination of cAMP-induced gene transcription occurs through the de-phosphorylation of CREB by PP1 or PP2B, or through the interaction of PKA with PKI, which drives the catalytic units back to the cytoplasm by exposing a nuclear export motif [Daniel et al., 1998 and Mayr and Montminy, 2001].

1.5.3 Guanine Nucleotide Exchange Protein Activated by cAMP

Ras is a monomeric GEF that is activated by receptor tyrosine kinases (RTKs) such as the epidermal growth factor (EGF) receptor and the insulin receptor [Malarkey et al., 1995]. Activation of these receptors through ligand binding results in the conversion of Ras from its inactive GDP-bound form to its active-GTP bound form. Rap1 and Rap2 are also members of the Ras-like family of small GTPases [Zwartkruis and Bos, 1999].

A novel 881-residue protein, guanine nucleotide exchange protein activated by cAMP (EPAC), was identified with a distinct region for cAMP binding and a second region capable of supporting GEF activity [de Rooij et al., 1998 and Kraemer et al., 2001]. Two EPAC proteins, EPAC1 and EPAC2 (cAMP-GEFI and cAMP-GEFII), so called because of the number of cAMP binding sites, have been described [de Rooij et al., 2000, Kraemer et al., 2001 and Rehmann et al., 2003]. EPAC1 is composed of an N-terminal regulatory module containing a Dishevelled, Egl-10, Pleckstrin (DEP) domain, the cyclic nucleotide binding site(s), and the Ras exchange motif (REM), with the GEF domain or catalytic machinery towards the C-terminal region [Kraemer et al.,

2001 and Rehmann et al., 2003]. EPAC2 has the same domains as EPAC1 but it differs in that it contains a second cAMP-binding site at the extreme N-terminus, and a Ras association domain between the REM and GEF domains [Bos, 2003 and Rehmann et al., 2006].

Physiological concentrations of cAMP bind EPAC and directly activate Rap1 and Rap2 through GDP/GTP exchange, a process that is independent of phosphorylation by PKA [de Rooij et al., 1998 and de Rooij et al., 2000 and Kraemer et al., 2001]. EPAC thus functions as a GEF for Rap1 and Rap2 [de Rooij et al., 1998]. Whilst half-maximal activation of PKA requires around 1μM of cAMP, half-maximal activation of EPAC2 requires approximately 40μM cAMP [Bos, 2003]. The binding of cAMP induces a conformational change in EPAC proteins that relieves the N-terminal inhibitory constraint by exposing, and thereby activating, the GEF domain. This is exemplified by truncation of the cAMP binding domain, the identification of a related to EPAC protein (rEPAC) that lacks the cAMP binding domain and constitutively activates both Rap1 and Rap2, and the use of N- and C-terminally tagged fluorescence resonance energy transfer (FRET) constructs [de Rooij et al., 1998, de Rooij et al., 2000, Bos, 2003 and Ponsioen et al., 2004].

EPAC is ubiquitously expressed in human tissues [Zwartkruis and Bos, 1999 and Bos, 2003]. Within the cell EPACs are localised at perinuclear and mitochondrial locations and may co-localise with soluble forms of AC [Taskén and Aandahl, 2004 and Bundey and Insel, 2004]. This localization is subject to change during the cell cycle [Bos, 2003]. Localisation is controlled by the DEP domain [de Rooij et al., 1998 and Kraemer et al., 2001]. Removal of the DEP and cAMP binding domains has no effect on EPAC activity, but it does affect its localisation at the plasma membrane [de Rooij et al., 2000 and Magiera et al., 2004]. Assessing the role of EPACs in a cellular signalling context, it is hardly surprising that EPAC1 also associates with AKAP6 using PDE4D3 as a bridge [McConnachie et al., 2006].

EPACs may also regulate other protein kinase activity, such as protein kinase B (PKB) or phospholipase Cε (PLCε). What is certain is that the

activation of EPAC, possibly augmented by the interaction with microtubule-associated protein 1A, light chain 2 (MAP1A-LC2), and Rap1 causes a significant increase in cell adhesion [Rangarajan et al., 2003, Gupta and Yarwood, 2005 and Yarwood, 2006]. The mobilisation of intra-cellular Ca^{2+} stores through EPAC2-mediated regulation of the ryanodine receptor has also been described and may play a role in insulin secretion from the pancreatic β-islets [Bos, 2003]. The availability of cAMP analogues, selective for EPAC over PKA, will allow the elucidation of a plethora of cell signalling pathways that are subject to the EPAC regulation [Christensen et al., 2003].

1.5.4 cAMP-gated Ion Channels

Cyclic nucleotide-gated (CNG) ion channels are members of the voltage-gated ion channel super-family [Kaupp and Seifert, 2002]. CNG ion channels are activated by both cAMP and cGMP but have ligand specificity [Young and Krougliak, 2004]. They have four subunits, each composed of six transmembrane-spanning regions with intra-cellular N- and C-terminal regions. There are six types of subunit, four "A" and two "B" subunits. Homo- and hetero-tetrameric channels are formed from combinations of subunits and these direct their specific means of regulation [Bradley et al., 2005]. Cyclic nucleotide binding occurs at the C-terminal of the channel and other sites of functional regulation are at sites within the N-terminal. The activation of the specific channel requires the co-operative binding of multiple cyclic nucleotide molecules and is not subject to any desensitisation mechanism. They are not cation-specific and allow the influx of either alkali Na^+ ions or divalent Ca^{2+} ions [Cooper, 2003]. CNG ion channel activity is modulated by both Ca^{2+}/CaM and phosphorylation. They are expressed in a wide variety of tissue but are most commonly studied in photoreceptors or olfactory sensory neurons [Bradley et al., 2005]. CNG ion channels have been exploited to investigate cAMP compartmentalisation [Rochais et al., 2004].

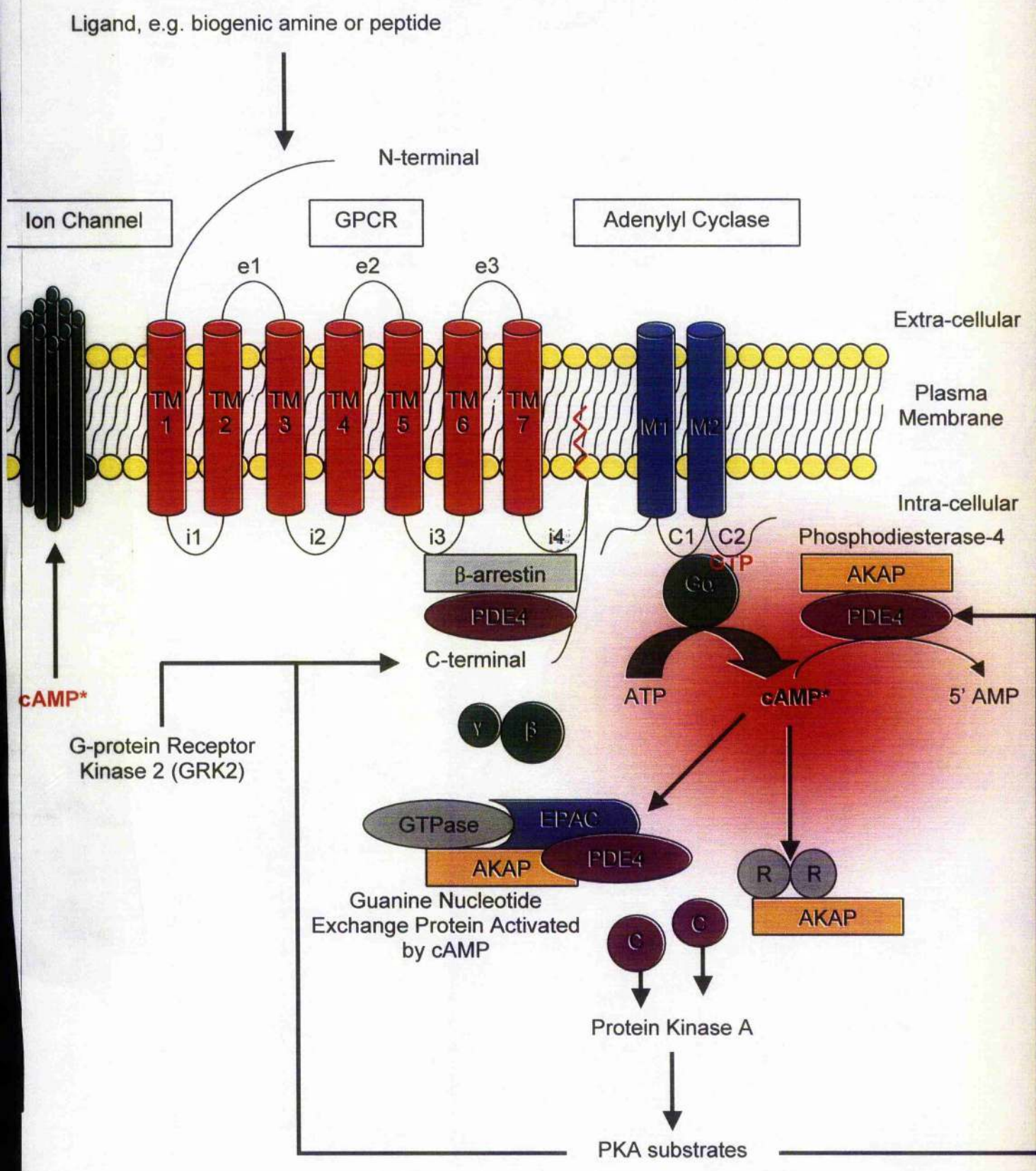

Figure 1.3 – Schematic representation of the cAMP signalling system.

1.6 Cyclic Nucleotide Phosphodiesterases

Cyclic nucleotide phosphodiesterases (PDEs) (EC 3.1.4.17) are enzymes that catalyse the hydrolysis of cyclic nucleotides to the associated 5' mononucleotide. This catalytic reaction is shown structurally in Figure 1.4 [Lugnier, 2006]. PDE activity is detectable at various locations within cells including the cytosol, the plasma membrane, the cytoskeleton and the nucleus [Houslay and Adams, 2003]. The PDE super-family, shown in Table 1.1, constitutes eleven PDEs characterised by their substrate specificity, i.e. their ability to hydrolyse cAMP and/or cGMP, their specific means of regulation, and their specific inhibition by selective inhibitors [Houslay, 2001]. A central theme for all PDEs appears to be the presence of N-terminal, tandem regulatory domains that function to control the activity of the core, conserved catalytic unit, as depicted in Figure 1.5 [Francis et al., 2001 and Houslay and Adams, 2003].

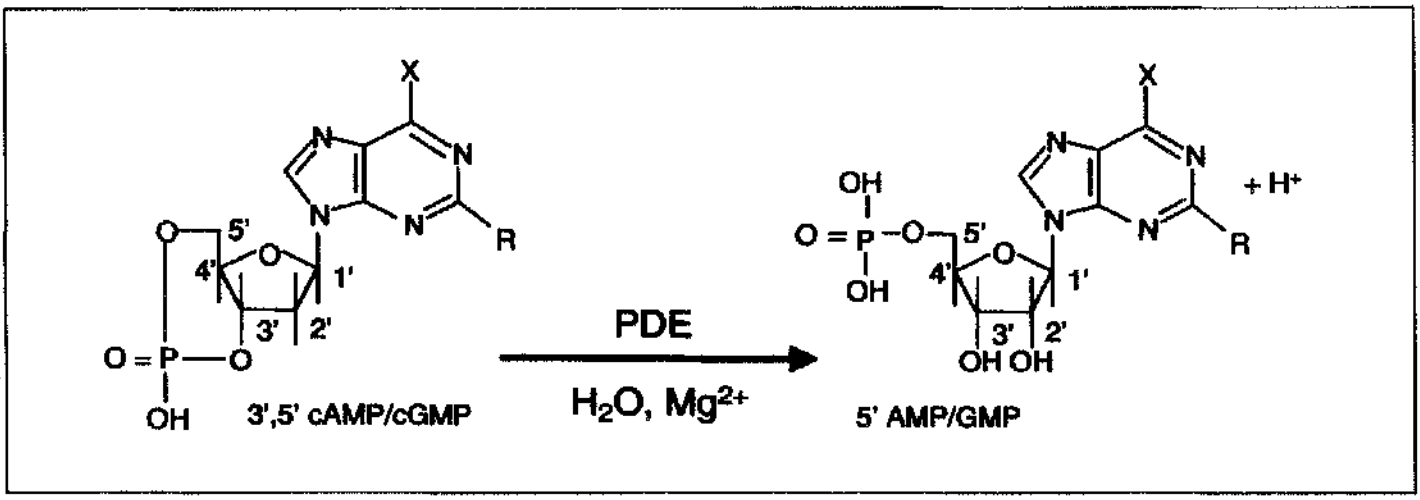

Figure 1.4 – Cyclic nucleotide hydrolysis by phosphodiesterases.

PDE	Genes	Substrates		Regulation	Regulatory Domains	Selective Inhibition
		cAMP	cGMP			
1	A, B and C	Yes	Yes	Ca^{2+}/CaM PKA and CaMK	Ca^{2+}/CaM Binding	Nicardipine and Vinpocetine
2	A	Yes	Yes	Activated by cGMP Phosphorylated by PKC	GAF	EHNA
3	A and B	Yes	No	Inhibited by cGMP Phosphorylated by PKA, PKB/Akt & PI3-K		Cilostimide and Milrinone
4	A, B, C and D	Yes	No	Phosphorylated by PKA and ERK1/2	UCR	Rolipram, Ro 20-1724, Cilomilast (Ariflo®), Denbufylline and Roflumilast
5	A	No	Yes	Binds cGMP Phosphorylated by PKA and PKG	GAF	Zaprinast and Sildenafil (Viagra®)
6	A, B and C	No	Yes	Activated by Rhodopsin and Transducin (G_t)		Zaprinast and Sildenafil (Viagra®)
7	A and B	Yes	No			BRL 50481 and ICI 242
8	A	Yes	No			Unknown, IBMX-insensitive
9	A	No	Yes			Zaprinast, SCH51866, IBMX-insensitive
10	A	Yes	Yes	Inhibited by cAMP		Dipyridamole and Zaprinast
11	A	Yes	Yes			Dipyridamole and Zaprinast

Table 1.3 – Classification of the PDE enzyme super-families.

1.6.1 Phosphodiesterase-1

There are three genes (A-C) encoding PDE1 and these are expressed as multiple splice variants arising from both 5' and 3' mRNA alternative splicing [Snyder et al., 1999]. PDE1 enzymes are dimers and can hydrolyse both cAMP and cGMP, with K_m values of 1-100μM and 1-5μM respectively [Francis et al., 2001]. They are composed of paired Ca^{2+}/calmodulin (CaM) binding domains and the co-operative occupancy of four Ca^{2+} ions, irrespective of intra-cellular origin, of the binding domains serves to activate enzymatic activity [Spence et al., 1995 and Lugnier, 2006]. PDE1 enzymes exist in an auto-inhibited state and are also inhibited directly, at the active site, by nicardipine and vinpocetine, and by the anti-schizophrenic drug tri-fluoro-perazine, a CaM antagonist [Houslay, 2001]. Activity can also be down-regulated by phosphorylation by both PKA and CaMK, by attenuating CaM binding. PDE1 is ubiquitously expressed and its expression profile can be dynamically regulated by 7-oxo-prostacyclin in the heart and phosphatidyl inositol signalling in Chinese Hamster Ovary (CHO) cells [Spence et al., 1995 and Kostic et al., 1997].

1.6.2 Phosphodiesterase-2

One gene (A) encodes three 5' mRNA splice variants of PDE2 [Francis et al., 2001]. PDE2 enzymes can hydrolyse both cAMP and cGMP, with a K_m value of 15-30μM. PDE2 enzymes are unique as they are activated through a decrease in K_m rather than an increase in V_{max}, as is observed for other PDEs. They contain tandem GAF domains that promote dimerisation and directly bind cGMP to activate and co-operatively increase the rate of hydrolysis of cAMP; a point of cross talk for the signalling pathways [Lugnier, 2006]. Activity is also enhanced by phosphorylation by PKC [Houslay, 2001]. PDE2 enzymes are inhibited through direct competition for cGMP binding by erythro-9-(2-hydroxy-3-nonyl)-adenine (EHNA), an adenosine deaminase inhibitor [Michie et al., 1995]. PDE2 is widely expressed in many human tissues and has a ubiquitous sub-cellular localisation [Lugnier, 2006]. It is

particularly abundant in the CNS and contributes to the compartmentalisation of olfactory signal transduction [Juilfs et al., 1997].

1.6.3 Phosphodiesterase-3

PDE3 enzyme splice variants are encoded by two genes (A and B), which are positioned at chromosome 11p15.1 and 11p15, and are not subject to mRNA splicing [Meacci et al., 1992, Lobbert et al., 1996 and Miki et al., 1996]. PDE3 dimers specifically hydrolyse cAMP and are competitively inhibited by cGMP [Lugnier, 2006]. The K_m values for PDE3 hydrolysis of both cyclic nucleotides are 0.1-0.8μM, but the V_{max} for cAMP hydrolysis is greater [Francis et al., 2001]. Excess cAMP in Jurkat T-cells induces expression of PDE3 [Erdogen and Houslay, 1996]. PDE3 is targeted to the endoplasmic reticulum through two N-terminal domains and as such are appropriately positioned to control the phosphorylation status of voltage-gated ion channels and Ca^{2+} release [Shakur et al., 2000]. Together with PDE4, PDE3 enzymes are responsible for the major cAMP hydrolysing activity in heart cells and platelets [Mongillo et al., 2004]. PDE3A has a fundamental role in controlling cardiac contractility through the modulation of Ca^{2+} channels, and inhibition of these enzymes in the heart by cilostimide and milrinone results in positive inotropy, i.e. increased contractility. Furthermore, PDE3 inhibition attenuates platelet aggregation [Francis et al., 2001]. PDE3B expression is altered and thought to play a role in type 2 diabetes mellitus [Matsumoto et al., 2003]. Increasing intra-cellular cAMP concentrations increases the rate of lipolysis in adipocytes, via PKA phosphorylation and activation of hormone-sensitive lipase, and in pancreatic β-cells enhances insulin secretion in response to glucose [Härndahl et al., 2002 and McConnachie et al., 2006]. More recently, a role has been identified for cAMP and PDE3B in GLUT-4 translocation in adipocytes [Zmuda-Trzebiatowska et al., 2006]. PDE3B is phosphorylated and activated by PKA and thus functions in a classical negative feedback loop to lower intra-cellular cAMP concentrations. PDE3B is also phosphorylated and activated by PKB/Akt, a protein kinase involved in the insulin signalling cascade, and is

therefore likely to utilise PDE3B activation to reduce further insulin secretion, in an autocrine manner [Rondinone et al., 2000 and Onuma et al., 2002].

1.6.4 Phosphodiesterase-4

PDE4 enzymes are the subject of this thesis and are discussed in much greater detail in Section 1.7 below.

1.6.5 Phosphodiesterase-5

PDE5 enzymes are widely known as being the drug target for the compound Viagra® (sildenafil) for the treatment of penile erectile dysfunction [Corbin and Francis, 1999 and Sung et al., 2003]. Viagra® prevents the PDE5 hydrolysis of cGMP promoting smooth muscle relaxation and increasing the blood flow to the corpus cavernosum. Zaprinast also inhibits the cGMP-hydrolysing activity of PDE5 enzymes [Lugnier, 2006]. One gene (A) located on chromosome 4q25-27 encodes three PDE5 isoforms that occur through both alternative mRNA splicing and the use of alternate promoters, regulated by cyclic nucleotide expression [Francis et al., 2001]. PDE5 enzymes exist as dimers and have a K_m of 5-20μM for cGMP binding at the N-terminal GAF domain. PDE5s are subject to activation and conformational change initially by cGMP binding and secondly by both PKA and protein kinase G (PKG) phosphorylation leading to a further increase in cGMP binding affinity [Lugnier, 2006]. PDE5 is expressed in lung, heart and the cerebellum and at lower levels in the brain and kidney [Francis et al., 2001 and Houslay, 2001].

1.6.6 Phosphodiesterase-6

PDE6 enzymes are light activated via rhodopsin and transducin, a G-protein, and are found to be expressed exclusively in the rod and cone sensory cells of the visual system [Houslay, 2001]. Within the cell PDE6 enzymes are predominantly membrane bound [Francis et al., 2001]. PDE6

enzyme subunits are encoded by distinct genes and are specific for cGMP, with a K_m in the region of 5-20μM. Structurally they are hetero-tetramers composed of α-catalytic and/or β-catalytic subunits and two γ-regulatory subunits with rod PDE6 enzymes composed of α, β and γ subunits and cones α, α, and γ subunits [Lugnier, 2006]. For photo-transduction, rhodopsin absorbs a photon of light and activates transducin, which exchanges GDP for GTP. GTP-bound transducin then displaces the γ-subunits and activates PDE6 catalytic activity.

1.6.7 Phosphodiesterase-7

PDE7 enzymes are encoded by two genes (A and B), which are located on chromosome 8q13-q22 and subject to 5' mRNA splicing [Houslay and Milligan, 1997 and Lugnier, 2006]. They have very low K_m values (approximately 0.1μM) for cAMP hydrolysis [Richter et al., 2002]. BRL 50481 and ICI 242 have been shown to inhibit PDE7 activity, whereas rolipram has no effect. Within the cell PDE7 associates with the golgi apparatus, as shown by co-localisation with the golgi marker GM130 [Asirvatham et al., 2004]. In the same study PDE7A has been shown to bind AKAP-MTG in T-cells, where its expression predominates and thus, may be subject to regulation by PKA.

1.6.8 Phosphodiesterase-8

PDE8 enzymes are encoded by one gene (A) and have similar K_m values for cAMP hydrolysis as PDE7 [Francis et al., 2001 and Lugnier, 2006]. They are insensitive to current PDE inhibitors, including IBMX. A Per-ARNT-Sim (PAS) domain is located at the N-terminal and may regulate intra-cellular distribution and activity, through protein-protein interactions [Soderling and Beavo, 2000]. Expression of PDE8 isoforms is highest in the testis and lower expression is detected in a plethora of other tissues including brain, liver and kidney.

1.6.9 Phosphodiesterase-9

Encoded by one gene (A) located on chromosome 21q22.3, PDE9 enzymes, of which there is four splice variants, are specific for cGMP with a K_m value of approximately 0.07μM [Soderling and Beavo, 2000]. They contain a REC domain, but as yet the precise role of this domain is unknown [Lugnier, 2006]. Intriguingly, cGMP-specific PDE9 is, like the cAMP-specific PDE8, insensitive to inhibition by IBMX but activity is attenuated with zaprinast and SCH 51866. PDE9 has broad tissue distribution including, kidney, liver, lung, brain, testis, skeletal muscle, heart, thymus and spleen [Soderling and Beavo, 2000].

1.6.10 Phosphodiesterase-10

Alternative mRNA splice variants of PDE10 enzymes are encoded by one gene (A) located on chromosome 6q26-27 and contain GAF domains of unknown function [Francis et al., 2001 and Lugnier, 2006]. PDE10 displays a K_m value of 0.05μM and a V_{max} value 5-fold higher for cAMP than cGMP, K_m 3μM. This kinetic profile may underlie the cAMP inhibition of cGMP hydrolysis by PDE10. IBMX, dipyridamole and zaprinast inhibit PDE10. PDE10 is ubiquitously expressed in human tissue. Unlike PDE10A1, PDE10A2 is phosphorylated at its extreme N-terminal by PKA and this phosphorylation prompts it redistribution from the membrane of the golgi apparatus to the cytosol [Kotera et al., 2004].

1.6.11 Phosphodiesterase-11

Similarly, PDE11 enzymes are encoded by just one gene (A) and also do not discriminate between cAMP and cGMP, with a K_m value of approximately 0.75μM for both cyclic nucleotides [Francis et al., 2001]. PDE11 isoforms show differential inclusion of tandem GAF domains, a likely result of alternative 5' mRNA splicing similar to that for the UCR regulatory domains of PDE4 isoforms [Houslay, 2001 and Lugnier, 2006]. Inclusion of

the extreme N-terminal GAF domain may allow PDE11 to be regulated by PKA and PKG phosphorylation, as putative consensus motifs exist [Lugnier, 2006]. IBMX, dipyridamole and zaprinast also inhibit PDE11. PDE11 has wide tissue distribution.

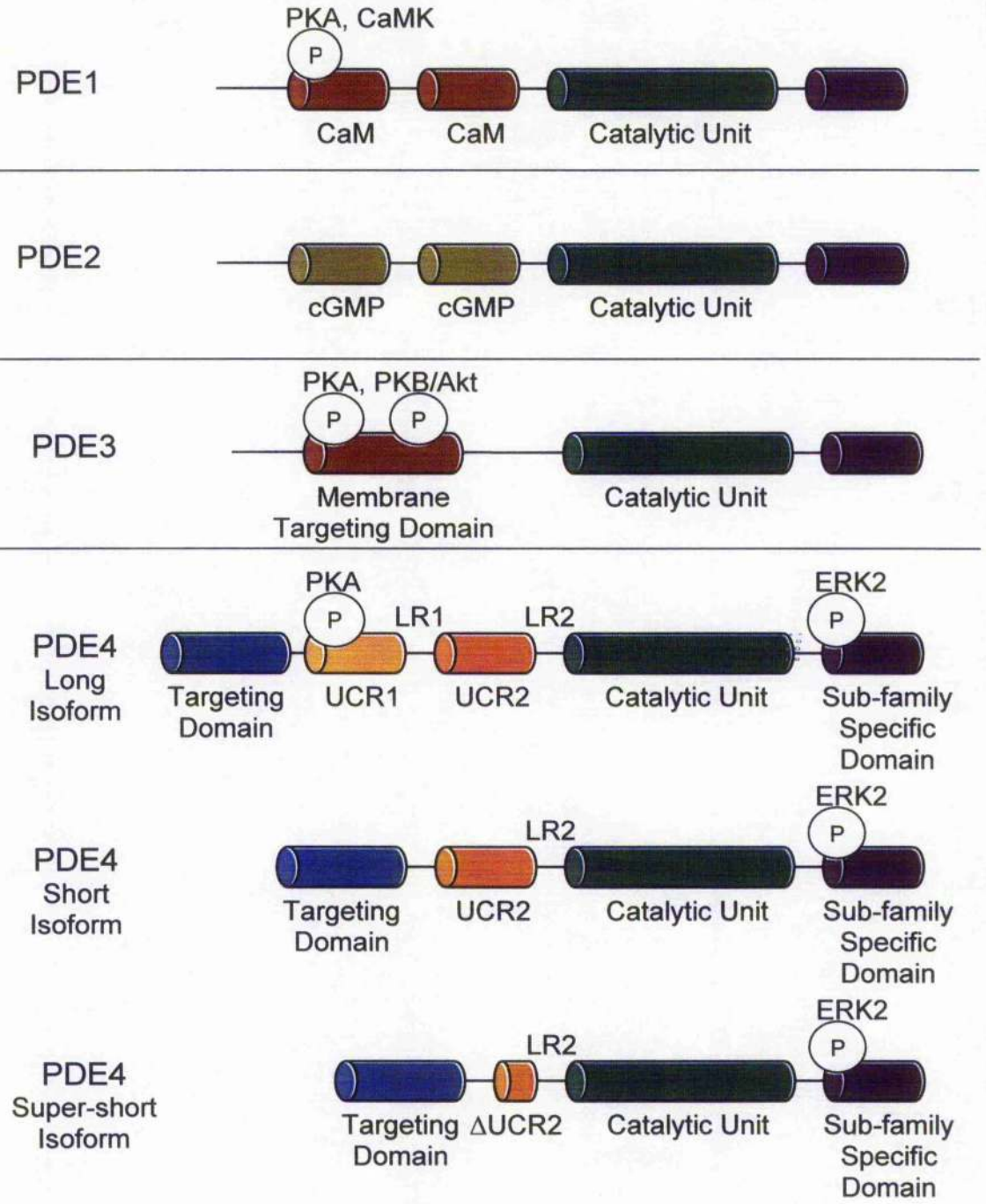
PDE1
PKA, CaMK
P
CaM
CaM
Catalytic Unit
PDE2
cGMP
cGMP
Catalytic Unit
PDE3
PKA, PKB/Akt
P
P
Membrane Targeting Domain
Catalytic Unit
PDE4 Long Isoform
PKA
P
LR1
LR2
ERK2
P
Targeting Domain
UCR1
UCR2
Catalytic Unit
Sub-family Specific Domain
PDE4 Short Isoform
LR2
ERK2
P
Targeting Domain
UCR2
Catalytic Unit
Sub-family Specific Domain
PDE4 Super-short Isoform
LR2
ERK2
P
Targeting Domain
ΔUCR2
Catalytic Unit
Sub-family Specific Domain
PDE5
cGMP
GAF A
GAF B
Catalytic Unit
PDE6
GAF A
GAF B
Catalytic Unit

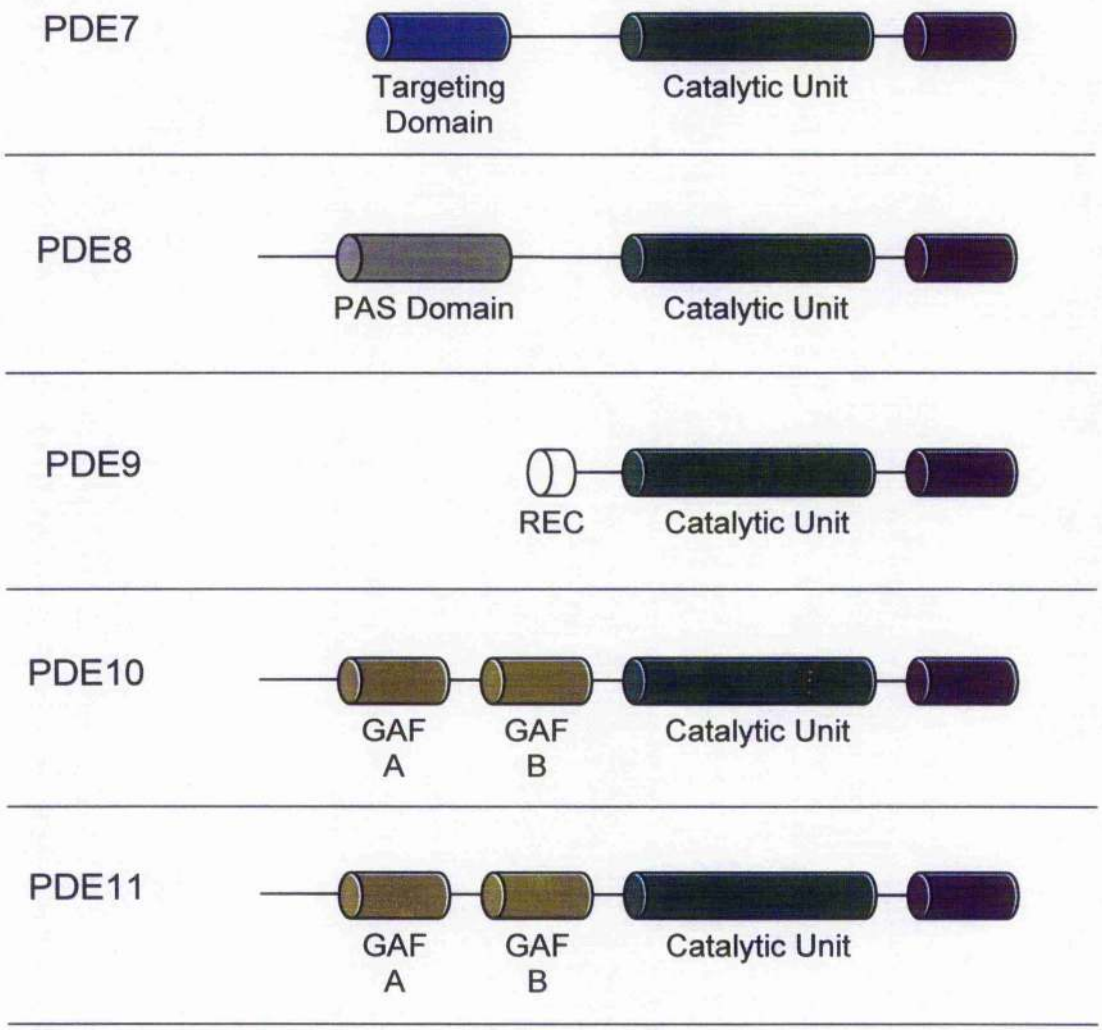

Figure 1.5 – Modular structures of the PDE enzyme super-family.

1.7 cAMP-specific Phosphodiesterase-4

1.7.1 Phosphodiesterase-4 Gene and Modular Structure

Phosphodiesterase-4 (PDE4) enzymes, or as they were once known "type-IV" or "type-4", are a family of over 20 proteins encoded by four distinct genes, PDE4A – PDE4D [Conti et al., 2003 and Houslay et al., 2005]. PDE4A1, originally known as RD1 (ratdnc-1), was the first PDE4 to be cloned. This was achieved using a probe based upon the *Drosophila melanogaster* dunce^{+} gene, which encodes a PDE4 enzyme [Davis et al., 1989]. This work was advanced with the identification of multiple PDE4 isoforms [Swinnen et al., 1989] and the classification of these into four related, but distinct, gene products [Bolger et al., 1993]. The four genes encoding the PDE4 enzymes are located on three different chromosomes in humans. Chromosome 19p13.2 encodes PDE4A [Milatovich et al., 1994 and Horton et al., 1995] with the PDE4C gene located on the same chromosome at 19p13.1 [Sullivan et al., 1999]. The other PDE4 genes encoding PDE4B and PDE4D are located on chromosomes 1p31 and 5q12 respectively [Milatovich et al., 1994 and Szpirer et al., 1995]. The genes are approximately 50,000 base pairs in length and consist of eighteen or more coding regions or exons [Szpirer et al., 1995, Houslay, 2001 and Houslay and Adams, 2003]. PDE4 isoforms occur through alternative splicing of 5' mRNA transcripts [Swinnen et al., 1989, Bolger et al., 1996, Bolger et al., 1997 and Richter et al., 2005]. Such splicing supports the remarkable homology of the PDE4 catalytic unit and the conserved sub-family specific C-terminal regions. The splice variants are individually characterised by their N-terminal regions, which are encoded by single, unique 5' exons. It is likely that the identification of hitherto unknown novel 5' exons, appropriately positioned downstream of promoter regions, will augment the current crop of known PDE4 isoforms and significantly contribute to the compartmentalisation and regulation of cAMP signalling [Rena et al., 2001 and Wallace et al., 2005]. However, PDE4 enzymes can also be classified by virtue of the differential inclusion of their upstream conserved regions 1 and 2 (UCR1 and UCR2) regulatory domains into long, short or

super-short forms. Long forms are characterised by their unique and specific 5' exons that take up the position of exon 1. A common long form region is encoded immediately 5' to exon 2. Exons 2-4 encode the UCR1 regulatory module, which consists of approximately 60 amino acids. This is connected to linker region 1 (LR1). LR1 is 24 amino acids in length and encoded by exons 4 and 5. Short forms of PDE4 enzymes result from a splice junction located between exons 5 and 6. Thus, the PDE4 short forms contain no UCR1 module. LR1 is sub-family specific and connects UCR1 to UCR2. UCR2 is encoded by exons 6-8 and produces a second regulatory domain of approximately 80 amino acids. A splice junction embedded between exons 6 and 7 results in the truncation of UCR2 producing super-short PDE4 enzymes. The UCR regulatory domains interact with the catalytic unit through a 10-28 amino acid sequence known as linker region 2 (LR2), a sub-family specific sequence encoded by exons 8 and 9. The catalytic unit itself is approximately 320-350 amino acids in length and is encoded by exons 10-15. It is highly conserved throughout all PDE4 enzymes. The C-terminal region, also encoded by exon 15, shows distinct homology within each gene family. The modular structures of PDE4 enzymes are shown in Figure 1.5.

1.7.2 Phosphodiesterase-4 Expression Profiles

PDE4 enzymes provide the major cAMP hydrolysing activity in many cell types [Houslay, 2001 and Conti et al., 2003]. PDE4 isoforms are ubiquitously expressed on a cell-type specific basis and the abundance of isoforms confers distinct intra-cellular targeting [Houslay and Adams, 2003 and Houslay et al., 2005]. Many studies have employed reverse transcriptase polymerase chain reaction (RT-PCR) to assess PDE4 transcripts within cells [Rena et al., 2001, Wallace et al., 2005 and Richter et al., 2005]. However, it should be understood that the presence of such RNA transcripts is not always representative at the level of protein expression. The expression and turnover of long PDE4 forms is considered to be a stable process with low protein degradation whereas the short and super-short splice variants typically show a greater level of variation in their expression and are more rapidly degraded

[Richter and Conti, 2004]. It is widely appreciated that any change in PDE4 isoform expression is likely to underpin a fundamental change in cAMP signalling in cells [Houslay and Adams, 2003 and Shepherd et al., 2004].

PDE4A isoforms have very prominent expression patterns in the brain [Shakur et al., 1994, McPhee et al., 1995, Engels et al., 1995, McPhee et al., 2001 and D'Sa et al., 2005]. Significant expression of PDE4A isoforms occurs in the granular layer of the olfactory bulb, the piriform cortex, the dentate gyrus and the CA1 and CA2 pyramidal cells [McPhee et al., 2001]. The long PDE4A isoforms, PDE4A5 and PDE4A10, show distinct expression in the striatum, thalamus and hippocampus but not the cerebellum. Transcripts for PDE4A11 were also detected in brain tissue and in the same study developmental changes in brain expression for this isoform were proposed [Wallace et al., 2005]. PDE4A1 expression was strongly evident in the cerebellum, the glomerular layer of the olfactory bulb and the CA3 pyramidal cells. Little or no expression of all three isoforms was detected in the medial nucleus of the amygdale. Expression of PDE4B isoforms in many regions of the brain has also been identified [Lobban et al., 1994]. These differential brain expression profiles may underlie the role of specific PDE4 isoform inhibition as potential therapeutics for the treatment of CNS disorders, such as depression, Alzheimer's and Parkinson's disease, and may explain the nausea and emetic side effects of PDE4 inhibitors [D'Sa et al., 2005].

PDE4 isoforms have been shown to provide the dominant cAMP hydrolysing activity in many inflammatory cells such as neutrophils, eosinophils, monocytes, macrophages and T-lymphocytes [Manning et al., 1999, Le Jeune et al., 2002, Barber et al., 2004, Shepherd et al., 2004, Abrahamsen, et al., 2004, Ariga et al., 2004, Wallace et al., 2005 and Jones et al., 2005]. Eosinophils and neutrophils are known to express PDE4A, PDE4B and PDE4D isoforms with no expression of PDE4C [Pryzwansky and Madden, 2003]. PDE4A showed different localisation patterns in each of these inflammatory cells with uniform distribution in all intra-cellular granules within the eosinophils but distinct and ordered localisation within specific myeloperoxidase-containing granules. Indeed, PDE4A appears to play a

significant role in the regulation of granule exocytosis. The U937 monocytic cell line has been shown to express isoforms from three of the four PDE4 sub-families. These include PDE4A4B, PDE4B2, PDE4D3 and PDE4D5 [MacKenzie and Houslay, 2000]. The activity of PDE4D and PDE4B isoforms predominate over that of PDE4A. No expression of PDE4C was detected. This is consistent with other studies that have shown an absence of PDE4C expression in inflammatory cells [Hansen et al., 2000]. U937 monocyte to macrophage differentiation shows a change in PDE4D to PDE4B isoform expression [Shepherd et al., 2004]. Jurkat T-cells express endogenous PDE4A and PDE4D isoforms but show no expression of PDE4B or PDE4C isoforms [Erdogen and Houslay, 1997].

Studies undertaken with isolated rat hearts have significant PDE4A, PDE4B and PDE4D transcript levels together with PDE1C [Kostic et al., 1997]. No transcripts for PDE4C expression were detected. Exposure to 7-oxo-prostacyclin, a known cardio-protective agent, elicits considerable alteration of these transcript levels, increasing PDE4B1 and PDE4B3 transcripts, decreasing PDE4D transcripts, while at the same time retaining PDE4A transcript levels at the basal state. Human pulmonary arterial smooth muscle cells express PDE4 isoforms, specifically PDE4A10, PDE4A11, PDE4B2, PDE4C and PDE4D5 [MacLean et al., 1997 and Millen et al., 2006]. In these cells the PDE4 isoform expression profile is altered in the hypoxic state, but intriguingly the overall PDE4 activity remains unchanged indicating some phosphorylation driven compensatory mechanism [Millen et al., 2006].

Furthermore, in human airway smooth muscle cells cAMP levels control the expression of the PDE4D5 isoform, the enzyme responsible for its degradation [Le Jeune et al., 2002]. Analysis of the promoter region directly up-stream of the initiating ATG start codon identified a crucial CRE, where on site-directed mutagenesis ablated any up-regulation of PDE4D5 expression on treatment of the cells with cAMP elevating agents such as forskolin or isoprenaline. This effect has been shown for PDE4B2, with prostaglandin, as well as other PDE4D isoforms in a variety of cell types [Méhats et al., 1999 and Oger et al., 2002]. Similarly, forskolin-induced transcription of PDE4D

isoforms occurred in Jurkat T-cells whereas the presence of transcripts for PDE4A isoforms was attenuated [Erdogen and Houslay, 1997]. These data indicates highly specific transcriptional control of distinct PDE4 sub-family expression through PKA-mediated gene transcription.

1.7.3 Phosphodiesterase-4 Catalytic Unit

The catalytic unit of all PDE4 enzymes has a common signature motif [Houslay, 2001]. This motif is His-Asp-[Leu/Ile/Val/Met/Phe/Tyr]-Xaa-His-Xaa-[Ala/Gly]-Xaa-Xaa-Asn-Glu-Xaa-[Leu/Ile/Val/Met/Phe/Tyr]. The common structures of the PDE4B (amino acids 152-528) and PDE4D (amino acids 183-510) catalytic unit have been resolved and have approximately 80% homology [Xu et al., 2000 and Lee et al., 2002]. Therefore, the catalytic unit of all PDE4 enzymes is composed of seventeen α-helices arranged in three sub-domains of eight, four and six helices respectively and a short β-hairpin [Xu et al., 2000 and Houslay and Adams, 2003]. The cAMP-binding pocket has a volume of 440 cubic angstroms and is lined with hydrophobic residues and residues with negatively charged side chains [Houslay, 2001]. The metal ion binding sites within the catalytic machinery are of extreme functional significance. Disruption of this binding could be exploited for selective PDE4 inhibition. There are two distinct binding sites for divalent cations. A tightly bound zinc ion (Zn^{2+}) is located in the first pocket with preferential binding for the second site given to a magnesium ion (Mg^{2+}), although the presence of Zn^{2+} or manganese (Mn^{2+}) ions in this site has been reported [Xu et al., 2000 and Xu et al., 2004]. Direct binding of Zn^{2+} in the first metal ion-binding site is mediated by interactions with His-238, His-274, Asp-275 and Asp-392 [Houslay and Adams, 2003]. Binding of the second metal ion is coordinated by five amino acids, His-274, Glu-304, His-307, Thr-345 and Asp-392. It should be noted that the annotation of the residue number above corresponds to the PDE4B2 isoform. Interestingly all of the residues involved in the binding of the metals ions are absolutely conserved across all of the PDE families [Houslay and Adams, 2003]. These bound ions are an essential feature of the catalytic machinery and their presence allows cAMP binding

and facilitates 5' AMP release [Percival et al., 1997, Liu et al., 2001 and Laliberté et al., 2002]. It was elucidated that Asp-440 in PDE4A1 was the critical residue that directs substrate specificity for either cAMP or cGMP [Richter et al., 2001]. Site-directed mutagenesis of this conserved residue in PDE4 isoforms to either asparagine or alanine rendered the PDE4 unable to discriminate between cAMP and cGMP [Herman et al., 2000 and Richter et al., 2001].

1.7.4 Phosphodiesterase-4 Isoforms

There are now some twenty human isoforms within the PDE4 family, as shown in Table 1.4, and a succinct nomenclature for describing these has been derived [Houslay, 2001]. PDE4 isoforms are described by indicating the species, followed by the PDE family, the gene family and then the isoform or splice variant number. For example, HSPDE4A11 describes the human form of a PDE4 expressed by gene A and is assigned the number 11 to denote the isoform or splice variant [Wallace et al., 2005].

It should be noted here that PDE4 isoforms migrate on SDS-PAGE with a higher molecular weight than their predicted amino acid sequence and the C-terminal region is fundamental [Johnston et al., 1997]. The molecular weights quoted below are determined from their primary amino acid structure.

PDE4	Accession Number	Predicted Molecular Weight (kDa)	Classification	References
PDE4A1	U97584	79	Super-short	Sullivan et al., 1998
PDE4A4B	L20965	99	Long	Huston et al., 1996
PDE4A7	U18088	38	Inactive	Horton et al., 1995 Johnston et al., 2004
PDE4A10	AF110461	93	Long	Rena et al., 2001
PDE4A11	AY618547	93	Long	Wallace et al., 2005
PDE4B1	CAH70628	83	Long	Bolger et al., 1993
PDE4B2	NP_002591	64	Short	Bolger et al., 1994 Houslay et al., 1998
PDE4B3	AAB96381	83	Long	Huston et al., 1997
PDE4B4	XP_001862	73	Long	Shepherd et al., 2003
PDE4C1	NP_000914	80	Long	
PDE4C2	AAD47055	68	Long	
PDE4C3	AAD47054	76	Long	
PDE4D1	AAA97890	66	Short	Némoz et al., 1996
PDE4D2	AAA97891	58	Super-short	Némoz et al., 1996
PDE4D3	AAA97892	77	Long	Némoz et al., 1996
PDE4D4	NP_006194	91	Long	Bolger et al., 1997
PDE4D5	AAC00069	84	Long	Bolger et al., 1997
PDE4D6	AF536975	59	Super-short	Wang et al., 2003
PDE4D7	AF536976	84	Long	Wang et al., 2003
PDE4D8	AF536977	77	Long	Wang et al., 2003 Richter et al., 2005
PDE4D9	AY245867	77	Long	Wang et al., 2003 Richter et al., 2005

Table 1.4 – The human PDE4 isoforms.

Table adapted from Zhang et al., 2005.

1.7.4.1 Phosphodiesterase-4A

PDE4A1 is expressed in both human and rat as a super-short isoform of 79kDa [Sullivan et al., 1998]. Human PDE4A4B and its rat homologue PDE4A5 are both long isoforms of 99kDa and 94kDa respectively [Huston et al., 1996 and McPhee et al., 1995]. PDE4A10 and PDE4A11 are long isoforms expressed in both humans and rats with indistinguishable molecular weights of approximately 93kDa [Rena et al., 2001 and Wallace et al., 2005]. PDE4A8 is a long isoform of 88kDa expressed solely in rats [Bolger et al., 1996]. No human expression has been identified. PDE4A7 is a catalytically inactive isoform that is 38kDa due to 5' and 3' alternative mRNA splicing [Horton et al., 1995 and Johnston et al., 2004]. PDE4A isoforms are unique amongst the other PDE4 gene families in that their C-terminal regions are not conserved across humans and rats. The different human isoforms have consistent K_m values of 2-4μM for cAMP hydrolysis and similar relative cytosolic V_{max} values compared to PDE4A4B. Interestingly the rat isoforms have significantly lower relative cytosolic V_{max} values. Elucidating endogenous PDE4A function in many cell types is difficult due to low expression levels.

1.7.4.2 Phosphodiesterase-4B

The most recent PDE4B to be cloned and characterised is the long rat isoform PDE4B4, which has a molecular weight of 73kDa [Shepherd et al., 2003]. Human and rat PDE4B1 and PDE4B3 are the other long isoforms of this gene family and are indistinguishable in terms of molecular weight at 83kDa [Bolger et al., 1993 and Huston et al., 1997]. PDE4B2 is a short isoform of 64kDa expressed in both human and rat [Bolger et al., 1994 and Houslay et al., 1998]. The different isoforms have K_m values of 2-6μM. The relative cytosolic V_{max} value of PDE4B2 is 2-fold higher than that of PDE4B1, with PDE4B3 and PDE4B4 having relative cytosolic V_{max} values 4-fold higher compared to PDE4B1 [Shepherd et al., 2003]. Endogenous PDE4B expression is detectable in most cells.

1.7.4.3 Phosphodiesterase-4C

The isoforms and splice variants of the PDE4C gene family have not been as rigorously investigated. This is in some part due to their very low expression levels. Currently there are three known long isoforms expressed by the PDE4C gene, namely PDE4C1, PDE4C2 and PDE4C3 [Houslay, 2001]. No short or super-short isoforms have been identified and these are unlikely to exist due to limited space between the long form exons for upstream functional promoter regions [Sullivan et al., 1999].

1.7.4.4 Phosphodiesterase-4D

The PDE4D gene family has been extensively investigated and encodes up to nine isoforms or splice variants [Bolger et al., 1997 and Richter et al., 2005]. PDE4D1 is a short isoform with a predicted molecular weight of 66kDa and PDE4D2 is a super-short isoform of 58kDa [Némoz et al., 1996]. PDE4D3 [Némoz et al., 1996], PDE4D4 and PDE4D5 [Bolger et al., 1997] are long isoforms of 77kDa, 91kDa and 84kDa respectively. A further two 5' differentially spliced isoforms were identified, namely PDE4D6 (super-short; 59kDa) and PDE4D7 (long; 84kDa) [Wang et al., 2003]. This was followed by the identification and cloning of two further long isoforms, PDE4D8 (long; 77kDa) and PDE4D9 (long; 77kDa) [Wang et al., 2003 and Richter et al., 2005]. Because the many PDE4D isoforms have very similar molecular weights the need for unique anti-sera to the N-terminal regions is of prime importance in determining the expression of these novel isoforms. PDE4D1 to PDE4D5 have been kinetically characterised and have K_m values of approximately 1μM and consistent relative cytosolic V_{max} values with the exception of PDE4D4, which exhibits a 3-fold increase. PDE4D isoforms are usually ubiquitously expressed at high levels, in particular PDE4D3 and PDE4D5.

1.7.5 Phosphorylation of Phosphodiesterase-4

1.7.5.1 cAMP-dependent Protein Kinase

The first evidence of PDE4 enzymes being phosphorylated and activated by a cAMP-dependent protein kinase was shown in thyroid FRTL-5 cells on stimulation with thyroid stimulating hormone (TSH) [Sette et al., 1994]. PKA phosphorylation sites on PDE4D3 were mapped to two serine residues (Ser-13 and Ser-54) [Hoffman et al., 1998]. PKA phosphorylation at Ser-13, within the unique N-terminal region of the enzyme, has been shown to facilitate the recruitment of AKAP6 [Carlisle Michel et al., 2004]. However, site-directed mutagenesis of Ser-13 to alanine and aspartate respectively exhibits no change in either specific enzymatic activity or in its susceptibility to inhibition by rolipram [Hoffman et al., 1998]. Significantly, PKA phosphorylation at Ser-54 within PDE4D3 serves to activate the enzyme (approximately 2.5-fold activation) and increases its affinity for inhibition by rolipram (approximately 7-fold left shift in IC_{50} concentration response curve) [Sette and Conti, 1996, Hoffman et al., 1998 and MacKenzie et al., 2002]. The activating serine residue is located within the UCR1 regulatory module where the consensus motif Arg-Arg-Glu-Ser-Phe is present. This motif is conserved in all PDE4 long isoforms and has been shown to activate long isoforms from each PDE4 sub-family [MacKenzie et al., 2002 and Manganiello, 2002]. It has been proposed that PKA phosphorylation within UCR1 affects the positioning of the Mg^{2+} ion bound at the second metal ion site within the catalytic unit and that this modification serves to enhance the catalytic efficiency of PDE4 long isoforms [Houslay and Adams, 2003]. Furthermore, it is now widely appreciated that the UCR1 and UCR2 domains electro-statically interact, through the positively charged residues contained within UCR1 and the negatively charged residues of UCR2, and thus regulate the PDE4 catalytic machinery [Beard et al., 2000]. Phosphorylation of the target serine leads to the attenuation of these ionic bonds by introducing a significant negative charge, i.e. phospho-serine, and affecting the C-terminal region of UCR1 and its subsequent interaction with the N-terminal of UCR2.

As a consequence, PKA phosphorylation of UCR1 reduces the affinity of the UCR1-UCR2 interaction and perhaps this attenuation relieves a down-regulation exerted by UCR2 upon the catalytic unit [Lim et al., 1999]. These data provide further ramification that the UCR domains of PDE4 enzymes provide regulation of catalytic activity.

1.7.5.2 Extra-cellular Signal-regulated Kinase

Mitogen-activated protein kinases (MAPK) are serine/threonine protein kinases whose activities are stimulated by the action of many growth factors and cytokines [Pearson et al., 2001]. They are the ultimate components of intra-cellular signal transduction cascades and can phosphorylate transcription factors that are then able to induce gene expression of many other proteins, including protein kinases. The MAPK consensus site for phosphorylation, found on many target proteins, is Pro-Xaa-[Ser/Thr]-Pro [Hoffman et al., 1999]. Extra-cellular signal-regulated kinases 1/2 (ERK1/2), or p44/p42 MAPK, are members of the MAPK family. Authentic cellular substrates for ERK1/2 require two kinase-docking motifs [MacKenzie et al., 2000 and Houslay and Adams, 2003]. A kinase interaction motif (KIM) can be found approximately 135 amino acids N-terminal of the MAPK consensus site. This has the consensus sequence [Leu/Val]-Xaa-Xaa-[Arg/Lys]-[Arg/Lys]-$Xaa_{(3-6)}$-Leu-Xaa-[Leu/Ser]. A second ERK1/2 docking site is a Phe-Xaa-Phe (FQF) motif. This motif is located approximately 16 residues C-terminally to the MAPK consensus site and this directs the specificity for ERK1/2 phosphorylation over c-Jun N-terminal kinase (JNK) [Sharrocks et al., 2000 and Biondi and Nebreda, 2003]. Site directed mutagenesis of either, or both, docking motifs result in the ablation of ERK1/2 interaction with, and phosphorylation of, the target protein [MacKenzie et al., 2000].

PDE4B2 was identified as a substrate for ERK1/2 phosphorylation through expression in baculovirus and mass spectrometry analysis [Lenhard et al., 1996]. This study identified the target residue as Ser-487 within an ERK1/2 consensus motif. The ERK phosphorylation signature motif is

present in PDE4B, PDE4C and PDE4D isoforms (Pro-Glu-Ser-Pro) but not in isoforms from the PDE4A sub-family (Arg-Glu-Ser-Pro) [Baillie et al., 2000]. The single replacement of a proline residue with an arginine residue in the ERK1/2 consensus site within the catalytic unit of PDE4A isoforms is enough to prevent ERK1/2 phosphorylation. Nevertheless, it should be noted that PDE4A isoforms possess both KIM and FQF docking motifs and could function as ERK1/2 scaffold proteins without being phosphorylated. ERK1/2 phosphorylation of a single serine residue within the catalytic units of PDE4B, 4C and 4D isoforms alters the specific activity of the enzyme [Hoffman et al., 1999, MacKenzie et al., 2000 and Baillie et al., 2000]. The nature of this functional activity change is dependent on the alternative splicing of the specific isoform, i.e. whether the isoform is considered to be a long or a short form PDE4. ERK1/2-mediated inhibition of PDE4 long isoforms (activity is approximately 60% of native PDE4 activity) is a transient effect that is overcome by a PKA-mediated activation through phosphorylation of UCR1, as discussed in Section 1.7.5.1 [Houslay and Kolch, 2000 and Baillie at al., 2001]. In contrast, ERK1/2 phosphorylation at the same serine residue within the catalytic unit of PDE4 short forms serves to activate these enzymes (activity is approximately 140% of native PDE4 activity) [MacKenzie et al., 2000 and Baillie et al., 2000]. ERK1/2 phosphorylation of super-short PDE4 isoforms induces a small inhibitory effect [MacKenzie et al., 2000]. The mechanism underlying the modulation of catalytic activity has been assigned to the positioning of the Mg^{2+} ion bound at the second metal ion site within the catalytic unit and that this modification serves to modulate the catalytic activity of PDE4 isoforms subjected to ERK1/2 phosphorylation [Houslay and Adams, 2003].

1.7.5.3 Phosphatidylinositol-3 Kinase-dependent Phosphorylation

PDE4A5, the rat homologue of human PDE4A4B, is phosphorylated and activated (activity is approximately 177% of native PDE4 activity) in 3T3-F442A pre-adipocytes by a hitherto unknown kinase that constitutes a crucial role in phosphatidylinositol-3 kinase (PI-3K) signalling [MacKenzie et al., 1998]. This phosphorylation event reduced the intra-cellular cAMP

concentration, an effect rescued by wortmannin, a PI-3K inhibitor, and the immuno-suppressant rapamycin, and prevented the differentiation to adipocytes. The exact mechanism through which this occurs remains to be elucidated. However, it is proposed that the activation of p70S6 kinase, downstream of both PI-3K and mTOR, is crucial. However, no consensus sequence for p70S6 kinase is present on PDE4A5. One candidate may be mTOR itself as it is known to contain intrinsic kinase activity. Subsequent work has shown that this differentiation process requires Janus Kinase-2 (JAK-2) and Signal Transducer and Activator of Transcription-5 (STAT-5) signalling and not MAPK or p70S6 kinase although their expression is essential [Yarwood et al., 1999]. In U937 monocytic cells, PDE4A4B is activated on challenge with lipopolysaccharide (LPS) or interferon-γ (IFN-γ) [MacKenzie and Houslay, 2000]. This activation was also sensitive to wortmannin and rapamycin. Consistent with these findings is the role of reducing intra-cellular cAMP concentrations through increased expression of PDE4B2 resulting in PI-3K signalling pathway activation, and cell proliferation and survival through PKB/Akt activation [Smith et al., 2005 and Song et al., 2005]. The mechanism through which cAMP achieves this activation is currently unknown. Taken together these data imply another important point of cross talk with respect to cAMP signalling.

1.7.6 Phosphodiesterase-4 Partner Proteins

Cell signalling pathways require the efficient and specific formation of protein complexes. Proteins within these complexes are then targeted to specific locations in the cell and as such are appropriately positioned to regulate cellular behaviour. Specific protein-protein interaction is not a random process. Protein binding motifs have been identified for many receptors, enzymes, protein kinases, scaffold, anchoring, and adaptor proteins. Screening of proteins for putative binding sites will give much needed insight into the molecular basis through which these proteins modulate cellular signal transduction.

1.7.6.1 Src Homology 3 Binding Domains

Src homology 3 (SH3) binding domains are approximately 60 amino acids in length and contain proline-rich sequences or proline recognition domains [Mayer, 2001, Jia et al., 2005 and Li, 2005]. They are found in a variety of proteins including receptors with intrinsic tyrosine kinase activity (GRB2), PDE4 isoforms (PDE4A4B, PDE4A5 and PDE4D4) PI-3K (p85/p110), PLCγ and *phox* proteins of the NADPH oxidase enzyme (p40-, p47- and p67-*phox*). The conventional class 1 and class 2 binding motifs are illustrated in Table 1.5 and are based around the core conserved Pro-Xaa-Xaa-Pro consensus sequence [Jia et al., 2005]. The affinity of a protein containing class 1 or class 2 SH3 binding motifs is moderate at best with K_d values no better than 1-200μM [Li, 2005]. A number of other so-called non-conventional motifs have been identified [Jia et al., 2005]. Elucidation of new motifs may underlie increasing specificity for SH3 binding.

SH3 Binding Domains	Consensus Sequences
Core	Pro-Xaa-Xaa-Pro
Class I	[Arg/Lys]-Xaa-Xaa-Pro-Xaa-Xaa-Pro
Class II	Pro-Xaa-Xaa-Pro-Xaa-[Arg/Lys]
Non-conventional	Pro-Xaa-Xaa-Asp-Tyr Arg-Lys-Xaa-Xaa-Tyr-Xaa-Xaa-Tyr Pro-Xaa-[Val/Ile]-[Arg/Asn]-Arg-Xaa-Xaa-Lys-Pro [Arg/Lys]-Xaa-Xaa-[Lys/Arg] Lys-Lys-Pro-Pro His-Xaa-Xaa-Lys [Lys/Arg]-Xaa-Xaa-Xaa-Xaa-Lys-Xaa-[Lys/Arg]-[Lys/Arg]

Table 1.5 – Core, classical and non-conventional SH3 binding domains.

Sequences rich in positively charged and/or basic residues can also serve as putative SH3 binding domains. The consensus sequences are presented using the three-letter amino acid abbreviation and Xaa represents any amino acid.

The SH3 domain of the Src tyrosyl protein kinase has been shown to interact with the unique N-terminal region of the rat PDE4A5 isoform [O'Connell et al., 1996 and Beard et al., 2002]. This interaction is mediated through two class 1 SH3 binding domains at Pro-4 (PAAPSER) and Pro-61 (PHRPIER), with a class 2 SH3 binding domain at Arg-35 (RQPRTP). The SH3 domain of the Lyn tyrosyl protein kinase has been shown to interact directly with PDE4A4B, the human homologue of rat PDE4A5 [McPhee et al., 1999]. PDE4A4B contains similar SH3 binding motifs within the unique N-terminal region. However, an additional binding site has been identified within LR2, a site not present within rat PDE4A isoforms. This is a further class 1 SH3 binding domain positioned at Arg-315 (RPRPSQP). Membrane-bound or particulate forms of PDE4A4B exhibit significantly different sensitivities for inhibition by rolipram when compared to the cytosolic form of the same enzyme [Huston et al., 1996]. The particulate forms have approximately 60-fold higher affinity for inhibition by rolipram. Allowing the SH3 domain of recombinant Lyn tyrosyl protein kinase to interact with the cytosolic form of PDE4A4B can mimic this high affinity rolipram binding state (HARBS). Consequently, the cytosolic form of PDE4A4B exists as a low affinity rolipram binding state (LARBS). Thus, the formation of PDE4A4B protein complexes with SH3 domain-containing proteins promotes a change in the catalytic conformation of the PDE4A4B isoform. Sequential deletion of the unique N-terminal SH3 domain binding sites contained within PDE4A5 has been shown to disrupt its intra-cellular distribution [Huston et al., 2000 and Beard et al., 2002]. Furthermore, proteins containing SH3 domains also bind PDE4D4 through specific N-terminal interactions and might also play a role in defining its intra-cellular localisation without necessarily affecting the catalytic conformation [Beard et al., 1999]. Like PDE4A5, SH3 domain binding is mediated through two distinct proline-rich regions within the unique N-terminal. These commence at Pro-58 and Pro-75 respectively.

The cleavage of PDE4A5 by caspase-3 causes intra-cellular disruption and redistribution of this isoform [Huston et al., 2000]. Caspase-3 cleavage requires the consensus motif Asp-Xaa-Xaa-Asp. Tandem caspase-3 cleavage sites are found within the unique N-terminal region of PDE4A5 at

Asp-69 and Asp-72 respectively. Caspase-3 cleavage can also occur in the human homologue PDE4A4B but not in the other long isoforms PDE4A10 or PDE4A11 [Wallace et al., 2005]. The interaction of PDE4A5 with the SH3 domain of Src tyrosyl protein kinases is ablated following caspase-3 cleavage and this promotes the dynamic redistribution of the enzymes intra-cellular localisation [Huston et al., 2000]. Over-expression and confocal immuno-fluorescence of PDE4A5 in COS cells confirms the localisation to the perinuclear region and to the cortical regions of the plasma membrane. On caspase-3 cleavage this highly organised distribution was attenuated rendering the cleaved species to exhibit a more even intra-cellular distribution. It is proposed that the correct intra-cellular localisation of PDE4A5 is prominent to cell survival and concomitant to the activation of PDE4A5 through the PI-3K cell survival signalling pathway [MacKenzie et al., 1998], as discussed in Section 1.7.5.3.

1.7.6.2 Phosphatidic Acid

Growth factors, cytokines and hormones can activate phospholipase D. Phospholipase D is an enzyme that catalyses the hydrolysis of phosphatidylcholine, the principal phospholipid in most membranes, to phosphatidic acid (PA). PA can also be formed by the phosphorylation of diacylglycerol by diacylglycerol kinase. PDE4 enzymes have been shown to interact with PA [Némoz et al., 1997, Grange et al., 2000 and Baillie et al., 2002]. Interestingly, PA interaction has been shown to occur in PDE4 isoforms from PDE4A, PDE4B and PDE4D sub-families respectively [Némoz et al., 1997]. In the case of the PDE4A1 super-short isoform, the binding of PA using the first twenty-five amino acids of the unique N-terminal region confers predominance (approximately 93%) for the enzyme to be membrane bound [Shakur et al., 1994 and Scotland and Houslay, 1995]. The structure of this region was delineated using NMR and identified the membrane association region to be composed of two helical structures separated by a so-called "hinge" region [Smith et al., 1996]. The first helical structure is composed of residues 1-7 and this forms a typical amphipathic α-helix. The "hinge" region is composed of residues 8-13. Deletion of either of these

regions of PDE4A1 does not disrupt the membrane association. Similarly, the deletion of amino acids 21-25 does not trigger release from the plasma membrane. Amino acids 14-20 are hydrophobic and located towards the N-terminal end of the second helical region. These have been deduced to be critical in directing the membrane association of PDE4A1. Further work has identified the second helix to contain a novel domain that allows the interaction with PA, an interaction that is modulated by intra-cellular Ca^{2+} concentrations [Baillie et al., 2002]. Due to its high tryptophan content this domain has become known as the tryptophan anchoring PA selective binding domain (TAPAS-1). TAPAS-1 has the consensus sequence Leu-Val-Xaa-Trp-Trp-Asp-Xaa-Xaa-(Lys/Arg). The first five amino acids are responsible for lipid bi-layer insertion with the final four amino acids responsible for the Ca^{2+} dependent control of the process. A similar hydrophobic region binding PA was identified within the N-terminal region of PDE4D3 (Asp-31 to Ser-59) [Grange et al., 2000]. The binding of endogenous PA in this case served to activate over-expressed long isoform PDE4D3, indicating a role for PA to control the levels of cAMP within cells. This activating effect was also measured with the other long isoforms PDE4A5 and PDE4B1 [Némoz et al., 1997]. The level of activation was analogous to that measured for the PKA activation of long isoforms, as discussed in Section 1.7.5.1, but not related to any phosphorylation event. Thus, it can be inferred that both events induce a similar conformational change on the catalytic unit. Furthermore, no synergistic activation of PDE4 long isoforms was measurable when both PKA phosphorylation and PA activation was induced. The binding and/or activation of PDE4 isoforms by PA add further complexity to the shaping of cAMP gradients within cells and the generation of localised pools of cAMP and the compartmentalisation of cAMP signalling.

1.7.6.3 XAP2/AIP

Hepatitis B virus X-associated protein (XAP2) or aryl hydrocarbon receptor-interacting protein (AIP) is an immunophilin-like protein, which was originally identified in a yeast-2-hybrid screen as interacting with and repressing hepatitis B virus X protein-mediated gene expression

[Kuzhandaivelu et al., 1996 and Kashuba et al., 2000]. XAP2 is highly expressed in the spleen and thymus, with lower levels of expression in the liver, kidney and lung [Sumanasekera et al., 2003]. Specific activation of lung AhRs by pollutants and carcinogens, such as dioxin and poly-halogenated aromatic hydrocarbons, increases neutrophil recruitment and the onset of the excessive inflammatory response, characteristics of COPD [Martinez et al., 2002 and Teske et al., 2005]. Therefore, activation of the AhR may be important in the pathogenesis of inflammatory lung disease. XAP2 is also proposed to modulate AhR stability and nucleocytoplasmic shuttling, thereby regulating gene transcription [Meyer and Perdew, 1999, Sumanasekera et al., 2003, Lees et al., 2003, Ramadoss et al., 2004 and Pollenz and Dougherty, 2005]. Recently, XAP2 has been assigned a role as a tumour suppressor, consistent with its role as a potent repressor of peroxisome proliferator-activated receptor α (PPARα) activity and with the identification of XAP2 mutations that increase susceptibility for pituitary adenomas [Sumanasekera et al., 2003 and Vierimaa et al., 2006]. Conversely, XAP2 may also be tumour promoting due to its recently identified interaction with survivin, an inhibitor of apoptosis via the inhibition of caspases [Kang and Altieri, 2006]. Its perceived mode of action is thought to be through the stabilisation of survivin and prevention of ubiquitination and subsequent proteasomal degradation. This may provide the first evidence of XAP2 promoting cancer cell survival although it is consistent with its ability to stabilise cytosolic proteins and prevent degradation.

XAP2 is a 38kDa protein composed of N-terminal immunophilin homology domains and a C-terminal tetratricopeptide repeat (TPR) domain. The TPR domain of XAP2 interacts with a Glu-Glu-Val-Asp binding motif on heat shock protein 90 (HSP90). PDE4A5 contains a highly conserved TPR binding motif in the UCR2 regulatory region, where the hydrophobic valine residue is replaced with a similarly hydrophobic leucine. Together with Ser-11 to Iso-43, within the unique N-terminal region, XAP2 can interact with PDE4A5 through its C-terminal TPR domain, with Arg-271 identified as the key residue [Bolger et al., 2003]. The XAP2-PDE4A5 interaction is specific in that PDE4A5 did not interact with other immunophilin family proteins and

neither did XAP2 interact with other PDE4 isoforms across all gene families. Interaction with the human PDE4A4B can occur due to species conservation of the critical residues. The N-terminal interaction is responsible for ameliorating PDE4A5 activity by approximately 60%, acting as a non-competitive inhibitor, i.e. it does not bind directly to the enzyme active site. XAP2 interaction with PDE4A5 also resulted in a 5-fold increase in the sensitivity to inhibition by rolipram, indicating a likely conformational change in the catalytic unit. Furthermore, it appears to protect PDE4A5 from activation by PKA.

1.7.6.4 Foci Formation

Accretion foci can form in cells over-expressing green fluorescent protein (GFP) fusion proteins of human PDE4A4B, and to a lesser extent rat PDE4A5, following extensive rolipram treatment [Terry et al., 2003]. The formation of foci is clearly dependent upon protein synthesis and the timely reformation of foci with subsequent rolipram treatment is likely to be representative of the required proteins being available. As a general rule formation of these accretion foci occurs with inhibitors known to sense HARBS, e.g. rolipram and Ro 20-1724, and not inhibitors that only sense LARBS, e.g. Ariflo®. A rolipram-induced conformational change within the catalytic unit of PDE4A4B may be enough to re-distribute PDE4A4B within the cell and modulate cAMP compartmentalisation in such a way that it promotes the formation of PDE4 oligomers [Lee et al., 2002 and Richter and Conti, 2004]. Simply increasing cAMP concentrations with forskolin or non-foci forming PDE4 inhibitors can also attenuate foci accumulation. The propensity for PDE4A4B and PDE4A5 to form foci appears to lie within the unique N-terminal region and not with any other property of GFP, other PDE4A isoforms, or PDE4 isoforms from the other gene families [Terry et al., 2003 and Wallace et al., 2005]. Alternatively, this effect may be of importance for PDE4 inhibitor development in dissecting whether compounds can sense HARBS, a state that is thought to underlie the severe side effects associated with the current available compounds [Huang et al., 2001].

1.7.6.5 Disrupted in Schizophrenia 1

The Disrupted in Schizophrenia 1 (DISC1) gene locus has been implicated in the generation of psychiatric illness through a balanced chromosomal translocation [Millar et al., 2005]. One such translocation occurs to the PDE4B gene on chromosome 1p31. DISC1 is a 71kDa protein expressed in the brain. Endogenous DISC1 and PDE4B co-localise at the mitochondria in human neuroblastoma-derived cells. The interaction of both proteins is confirmed by co-immuno-precipitation and is mediated through a direct interaction with the N-terminal region of DISC1 and the UCR2 regulatory module of PDE4B. As the UCR2 domain is conserved throughout all PDE4 isoforms then it is likely that DISC1 will interact with all long and short PDE4s. The activation of PDE4 long isoforms by PKA phosphorylation of the UCR1 domain results in release of DISC1 from PDE4B [Millar et al., 2005].

1.7.6.6 β-arrestin

β-arrestin is a cytosolic signalling scaffold protein involved in the integration of countless signal transduction pathways [Lefkowitz and Shenoy, 2005]. These include receptor mediated endocytosis via clathrin binding, activation of multiple components of MAPK cascades, regulation of cytosolic tyrosine kinases, scaffolding of E3 ligase for ubiquitination and degradation of target proteins, recruitment of PDE4s in receptor signalling, and de-phosphorylation events through PP binding. There are four types of arrestin, β-arrestin1, β-arrestin2 and two visual arrestins [Luttrell and Lefkowitz, 2002]. Extensive investigation of β-arrestin in β_2-adrenoreceptor signalling has uncovered important functional properties of this scaffolding protein. Agonist stimulation of the β_2-adrenoreceptor results in the coupling of the stimulatory G-protein, G_s, which in turn stimulate AC to catalyse the formation of cAMP, as shown in Figure 1.2. cAMP instigates a plethora of signalling events through AKAP-bound PKA, EPAC and CNG ion channels, as discussed in more detail in Section 1.5 and illustrated in Figure 1.3. The β_2-adrenoreceptor is phosphorylated directly by constitutively AKAP5-bound PKA or agonist-

dependent AKAP12-bound PKA resulting in the uncoupling of G_s, the coupling of G_i, the subsequent attenuation of PKA activity and the activation of ERK1/2 activity through Src [Fraser et al., 2000, Baillie et al., 2003, Tao et al., 2003, Lynch et al., 2005 and Willoughby et al., 2006]. Of course, ERK1/2 may also, in certain cells, be activated directly by cAMP through the activation of Rap1 [Houslay and Kolch, 2000, Lefkowitz et al., 2002 and Wang et al., 2006]. Adding further complexity to this signalling system, it has been recently shown that phosphorylation of the β_2-adrenoreceptor by GRK5/6 can also recruit β-arrestin and activate ERK1/2 unaided by G-protein interactions [Shenoy et al., 2006]. Continued agonist occupancy results in the PKA phosphorylation of GRK2 at Ser-685, activation and translocation to the plasma membrane, through the enhanced interaction of Gβγ subunits, where it phosphorylates and desensitises the β_2-adrenoceptor [Kohout and Lefkowitz, 2003 and Li et al., 2006]. Incidentally, the phosphorylation of GRK2 by ERK1/2 reduces its ability to interact with the Gβγ subunits and removes it from the plasma membrane. This phosphorylation recruits β-arrestin2 and specific PDE4 isoforms, predominately PDE4D5, to the β_2-adrenoreceptor where they degrade the localised pool of cAMP attenuating PKA activity [Perry et al., 2002]. The recruitment of β-arrestin also mediates β_2-adrenoreceptor internalisation into early endosomes via clathrin-coated pits, dissociation of β-arrestin through receptor de-phosphorylation by PP2, and the rapid re-cycling of the functional receptor to the plasma membrane [Oakley et al., 1999, Simaan et al., 2005 and Vaughan et al., 2006]. It has been shown that β-arrestin can interact with all PDE4 isoforms from each sub-family and does not distinguish between long, short and super-short forms [Perry et al., 2002 and Wallace et al., 2005]. This implies that the primary interaction site on PDE4 isoforms is the catalytic unit, as the catalytic unit is highly conserved [Xu et al., 2000]. However, β-arrestin preferentially interacts with the PDE4D5 isoform by virtue of the unique N-terminal targeting region, which provides additional binding sites for β-arrestin [Bolger et al., 2003]. Indeed, small interfering RNA (siRNA) knockdown of PDE4D does not induce a compensatory mechanism whereby PDE4s from the other gene families are recruited to the β_2-adrenoreceptor by β-arrestin [Xiang et al., 2005 and Lynch et al., 2005]. There are two distinct binding sites on β-arrestin, one at the

extreme N-terminal region (residues 1-28) and one at the N-terminal region of the C-terminal domain (residues 192-255) [Bolger et al., 2003]. These regions mediate the interaction with Thr-11 to Ala-85 of the unique N-terminal region and Phe-670 to Leu-676 of the C-terminal region of the catalytic unit of PDE4D5 [Bolger et al., 2006].

The β-arrestin-PDE4 interaction also plays a fundamental role enhancing T-cell receptor (TCR) function [Abrahamsen et al., 2004]. On TCR stimulation, coupling to G_s, activation of AC, production of intra-cellular pools of cAMP and activation of PKA results in the amelioration of TCR function through the activation of C-terminal Src kinase. Co-stimulation and ligation of CD28 recruits the β-arrestin-PDE4 complex and degrades the localised pool of cAMP preventing the PKA phosphorylation of C-terminal Src kinase and enhancing TCR function. This dissects one mechanism of the anti-inflammatory effects of PDE4 inhibition by preventing optimal TCR activation.

1.7.6.7 A-kinase Anchoring Proteins

An introduction to AKAPs and their functional role has been given in Section 1.5.2.1. PKA co-localises with PDE4 isoforms through interactions mediated by AKAPs [Dodge et al., 2001, Taskén et al., 2001, Asirvatham et al., 2004 and Bajpai et al., 2006]. This trimeric complex facilitates the generation of cAMP gradients and compartmentalised phosphorylation of PKA target proteins, coupled with the control of such response by the recruited PDE4 [Houslay and Adams, 2003].

PDE4D3 interacts with AKAP6 (or m-AKAP) in rat cardio-myocytes using the first fifteen residues contained within the unique N-terminal region of the PDE4 and residues 1286 to 1831 of the AKAP6 [Dodge et al., 2001]. As previously discussed in Section 1.7.5.1, PDE4 enzymes are phosphorylated by PKA at sites within the unique N-terminal region and UCR1 and the PDE4 interaction with AKAPs is likely to control this event. The N-terminal phosphorylation at Ser-13 serves to increase the affinity of PDE4D3 for AKAP6 binding [Carlisle Michel et al., 2004]. Thus, increases in cAMP

concentrations within micro-domains will activate AKAP-tethered PKA to phosphorylate PDE4, increasing PDE4 activity and AKAP affinity, coupled with the simultaneous degradation of cAMP and recruitment of PP1/2 [Baillie et al., 2005]. Furthermore, EPAC1 and ERK5 have been shown as additional signalling molecules in these protein complexes in cardiac myocytes [Dodge-Kafka et al., 2005]. PDE4D3 is the crucial signalling molecule and is regulated by localised changes in intra-cellular cAMP concentrations. PKA is activated by sub micro-molar concentrations of cAMP whereas PDE4D3 and EPAC1 require concentrations in the micro-molar range. Thus, increasing cAMP activates PKA then PDE4D3 with a concomitant activation of EPAC1. The phosphorylation promotes the mAKAP interaction through Ser-13 and the activation of PDE4D3 through Ser-54 [Carlisle Michel et al., 2004, Sette and Conti, 1996, Hoffman et al., 1998 and MacKenzie et al., 2002]. EPAC1 activation prevents ERK5 inhibition of PDE4D3. Ultimately, cAMP concentrations decrease, the de-phosphorylation of target proteins occurs through PP1/2, and the system is reset.

In Sertoli cells of the rat testis, PDE4D3 has been observed to co-immuno-precipitate with PKA-RIIα and PKA-RIIβ subunits, and AKAP9 (or AKAP450) [Taskén et al., 2001]. The RII-AKAP9-PDE4D3 complex was distributed within the golgi/centrosomal region of the cells. PDE4D3 interacts with amino acids 1710 to 2872 of AKAP9. A similar interaction has been observed in COS1 cells where dominant negative forms of PDE4C2 and PDE4D3 interact with the RII-AKAP9 complex and are constitutively PKA phosphorylated, whereas PDE4A4B and PDE4B1 phosphorylation requires a global increase in cAMP, indicating a degree of compartmentalisation tailored through AKAP9 [McCahill et al., 2005]. Over-expression of PDE4A5 or PDE4A8 with AKAP3 (or AKAP110) facilitated the co-immuno-precipitation of PDE4A and AKAP3 but co-immuno-precipitation was not achieved with PDE4D3, indicating a PDE4A specific effect [Bajpai et al., 2006]. The likely interaction sites for AKAP3 binding are the conserved regions of rat PDE4A isoforms. It will be interesting to elucidate whether human PDE4A isoforms can interact with AKAP3 thus indicating whether the species difference at C-terminal region or the common LRs are responsible. These interactions

support the notion that the endogenous co-localisation of both proteins indicates a functional interaction in spermatozoa [Bajpai et al., 2006].

Further indication for PDE4A binding of AKAPs has been proposed in T-lymphocytes [Asirvatham et al., 2004]. PDE activity was detected from RIIα-AKAP immuno-precipitates and identified as PDE4A and PDE7A, by immuno-probing with specific anti-sera. PDE4A interacts with AKAP1, AKAP8 and MTG, but not AKAP5, whereas PDE7A only interacts with MTG. Thus, one would expect the interaction of PDE4 with these AKAPs to direct their sub-cellular localisation, e.g. AKAP1 directing PDE4A to the mitochondria and MTG directing PDE7A to the golgi apparatus.

1.7.6.8 Receptor for activated C-kinase 1

Receptor for activated C-kinase 1 (RACK1) is a unique, high affinity partner protein of 36kDa that specifically interacts with PDE4D5 through a domain known as the RACK1 interaction domain (RAID1) [Yarwood et al., 1999, Steele et al., 2001 and Bolger et al., 2006]. RACK1 contains seven repetitive tryptophan and aspartate residues, known as WD-repeats, in a propeller-like structure, and scaffolds activated PKC isoforms in a similar way to AKAPs for PKA [McCahill et al., 2002]. Such activation of PKC with PMA has no effect on the interaction with PDE4D5 and thus it is likely that the interaction is constitutive in cells where they are endogenously expressed [Yarwood et al., 1999]. RACK1 interacts at an exclusive site within the catalytic unit, i.e. Gly-609 to Asp-658, but the primary interaction site is the unique N-terminal region, i.e. Asp-22 to Leu-38, analogous to that of β-arrestin [Bolger et al., 2006]. On RACK1, the interaction sites have been mapped to the final three WD-repeats, amino acids 179-317 although the interaction with the truncated protein was approximately 25% of wild type, indicating the requirement of additional interaction sites or a failing in the truncated protein to form the correct quaternary structure [Steele et al., 2001]. The functional consequence of this interaction is currently unknown as no effect on PDE4D5 enzymatic activity was measured, but a significant 4-fold reduction in sensitivity to inhibition by rolipram occurred indicating a possible

conformational change of the PDE4D5 catalytic unit mediated through the unique N-terminal region [Yarwood et al., 1999]. RACK1 can also translocate to the nucleus on treatment with forskolin and may play a role in cAMP-PKA-CREB gene expression, and perhaps of PDE4D5 itself [Le Jeune et al., 2002 and McCahill et al., 2002].

1.7.6.9 Myomegalin

Myomegalin is a scaffold protein that is involved in cytoskeletal organisation and/or cell movement [Verde et al., 2001]. The 240kDa full-length protein is abundantly expressed in both skeletal and cardiac muscle, with a 65kDa splice variant occurring in testis [Verde et al., 2001]. It is localised at the sarcoplasmic reticulum in the muscle cells and at the golgi apparatus in COS7 cultured cells, via its C-terminal region. The long PDE4D isoforms, PDE4D3, PDE4D4 and PDE4D5 are targeted to sub-cellular particulate locations within the cell and are present within the cytosol. The 65kDa species of myomegalin is able to interact with PDE4D isoforms through a putative site at the N-terminal of UCR2 and as such is likely to play a key role in the particulate localisation of long form PDE4Ds. As with DISC1, any protein interactions mediated through the UCR2 domain are likely to be conserved across the four PDE4 gene families.

1.7.6.10 Phosphodiesterase-4 Dimerisation

It has been suggested that PDE1 to PDE6 may exist as dimers and that this interaction is mediated through their N-terminal regulatory domains and, as such, is likely to represent an important structural property [Richter and Conti, 2004]. Various studies have proposed that PDE4 enzymes may exist as dimers or oligomers [Rocque and Holmes et al., 1997, Rocque and Tian et al., 1997, Richter et al., 2000, Lee et al., 2002, Richter and Conti, 2002 and Richter and Conti, 2004]. From expression, purification and analyses, by size exclusion chromatography and ultra-centrifugation, of the short PDE4B2 isoform it was appreciated that the protein could exist in an oligomeric state, with a molecular weight in excess of 600kDa compared to

the monomeric molecular weight of approximately 64kDa [Rocque and Holmes et al., 1997]. Interestingly, removal of the first 80 amino acids from PDE4B2 results in a protein species that is expressed in a significantly reduced oligomeric state, i.e. monomer to tetramer [Rocque and Holmes et al., 1997 and Rocque and Tian et al., 1997]. Thus, it can be inferred from these studies that the unique N-terminal region and UCR modules play a pivotal role in the oligomerisation of PDE4 enzymes. Furthermore, this function for the unique N-terminal and UCR domains may underlie the difficulties encountered to date in expression and purification studies to resolve the crystal structure of these regions. Expression and purification of PDE4A4B has also assigned a potential role for the C-terminal region in the formation of dimers and oligomers of PDE4 enzymes [Richter et al., 2000]. Analyses, by size exclusion chromatography and ultra-centrifugation, have shown that the presence of an intact C-terminal region results in oligomerisation whereas truncation of the C-terminal region returns a dimeric form. It is proposed that a dimerisation interface exists involving helices nine, ten and eleven of the catalytic unit and mutation of one of two residues (Arg-358-Asp or Asp-322-Arg) can prevent dimerisation [Lee et al., 2002]. This change in charge prevents dimerisation as assessed by later elution on a gel filtration column. The residues involved in the dimerisation interface are highly conserved in PDE1, 3, 4, 8 and 9, but not in the other PDE families and thus one would expect only isoforms from these families to exist as dimers. Data from both the Houslay and Conti laboratories claim that the UCR modules are the major players responsible for mediating dimerisation of PDE4 enzymes, whereas the catalytic unit and C-terminal region may be involved in stabilising such a complex [Beard et al., 2000, Richter and Conti, 2002 and Richter and Conti, 2004]. It is now understood that the C-terminal region of UCR1 and the N-terminal region of UCR2 of PDE4 enzymes interact with each other and regulate catalytic activity [Beard et al., 2000]. This contact is formed through the interaction of positively charged residues contained within the UCR1 domain (Arg-98 and 101 in PDE4D3) and negatively charged residues present within the UCR2 domain (Glu-146 and 147, and Asp-149). Although this interaction was thought to represent intra-molecular contacts, it may also be able to mediate inter-molecular complex formation, and thus may

contribute to the formation of PDE4 dimers or oligomers [Richter and Conti, 2002 and Richter and Conti, 2004]. Indeed, the long isoform PDE4D3 was shown to exist as a dimer, whereas the super-short isoform PDE4D2 was shown to exist as a monomer. These data indicate the involvement of UCR1 and at least the N-terminal portion of UCR2. Interestingly the regions involved in inter-molecular dimerisation appear to be distinct from those involved in the electrostatic intra-molecular interactions, as mutation of the respective charged residues does not ablate the dimerisation of PDE4 long isoforms. Site-directed mutagenesis of hydrophobic amino acids, distinct from those involved in mediating UCR1-UCR2 intra-molecular interactions (Val-100, Phe-104, and Leu-145, 148, 152 and 155), ablates the ability of PDE4D3 to exist as a dimer [Richter and Conti, 2004]. PKA phosphorylation status of PDE4 enzymes does not affect dimer formation. PKA phosphorylation of PDE4 enzymes is discussed in Section 1.7.5.1.

The role of the C-terminal region of PDE4 sub-families with respect to dimerisation should be approached with caution, as it is well understood that the apparent molecular weights of PDE4 isoforms migrate with a larger mobility on SDS-PAGE, and are eluted at larger molecular weights using gel filtration techniques than is predicted from its primary structure [Conti and Richter, 2002 and Johnston et al., 2004].

What is the functional significance of PDE4 dimerisation? Richter and Conti have shown that PDE4 dimerisation causes an increase V_{max} but not the K_m over the monomeric form, that it is a pre-requisite for activation by both PKA and phosphatidic acid (PA), and that it results in increased affinity for rolipram binding; a likely consequence of stabilisation in a high affinity rolipram binding state (HARBS) [Richter and Conti, 2004]. Thus, disruption of PDE4 dimerisation will promote a low affinity rolipram binding state (LARBS) and may attenuate the undesirable side effects associated with the current PDE4 inhibitors.

1.7.7 Phosphodiesterase-4 as a therapeutic target

PDE4 inhibitors are currently being developed by many of the major pharmaceutical companies to treat a variety of inflammatory diseases such as asthma, chronic obstructive pulmonary disease (COPD), rheumatoid arthritis and psoriasis [Houslay et al., 2005 and Zhang et al., 2005]. Furthermore, their potential is being investigated for the treatment of a number of CNS disorders such as depression, Schizophrenia, Parkinson's and Alzheimer's disease [O'Donnell and Zhang, 2004 and Millar et al., 2005]. Inhibition of PDE4 enzymes has also been proposed for the treatment of cardiovascular disorders such as stroke, restenosis, and pulmonary hypertension [Gretarsdottir et al., 2003, Maurice et al., 2003, Tilley and Maurice, 2005, Houslay, 2005 and Millen et al, 2006]. Moreover, PDE4 inhibition may promote cancerous cell apoptosis, e.g. in diffuse large B-cell lymphoma where PDE4B expression is up-regulated [Smith et al., 2005].

PDE4 isoforms are localised within the airway smooth muscle cells [Burnouf and Pruniaux, 2002]. PDE4 inhibition reduces airway smooth muscle tone through cAMP-mediated activation of PKA. PKA phosphorylation inhibits the myosin light chain kinase thereby preventing the phosphorylation of the myosin fibres in the smooth muscle cells. PDE4D isoforms are critical in the control smooth muscle contraction [Méhats et al., 2003]. Indeed, PDE4D knockout ($PDE4D^{-/-}$) mice show a loss of muscarinic cholinergic airway signalling and a loss of airway hyper-reactivity [Hansen et al., 2000]. Interestingly, the $PDE4D^{-/-}$ mice showed an equivalent lung inflammatory response compared to wild type mice. This loss of function was specific to the airway smooth muscle cells and these data support the notion that sub-family specific PDE4 isoforms have distinct, not coincidental functions.

The cystic fibrosis transmembrane conductance regulator (CFTR) in airway epithelial cells drives mucociliary clearance [Houslay et al., 2005]. Inhibition of PDE4 may prevent mucus accumulation by promoting the PKA phosphorylation of the CFTR and increasing probability of channel conductance. The cAMP-dependent regulation of the CFTR has also been

identified in the corneal endothelium and this mechanism may translate to airway epithelial cells [Sun et al., 2003].

The pathogenesis of inflammation is a complex process involving a multitude of inflammatory cells such as B-cells, T-cells, neutrophils, eosinophils, basophils, monocytes, macrophages and mast cells, and their function is regulated by the generation of both pro- and anti-inflammatory cytokines. cAMP is known to antagonise the action of pro-inflammatory mediators and PDE4 is localised within immune and inflammatory cells [Wong and Koh, 2000, Souness et al., 2000 and Barber et al., 2004]. Thus, inhibition of sub-family specific PDE4s and the elevation of intra-cellular cAMP concentrations may dampen the inflammatory response. This is corroborated in studies undertaken in PDE4B$^{-/-}$ and PDE4D$^{-/-}$ mice that show that PDE4B activity is essential for the expression of the pro-inflammatory cytokine tumour necrosis factor α (TNFα) where knockout elicits a 90% reduction in expression [Jin and Conti, 2002]. At the level of gene transcription, T-cell expression of TNFα is inhibited via PDE4 inhibition by rolipram and is accompanied by an increase in the expression of the anti-inflammatory cytokine interleukin-10 (IL-10) [Houslay et al., 2005]. Similar attenuation of TNFα expression occurred in monocytes with the more potent PDE4 inhibitor, roflumilast [Hatzelmann and Schudt, 2001, Bundschuh et al., 2001 and Muise et al., 2002]. The recruitment of PDE4 and β-arrestin with CD28 to the T-cell receptor is a pre-requisite for full T-cell activation [Abrahamsen et al., 2004]. Inhibition of PDE4 will blunt such co-ligation and activation providing a potential mechanism for the associated anti-inflammatory effects. Increased intra-cellular levels of cAMP are known to attenuate the de-granulation of neutrophils and eosinophils [Teixeira et al., 1997, Pryzwansky and Madden, 2003 and Jones et al., 2005]. In PDE4B$^{-/-}$ and PDE4D$^{-/-}$ mice neutrophil recruitment to the bronchoalveolar lavage was attenuated and this effect was hypothesised to be due to decreased cell surface expression of adhesion molecules and chemotaxis [Ariga et al., 2004]. Reductions in endothelial cell permeability and the endothelial cell expression of adhesion molecules also results from PDE4 inhibition [Teixeira et al., 1997]. Moreover, adaptation of inflammatory cell expression of PDE4 isoforms has been observed in people diagnosed

with the inflammatory respiratory disease COPD, indicating a need for sub-family or even isoform specific inhibitors of PDE4 [Barber et al., 2004].

Learning and memory are affected by disruptions in intracellular cAMP concentrations. PDE4 enzymes are related to the dunce gene product of *Drosophila melanogaster*, the learning and memory gene [Bolger et al., 1993]. Therefore, it is hardly surprising that modulation of cAMP by PDE4 affects cognition. N-methyl-D-aspartic acid (NMDA) and α-amino-5-hydroxy-3-methyl-4-isoxazole propionic acid (AMPA) receptor expression in the hippocampal and cerebral cortical neurons underlie the ability to learn and the formation of long- and short-term memory. NMDA receptor activation results in an increase in intra-cellular Ca^{2+} levels and the activation of AC to generate a cAMP-PKA-CREB-mediated synaptic plasticity [Zhang et al., 2005]. RACK1 is known to associate with the NMDA receptor [Ron et al., 2004]. As discussed above in Section 1.7.6.8, RACK1 also specifically interacts with PDE4D5 [Yarwood et al., 1999]. AKAPs also interact with both the NMDA receptors and PDE4D isoforms [Taskén and Aandahl, 2004]. Therefore, it is not difficult to appreciate the control of cAMP compartmentalisation and PKA activity in close proximity to the NMDA receptor. Indeed, PDE4D specific knockout has been assigned as cognitive enhancing [Houslay et al., 2005]. The PKA phosphorylation of AMPA receptors is a pre-requisite for synaptic delivery in hippocampal cells [Esteban et al., 2003 and Esteban, 2003]. Again, prevention of cAMP degradation through PDE4 inhibition will enhance AMPA receptor delivery to neuronal synapses via a similar mechanism to the NMDA receptors in mediating cognitive enhancement.

The pharmacological explanation of depression is a lack of the monoamine transmitters nor-adrenaline and 5-hydroxytryptamine (5-HT or serotonin) in the brain. Current anti-depressants promote the synthesis, and prevent the degradation and re-uptake of both transmitters. They have also been shown to induce the expression of PDE4A and PDE4B isoforms, two examples being despiramine and fluoxetine [O'Donnell and Zhang, 2004]. Thus, the anti-depressant effects of cAMP have been promoted because both cAMP generation is fundamental in intra-cellular signalling induced by nor-

adrenaline and 5-HT, and because PDE4 isoforms are differentially expressed in the brain. At present it is difficult to reconcile which PDE4 sub-family is important in mediating the anti-depressant effects elicited by PDE4 inhibitors but PDE4B$^{-/-}$ and PDE4D$^{-/-}$ mice show similar anti-depressant properties to mice treated with current compounds. It is now appreciated that PDE4 enzymes expressed in the brain predominate in HARBS and may also underlie the anti-depressant effects.

However, many of the current inhibitors to date have nausea, emesis and sedation as particularly severe side effects [Huang et al., 2001 and Zhang et al., 2005]. Such has been the hindrance of the side effects associated with PDE4 inhibition, the development of a highly emetic photo-affinity probe able to inhibit PDE4 has been developed to try and elucidate the emetic targets [MacDonald et al., 2000]. In simplistic terms, it has been proposed that inhibition of high affinity PDE4 conformers may be involved in manifestation of these side effects with inhibition of low affinity conformers providing the beneficial effects [Giembycz, 2000 and O'Donnell and Zhang, 2004]. However, this theory is now not given much credence. Another theory is isoform specific, where it is thought that PDE4 inhibitors selective for PDE4B over PDE4D may be more successful in overcoming the side effects associated with the current compounds [Giembycz, 2002, Lipworth, 2005 and Zhang et al., 2005]. PDE4D is expressed at very high levels in the area postrema of the hindbrain [Giembycz, 2002]. The area postrema contains the chemoreceptor trigger zone, which is involved in the reflex mechanism of vomiting. Receptors are expressed on the chemoreceptor trigger zone and are coupled to the stimulation and inhibition of AC. Thus, disruption of cAMP signalling through these receptors within this brain region by inhibition of PDE4D may explain the emetic effects [O'Donnell and Zhang, 2004]. Furthermore, the generation of PDE4 inhibitors that do not permeate the blood brain barrier may significantly reduce these side effects [Zhang et al., 2005]. However, PDE4 inhibitors have been produced that exhibit broncho-dilatation, anti-inflammatory and non-emetic properties but many have been discontinued as development compounds due to aberrant metabolism [Alexander et al., 2002, Guay et al., 2002 and Burnouf and Pruniaux, 2002].

PDE4 inhibitors show much promise as potential targets for the treatment of respiratory failure, inflammation, cardiovascular disease, CNS disorders and cancer. However, the design of sub-family specific inhibitors, inhibitors with affinity for LARBS, and inhibitors that are unable to penetrate the blood brain barrier provide the best opportunity to further evaluate PDE4 inhibition for therapeutic benefit. Furthermore, the elucidation of the full crystal structure of PDE4 long isoforms will provide much needed insight into isoforms specific regulation of activity.

1.8 Thesis Aims

The work in this thesis can be separated into three distinct chapters. Each of these chapters focuses upon the PDE4A sub-family of enzymes and the expression and regulation of distinct isoforms. These isoforms are likely to contribute to the compartmentalisation of cAMP signalling in cells in which they are expressed. Modifications of PDE4A isoforms, by phosphorylation and/or protein-protein interactions, add further complexity to the PDE4A regulation of intra-cellular cAMP concentrations and the downstream signalling events.

The human PDE4 family currently comprises of twenty-one isoforms. Of these, five are assigned to the PDE4A gene family. The PDE4A gene, located on chromosome 19p13.2, encodes an active super-short form called PDE4A1, a catalytically inactive isoform called PDE4A7, and three active long isoforms called PDE4A4B, PDE4A10 and a new isoform, PDE4A11. This thesis aims to characterise the novel PDE4A11 isoform, summarise its key distinguishing features, and attempts to elucidate the functional significance of its expression.

Previous studies from the Houslay laboratory have described the regulation of PDE4 activity through direct phosphorylation by both PKA and ERK1/2 [Hoffman et al., 1998, Baillie et al., 2000, Baillie et al., 2001 and MacKenzie et al., 2002]. PDE4 long isoforms are phosphorylated and

activated by PKA at one distinct serine site within the UCR1 regulatory module, which is conserved in all PDE4 isoforms. ERK1/2 phosphorylation of all PDE4 isoforms, except PDE4A, occurs at a single serine residue within the catalytic unit. This phosphorylation exerts differential effects upon PDE4 catalytic activity dependent upon the inclusion of the UCR regulatory domains. Work in this thesis strives to identify novel phosphorylation sites for PDE4 enzymes, which may contribute to the regulation of cAMP compartmentalisation, PDE4 activity, and cross talk between cAMP and other signalling pathways.

The production of super-oxide (O_2^-) and other reactive oxygen species (ROS) constitutes a key component of the inflammatory response. The expression of PDE4 enzymes is particularly abundant in immune and inflammatory cells. Inhibition of PDE4 attenuates the production of ROS. However, the molecular mechanism through which PDE4 inhibitors achieve this is largely unknown. Preliminary work to address this is described in the final chapter of this thesis. This chapter aims to elucidate the mechanism through which cAMP signalling controls the production of ROS.

Chapter 2 Materials and Methods

2.1 Materials

All equipment, materials and chemicals were supplied by Sigma-Aldrich® (Poole, U.K.) unless otherwise stated.

2.2 Plasmid Preparation

All molecular biology techniques were undertaken in a sterile environment using sterilised equipment. Buffers were of molecular biology grade and were sterilised by autoclaving or sterile filtration.

2.2.1 Transformation of Competent Cells

Competent cells are cells that have the ability to incorporate DNA plasmids. Not all cells are competent and have this capacity so cells can be manipulated to become chemically competent. Most competent cell types have their own optimal transformation protocol but they follow the same general principle described below. Follow the manufacturers instructions for protocols tailored to individual bacterial cell types. Competent bacterial cells were stored at –80°C and thawed on ice. 50µl of competent cells were required per transformation reaction. 1-10ng of DNA was added to each 50µl aliquot of cells and the cells were incubated on ice for up to 15min. Longer incubations generally have no effect on transformation efficiency. The cells were then heat shocked for 45-90s at 42°C and returned to ice for a further 2min. 450µl of pre-warmed LB media (1% (w/v) bacto-tryptone, 0.5% (w/v) bacto-yeast extract and 170mM NaCl) was added to the cells and then incubated in the orbital shaking incubator for 45min at 37°C. Agar plates containing the appropriate antibiotic(s) were produced using LB media containing 1.5% (w/v) agar. The commonly used antibiotics and their effective

final concentrations are shown in Table 2.1. The LB media/agar solution was autoclaved and cooled to less than 50°C before the addition of the antibiotic(s). 100-200µl of transformation mix was then spread on the agar plates and the plates incubated overnight at 37°C. Colony growth on the plates was indicative of successful cell transformation. Plates were stored at 4°C for up to 1 month before being discarded.

Antibiotic	Stock Concentration	Storage	Working Concentration
Ampicillin	100mg/ml in H_2O	-20°C	100µg/ml
Kanamycin	10mg/ml in H_2O	-20°C	50µg/ml
Chloramphenicol	17mg/ml in ethanol	-20°C	34µg/ml

Table 2.1 – Concentrations of commonly used antibiotics.

2.2.2 Isolation of Plasmid DNA

From single colonies on agar plates, see Section 2.2.1, or glycerol stocks, see Section 2.2.3.1, 5ml bacterial cultures were grown overnight in LB media containing the appropriate antibiotic(s) in the orbital shaking incubator at 37°C. 1ml of the bacterial culture was used directly for glycerol stock production and the remaining bacterial culture for plasmid DNA isolation using the QIAGEN® (Crawley, U.K.) QIAprep® Miniprep Kit. Alternatively, the 5ml overnight bacterial culture was used to inoculate a larger LB media culture flask (approximately 500ml), supplemented with the appropriate antibiotic(s), for overnight growth and isolation of significantly greater plasmid DNA concentrations and volumes using the QIAGEN® (Crawley, U.K.) QIAprep® Maxiprep Kit. For in-depth details of the plasmid DNA isolation protocols please refer to the manufacturers instructions.

2.2.3 Storage of Plasmid DNA

2.2.3.1 Glycerol Stocks

To produce a glycerol stock, 1ml of overnight bacterial culture was removed and mixed with 500µl of sterile glycerol in a sterile cryo-vial. The cryo-vial was snap frozen and stored at –80°C until required. Generally, the *E.coli* bacterial strain, JM109, was used as the host strain for the generation of glycerol stocks for long-term storage.

To inoculate culture media from a glycerol stock, the glycerol stock was stabbed with a sterile pipette tip, which was then transferred to approximately 5ml of sterile LB media containing the appropriate antibiotic(s) for the bacterial host strain and/or the DNA plasmid with which they are transformed. The inoculated culture was then grown overnight at 37°C in an orbital shaking incubator.

2.2.3.2 Purified Plasmid DNA

Purified plasmid DNA produced, as described in Section 2.2.2, using the QIAGEN® (Crawley, U.K.) QIAprep® Kits was stored at 4°C, if eluted in 10mM Tris-Cl; pH 8.5, and –20°C, if eluted in sterile water.

2.2.4 Analysis of Plasmid DNA

2.2.4.1 Agarose Gel Electrophoresis

Agarose gel electrophoresis is a method of separating DNA plasmids or fragments by virtue of their charge, by the migration of the DNA through a matrix under the influence of an electric field. DNA is highly negatively charged and therefore moves through the matrix towards the positive electrode. 1% (w/v) agarose gels resolves DNA fragments between 0.5-10kb and allows detection of 20-500ng of DNA per band, which can be used to determine the DNA concentration of a plasmid preparation or fragment. 1% (w/v) agarose was dissolved in 40mM Tris-Cl; pH 8.5, 0.114% (v/v) glacial acetic acid and 2mM EDTA (TAE) by heating in a microwave oven. Care was taken not to super-heat the solution. 0.5µg/ml (final concentration) ethidium bromide was added to the cooled (55-60°C) 1% (w/v) agarose solution and poured into the Bio-Rad® (Hemel Hempstead, U.K.) Sub-Cell GT gel apparatus, with the well comb in place and the ends sealed with autoclave tape, and allowed to set. For more details about the Bio-Rad® Sub-Cell GT gel apparatus please consult the manufacturers instructions. Once set, normally around 30-40min, the comb and autoclave tape were removed and the gel was placed in the tank and immersed in a volume of 1x TAE buffer that was sufficient to cover the top of the gel by approximately 1mm. 6x loading buffer composed of 0.25% (w/v) bromophenol blue, 0.25% (w/v) xylene cyanol FF and 40% (w/v) sucrose was diluted 1:6 into the DNA solution and mixed gently. 5µl of Promega® (Southampton, U.K.) 1kb DNA ladder was also loaded to an appropriate well of the gel to allow the size of the DNA plasmid or fragment within the sample to be determined. The gels

were run at 100V for approximately 1h. The gel was removed from the tank and analysed under ultra-violet light where ethidium bromide stained DNA is visualised. All DNA agarose gel images were captured using a Kodak® DC290 camera controlled via Kodak® 1D, Version 3.5.4 computer software.

2.2.4.2 Quantification of DNA Concentration

The concentration of any DNA sample, produced following the protocol described in Section 2.2.2, was determined using a Jenway and Genova MK2 spectrophotometer, measuring the absorption at 260nm (A_{260}). 1ml of sterile water was added to a quartz cuvette and the absorption measured. The DNA solution was diluted 1:200 in the sterile water and the new absorption reading measured. The concentration of DNA was determined on the basis that an absorbance of 1 unit at 260nm corresponds to 50µg plasmid DNA per millilitre based on a standard quartz cuvette with a 1cm path length. The ratio of the absorbance readings at 260nm (A_{260}) over 280nm (A_{280}) is indicative of the purity of the DNA preparation. An A_{260}/A_{280} ratio of 1.8 is typical of a pure DNA preparation in a low-salt buffer and is generally reproducible.

2.2.4.3 DNA Sequencing

DNA samples for sequencing were prepared as described in Section 2.2.2. BaseClear Lab Services (Leiden, Netherlands) carried out the sequencing of 500bp lengths of plasmid DNA using standard and/or custom DNA sequencing primers. Analyses of the DNA sequencing reactions aligned with the predicted DNA sequences was done using either Gene Jockey®, Version 2.2 or Chromas® 1.45 computer software programmes.

2.2.5 Site-Directed Mutagenesis of Plasmid DNA

Site-directed mutagenesis of plasmid DNA was carried out using the Stratagene® (La Jolla, CA, U.S.A.) QuikChange® Site-Directed Mutagenesis Kit, according to the manufacturers instructions. Briefly, sample polymerase chain reactions (PCRs) were set up in 1x reaction buffer containing various concentrations of purified, template plasmid DNA (5-50ng), 125ng of each primer and 1µl of deoxynucleotide tri-phosphate (dNTP) mix in a final reaction volume of 50µl. Primer pairs used for site-directed mutagenesis are shown in Table 2.2. 1µl of *Pfu Turbo* DNA polymerase (2.5U/µl) was added to each reaction. The PCR conditions used were 95°C for 30s, and 18 cycles of 95°C for 30s, 55°C for 1min, and 68°C for 1min per kb of the plasmid length. 1-4µl of the *Dpn I* restriction enzyme was added to each reaction and incubated at 37°C for 1h. 1µl of the *Dpn I*-treated DNA was used to transform 50µl of XL1-Blue super-competent cells as described in Section 2.2.1. Plasmid DNA was isolated from single colonies on agar plates, as described in Section 2.2.2, and subsequently the DNA sequenced, as described in Section 2.2.4.3, to assess whether successful site-directed mutagenesis had been achieved.

Protein	Mutation	Forward (5') Primer	Reverse (3') Primer
PDE4A11	Ser119Ala	CCACCAGCCAGCGCCGG GAGGCCTTCCTGTACCG CTCAGACAG	CTGTCTGAGCGGTACAG GAAGGCCTCCCGGCGCT GGCTGGTGG
PDE4A5	Ser147Ala	CTTCCTCTACCGCTCAGA CGCCGACTATGACATGTC ACCGAAG	CTTCGGTGACATGTCATA GTCGGCGTCTGAGCGGT AGAGGAAG
PDE4A5	Ser161Ala	GCTGTGTCCAGGAGCTC GGCTGTCGCCAGCGAAG CGCACG	CGTGCGCTTCGCTGGCG ACAGCCGAGCTCCTGGA CACAGC
PDE4A5	Thr437Ala	CACACGTGCTGCTGGCC GCGCCCGCACTGGACGC TGTG	CACAGCGTCCAGTGCGG GCGCGGCCAGCAGCACG TGTG
PDE4A5	Thr776Ala	CTGTTCCTTCAGCCCTGG GGCCCCTATTCTGCCTGA CG	CGTCAGGCAGAATAGGG GCCCCAGGGCTGAAGGA ACAG
p47-*phox*	Ser304Ala	GGCGCCGCCCCGCAGGT CGGCCATCCGCAACGCG CACAGC	GCTGTGCGCGTTGCGGA TGGCCGACCTGCGGGGC GGCGCC
p47-*phox*	Ser320Ala	GGTCGCGGAAGCGCCTC GCCCAGGACGCCTATCG CCGC	GCGGCGATAGGCGTCCT GGGCGAGGCGCTTCCGC GACC
p47-*phox*	Ser328Ala	GGACGCCTATCGCCGCA ACGCCGTCCGTTTTCTGC AGCAG	CTGCTGCAGAAAACGGA CGGCGTTGCGGCGATAG GCGTCC

Table 2.2 – Primer pairs used for site-directed mutagenesis.

The nucleotides highlighted in red indicate the nucleotide sequence change to alanine codons.

2.3 Reverse Transcriptase Polymerase Chain Reaction

2.3.1 Using mRNA

Amplification of generic PDE4A and specific PDE4A11 fragments were carried out using intron-spanning primer pairs as detailed in Table 2.3, primers pairs 1-4. Reverse transcriptase polymerase chain reaction (RT-PCR) was done with 2µg of mRNA extracted from brain tissue or HEK293 cells using the QIAGEN® One-Step RT-PCR Kit (Crawley, U.K.). PCR conditions of 50°C for 30min, 94°C for 15min, and 35 cycles of 94°C for 1min, 50°C for 1min, and 72°C for 1min. Final extension was undertaken at 72°C for 10min. The PCR products were visualised by 1% (w/v) agarose gel electrophoresis, as described in Section 2.2.4.1.

2.3.2 Using cDNA for Tissue Expression Profiling

To assess the expression profile of PDE4A11 in twenty-four human tissues, a Rapid-Scan™ Gene Expression Panel of first strand cDNAs supplied by OriGene Technologies Inc. (Rockville, MD, U.S.A) were used according to the manufacturers instructions. These were used as PCR templates and primer pair 5 used to generate the 494bp product is detailed in Table 2.3. QIAGEN® HotStar Taq DNA Polymerase (Crawley, U.K.) was used together with PCR conditions of 95°C for 15min, and 35 cycles of 95°C for 30s, 50°C for 30s and 72°C for 1 min. Final extension was undertaken at 72°C for 10 min. The PCR products were visualised by 1% (w/v) agarose gel electrophoresis, as described in Section 2.2.4.1.

Primer Pair	Region of PDE4A11	Fragment Length (bp)	Forward (5') Primer	Reverse (3') Primer
1	UCR2 to catalytic unit	506	ATGCAGACCTATCGC TCTGTCAGC	ACCATCGTGTCCACAGG GATGC
2	Unique N-terminal to UCR1	497	ATGGCGCGGCCGCG CGGCCTAGGCC	CGGACGCTCCGGAGGC TGGCCAGCACC
3	Unique N-terminal to LR2	886	ATGGCGCGGCCGCG CGGCCTAGGCC	GCGGCTGGGAGGGTCT TGGTCGCGGCGC
4	Unique N-terminal to catalytic unit	1794	ATGGCGCGGCCGCG CGGCCTAGGCC	GCCACGCTCGCGCTCT CGGTCACCCTGC
5	Unique N-terminal to LR1	494	GGAGCTGCAACTGG TGGC	GGCACATTGGTCAGGA GTGAG

Table 2.3 – Primer pairs used for RT-PCR.

2.4 Expression and Purification of Recombinant Fusion Proteins

2.4.1 Maltose Binding Protein (MBP) Fusion Proteins

Competent *E.coli* BL21 pLysS (DE3) cells were transformed, as described in Section 2.2.1, with the appropriate pMAL plasmid, as described in Table 2.4, and grown directly in 30ml of sterilised LB media, supplemented with 100ug/ml ampicillin, overnight in an orbital shaking incubator at 37°C. 450ml of sterilised LB media, supplemented with 100ug/ml ampicillin, was inoculated with the overnight culture and grown in the orbital shaker at 37°C for 1-2h. A 1ml sample of culture was removed to a plastic cuvette and the optical density measured at 600nm (OD_{600}) against an LB media control. Expression of the fusion protein was induced with 0.2mM isopropyl-β-D-thiogalactopyranoside (IPTG) when an OD_{600} of 0.6-1 was achieved. An OD_{600} at this level ensured that the culture was in the logarithmic phase, where bacteria will grow exponentially. Expression of the target protein was undertaken for 4h in an orbital shaker set at 30°C. Hourly 1ml samples of LB media were removed to monitor protein expression. These samples, including the sample used for OD_{600} measurement (un-induced control sample), were centrifuged at 16,060 x *g* and the pellet was re-suspended in 100µl SDS sample buffer for analysis by SDS-PAGE and Coomassie® staining, as described in Section 2.12. The cells were then harvested by centrifugation at 6,500 x *g* for 10min. The cells were re-suspended in 12ml of 50mM Tris-HCl; pH 8.0, 10mM NaCl and 10mM β-mercaptoethanol containing a 1x solution of Roche Diagnostics (Mannheim, Germany) protease inhibitor cocktail tablets. The re-suspended cells were then frozen at –80°C and thawed on ice. Lysozyme was added at a final concentration of 1mg/ml and the cell suspension subjected to sonication to achieve sufficient cell lysis. A final concentration of 0.05% (v/v) NP-40 was added to aid cell lysis and the subsequent cell debris removed by centrifugation at 20,000 x *g* for 15 min. 1ml of New England BioLabs® (Hitchin, U.K.) amylose resin was pre-equilibrated with re-suspension buffer containing 0.05% (v/v) NP-40. The cell supernatant was applied to the pre-equilibrated resin and incubated end-over-

end for 1h at 4°C to bind the expressed fusion protein. The resin was collected by centrifugation at 5,200 x *g* for 2min and washed three times with 750µl of re-suspension buffer containing 0.05% (v/v) NP-40. The fusion protein was eluted from the amylose resin with 500µl of 10mM maltose, 50mM Tris-HCl; pH 8.0 by incubating end-over-end for 20min at 4°C. This was repeated up to three times, if necessary. The eluted fractions were pooled and dialysed using Pierce® (Rockford, IL, U.S.A.) Slide-A-Lyser® dialysis cassettes against three 650ml volumes of 100mM NaCl, 50mM Tris-HCl; pH 8.0, 5% (v/v) glycerol, for 1h each at 4°C. The purified fusion protein was frozen on dry ice, and stored as aliquots, at –80°C. The expression time-course and final purification to homogeneity was analysed by SDS-PAGE and Coomassie® staining, described in Section 2.12.

2.4.2 Glutathione-S-Transferase (GST) Fusion Proteins

The *E.coli* expression and purification of recombinant GST fusion proteins mirrors the experimental protocol described in Section 2.4.1 for the expression and purification of MBP fusion proteins. Competent *E.coli* BL21 pLysS (DE3) cells were transformed, as described in Section 2.2.1, with the appropriate pGEX plasmid, as described in Table 2.4. For the purification of GST fusion proteins the use of Amersham Biosciences (Little Chalfont, U.K.) glutathione sepharose resin was required and successful elution required an elution buffer composition of 10mmM glutathione, 50mM Tris-HCl; pH 8.0. The expression time course and final purification to homogeneity was analysed by SDS-PAGE and Coomassie® staining, described in Section 2.12.

2.5 Mammalian Cell Culture

All cell culture techniques were performed in a class two hood using standard aseptic techniques and reagents that had been sterilised by either autoclaving or sterile filtration.

2.5.1 Maintenance of Cell Lines

The storage of cells with a low passage number at –200°C ensured the long-term integrity of the specific cell line. To revive cells from this temperature the individual vial was quickly thawed and added directly to 10ml of pre-warmed fresh growth media, under sterile conditions. Once the cell line was established and confluent, further 1ml aliquots of cells were re-suspended in cell freezing media. These were initially frozen at –80°C before being transferred to –200°C for long-term storage.

2.5.1.1 COS1 and COS7 Cells

COS1 and COS7 cell lines are derived from African green monkey kidney cells and have been transformed with the SV40 virus. The cells were propagated in growth media containing Dulbecco's modified Eagle's medium (DMEM) supplemented with 0.1% (v/v) penicillin/streptomycin (10000U/ml), 2mM glutamine and 10% (v/v) foetal calf serum (FCS). The cell line was maintained at 37°C in an atmosphere of 95% (v/v) air and 5% (v/v) CO_2. The cells were passaged when approximately 90% confluence was reached. To passage the cells the growth media was removed and 5ml of pre-warmed sterile phosphate buffered saline (PBS) was added. The cells were washed by gentle agitation with sterile PBS, which was then aspirated. 5ml of trypsin-EDTA solution was added and cells were incubated for 5min at 37°C. The cells were vigorously agitated and then analysed under the microscope to check for efficient cell detachment. Once this state was achieved, 10ml of growth media was added to inactivate the trypsin-EDTA solution. The cells were collected by centrifugation at 1,000 x *g* for 3min. The growth media supernatant was removed and the cell pellet re-suspended in the appropriate volume of growth media. Once fully re-suspended 1ml of cells were added to fresh growth media in a sterile flask(s). The cells were returned for incubation at 37°C in an atmosphere of 95% (v/v) air and 5% (v/v) CO_2 until required or confluent.

2.5.1.2 HEK293 Cells

The human embryonic kidney 293 (HEK293) cell line has epithelial cell morphology. These cells were maintained as described in Section 2.5.1.1 for COS1 and COS7 cells.

2.6 Mammalian Cell Transfection of Plasmid DNA

A list of DNA plasmids used for the transfection of mammalian cell lines are described in Table 2.4.

2.6.1 DEAE-Dextran Transient Transfection

This method of mammalian cell transfection was used for the transfection of COS1 and COS7 cell lines only. Flasks of confluent cells were passaged the day prior to transfection and plated to ensure 70% confluence on the day of transfection. These plates were incubated overnight at 37°C in an atmosphere of 95% (v/v) air and 5% (v/v) CO_2. The amount of DNA required for each transfection plate is dependent on the number of cells to be transfected and should be scaled accordingly. This protocol is accurate for 100mm plates of 70% confluent cells in 10ml of growth media. 10µg of the desired DNA plasmid was diluted in 10mM Tris-Cl; pH 7.6, 0.1mM EDTA to a final volume of 250µl. 200µl of 10mg/ml DEAE-Dextran was added to the DNA solution, mixed, and incubated for 15min at room temperature. Where co-transfection of two DNA plasmids was required 10µg of each plasmid, in a final volume of 250µl of 10mM Tris-Cl; pH 7.6, 0.1mM EDTA, was added to 200µl of 10mg/ml DEAE-Dextran. During the incubation period the growth media was removed from the plates and replaced with 10ml of fresh growth media supplemented with 100µM sterile chloroquine. Following incubation, the DNA-DEAE-Dextran solution was added directly to the appropriate transfection plate and incubated for 3-4 hrs at 37°C. The growth medium was removed from the plates and 10ml of sterile PBS containing 10% (v/v) di-

methyl sulphoxide (DMSO) added and aspirated immediately. The plates were washed twice with 10ml of sterile PBS before the introduction of 10ml of fresh growth media. The plates were incubated for approximately 2 days at 37°C in an atmosphere of 95% (v/v) air and 5% (v/v) CO_2 prior to any cell treatments and harvesting. Details of ligands and inhibitors used for cell treatments are described in Table 2.5.

2.6.2 PolyFect® Transient Transfection

The PolyFect® method of mammalian cell transfection, from QIAGEN® (Crawley, U.K.), was used for the transfection of COS1, COS7 and HEK293 cell lines. Flasks of confluent cells were passaged the day prior to transfection and plated to ensure 40-80% confluence on the day of transfection. These plates were incubated overnight at 37°C in an atmosphere of 95% (v/v) air and 5% (v/v) CO_2. The amount of DNA required for each transfection plate is dependent on the number of cells to be transfected and should be scaled accordingly. This protocol is accurate for 100mm plates of 40-80% confluent cells in 8ml of growth media. 4µg of the desired DNA plasmid for the transfection of COS1 or COS7 cells was diluted in antibiotic- and FCS-free DMEM to a final volume of 300µl. 8µg of the desired DNA plasmid for the transfection of HEK293 cells was diluted in antibiotic- and FCS-free DMEM to a final volume of 300µl. 25µl of PolyFect® Transfection Reagent was added to the DNA solution for COS cell transfections whereas 80µl was required for efficient transfection of HEK293 cells. The transfection reagents were incubated at room temperature for 5-10min to allow complex formation. Where co-transfection of two DNA plasmids was required the amount indicated above of each plasmid was diluted in 300µl of antibiotic- and FCS-free DMEM before the addition of the specific volume of PolyFect® Transfection Reagent indicated above for the cell type. During the incubation period the growth media was removed from the plates and replaced with 7ml of fresh DMEM supplemented with 0.1% (v/v) penicillin/streptomycin (10000U/ml), 2mM glutamine and 10% (v/v) foetal calf serum (FCS). Following incubation, 1ml of supplemented DMEM

containing the antibiotics and 10% (v/v) FCS was added to the DNA-DMEM-PolyFect® complex. This was mixed gently and added directly to the appropriate transfection plate. The plates were then incubated for approximately 2 days at 37°C in an atmosphere of 95% (v/v) air and 5% (v/v) CO_2 prior to any cell treatments and harvesting. Details of ligands and inhibitors used for cell treatments post-transfection are described in Table 2.5.

2.6.3 FuGENE® 6 Transient Transfection

The FuGENE® 6 method of mammalian cell transfection, from Roche Diagnostics (Mannheim, Germany), was used for the transfection of COS1, COS7 and HEK293 cell lines that were to be used for confocal microscopy analyses. Flasks of confluent cells were passaged the day prior to transfection and plated to ensure 50-80% confluence on the day of transfection. These plates were incubated overnight at 37°C in an atmosphere of 95% (v/v) air and 5% (v/v) CO_2. The amount of DNA required for each transfection plate is dependent on the number of cells to be transfected and should be scaled accordingly. This protocol is accurate for one well of a 6-well plate containing 40-80% confluent cells in 2ml growth media per well. 5µl of FuGENE® 6 Transfection Reagent was added to 95µl of antibiotic- and FCS-free DMEM and incubated at room temperature for 5 min. 1µg of the desired DNA plasmid for cell transfection was added to the FuGENE® 6-DMEM solutions and this were incubated for 15-45min allowing complex formation. The transfection reagents were then added directly to the appropriate well of the transfection plate. The plates were incubated for approximately 24h at 37°C in an atmosphere of 95% (v/v) air and 5% (v/v) CO_2 prior to any cell treatments and harvesting. Details of ligands and inhibitors used for cell treatments post-transfection are described in Table 2.5.

Plasmid	Antibiotic Resistance	Expression	Description	Source
hRD1/pcDNA3	Ampicillin	Mammalian	Full open reading frame of human PDE4A1 in pcDNA3	Dr. Fiona Begg (Houslay Laboratory)
pcDNA46	Ampicillin	Mammalian	Full open reading frame of human PDE4A4B in pcDNA3	Prof. Graeme Bolger University of Alabama, Alabama, U.S.A.
pcDNAR6-VSV	Ampicillin	Mammalian	Full length open reading frame of rat PDE4A5 in pcDNA3 tagged with VSV	Prof. Graeme Bolger University of Alabama, Alabama, U.S.A.
pcDNAR6-VSV S147A	Ampicillin	Mammalian	Full length open reading frame of rat PDE4A5 with Serine 147 mutated to Alanine in pcDNA3 tagged with VSV	Derek Wallace (Houslay Laboratory)
pcDNAR6D147	Ampicillin	Mammalian	Full length open reading frame of rat PDE4A5 with Serine 147 mutated to Aspartate in pcDNA3	Prof. Graeme Bolger University of Alabama, Alabama, U.S.A.
pcDNAR6-VSV S161A	Ampicillin	Mammalian	Full length open reading frame of rat PDE4A5 with Serine 161 mutated to Alanine in pcDNA3 tagged with VSV	Derek Wallace (Houslay Laboratory)
pSV.R6ΔP5	Ampicillin	Mammalian	Rat PDE4A5 with N-terminal region removed (Serine 135 to end) in pSV	Dr. Grant Scotland (Houslay Laboratory)
pSV.R6ΔP6	Ampicillin	Mammalian	Rat PDE4A5 with N-terminal region and UCR1 removed (Proline 197 to end) in pSV	Dr. Grant Scotland (Houslay Laboratory
pMalR6	Ampicillin	*E.coli*	Full open reading frame of rat PDE4A5 in pMalC2X with MBP in fusion with the N-terminal region	Prof. Graeme Bolger University of Alabama, Alabama, U.S.A.

Plasmid	Antibiotic Resistance	Expression	Description	Source
pMalR6 S147A	Ampicillin	*E.coli*	Full open reading frame of rat PDE4A5 with Serine 147 mutated to Alanine in pMalC2X with MBP in fusion with the N-terminal region	Derek Wallace (Houslay Laboratory)
pMalR6 S161A	Ampicillin	*E.coli*	Full open reading frame of rat PDE4A5 with Serine 161 mutated to Alanine in pMalC2X with MBP in fusion with the N-terminal region	Derek Wallace (Houslay Laboratory)
pMalR6 T437A	Ampicillin	*E.coli*	Full open reading frame of rat PDE4A5 with Threonine 437 mutated to Alanine in pMalC2X with MBP in fusion with the N-terminal region	Derek Wallace (Houslay Laboratory)
pMalR6 T776A	Ampicillin	*E.coli*	Full open reading frame of rat PDE4A5 with Threonine 776 mutated to Alanine in pMalC2X with MBP in fusion with the N-terminal region	Derek Wallace (Houslay Laboratory)
pcDNA3 PDE4A8VSV	Ampicillin	Mammalian	Full open reading frame of rat PDE4A8 in pcDNA3 tagged with VSV	Prof. Graeme Bolger University of Alabama, Alabama, U.S.A.
4A10 ATG2	Ampicillin	Mammalian	Full open reading frame of human PDE4A10 in pSV Sport	Dr. Fiona Begg (Houslay Laboratory
TM3	Ampicillin	Mammalian	Full open reading frame of human PDE4A11 in pcDNA3	Dr. Ian McPhee (Houslay Laboratory)

Plasmid	Antibiotic Resistance	Expression	Description	Source
PDE4A11 S119A	Ampicillin	Mammalian	Full open reading frame of human PDE4A11 in pcDNA3 with Serine 119 mutated to Alanine in pcDNA3	Derek Wallace (Houslay Laboratory)
PDE 4B1	Ampicillin	Mammalian	Full open reading frame of human PDE4B1 in pEE7 (Cell-Tech)	Dr. Elaine Huston (Houslay Laboratory)
PDE 4B2	Ampicillin	Mammalian	Full open reading frame of human PDE4B2 in pEE7 (Cell-Tech)	Dr. Elaine Huston (Houslay Laboratory
PDE 4B3/pCMV4A	Ampicillin	Mammalian	Full open reading frame of human PDE4B3 in pCMV4A	Dr. Shaun Mackie University of Edinburgh, Edinburgh, U.K.
PDE 4B4	Ampicillin	Mammalian	Full open reading frame of human PDE4B4 in pEE7 (Cell-Tech)	Prof. Graeme Bolger University of Alabama, Alabama, U.S.A.
pcDNANDUN	Ampicillin	Mammalian	Full open reading frame of human PDE4D1 in pcDNA3	Prof. Graeme Bolger University of Alabama, Alabama, U.S.A.
pcDNAN43	Ampicillin	Mammalian	Full open reading frame of human PDE4D3 in pcDNA3	Prof. Graeme Bolger University of Alabama, Alabama, U.S.A.
pcDNAN79-VSV	Ampicillin	Mammalian	Full open reading frame of human PDE4D5 in pcDNA3 tagged with VSV	Prof. Graeme Bolger University of Alabama, Alabama, U.S.A.
pFLAG CMV RB3	Ampicillin	Mammalian	Full open reading frame of XAP2 in pFLAG CMV with FLAG in fusion with the N-terminal region	Prof. Graeme Bolger University of Alabama, Alabama, U.S.A.

Plasmid	Antibiotic Resistance	Expression	Description	Source
pcDNAARB2 FLAG	Ampicillin	Mammalian	Full open reading frame of β-arrestin2 in pcDNA3 with FLAG in fusion with the C-terminal	Prof. Graeme Bolger University of Alabama, Alabama, USA
pGEX NARB2	Ampicillin	*E.coli*	Full open reading frame of human β-arrestin2 in pGEX-5X3 with GST in fusion	Prof. Graeme Bolger University of Alabama, Alabama, USA
pGEX-hLyn	Ampicillin	*E.coli*	SH3 domain of human Lyn tyrosyl kinase in pGEX-2T with GST in fusion	Dr. William Wishart Sandoz Pharma, Basel, Switzerland
pGEX-p47*phox*	Ampicillin	*E.coli*	Human p47-*phox* in pGEX-6P1 with GST in fusion	Dr. Katrin Rittinger N.I.M.R., London, U.K.
pGEX-p47*phox* S304A	Ampicillin	*E.coli*	Human p47-*phox* in pGEX-6P1 with Serine 304 mutated to Alanine with GST in fusion	Derek Wallace (Houslay Laboratory)
pGEX-p47phox S320A	Ampicillin	*E.coli*	Human p47-*phox* in pGEX-6P1 with Serine 320 mutated to Alanine with GST in fusion	Derek Wallace (Houslay Laboratory)
pGEX-p47*phox* S328A	Ampicillin	*E.coli*	Human p47-*phox* in pGEX-6P1 with Serine 328 mutated to Alanine with GST in fusion	Derek Wallace (Houslay Laboratory)
pGEX-p47*phox* PX	Ampicillin	*E.coli*	*Phox* domain (5-122) of human p47-*phox* in pGEX-6P1 with GST in fusion	Dr. Katrin Rittinger N.I.M.R., London, U.K.
pGEX-p47*phox* SH3	Ampicillin	*E.coli*	SH3 domains (155-390) of human p47-*phox* in pGEX-6P1 with GST in fusion	Dr. Katrin Rittinger N.I.M.R., London, U.K.
pGEX-p67*phox*	Ampicillin	*E.coli*	Human p67-*phox* in pGEX-4T1 with GST in fusion	Dr. Katrin Rittinger N.I.M.R., London, U.K.

Table 2.4 – cDNA plasmid constructs used for protein over-expression in either *E.coli* or mammalian cells.

2.7 Mammalian Cell Transfection of siRNA

Small interfering RNAs (siRNAs) are 19-25 nucleotides long and can be used to knockdown protein expression in a plethora of mammalian cell types. The PolyFect® method of mammalian cell transfection, from QIAGEN® (Crawley, U.K.), was used for the transfection of the COS1 cell line with the Santa Cruz Biotechnology Inc. (Santa Cruz, CA, U.S.A.) MAPKAPK2 siRNA nucleotide. Flasks of confluent cells were passaged the day prior to transfection and plated to ensure 40-80% confluence on the day of transfection. These plates were incubated overnight at 37°C in an atmosphere of 95% (v/v) air and 5% (v/v) CO_2. The amount of siRNA required for each transfection plate is dependent upon the number of cells to be transfected and should be scaled accordingly. This protocol is accurate for 100mm plates of 40-80% confluent cells in 8ml growth media. 50-100nM of the siRNA nucleotide was diluted in antibiotic- and FCS-free DMEM to a final volume of 300µl. 25µl of PolyFect® Transfection Reagent was added to the siRNA-DMEM solution for COS1 cell transfection. The transfection reagents were incubated at room temperature for 5-10min to allow complex formation. Where co-transfection of a DNA plasmid and siRNA nucleotide was required 4µg of plasmid DNA and 50-100nM of siRNA was diluted in a final volume of 300µl of antibiotic- and FCS-free DMEM. 25µl of PolyFect® Transfection Reagent was then added to this DNA-siRNA-DMEM mix and incubated as described above. During the incubation period the growth media was removed from the plates and replaced with 7ml of fresh DMEM supplemented with 0.1% (v/v) penicillin/streptomycin (10000U/ml), 2mM glutamine and 10% (v/v) foetal calf serum (FCS). Following incubation, 1ml of supplemented DMEM containing antibiotics and 10% (v/v) FCS was added to the siRNA/DNA-DMEM-PolyFect® complex. This was mixed gently and added directly to the appropriate transfection plate. The plates were then incubated for approximately 2 days at 37°C in an atmosphere of 95% (v/v) air and 5% (v/v) CO_2 prior to any cell treatments and harvesting. Details of ligands and inhibitors used for cell treatments post-transfection are described in Table 2.5. Samples of native and siRNA transfected cell lysate were subjected to SDS-

PAGE and Western immuno-blotting, as described in Section 2.12, to determine protein expression knockdown.

2.8 Preparation of Rat Cardiac Myocytes

The preparation of rat cardiac myocytes from isolated rat hearts was undertaken in a sterile hood, according to the procedure described by Dostal et al., 1992. In detail, ADS buffer was prepared containing 120mM NaCl, 20mM N-2-hydroxyethylpiperazine-N'-2-ethanesulphonic acid (HEPES)-OH; pH 7.35, 0.8mM NaH_2PO_4/H_20, 5mM KCl, 0.4mM $MgSO_4/7H_2O$, 1% (w/v) glucose and 1% (v/v) penicillin/streptomycin (10000U/ml). To culture rat cardiac myocytes 100ml of ADS buffer alone, 100ml of ADS buffer containing 48mg collagenase II and 100ml of ADS buffer containing 60mg pancreatin were prepared and filter sterilised to produce the enzyme solution. Non-heart tissue was removed using forceps and blood drained by teasing apart the heart. The hearts were then diced using a scalpel and then removed to a 50ml universal. 25ml of ADS was used to wash any residual tissue into the universal and the tissue was allowed to settle at the bottom of the tube. The supernatant was then removed and discarded. 10ml of enzyme solution was added to the universal and incubated, at an angle, in a shaking water bath at 37°C, 130rpm for 4min. The supernatant was removed, discarded and a further 10ml of enzyme solution was added and the universal incubated at 37°C, 160rpm for 20min. This supernatant was added to 8ml of FCS in a fresh universal and tube inverted on ice. A further 10ml of enzyme solution was added to the rat hearts and incubated at 37°C, 160rpm for 20min. The supernatant was again removed and added to the tube containing FCS. This digestion process was repeated a further three times and each time the supernatant was added to FCS-containing tube. The tube was then centrifuged at 1,300 x *g* for 10min. The supernatant was discarded and the small pellet of cardiac myocytes carefully re-suspended, by pipetting, in 25ml of plating media composed of 66% (v/v) DMEM, 20% (v/v) M199, 8% (v/v) horse serum, 5% (v/v) FCS and 1% (v/v) penicillin/streptomycin (10000U/ml). The cell re-suspension was then centrifuged again, the supernatant

discarded, and re-suspended in 20ml of plating media (this was approximate for fifty rat hearts and scaled accordingly). The re-suspension solution was then added to a 100mm culture plate and incubated at 37°C for 1h. This allowed fibroblasts to adhere to the culture dish and cardiac myocytes to remain in the plating media. During this incubation, 10ml of sterile 70% (w/v) gelatin solution was added to each 100mm culture plate, incubated for 5-10min at room temperature, and then removed. Following incubation the cell media containing the cardiac myocytes was removed and centrifuged at 1,300 x *g* for 10min. The supernatant was discarded and the cells re-suspended in a sufficient volume of plating media for the number of 100mm plates required. For a single 100mm culture plate of cardiac myocytes approximately five rat hearts were required. The cells were incubated for approximately 24h at 37°C in an atmosphere of 95% (v/v) air and 5% (v/v) CO_2. The plating media was then replaced with maintenance media consisting of 75% (v/v) DMEM, 20% (v/v) M199, 4% (v/v) horse serum and 1% (v/v) penicillin/streptomycin (10000U/ml). The cells were then incubated for a further 24h at 37°C in an atmosphere of 95% (v/v) air and 5% (v/v) CO_2 prior to any cell treatments and harvesting. Details of ligands and inhibitors used for cell treatments are described in Table 2.5.

Compound	Desired Mode of Action	Concentration	Time
Forskolin	Directly activates adenylyl cyclase	100µM	10-20min
EGF	Activation of ERK1/2 and Akt/PKB	50ng/ml	30min
PMA	Activation of ERK1/2	100nM	20min
Insulin	Activation of Akt/PKB	1-10nM	15min
Anisomycin	Activation of p38 MAPK and MAPKAPK2	10µg/ml	60min
TNFα	Activation of p38 MAPK and MAPKAPK2	10ng/ml	5min
Angiotensin II	Assembly and activation of NADPH Oxidase	100nM	5min
H89	PKA inhibitor	1-10µM	10min
U0126	MEK inhibitor	10µM	60min
SB203580	p38 MAPK inhibitor	10µM	60min
IBMX	Non-specific PDE inhibitor	100µM	10min
Rolipram	Specific PDE4 inhibitor	10µM	10min

Table 2.5 – Desired mode of action, final concentrations and incubation times for ligands and inhibitors used for the treatment of mammalian cell lines.

2.9 Confocal Microscopy Analysis

COS1 or COS7 cells were transfected in 6-well plates with the appropriate DNA plasmid using the Roche® Diagnostics (Mannheim, Germany) FuGENE® 6 Transfection Reagent, as described in Section 2.6.3. Following protein expression for 24h and any subsequent cell treatments, as detailed in Table 2.5, the cells were fixed in sterile PBS containing 4% (v/v) para-formaldehyde, 5% (w/v) sucrose, 10mM $MgCl_2$, 150mM NaOH, and the pH was adjusted to 7.5 with 1.2ml HCl. The cells were then washed three times with 2ml of sterile PBS and the cover slips removed to the immunohistochemistry box. The cells were permeabilised with 200µl of 0.2% (v/v) TritonX-100. This was repeated three times and excess TritonX-100 removed by blotting with napkins. The proteins were then blocked using 10% (v/v) goat serum (dependent upon primary antibody host animal) and 2% (w/v) BSA diluted in 20mM Tris-Cl; pH 7.5 and 150mM NaCl. The protein of interest was detected using a specific primary anti-serum. 200µl of primary anti-serum diluted in TBS and blocking solution was added to the cover slips for 2h at room temperature. The cover-slips were washed three times with 200µl of blocking solution and incubated with 200µl of secondary antibody conjugated to Alexa® 594 from Molecular Probes (Eugene, OR, U.S.A.). The cells were fixed to the confocal slide using immuno-mount and observed using a Zeiss® Pascal laser-scanning microscope (Jena, Germany).

2.10 Preparation of Cell Lysates

2.10.1 Whole Cell Lysate

Confluent cells were harvested at temperatures less that 4°C using buffers that had been previously chilled to minimise protein degradation in the whole cell extract. The cell culture media was aspirated and the cells were washed twice with ice cold sterile PBS. The cell plates were drained thoroughly and the appropriate volume of cell lysis buffer added. For a 6-well plate, 100µl of cell lysis buffer was added whereas a 100mm plate received

500µl of cell lysis buffer. For the production of whole cell lysate, 3T3 lysis buffer composed of 25mM HEPES-OH; pH 7.5, 50mM NaCl, 10% (v/v) glycerol, 1% (v/v) Triton, 50mM NaF, 30mM Na pyrophosphate, 5mM EDTA and 1x solution of Roche® Diagnostics (Mannheim, Germany) protease inhibitor cocktail tablets was used. The cells were incubated for 5min with buffer on ice and then scraped into a 1.5ml Eppendorf® tube. The cell lysates were centrifuged in a bench-top, refrigerated centrifuge at 16,060 x *g* at 4°C and the supernatant retained. The cell lysates were then snap frozen on dry ice and stored at –80°C until required.

2.10.2 Sub-cellular Fractionation

This procedure was undertaken as described in numerous publications [Sullivan et al., 1998, McPhee et al., 1999, Rena et al., 2001 and Wallace et al., 2005]. Confluent cells were harvested at temperatures less that 4°C using buffers that had been previously chilled to minimise protein degradation in the sub-cellular fractions. The growth media was removed from the plates and the cells washed twice with ice cold, sterile PBS. The PBS was aspirated and the plates were left to drain. The plates were then washed with 500µl of sterile 50mM KCl, 50mM HEPES; pH 7.2, 10mM EGTA, 1.92mM $MgCl_2$, 1mM dithiolthreitol (DTT) and 1x solution of Roche® Diagnostics (Mannheim, Germany) protease inhibitor cocktail tablets (KHEM). The plates were left to drain for 5min and any excess KHEM was aspirated. The cells were then isolated by scraping into a 1.5ml Eppendorf® tube. The cells were homogenised on ice by drawing through a 26G needle and 1ml syringe, approximately 30 times, and centrifuged at 950 x *g* in a bench-top, refrigerated centrifuge for 10min at 4°C. The pellet formed at this stage was the P1 fraction (unbroken cells and nuclei). The supernatant was transferred into an ultra-centrifuge tube and centrifuged at 154,000 x *g* in a Beckman® TL-100 ultra-centrifuge for 30min at 4°C. The pellet formed at this stage was the P2 fraction (plasma membrane, golgi vesicles, endoplasmic reticulum, lysosomes and endosomes). The supernatant from this fraction was retained as the S fraction (enriched cytosolic proteins) and the volume noted. Both P1

and P2 fractions were washed twice in 500µl of KHEM at the centrifuge speeds described above for the relevant fraction (P1 = 950 x *g* for 10min and P2 = 154,000 x *g* for 30min). The pellets were then re-suspended in a volume of KHEM analogous to that of the supernatant fraction. All fractions were snap frozen on dry ice and stored at –80°C until required. To assess the sub-cellular distribution of a given protein equal volumes of P1, P2 and S fractions were subjected to SDS-PAGE and Western immuno-blotting, as described in Section 2.12. Western immuno-blots, within the linear range to the light produced from ECL, were then scanned and quantified using The Discovery Series™ Quantity One® 1-D Analysis Software, Version 4.4.0. The specific intensity of the immuno-reactive bands in the P1, P2 and S fractions, together with an appropriate background control reading, was determined within a constant measurement area. The sub-cellular distribution was then calculated as the relative percent contribution of P1, P2 and S immuno-reactivity, less the background response, as a function of the total densitometry readings (100%). Where any alteration in the sub-cellular distribution of a protein was to be determined Two-Sample t-test statistical analysis was applied to the densitometry data using MINITAB® Release 14.13 computer software. Alterations in the relative expression of a protein within a sub-cellular fraction was determined as statistically significant when $p < 0.05$ compared to the no treatment control.

2.11 Determination of Protein Concentrations (Bradford's Assay)

The protein concentration of purified recombinant proteins or cell lysates (whole or sub-cellular fractions) was determined using bovine serum albumin (BSA) as a standard in a spectrophotometric assay. The assays were undertaken in clear 96-well micro-titre plates. A standard curve of known BSA concentrations between 0µg/µl and 5µg/µl was generated diluted in sterile water to a final volume of 50µl. The protein sample of interest was assayed at various dilutions in a final volume of 50µl to ensure it was within the range of the standard curve. The extent of the dilution was factored into the final determination. Bradford reagent from Bio-Rad® (Hemel Hempstead,

U.K.) was diluted 1:5 with sterile water and 200µl was added to each well of the 96-well micro-titre plate [Bradford, 1976]. The intensity of the colour change (brown to blue) produced with this reagent on interaction with protein is directly proportional to the protein concentration. The 96-well plate was analysed with a 590nm test filter using a Dynex MRX micro-titre plate reader controlled through Dynex Revelation, Version 3.04 computer software. Protein concentrations were determined by plotting the standard curve and using least squared regression analysis to obtain the best-fit line. The equation of the line was used to determine the concentration of the protein samples and adjusted to account for any dilution factor.

2.12 Protein Analysis

2.12.1 SDS-PAGE

Sodium dodecyl sulphate-polyacrylamide gel electrophoresis (SDS-PAGE) is a method that is routinely employed to separate proteins by virtue of their molecular weight. Protein samples of 1-100µg were denatured and reduced by dilution in 10% (w/v) SDS, 300mM Tris-Cl; pH 6.8, 0.05% (w/v) bromophenol blue, 50% (v/v) glycerol and 10% (v/v) β-mercaptoethanol, herein referred to as 5x SDS sample buffer. The samples were boiled for 5min and then loaded directly to an appropriate well of an Invitrogen™ (Paisley, U.K.) NuPAGE® 4-12% Bis-Tris polyacrylamide gel immersed in Invitrogen™ NuPAGE® MES or MOPS SDS running buffer. 5µl of Bio-Rad® (Hemel Hempstead, U.K.) pre-stained molecular weight protein marker was also loaded to an appropriate well of the gel to allow the molecular weight of the proteins within the sample to be determined. The gels were run at 200V for 1h. For a more detailed description of Invitrogen™ NuPAGE® pre-cast gels and associated XCell II™ apparatus please consult the manufacturers instructions.

2.12.2 Coomassie® Staining

Proteins separated by SDS-PAGE can be visualised by a variety of methods. The limit of Coomassie® staining is approximately 0.1-0.5µg of protein per band on a polyacrylamide gel and resolves all proteins within a sample. Gels that required Coomassie® staining were removed form the pre-cast gel cassette and washed with sterile water to remove residual running buffer. Coomassie® stain consisting of 1.25g Coomassie® Brilliant Blue R_{250} (omit for de-stain), 444ml methanol, 56ml acetic acid in a final volume of 1000ml sterile water was added to the gel with gentle shaking for 2h at room temperature. The Coomassie® stain was removed and replaced with de-stain. De-stain removed all background staining with the Coomassie® stain remaining bound to the proteins resulting in the detection of all proteins present in the sample. The gel was then washed with sterile water and incubated with sterile water plus 10% (v/v) glycerol to aid the prevention of gel cracking following drying.

2.12.3 Western Immuno-blotting

Proteins separated by SDS-PAGE can be visualised by a variety of methods. Western immuno-blotting allows the detection of individual proteins with specific anti-sera. The proteins separated by SDS-PAGE were transferred to a nitrocellulose membrane using the XCell II™ blotting apparatus and NuPAGE® Transfer Buffer containing 20% (v/v) methanol. The proteins were transferred with an applied voltage of 30V for 1h. For a more detailed description of the XCell II™ apparatus set-up and buffer compositions please consult the manufacturers instructions. Following transfer of the sample proteins, as indicated by successful transfer of the pre-stained molecular weight markers, the nitrocellulose membrane was incubated or blocked in 5% (w/v) milk powder (Marvel®), re-constituted in 20mM Tris-Cl; pH 7.6, 150mM NaCl and 0.1% (v/v) Tween20 (TBST), for 1h at room temperature with gentle agitation. The primary antibody was added at the appropriate dilution (general dilution range 1:1000 to 1:10000) to a 1% (w/v)

milk powder TBST solution. Details of the primary antibodies used in experiments described in this thesis are shown in Table 2.6. The blocked nitrocellulose membrane was then sealed in an airtight plastic carrier containing the primary antibody solution and this was incubated for 1h at room temperature, or overnight at 4°C, with vigorous agitation. The membrane was then washed several times with TBST before the application of the appropriate horseradish peroxidase (HRP) conjugated anti-immunoglobulin G (IgG) secondary antibody diluted 1:5000 in 1% (w/v) milk powder TBST solution in a sealed, airtight plastic carrier. Similarly, this was incubated for 1h at room temperature, or overnight at 4°C, with vigorous agitation. The membrane was again washed several times with TBST before employing the Amersham Biosciences (Little Chalfont, U.K.) enhanced chemiluminescence (ECL) Western immuno-blotting kit as the visualisation protocol for detecting bound antibodies. Briefly, the bound antibodies were detected by exposure of the membrane, following washing in ECL solution, to blue-light sensitive autoradiography film and developed using the Kodak® X-Omat Model 2000 processor. For a more detailed description of the visualisation kit and autoradiography film processor please consult the manufacturers instructions.

2.12.4 Antibody Generation

The generation of anti-sera specific for the unique N-terminal region of PDE4A11 and the phosphorylated Ser-147 residue of PDE4A5 was undertaken by Cambridge Research Biochemicals Limited (Cleveland, U.K.). Briefly, rabbit anti-sera were generated against the following keyhole limpet haemocyanin (KLH)-conjugated peptides, Ala-Arg-Pro-Arg-Gly-Leu-Gly-Arg-Iso-Pro-Glu-Leu-Gln-Leu-Val-[Cys]-amide for PDE4A11 and [Cys]-Ser-Phe-Leu-Tyr-Arg-Ser-Asp-(p-Ser)-Asp-Tyr-Asp-Met-Ser-Pro-Lys-amide for the phosphorylated PDE4A5. The crude anti-sera for PDE4A11 were purified by affinity chromatography on Thiopropyl Sepharose 6B derivatised with antigen. The phospho-reactive serum to phosphorylated PDE4A5 peptide was affinity purified on a Thiopropyl Sepharose 6B column derivatised with non-phosphorylated antigen. The unbound serum was then applied to a similar

column derivatised with phosphorylated antigen. The eluate was retained where significant phospho-specific immuno-reactivity was demonstrated on peptide coated ELISA plates. Resultant glycine eluates for both PDE4A11 and Ser-147 phosphorylated PDE4A5 were used for Western immuno-blot analysis, as described above in Section 2.12.3.

Protein	Specificity	Type	Dilution*	Animal	Source
Human PDE4A	Conserved C-terminal region of human PDE4A isoforms	Serum	1:10000	Goat	Houslay Laboratory
Rat PDE4A	Conserved C-terminal region of rat PDE4A isoforms	Serum	1:5000	Goat	Houslay Laboratory
Rat PDE4A	Conserved C-terminal region of rat PDE4A isoforms	Serum	1:5000	Rabbit	Houslay Laboratory
PDE4B	Conserved C-terminal region of PDE4B isoforms in all species	Serum	1:5000	Goat	Houslay Laboratory
PDE4D	Conserved C-terminal region of PDE4D isoforms in all species	Serum	1:10000	Goat	Houslay Laboratory
PDE4A11	Unique N-terminal region of PDE4A11	Polyclonal	1:2000	Rabbit	Cambridge Research Biochemicals
PKA phosphorylated PDE4	Phosphorylated Ser residue in RRE**S***F motif in UCR1 of all PDE4 long isoforms	Serum	1:1000	Rabbit	Houslay Laboratory
MAPKAPK2 phosphorylated PDE4	Phosphorylated Ser residue in LYRSD**S*** motif in UCR1 of all PDE4 long isoforms	Polyclonal	1:1000	Rabbit	Cambridge Research Biochemicals
p44/p42 MAPK (ERK1/2)	Endogenous levels of p44/p42 MAPK. More specific for p42 MAPK	Polyclonal	1:1000	Rabbit	Cell Signaling Technology®
Activated p44/p42 MAPK (ERK1/2)	Endogenous levels of phosphorylated p44/p42 MAPK at Thr202 and Tyr204	Monoclonal	1:2000	Mouse	Cell Signaling Technology®
Akt	Endogenous levels of Akt1, Akt2 & Akt3 proteins	Polyclonal	1:1000	Rabbit	Cell Signaling Technology®
Activated Akt	Endogenous levels of phosphorylated Akt at Ser473 only & not Thr308	Monoclonal	1:1000	Mouse	Cell Signaling Technology®
p38 MAPK	Endogenous levels of p38 MAPK	Polyclonal	1:1000	Rabbit	Cell Signaling Technology®

Protein	Specificity	Type	Dilution*	Source	Supplier
Activated p38 MAPK	Endogenous levels of phosphorylated p38 MAPK at Thr180 & Tyr182	Polyclonal	1:1000	Rabbit	Cell Signaling Technology®
MAPKAPK2	Endogenous levels of MAPKAPK2	Polyclonal	1:1000	Rabbit	Cell Signaling Technology®
Activated MAPKAPK2	Endogenous levels of phosphorylated MAPKAPK2 at Thr334 only & not Thr25, Thr222 & Ser272	Polyclonal	1:1000	Rabbit	Cell Signaling Technology®
XAP2	Recognises immunophilin ARA9, AIP or XAP2	Serum	1:1000	Rabbit	Houslay Laboratory
β-arrestin2	Recognises C-terminal region of β-arrestin1/2	Polyclonal	1:1000	Rabbit	Houslay Laboratory
p47-*phox*	Human p47-*phox* with minimal cross-reactivity with bovine p47-*phox*	Serum	1:1000	Rabbit	Upstate®
GST	Recognises GST-tag fusion proteins	Polyclonal	1:1000	Rabbit	Houslay Laboratory
VSV	Recognises an epitope containing the five C-terminal amino acids of VSV glycoprotein	Monoclonal	1:5000	Mouse	Sigma-Aldrich®
FLAG	Recognises an epitope containing DYKDDDDK	Monoclonal	1:5000	Source	Sigma-Aldrich®

Table 2.6 – Anti-sera used for Western immuno-blotting.

*Dilution factor is correct for Western immuno-blotting. Antibody titrations should be undertaken for immuno-precipitation and immuno-histochemistry.

2.13 Fusion Protein Interactions

2.13.1 Pull-down Assays

The expression and purification of GST fusion proteins in *E.coli* was undertaken as described in Section 2.4.2. COS7 cells were transfected to transiently express specific PDE4A isoforms as described in Section 2.6.1 and subjected to sub-cellular fractionation as described in Section 2.10.2. Assessment of the interaction of PDE4A isoforms with GST fusion proteins has been described previously [McPhee et al., 1999, Huston et al., 2000 and Rena et al., 2001]. Briefly, 400µg of the GST fusion protein, or GST alone as a control, was immobilised on a 40µl bed volume of Amersham Biosciences (Little Chalfont, U.K.) glutathione sepharose resin. The resin was pelleted by centrifugation at 1,000 x *g* for 5min at 4°C using a refrigerated bench-top centrifuge. The supernatant was discarded. The pellets were then re-suspended in 500µl (approximately 200µg of protein) of cytosolic, or S fraction, produced from COS7 cells expressing equal immuno-reactive amounts of PDE4A isoforms, as determined by Western immuno-blotting with a PDE4A C-terminal specific anti-serum. The protein samples were diluted in KHEM, the buffer used for sub-cellular fractionation of mammalian cells. The immobilised fusion protein and cytosol were incubated together for 1h end-over-end at 4°C. The glutathione sepharose resin was then collected by centrifugation at 1,000 x *g* for 5min at 4°C. The supernatant was retained for Western immuno-blotting to measure the extent of PDE4A remaining unbound to the GST fusion protein. The beads were washed three times with 500µl of KHEM by centrifugation at 1,000 x *g* for 5min at 4°C. The supernatant was discarded and the beads re-suspended in 40µl of SDS sample buffer to elute the bound proteins. Protein samples of PDE4A expressed in cytosolic cell lysate, PDE4A bound to GST, PDE4A unbound to the GST fusion protein and PDE4A bound to the GST fusion protein were analysed by SDS-PAGE, as described in Section 2.12.1, and immuno-probed for PDE4A using a C-terminal, species and sub-family specific anti-serum, as described in Section 2.12.3.

2.13.2 Peptide Arrays

Peptide arrays are Whatman® 50 cellulose membranes on which peptide sequences are directly synthesised [Reineke et al., 2001 and Frank, 2002]. These peptide arrays are able to bind purified recombinant proteins and provide evidence for direct protein interaction and the elucidation of the critical domains and residues involved [Espanel and Hooft van Huijsduijnen, 2005 and Bolger et al., 2006]. The peptide arrays used in the experiments detailed in this thesis were kindly produced by Dr. E. Klussmann (Forschungsinstitut für Molekulare Pharmakologie, Berlin, Germany) using the Intavis Bioanalyical Instruments (Köhn, Germany) AutoSpot-Robot ASS 222 and utilising Fmoc-chemistry. Recombinant GST fusion proteins were produced to homogeneity, as described in Section 2.4.2. The peptide arrays were activated by immersion in 100% (v/v) ethanol and then washed in TBST for 10min at room temperature on an orbital shaker. The peptide arrays were then incubated or blocked with 5% (w/v) milk powder (Marvel®), re-constituted in 20mM Tris-Cl; pH 7.6, 150mM NaCl and 0.1% (v/v) Tween20 (TBST) for 1h at room temperature with vigorous agitation. 3-10µg/ml of recombinant GST fusion protein, or GST alone as a control, was then diluted in 1% (w/v) milk powder TBST solution and incubated with the peptide array in an airtight plastic carrier overnight at 4°C with vigorous agitation. The peptide array was then subjected to three 10min washes in TBST. The recombinant GST fusion protein was then detected for direct binding to the peptide array by probing with a specific primary anti-serum or an anti-serum specific for GST. As a general rule the primary anti-sera were used at two-fold less than the recommended dilution for Western immuno-blotting. Details of the primary antibodies used in the experiments described in this thesis are shown in Table 2.6. The membrane was then washed several times with TBST before application of the appropriate horseradish peroxidase (HRP) conjugated anti-immunoglobulin G (IgG) secondary antibody diluted 1:5000 in 1% (w/v) milk powder TBST solution in a sealed, airtight plastic carrier. Similarly, this was incubated for 1h at room temperature, or overnight at 4°C, with vigorous agitation. The membrane was again washed several times with TBST before

employing the Amersham Biosciences (Little Chalfont, U.K.) enhanced chemiluminescence (ECL) Western immuno-blotting kit as the visualisation protocol for detecting bound antibodies. Briefly, the bound antibodies were detected by exposure of the peptide array, following washing in ECL solution, to blue-light sensitive autoradiography film and developed using the Kodak® X-Omat Model 2000 processor. For a more detailed description of this kit or the autoradiography film processor please consult the manufacturers instructions. The resolution of spots, distinct from the GST control peptide array, on the autoradiography film were indicative of a positive interaction of the recombinant fusion protein with the peptide array and the critical sequences were analysed for putative consensus sites or binding motifs.

2.14 Co-immuno-precipitation

Mammalian cell lines were co-transfected, as described above in Section 2.6 and cell lysates were produced by sub-cellular fractionation as described above in Section 2.10.2. The protein concentrations of the cytosolic, or S fractions were determined, as described above in Section 2.11, and the concentrations equalised for all samples to contain approximately 250µg of protein in a 500µl volume of ice-cold KHEM. A 30µl sample of the diluted lysate was removed for Western immuno-blotting to determine the relative immuno-reactive inputs of the co-expressed proteins for the co-immuno-precipitation experiment. Anti-FLAG or anti-VSV agarose beads were pre-equilibrated in ice-cold KHEM to produce a 50% slurry. 60µl of the slurry was added to each 500µl protein sample and these were incubated end-over-end for 2h at 4°C. The samples were centrifuged at 16,060 x *g* for 5min at 4°C using a bench-top refrigerated centrifuge. 30µl of supernatant was removed to screen for unbound proteins. The agarose resin was washed three times in 500µl of ice-cold KHEM and once in 500µl of ice-cold PBS by centrifugation at 16,060 x *g* for 1min at 4°C. Bound proteins were then eluted in SDS sample buffer and subjected to SDS-PAGE and Western immuno-blotting, as described in Sections 2.12.1 and 2.12.3 respectively. Using The Discovery Series™ Quantity One® 1-D Analysis Software, Version 4.4.0, the

intensity of the immuno-reactive amounts of the co-expressed proteins, in both the initial cell lysate and following co-immuno-precipitation, was determined. Each measurement was undertaken within a constant measurement area using scanned Western immuno-blots within the linear range to the light produced from ECL. In each case the densitometry readings were corrected with an appropriate background control. The immuno-reactive amounts of protein co-immuno-precipitated were then corrected for the immuno-reactivity of the same protein in the initial cell lysate. These ratios were then used to compare the interaction efficiency of the two proteins and to assess conditions that may facilitate the modulation of the specific interaction. Any modifications to the interaction efficiency were compared relative to the control co-immuno-precipitation (100%). Paired t-test statistical analysis was applied to the quantified data using MINITAB® Release 14.13 computer software, where $p < 0.05$ indicates a statistically significant difference in the relative amounts of protein co-immuno-precipitated compared to the untreated control. Control immuno-precipitations were undertaken in a similar manner with cell lysates produced from cells singly transfected with the protein that was to be co-immuno-precipitated. This facilitated screening for non-specific binding to the chosen agarose bead conjugate.

2.15 Phosphodiesterase Activity Assay

To measure PDE activity a radioactive cAMP hydrolysis assay was employed. This procedure has been described previously [Marchmont and Houslay, 1980] and is a modification of a historical two-step procedure [Thomson and Appleman, 1971]. PDE enzymes hydrolyse cAMP, which results in the formation of 5' AMP. In this assay, both [8-^{3}H] adenosine 3', 5'-cyclic mono-phosphate from Amersham Biosciences (Little Chalfont, U.K.) and adenosine 3', 5'- cyclic mono-phosphate are hydrolysed. Addition of Snake Venom from Ophiophagus Hannah prevents re-circularisation of uncharged 5' AMP by further hydrolysis to adenosine and the Dowex slurry binds charged, un-hydrolysed cAMP.

2.15.1 Activation of Dowex 1x8-400 Anion Exchange Resin

Dowex 1x8-400 was prepared and activated by dissolving 400g of Dowex resin in 4l of 1M NaOH. The solution was stirred for 15min at room temperature and the resin allowed to settle. The supernatant was removed and the Dowex resin extensively washed thirty times with 4l of distilled water and allowed to settle after each wash. After thirty washes the resin was washed with 4l of 1M HCl for 15min at room temperature and allowed to settle. The resin was then washed a further 5 times with distilled water and stored at 4°C as 1:1 slurry with distilled water. Following this procedure generally produced approximately 1l of Dowex slurry. This Dowex slurry was utilised in the PDE assay as a 2:1 solution of slurry to 100% (v/v) ethanol.

2.15.2 Assay Procedure

The entire assay procedure was undertaken using 1.5ml Eppendorf® tubes per reaction. The cAMP substrate solution for the assay was composed of 2µl of 1mM 3', 5' cyclic adenosine mono-phosphate and 3µl of [8-^{3}H] 3', 5' cyclic adenosine mono-phosphate per millilitre of 20mM Tris-Cl; pH 7.4 and 10mM $MgCl_2$. The appropriate volume of purified protein or cell extract was diluted to a final volume of 50µl in 20mM Tris-Cl; pH 7.4. 50µl in 20mM Tris-Cl; pH 7.4 was used as the blank control. The exact volume of purified protein or cell extract required in the assay was pre-determined in a pilot assay using increasing concentrations of protein samples. 50µl of cAMP substrate was added to 50µl of the PDE containing sample, mixed, and these were then incubated in a water bath at 30°C for 10min. The samples were then placed in a boiling bath for 2min to inactivate the PDE and stop the reaction. The tubes were then cooled on ice for a minimum of 15min. 25µl of 1mg/ml snake venom from *Ophiophagus Hannah* was then added to the reaction tubes, mixed, and incubated for a further 10min at 30°C. 400µl of Dowex/ethanol solution was added to each reaction tube, mixed, and incubated on ice for a further 15min. Following incubation the tubes were then mixed again and centrifuged at 16,060 x *g* for 3min at 4°C in a

refrigerated bench-top centrifuge. 1ml of Opti-Flow SAFE 1 scintillant was added to fresh 1.5ml Eppendorf® tubes. 150µl of supernatant from the reaction tubes was added to an individual tube containing scintillant with 50µl of cAMP substrate solution added to a scintillant vial to determine total counts per minute for the assay. All tubes containing scintillant were mixed and hydrolysed 3', 5' cyclic adenosine mono-phosphate and [8-^{3}H] 3', 5' cyclic adenosine mono-phosphate was measured using a Wallac® 1409 Liquid Scintillation Counter.

2.15.3 Determination of Phosphodiesterase Activity

To determine specific PDE activity contained within any reaction tube the following formula was applied, 2.61 x (value – blank / average total) x 10^{-11} x 10^{12} x (1000 / µg protein) resulting in PDE activity in pmoles/min/mg protein. To assess the effect of PDE inhibition, the activity of samples containing inhibitor were directly compared to an uninhibited control reaction and was expressed as the percentage of the aforementioned uninhibited control.

2.16 Thermal Stability Assays

Twenty assay tubes were set-up for a PDE activity assay, as described in Section 2.15.2. Each tube contained a pre-determined volume of cell extract, expressing the desired PDE4A, in a final volume of 50µl in 20mM Tris-Cl; pH 7.4. The assay tubes were placed in a 55°C water bath and one assay tube was removed to ice every 30s until none were remaining. 50µl of cAMP substrate was then added to 50µl of the de-natured PDE sample and the activity assay continued as described above. The log residual PDE activity was determined against a control cell extract and the thermal stability profile plotted as a function of time, with the half-life ($t_{1/2}$) determined as the time in which 50% of the activity remained. Statistical comparison of the determined half-life values for each PDE4A enzyme preparation was undertaken using MINITAB® Release 14.13 computer software and a Paired t-test, where $p < 0.05$ indicates statistical significance.

2.17 Phosphorylation Assays

All phosphorylation assays were undertaken using Amersham Biosciences (Little Chalfont, U.K.) ^{32}P labelled radioisotopes. All radioactive experiments were undertaken in accordance with the Ionising Radiations Regulations 1999 and local rules. All experiments requiring the use of ^{32}P labelled radioisotopes were undertaken behind Perspex® shields. The wearing of a film badge dosimeter monitored all personal exposure. In every phosphorylation experiment using ^{32}P labelled radioisotopes, the rate of disintegration (half-life = 14.3 days) was taken into account and the activity of the source adjusted accordingly.

2.17.1 In Vitro Phosphorylation

The expression and purification of MBP or GST fusion proteins in *E.coli* was undertaken as described in Section 2.4 and the concentration of the purified protein determined as described in Section 2.11. 1µg of fusion protein and a defined amount of Upstate (Dundee, U.K.) recombinant protein kinase (concentration required was detailed on the accompanying information sheet for the specific lot of recombinant protein kinase) were diluted in 20mM MOPS; pH 7.2, 25mM β-glycerol phosphate, 5mM EGTA, 1mM sodium orthovanadate and 1mM DTT to a final volume of 40µl. 10µl of 1µCi/µl ^{32}P-ATP diluted in 75mM $MgCl_2$ and 500µM ATP was added to the target recombinant fusion protein and specific kinase mix. The reaction was incubated at 30°C for 10min. The reaction was stopped by the addition of 12.5µl of 5x SDS sample buffer. The reaction tubes were mixed and heated for 10min at 70°C on a heating block. The tubes were then centrifuged at 16,060 x *g* for 1min and 30µl of the sample subjected to SDS-PAGE and transferred to a nitro-cellulose membrane, as described in Sections 2.12.1 and 2.12.3 respectively. The nitro-cellulose membranes were then air-dried and scanned using the Bio-Rad® (Hemel Hempstead, U.K.) Personal Molecular Imager® FX to resolve the radioactive regions utilising phosphor image screen technology. The Discovery Series™ Quantity One® 1-D

Analysis Software, Version 4.4.0 was used to quantify the intensity of each radioactive band. These measurements were undertaken within a constant measurement area and any appropriate background readings were subtracted. The membranes were then used for standard Western immuno-blotting, as described in Section 2.12.3. Western immuno-blots, within the linear range to the light produced from ECL, were scanned and quantified as a measurement of the relative immuno-reactive amount of target protein in the assay Again, these data were generated using The Discovery Series™ Quantity One® 1-D Analysis Software, Version 4.4.0. In all cases the extent of the phosphorylation was corrected for the immuno-reactive amount of target protein in the assay and any change expressed as a percentage of the wild type control (100%). Paired t-test statistical analysis of data were undertaken using MINITAB® Release 14.13 computer software, where $p < 0.05$ indicates a statistically significant change in the degree of phosphorylation compared to the wild type control.

2.17.2 In Vivo Phosphorylation

2.17.2.1 Detection by Western Immuno-blotting

Mammalian cells were transfected to express the desired protein using any of the transfection methods described in Section 2.6. Approximately 24-48h after transfection the cells were treated with the appropriate ligands and inhibitors as detailed in Table 2.5. The cells were then harvested in 3T3 lysis buffer, as described in Section 2.10.1 and the protein concentration determined, as described in Section 2.11. All samples were diluted to contain equal protein concentrations and 30µl was subjected to SDS-PAGE, as described in Section 2.12.1. The resolved proteins were then transferred to a nitro-cellulose membrane and probed for the specific phosphorylated residue on the expressed target protein using a specific phospho anti-serum. The native protein was also probed using a specific anti-serum to assess expression levels. The Western immuno-blotting procedure is described in Section 2.12.3 and the anti-sera used to probe for phosphorylated and native

proteins detailed in Table 2.6. Using The Discovery Series™ Quantity One® 1-D Analysis Software, Version 4.4.0 and scanned Western immuno-blots within the linear range to the light produced from ECL, the relative intensity of the immuno-reactive amounts of phosphorylated protein, as detected using the specific phospho anti-serum, was determined. These data were then corrected against the intensity of the immuno-reactive amounts of native, non-phosphorylated protein, using an anti-serum to detect expression levels. Each densitometry reading was undertaken within a constant measurement area and was corrected using an appropriate background control. The degree of phosphorylation was calculated as the ratio of the phosphorylated protein densitometry reading over the corresponding non-phosphorylated densitometry reading. Changes in the degree of phosphorylation were expressed as a percentage of the maximum response (100%).

2.17.2.2 Radioactive Whole Cell Labelling

COS1 cells were transfected to express the desired protein using any of the transfection methods described in Section 2.6. Approximately 24h after transfection the DMEM supplemented with 0.1% (v/v) penicillin/streptomycin (10000U/ml), 2mM glutamine and 10% (v/v) FCS was removed and replaced with 5ml of phosphate-free DMEM containing 0.1% (v/v) penicillin/streptomycin (10000U/ml), 2mM glutamine and 10% (v/v) FCS. The phosphate was then re-introduced to the medium using 500µCi of [^{32}P]-orthophosphate. The cells were then incubated overnight in an atmosphere of 95% (v/v) air and 5% (v/v) CO_2 in a Perspex® box with the lid slightly open to allow for sufficient aeration. The cells were then treated with the appropriate ligands and inhibitors, as detailed in Table 2.5. The cell media was removed, washed twice with ice-cold PBS and then harvested in ice-cold 100mM sucrose, 80mM β-glycerol phosphate, 20mM EGTA, 15mM $MgCl_2$, 1mM DTT, 2mM ATP, 0.5% (v/v) NP-40 and containing 1x Roche® Diagnostics (Mannheim, Germany) protease inhibitor cocktail tablets. The whole cell lysate was subsequently prepared as described in Section 2.10.1. 30µl of whole cell lysate was removed for standard Western immuno-blotting to

ensure that the appropriate endogenous kinase had been activated and inhibited by the respective cell treatments, as shown in Table 2.5. Anti-sera specific for activation and expression of the kinases are detailed in Table 2.6. The cell lysates were then divided equally and 5µl of anti-sera for the specific protein or appropriate fusion tag was added to one aliquot for immuno-precipitation. Aliquots of cell lysate without antibody were used as agarose resin only control immuno-precipitations. The lysates were incubated for 1h on ice with mixing every 10min. Amersham Biosciences (Little Chalfont, U.K.) Protein G agarose resin was pre-equilibrated with cell lysis buffer to produce a 50% slurry. Following the 1h incubation on ice with antibody, 60µl of Protein G agarose resin slurry was added to each tube, i.e. both control and PDE4 immuno-precipitations. The lysates were incubated for 1h on ice with mixing every 10min. The samples were then centrifuged at 16,060 x *g* for 1min and the supernatant removed. The immuno-precipitated proteins bound to the Protein G agarose resin were washed twice in 500µl of lysis buffer before a final wash in 500µl of ice-cold PBS. The final supernatant was removed and the bed volume of agarose resin was re-suspended in 30µl of 5x SDS sample buffer. The reaction tubes were mixed and heated for 10min at 70°C on a heating block. The tubes were then centrifuged at 16,060 x *g* for 1min and 30µl of the sample subjected to SDS-PAGE and transferred to a nitro-cellulose membrane, as described in Sections 2.12.1 and 2.12.3 respectively. The nitro-cellulose membranes were then air-dried and scanned using the Bio-Rad® (Hemel Hempstead, U.K.) Personal Molecular Imager® FX to resolve the radioactive regions utilising phosphor image screen technology. The Discovery Series™ Quantity One® 1-D Analysis Software, Version 4.4.0 was used to determine the densitometry of the relevant radioactive regions, less an appropriate background control. Each densitometry reading was taken within a consistent measurement area. The membranes were then used for standard Western immuno-blotting, as described in Section 2.12.3, to assess the immuno-reactive amounts of target protein immuno-precipitated. The Discovery Series™ Quantity One® 1-D Analysis Software, Version 4.4.0 was also used to assess the relative immuno-reactive band intensity of the target protein immuno-precipitated using scanned Western immuno-blots within the linear range to the light produced from ECL. All measurements

were undertaken in a consistent measurement area, less any relevant background control reading. To determine the degree of phosphorylation the densitometry of specific radioactive bands were corrected for the densitometry reading for the corresponding immuno-precipitated target protein. All data were expressed as a percentage of the no treatment control (100%). Paired t-test statistical analysis of data were undertaken using MINITAB® Release 14.13 computer software, where $p < 0.05$ indicates statistical significance in the level of phosphorylation as a result of the indicated cell treatments compared to the no treatment control.

2.17.3 Peptide Array Phosphorylation

Peptide arrays are Whatman® 50 cellulose membranes on which peptide sequences are directly synthesised [Reineke et al., 2001 and Frank, 2002]. The peptide arrays used in the experiments detailed in this thesis were kindly produced by Dr. E. Klussmann (Forschungsinstitut für Molekulare Pharmakologie, Berlin, Germany) using the Intavis Bioanalyical Instruments (Köhn, Germany) AutoSpot-Robot ASS 222 and utilising Fmoc-chemistry. The peptide array was activated by immersion in 100% (v/v) ethanol and then incubated in 20mM HEPES; pH 7.4, 100mM NaCl, 5mM $MgCl_2$, 1mM DTT and 0.2mg/ml BSA, herein referred to as membrane phosphorylation buffer, for 1h at room temperature on an orbital shaker. The peptide array was then blocked overnight at 4°C in membrane phosphorylation buffer containing 1mg/ml BSA and 100µM ATP. The peptide array was then incubated in membrane phosphorylation buffer containing 50µM ATP, 10µCi [^{32}P]-ATP plus Upstate (Dundee, U.K.) recombinant protein kinase (concentration required was detailed on the accompanying information sheet for the specific lot of recombinant protein kinase). The peptide array was incubated for 30min at 30°C on an orbital shaker contained in a Perspex® box. A control peptide array phosphorylation was undertaken without the addition of the recombinant protein kinase to screen for any non-specific [^{32}P]-ATP binding. The peptide array was extensively washed ten times for 15min in 1M NaCl, three times for 5min in water, three times for 15min in 5% (w/v) H_3PO_4 in water, three times

for 5min in water and finally twice for 2min in 100% (v/v) ethanol. The peptide arrays were then air-dried and scanned using the Bio-Rad® (Hemel Hempstead, U.K.) Personal Molecular Imager® FX to resolve the radioactive regions utilising phosphor image screen technology.

2.18 Caspase-3 Cleavage Assay

Recombinant caspase-3 was produced as an active species, as described elsewhere [Huston et al., 2000]. COS7 cells were transfected to transiently express specific PDE4A isoforms as described in Section 2.6.1 and subjected to sub-cellular fractionation as described in Section 2.10.2. 10µg of cytosolic, of S fraction, expressing the required PDE4A isoform, was incubated with 147ng of active p20 caspase-3 for 2h at 37°C and the final reaction volume made up to 25µl with KHEM. 5µl of 5x SDS sample buffer was added to stop the reaction and the resultant protein degradation analysed by SDS-PAGE, as described in Section 2.12.1, and immuno-probed for PDE4A using a C-terminal, species and sub-family specific anti-serum, as described in Section 2.12.3.

2.19 Analysis Software

The primary amino acid sequences of proteins were analysed by ScanSite (http://scansite.mit.edu/cgi-bin/motifscan_seq), a protein phosphorylation and protein-protein interaction database centred upon peptide library data. These protein scans were carried out on high or medium stringency to identify putative phosphorylation and interaction motifs.

All schematic diagrams were generated using Microsoft® PowerPoint® and all graphs were generated using Microsoft® Excel®. All concentration response curves were generated using Kaleidograph® curve fitting computer software and fitting the IC_{50} equation. All densitometry of Western immuno-blots, within the linear range to the light produced from ECL, and phosphor image scans were quantified using The Discovery Series™ Quantity One® 1-

D Analysis Software, Version 4.4.0. Paired t-test or Two-Sample t-test statistical analysis of data were undertaken using MINITAB® Release 14.13 computer software and statistical significance is indicated using the convention * $p < 0.05$, ** $p < 0.01$ and *** $p < 0.001$.

Chapter 3 Characterisation of a novel PDE4 isoform, PDE4A11

3.1 Introduction

There are now approximately 21 proteins within the human PDE4 family of enzymes and these are encoded by up to four genes, PDE4A – 4D [Zhang et al., 2005]. A single gene mapped to the p13.2 region on human chromosome 19 encodes the PDE4A isoforms [Sullivan et al., 1998]. PDE4A isoforms are individually characterised by their unique N-terminal regions, which are encoded by a single 5' exon. Furthermore, three distinct types of enzyme are generated as a consequence of alternative mRNA splicing [Bolger et al., 1996 and Bolger et al., 1997]. Splicing results in the differential inclusion of UCR1 and/or UCR2 regulatory modules. This generates long isoforms that include both UCR1 and UCR2, short isoforms that lack UCR1, and super-short isoforms that lack UCR1 and have a truncated UCR2. To date, five human PDE4A isoforms have been identified and characterised. These include the long isoforms PDE4A4B (pde46) [Huston et al., 1996], PDE4A10 [Rena et al., 2001] and PDE4A11 [Wallace et al., 2005]. PDE4A1 (hRD1) is expressed as a super-short enzyme [Sullivan et al., 1998]. PDE4A7 (2el) is a unique PDE4 in that it is truncated from both the N- and C-terminal regions rendering the enzyme catalytically inactive [Horton et al., 1995 and Johnston et al., 2004]. PDE4A isoforms are ubiquitously expressed on a cell-type specific basis and endogenous expression is considered to be lower than that of the PDE4B and PDE4D isoforms.

The sequencing and analysis of the PDE4A gene locus on chromosome 19 proposed that a third PDE4A long isoform exists [Sullivan et al., 1998]. The identification and characterisation of the third human PDE4A long isoform, known as PDE4A11, is described here in Chapter 3.

3.2 Results

3.2.1 Identification of the PDE4A11 Exon and Predicted Amino Acid Sequences

Genomic analysis of the 38kb human PDE4A gene locus identified a putative unique 5' exon thought to encode a novel PDE4A long isoform, now known as PDE4A11 [Sullivan et al., 1998 and Wallace et al., 2005]. Figure 3.1 illustrates the positioning of this 5' exon that encodes the unique N-terminal region of PDE4A11. The PDE4A gene is orientated 5' to 3' telomere to centromere with exon 1 of PDE4A4B positioned furthest, in the 5' direction, from the PDE4A common exon 2. Exon 1 of PDE4A11 is located approximately 10kb in the 3' direction with exon 1 of PDE4A10 found a further 1kb downstream. Using the putative nucleotide sequence of the PDE4A11 encoding exon, the BLAST algorithm, and the expressed sequence tag (EST) and high-throughput sequence nucleotide databases, PDE4A11 sequences were identified in a number of species including human, mouse, rat, bat and pig [Wallace et al., 2005]. These EST data clearly exhibited sequence homology akin to a PDE4A long form and supports the notion that exon 1 of PDE4A11 splices directly to exon 2, which encodes the PDE4A common long form region (CLFR) and a proportion of UCR1. Expression of exon 1 encoding PDE4A11 yields an 81 amino acid unique N-terminal region. Figure 3.2 shows the comparison of the similar sequences found in mouse, rat, bat and pig where distinct homology is observed. Although the homology between human and mouse sequences is only approximately 50%, and the human sequence is 81 amino acids compared to the mouse sequence at 66 amino acids, and at variance with the sequences for PDE4A1 [Sullivan et al., 1998], PDE4A4B [Huston et al., 1996 and Sullivan et al., 1998] and PDE4A10 [Rena et al., 2001], a cross species consensus sequence that accurately represents the PDE4A11 N-terminal region can be resolved. Bat and pig homology is much greater with approximately 90% of amino acids conserved.

3.2.2 Analysis of 5' Promoter Activity

Analysis of the 5' sequence preceding the PDE4A11 exon identified possible DNA polymerase II promoter regions capable of supporting DNA transcription complexes [Wallace et al., 2005]. Promoter activity of the 1kb region preceding the initiating ATG start codon for PDE4A11 was assessed using a luciferase reporter assay system [Wallace et al., 2005]. Luciferase activity was optimal when transcription was driven by the first 250bp immediately upstream of the PDE4A11 start codon. Luciferase activity was attenuated by approximately 50% when the preceding 500bp were assessed indicating a level of repressive transcription control in the second 250bp region. Similar levels of promoter activity were measured with the first 1kb preceding the PDE4A10 start codon whereas lower promoter activity was measured with the corresponding region preceding the PDE4A4B start codon [Rena et al., 2001 and Wallace et al., 2005].

3.2.3 Expression Profile of PDE4A11

As discussed previously in Section 1.7.1, the structure of long form PDE4 enzymes is generally constructed of a unique N-terminal region, two common UCRs, linked to each other and the common catalytic unit through two sub-family specific LRs, and terminate with a sub-family specific C-terminal tail. This modular structure is shown schematically in Figures 1.5 and 3.3. Intron-spanning primers to the unique N-terminal region of PDE4A11 and the common UCR1, LR1 and LR2 domains were designed, as detailed in Table 2.3, to establish the authenticity of the novel PDE4A11 isoform. Generic PDE4A primers to the common UCR2 and catalytic domain were also designed to function as control primers. Using mRNA from HEK293 cells and brain tissue respectively, the validity of the PDE4A11 isoform was demonstrated utilising RT-PCR across the long form splice junctions. Generic PDE4A transcripts of 506bp (UCR2 to catalytic unit), and two PDE4A11 specific transcripts of 497bp (N-terminal to UCR1) and 886bp (N-terminal to LR2) respectively were generated, as shown in Figure 3.3, confirming the

aforementioned EST data demonstrating PDE4A11 as a bona fide PDE4A long isoform.

To profile the tissue expression of PDE4A11, a panel of first strand cDNA isolated from various human tissues were used as PCR template sequences. Utilising RT-PCR and a primer pair designed to the unique N-terminal region of PDE4A11 and the PDE4A common LR1 domain, PDE4A11 specific transcripts of 494bp were detected, as shown in Figure 3.4. Significant detection of PDE4A11 transcripts was observed in adult liver, stomach, testis, thyroid, adrenal gland, polymorphonuclear blood leukocytes (PBLs), and foetal brain. To a lesser degree transcripts were also detected in adult brain, kidney, placenta, pancreas, ovary, uterus, skin and foetal liver. This expression profiling shows PDE4A11 to be widely expressed in various human tissues. Of particular interest is the change in transcript levels from foetal to adult tissue indicating the possibility for developmental changes in PDE4A11 expression. PDE4A11 transcripts in the brain were attenuated in adult on comparison with the transcript levels in foetal brain tissue. Conversely, PDE4A10 transcripts were not detected in foetal brain, but are clearly present in the adult [Rena et al., 2000]. PDE4A11 transcripts in the liver are enhanced in adult tissue when compared to the foetal tissue transcript level. Significant detection of PDE4A11 transcripts emerged in PBLs. Indeed, it appears that PDE4A11 transcripts are the major transcripts in nearly all immune and inflammatory cell types [Wallace et al., 2005]. Mast cells, eosinophils, macrophages, natural killer cells and monocytes show significant PDE4A11 transcripts when compared to PDE4A4B and PDE4A10. Interestingly, PDE4A11 is also the major PDE4A transcript in bronchial smooth muscle cells.

3.2.4 *Expression of Recombinant PDE4A11 in COS7 Cells*

The entire open reading frame (ORF) of human PDE4A11 was generated by PCR and sub-cloned into pcDNA3 for transient expression in COS7 cells. COS7 cells have basal PDE activity of 4-6pmol/min/mg of

protein. On transient transfection of the PDE4A11 expression construct this activity increases to 4-6ηmol/min/mg of protein [Wallace et al., 2005]. Cell lysates from COS7 cells expressing human PDE4A1, PDE4A4B, PDE4A10 and PDE4A11 were subjected to SDS-PAGE and Western immuno-blotting with a human PDE4A sub-family specific C-terminal anti-serum and a PDE4A11 specific N-terminal antibody. Figure 3.5(a), left panel, shows the detection of immuno-reactive bands for all PDE4A isoforms with the PDE4A sub-family specific anti-serum. The molecular weight of the super-short PDE4A1 was approximately 85kDa whereas the molecular weights of PDE4A4B, PDE4A10 and PDE4A11 were virtually indistinguishable at approximately 120-125kDa. Because these isoforms are of similar molecular weights specific detection requires the use of an anti-serum to the N-terminal regions. Figure 3.5(a), right panel, shows the same Western immuno-blot probed with an anti-serum generated specifically for the unique N-terminal region of PDE4A11 and this allowed the sole detection of a single immuno-reactive species at 126kDa +/- 4kDa. An intriguing attribute of all PDE4 isoforms is their ability to migrate on SDS-PAGE at molecular weights larger than those predicted by their primary structure. The predicted molecular weight of PDE4A11 is 95.3kDa. As this characteristic is consistent amongst all PDE4 isoforms a common domain must drive it, and indeed, the catalytic core is responsible for mediating this aberrant SDS-PAGE migration [Johnston et al., 2004].

3.2.4.1 Intra-cellular Distribution of PDE4A11

Using differential centrifugation the intra-cellular distribution of a protein can be quantified. Cell lysates can be separated into P1 (low-speed pellet) that contains intact cells and other cellular debris, P2 (high-speed pellet) that contains the plasma membrane and internal organelles, and S2 (high-speed supernatant) that contains cytosolic cellular components. The sub-cellular distribution of PDE4A1, PDE4A4B and PDE4A10 in COS7 cells has been determined [Sullivan et al., 1998, McPhee et al., 1999 and Rena et al., 2001]. PDE4A1 is considered to be primarily membrane-bound with approximately 85% located in the pellet fractions and only 15% found in the cellular cytosol.

Membrane insertion is mediated through a novel micro-domain called TAPAS-1 [Baillie et al., 2002]. PDE4A4B shows a more equal distribution with 45% located in the pellet fractions and 55% in the cellular cytosol. PDE4A10 is different again with only 17% located in the pellet fractions and 83% found in the cellular cytosol. Assessment of the sub-cellular localisation of PDE4A11 by sub-cellular fractionation and analysis by SDS-PAGE, is shown in Figure 3.5(b), and concluded that 57% of PDE4A11 was located in the pellet fractions with 43% found as a cellular cytosolic protein. These data are shown in more detail in Table 3.1. However, sub-cellular distribution is a crude means of assessing the intra-cellular distribution. Analysis of PDE4A11 intra-cellular distribution using laser-scanning confocal microscopy and immuno-histochemistry is shown in Figure 3.5(c) and deemed PDE4A11 expression to be localised at the peri-nuclear regions of the cell and distinct distribution within membrane ruffles, unlike both PDE4A4B and PDE4A10 [Huston et al., 1996 and Rena et al., 2001]. No nuclear expression of PDE4A11 was detected.

The PDE4A11 primary amino acid sequence was analysed by ScanSite (http://scansite.mit.edu/cgi-bin/motifscan_seq), a protein phosphorylation and protein-protein interaction database centred upon peptide library data. On high stringency, i.e. using tight motif scanning parameters, it was postulated that the unique N-terminal region contained putative phosphorylation sites for ERK1 at Ser-48, which may prime for a putative GSK-3 phosphorylation at Ser-44, and a potential SH3 binding domain at Pro-39 and a phosphatidyl-inositol-3,4,5-phosphate (PIP3) binding Pleckstrin homology (PH) domain at Phe-59. Analyses of the identified phosphorylation sites are shown in Figures 3.12 and 3.13 and the interaction with the SH3 domain of Lyn via the putative PDE4A11 N-terminal SH3 binding domain is assessed in Figure 3.15.

It was hypothesised that N-terminal PDE4A11 binding of PIP3 may be responsible for its intra-cellular targeting. To investigate this hypothesis, the activation of PI-3K to generate PIP3 was initiated using EGF in COS7 cells

and Insulin in HEK293 cells. The intra-cellular distribution of PDE4A11 was determined.

Figure 3.6(a) shows a timely and robust activation of the PI-3K signalling pathway, through phosphorylation of PKB/Akt, after 2.5min and that this activation was sustained for up to 30min. Figure 3.6(b) shows no significant visual change in the sub-cellular distribution of native PDE4A11 and following EGF treatment. Quantification of the sub-cellular distribution as shown in Figure 3.6(c), confirms that no change in the sub-cellular distribution of PDE4A11 was achieved on activation of the PI-3K pathway in COS7 cells. The percentage of PDE4A11 that was located in the membrane P2 fraction in untreated cells was calculated as 27% +/- 4%. No statistically significant change was observed with EGF where the distribution of PDE4A11 P2 expression was 26% +/- 3% ($p > 0.05$) with 10ng/ml EGF, 26% +/- 2% ($p > 0.05$) with 20ng/ml EGF and 22% +/- 9% ($p > 0.05$) with 50ng/ml EGF.

A time- and concentration-dependent activation of PI-3K was detected by phosphorylation of PKB/Akt in HEK293 cells, on treatment with insulin, as shown in Figure 3.7(a). Figure 3.7(b) exhibits a potential change in PDE4A11 sub-cellular distribution on insulin treatment but this was not confirmed through quantification of the PDE4A11 localisation in the membrane P2 fraction, as shown in Figure 3.8(c). In native cells 16% +/- 2% of total PDE4A11 expression was located in the P2 fraction. With 0.1ηM insulin, this increased directionally, but not significantly to 25% +/- 11% ($p > 0.05$), compared to 25% +/- 7% ($p > 0.05$) and 28% +/- 11% ($p > 0.05$) with 1ηM and 10ηM insulin respectively.

Transient over-expression of PDE4A4B, tagged with green fluorescent protein (GFP) in HEK293, CHO, and rat basophilic leukaemia cells coupled chronic rolipram treatment induces a redistribution of PDE4A4B into accretion foci [Terry et al., 2003]. Similar experiments using GFP-tagged PDE4A10 and PDE4A11 exhibited no change in the localisation and no formation of accretion foci indicating a PDE4A4B isoform-specific effect [Wallace et al., 2005].

3.2.4.2 Kinetic Profile of PDE4A11

The hydrolysis of cAMP by PDE4 follows a simple scheme where cAMP binds to the active site of PDE4 and forms an intermediate complex. The PDE4 is available to participate in further hydrolysis following release of the 5' AMP product. At steady state, cAMP and PDE4 form a complex for hydrolysis that reaches equilibrium. This is defined by the Michaelis-Menten constant, K_m, which is described as the concentration of cAMP at which PDE4 is hydrolysing at 50% of its maximal rate (V_{max}). As with other enzyme reactions, PDE4s follow saturation kinetics. V_{max} is reached with excess concentrations of cAMP and in these conditions, PDE4 is saturated with cAMP as the Michaelis intermediate complex.

PDE4A11 forms an active cAMP-hydrolysing enzyme when over-expressed in mammalian cells. As described above, PDE4A11, when transiently over-expressed in COS7 cells, was localised at both the plasma membrane and within the cytosolic compartment of the cell. Cytosolic PDE4A11 has a K_m of 4.2μM +/- 1.1μM [Wallace et al., 2005]. As a membrane-bound species the K_m of PDE4A11 showed no change at 3.7μM +/- 1.8μM [Wallace et al., 2005]. These values are comparable to the other PDE4A long isoforms PDE4A4B and PDE4A10 [Huston et al., 1996 and Rena et al., 2001]. The "relative V_{max}" values were also determined by assaying equal immuno-reactive amounts of cytosolic PDE4A11 against cytosolic PDE4A4B and cytosolic PDE4A10. Using cytosolic PDE4A4B and PDE4A10 as a reference point, as they both have similar "relative V_{max}" values, the analogous "relative V_{max}" for PDE4A11 was 1.1 +/- 0.1. Moreover, no change in "relative V_{max}" was determined between cytosolic and membrane-bound PDE4A11, with the "relative V_{max}" for membrane-bound 1.1 +/- 0.1. An alteration in the V_{max} value between particulate and cytosolic forms has been observed for PDE4A4B where the particulate form has a 50% lower "relative V_{max}" value [Huston et al., 1996].

3.2.4.3 Inhibition of PDE4A11 by PDE4-selective Inhibitors

Inhibition of PDE4 enzymes has been the subject of much pharmaceutical research and has led to the production of many PDE4 chemical inhibitors [Burnouf and Pruniaux, 2002, Houslay et al., 2005 and Zhang et al., 2005]. Rolipram (Schering-Plough) is the established PDE4 inhibitor and is generally classified as a first generation compound, together with its derivative Ro 20-1724. Second generation inhibitors include Ariflo®, or cilomilast, (GlaxoSmithKline) and roflumilast (Altana). Xanthine derivatives such as denbufylline are also effective inhibitors of PDE4 enzyme activity. The chemical structures of these inhibitors are shown in Figure 3.8.

Each of these inhibitors concentration-dependently inhibited PDE4A11 activity in both membrane (P2) and cytosolic (S2) sub-cellular fractions from COS7 cells transiently over-expressing PDE4A11. The concentration range required to inhibit PDE4A11 is indicated in the concentration response curves in Figure 3.9.

PDE4A4B can exist in two conformations as indicated by differential sensitivity to inhibition by rolipram [Huston et al., 1996 and McPhee et al., 1999]. PDE4A4B localised in the cytosol of the cell was approximately 5-fold less sensitive to inhibition by rolipram than the particulate or membrane-bound form (0.26μM +/- 0.09μM), and as such the concentration-response curve showed a distinct shift to the left (data not shown). This effect is not observed with PDE4A10, as it is predominantly expressed as a cytosolic species [Rena et al., 2001]. PDE4A11 has a similar intra-cellular distribution profile to PDE4A4B but was not subject to increased affinity to rolipram when present in the particulate fraction. Rolipram inhibits cytosolic PDE4A11 with an IC_{50} of 0.72μM +/- 0.08μM and the particulate form with an IC_{50} of 0.66μM +/- 0.12μM. Cytosolic PDE4A10 appears to be the most sensitive PDE4A long isoform to inhibition by rolipram with an IC_{50} of 0.13μM +/- 0.03μM, followed by cytosolic PDE4A11 and then cytosolic PDE4A4B with an IC_{50} of 1.31μM +/- 0.08μM.

No significant difference between the IC_{50} for inhibition of cytosolic versus particulate preparations of PDE4A4B by Ariflo®, denbufylline or Ro 20-1724 was determined, but a 3-fold increase in the sensitivity for inhibition of the particulate form was measured with roflumilast. Cytosolic PDE4A10 had similar sensitivity to inhibition by Ariflo® and denbufylline, compared to cytosolic PDE4A4B, but was 2-fold more sensitive to inhibition by Ro 20-1724 and roflumilast. PDE4A11 was more sensitive to inhibition by Ariflo®, denbufylline and Ro 20-1724 on comparison to the relevant sub-cellular preparation of PDE4A4B. In the case of roflumilast, cytosolic PDE4A11 was more sensitive than cytosolic PDE4A4B, whereas the converse was true for the particulate preparations.

The precise IC_{50} values for inhibition of particulate, where appropriate, and cytosolic preparations of PDE4A4B, PDE4A10 and PDE4A11 are detailed in Table 3.2.

3.2.4.4 Thermal Stability of PDE4A11

Thermal stability or denaturation of an enzyme is described as the loss of catalytic activity over time, when heated. This technique allowed a rudimentary structural comparison of PDE4A11 expressed at distinct locals within the cell. When particulate and cytosolic forms of PDE4A11 were heated at 55°C, their denaturation, and subsequent loss of cAMP hydrolysing activity occurred at different rates. As shown in Figure 3.10, PDE4A11 activity decayed as a single exponential and the half-life ($t_{1/2}$) of inactivation was determined. The cytosolic form of PDE4A11 had a $t_{1/2}$ of 2.5min +/- 0.3min whereas the particulate form was significantly more stable with a $t_{1/2}$ of 4.4min +/- 0.3min ($p < 0.05$).

3.2.5 Phosphorylation of PDE4A11

Long isoforms from all four PDE4 sub-families are phosphorylated and activated by PKA at a single target serine residue contained within an Arg-

Arg-Glu-Ser-Phe consensus motif located within the common UCR1 regulatory module [Sette and Conti, 1996, Hoffmann et al., 1998 and MacKenzie et al., 2002]. Phosphorylation of this residue results in the activation of PDE4 enzymes. Isoforms from all PDE4 sub-families have appropriate docking sites for ERK2 but only PDE4B, PDE4C and PDE4D contains an ERK2 phosphorylation consensus sequence within the C-terminal catalytic unit [Hoffmann et al., 1999, MacKenzie et al., 2000 and Baillie et al., 2000]. Functionally this phosphorylation exerts and inhibitory effect on PDE4 long isoforms and activates PDE4 short isoforms. These phosphorylation events are discussed in more detail in Section 1.7.5.

3.2.5.1 Protein Kinase A

Phosphorylation and activation of PDE4A11 was induced through the treatment of cells, transfected to transiently express PDE4A11, with the non-specific PDE inhibitor, IBMX and the adenylyl cyclase activator, forskolin. These treatments significantly raised the cAMP concentrations within the cells and induced activation of PKA. Figure 3.11(a) and Figure3.11(d) shows the time-dependent induction of a single phospho-UCR1 immuno-reactive band of approximately 125kDa. The peak of the phosphorylation response was measured at 2.5min with IBMX/forskolin. A significant increase in cAMP hydrolysing activity, from the 100% +/- 8% control level to 184% +/- 16% with forskolin was measured and similarly peaked after 2.5min. The immuno-reactive band, indicative of PDE4 UCR1 PKA phosphorylation was not detected in non-transfected cells [Wallace et al., 2005], and the immuno-reactivity was severely attenuated at time zero and in cells concentration-dependently treated with the PKA inhibitor, H89, as shown in Figure 3.11(b). Abolishment of PDE4A11 phosphorylation was detected in cells transfected to express a Ser-119-Ala phosphorylation defective mutant form of PDE4A11, as illustrated in Figure 3.11(c).

3.2.5.2 Extra-cellular Signal-regulated Kinase

As discussed above in Section 3.2.4.1, the unique N-terminal region of PDE4A11 contains a putative ERK1 phosphorylation site. Ser-48 was identified as the phosphorylation target residue contained within the consensus sequence, Pro-Ser-Ser-Pro. A possible ERK docking domain towards the extreme N-terminal of PDE4A11 was also presented following a further ScanSite (http://scansite.mit.edu/cgi-bin/motifscan_seq) analysis of PDE4A11, on medium stringency. Any change in the degree of PDE4A11 phosphorylation, following ERK1/2 activation with either EGF or PMA in COS1 cells, was determined.

PDE4A11 was analysed for alterations to the extent of phosphorylation by ERK1/2 in COS1 cells, grown in phosphate-free media, and radiolabelled with [^{32}P]-orthophosphate. The cells were treated with EGF, which initiated a robust activation of ERK1/2 at 2.5min, which was sustained for 30min, as shown in Figure 3.12(a). Evaluation of Figure 3.12(b) indicated an increase in the level of phosphorylation of PDE4A11 with EGF and comparable immuno-reactive amounts of PDE4A11 were immuno-precipitated. The quantification of any difference in phosphorylation, taking into account the relative amounts of PDE4A11 immuno-precipitated, showed no significant change in phosphorylation, with the degree of phosphorylation at 104% +/- 34% ($p > 0.05$) with EGF, and reduced to 85% +/- 12% ($p > 0.05$) with EGF plus U0126, as shown in Figure 3.12(b). Figure 3.12(c), top panel, confirmed low basal levels of active ERK1/2 in COS1 cells, the strong induction of ERK1/2 activation with EGF, and inhibition of active ERK1/2 with the MEK inhibitor, U0126.

COS1 cells transfected to over-express PDE4A11, in media where the endogenous phosphate was replaced with [^{32}P]-orthophosphate, were treated with PMA to activate ERK1/2. PMA treatment of COS1 results in the activation of ERK1/2, to a level comparable with that instigated by EGF, as shown in Figure 3.13(b), top panel, with PMA and Figure 3.12(c), top panel, with EGF. Indeed, appraisal of Figure 3.13(a), top panel, demonstrated a

visible increase in the degree of PDE4A11 phosphorylation on treatment with PMA, and the effect was sensitive to inhibition by U0126. Analogous immuno-reactive amounts of PDE4A11 were immuno-precipitated, as shown in Figure 3.13(a), bottom panel. Quantification of the variation in phosphorylation with PMA is shown in Figure 3.13(a) and revealed that no significant increase was observed at 128% +/- 23% ($p > 0.05$), with the effect of PMA plus U0126 measured at 85% +/- 5% ($p > 0.05$).

3.2.6 PDE4A11 Protein Interactions

In characterising the significance of PDE4A11 expression, it was important to elucidate whether PDE4A11 was able to support similar protein interactions and confer the functional attributes akin to the other PDE4A long isoforms.

3.2.6.1 SH3 Domain of Lyn

The SH3 domain of the tyrosyl kinase Lyn, interacts with PDE4A4B and PDE4A10 [McPhee et al., 1999 and Rena et al., 2001]. This interaction is discussed in more detail in Section 1.7.6.1. PDE4A4B contains four putative SH3 binding domains for interaction with the SH3 domain of Lyn, i.e. the unique N-terminal region, the PDE4A specific LR2, the C-terminal portion of the catalytic unit and the PDE4A specific C-terminal tail. Previously, the principal interaction site was mapped to the unique N-terminal region of PDE4A4B, with a secondary site confined within LR2 [McPhee et al., 1999]. Similarly, PDE4A10 exclusively interacts with the SH3 domain of Lyn through the common LR2 [Rena et al., 2001].

To assess the possible interaction of PDE4A11 with the SH3 domain of Lyn, the recombinant GST fusion protein was expressed and purified in *E.coli*, to a single band on a Coomassie® stained SDS-PAGE, as shown in Figure 3.14(a). Lyn-SH3 was expressed as soluble protein in *E.coli* and purified to final concentration of 7.7mg/ml. In Figure 3.15(a), panel (i), it was observed

that PDE4A4B interacted significantly with Lyn-SH3 accompanied with negligible non-specific interaction with the GST alone control. Interestingly, PDE4A4B was not detected in the residual cell lysate following incubation with Lyn-SH3 indicating a potentially high affinity interaction. On the other hand, PDE4A11 showed a significant reduction in binding to Lyn-SH3, as shown in Figure 3.15(c), panel (i). A similar level of non-specific interaction with the GST control was observed, but strikingly, a large proportion of PDE4A11 remained unbound to Lyn-SH3, indicating a much-reduced affinity of interaction. The level of interaction with Lyn-SH3, using the pull-down assay was akin to that observed previously with PDE4A10 [Rena et al., 2001]. To map the critical residues for PDE4A long form interaction with Lyn-SH3, a peptide array approach was utilised using the recombinant GST fusion protein of Lyn-SH3. GST showed an absence of non-specific binding to all of the peptide arrays used in these experiments (data not shown). Using the peptide array of full length PDE4A4B, this approach accurately assigned the major interaction site for Lyn-SH3 as Lys-306 to Lys-340 within LR2, as illustrated in Figure 3.15(a), panel (iii). A secondary interaction site was mapped to the PDE4A specific C-terminal tail, between Val-806 and Glu-835, as shown in Figure 3.15(a), panel (iv). Figure 3.15(a), panel (ii), showed nominal binding within the N-terminal region, compared to the detection of binding at the other sites. However, utilising the peptide array of the unique N-terminal region of PDE4A10, Figure 3.15(b) identified the first thirty amino acids as capable of supporting Lyn-SH3 binding. Removal of the first ten amino acids ablated the interaction of Lyn-SH3. Similarly, an extensive proline- and arginine-rich region exists within the unique N-terminal of PDE4A11. Pull-down analysis, Figure 3.15(c), panel (i), indicated that PDE4A11 was able to interact with Lyn-SH3 and the peptide array maps this interaction from Val-22 to Arg-60, as shown in Figure 3.15(c), panel (ii).

3.2.6.2 β-arrestin

β-arrestin can interact with two distinct sites within PDE4D5, the unique N-terminal region and a site towards the C-terminal of the conserved catalytic

unit [Perry et al., 2002, Bolger et al., 2003 and Bolger et al., 2006]. Therefore, PDE4A isoforms also have the potential to interact with β-arrestin.

A recombinant GST fusion protein of β-arrestin2 was expressed and purified in *E.coli* to a single band on a Coomassie© stained SDS-PAGE, as shown in Figure 3.14(b). β-arrestin2 was expressed at a lower level than Lyn-SH3 and consequently the yield was lower, with a final purified concentration of 1.2mg/ml. Using a pull-down assay with GST-β-arrestin2 and COS7 cell lysates expressing either PDE4A4B or PDE4A11, Figure 3.16 concluded that both PDE4A4B, (a), and PDE4A11, (b), were able to interact with β-arrestin2, with minimal interaction observed with GST alone.

3.2.6.3 Immunophilin XAP2

The immunophilin XAP2 specifically interacts with rat PDE4A5 and inhibits PDE4A5 cAMP hydrolysing activity [Bolger et al., 2003]. The interaction sites have been mapped to a region with the unique N-terminal of PDE4A5, responsible for the inhibition of catalytic activity, and the common PDE4 UCR2 domain. Thus, one would expect XAP2 to interact, at least to some extent, with PDE4 isoforms across all gene families, but this was not observed.

It was concluded in Figure 3.17(a) that PDE4A4B was able to interact with XAP2 when transiently co-expressed in COS7 cells. This is consistent with the previous data identifying XAP2 as a specific protein that can exclusively interact with PDE4A5 because of sequence conservation between the human and rat homologues [Bolger et al., 2003]. A similar degree of interaction with XAP2 was indicated following immuno-precipitation of XAP2, as shown in Figure 3.17(b), in COS7 cells over-expressing both XAP2 and PDE4A11. Non-specific co-immuno-precipitation interactions were negligible in both cases.

3.2.6.4 Action of Caspase-3

The unique N-terminal region of PDE4A5 contains the sequence, Asp-Ala-Val-Asp at Asp-69, which is a consensus sequence for caspase-3 cleavage. Thus, the unique intra-cellular targeting region of PDE4A5 is able to undergo caspase-3 cleavage, indicated by a increase in the migration mobility of PDE4A5 on SDS-PAGE from 109kDa to 100kDa, to prevent its interaction with SH3 domain containing proteins [Huston et al., 2000]. PDE4A5 does not contain the required proline- and arginine-rich sequence within LR2 and therefore, does not provide any compensatory binding with SH3 domains [McPhee et al., 1999]. Homology between rat PDE4A5 and human PDE4A4B gives rise to a similar site in the N-terminal region of PDE4A4B, Asp-Ala-Met-Asp at Asp-69. Caspase-3 cleavage was able to occur in PDE4A4B, as indicated by a faster migrating species on SDS-PAGE, but no equivalent digestion of PDE4A10 or PDE4A11 followed due to their unique N-terminal regions lacking the Asp-Xaa-Xaa-Asp consensus sequence [Wallace et al., 2005].

(a)

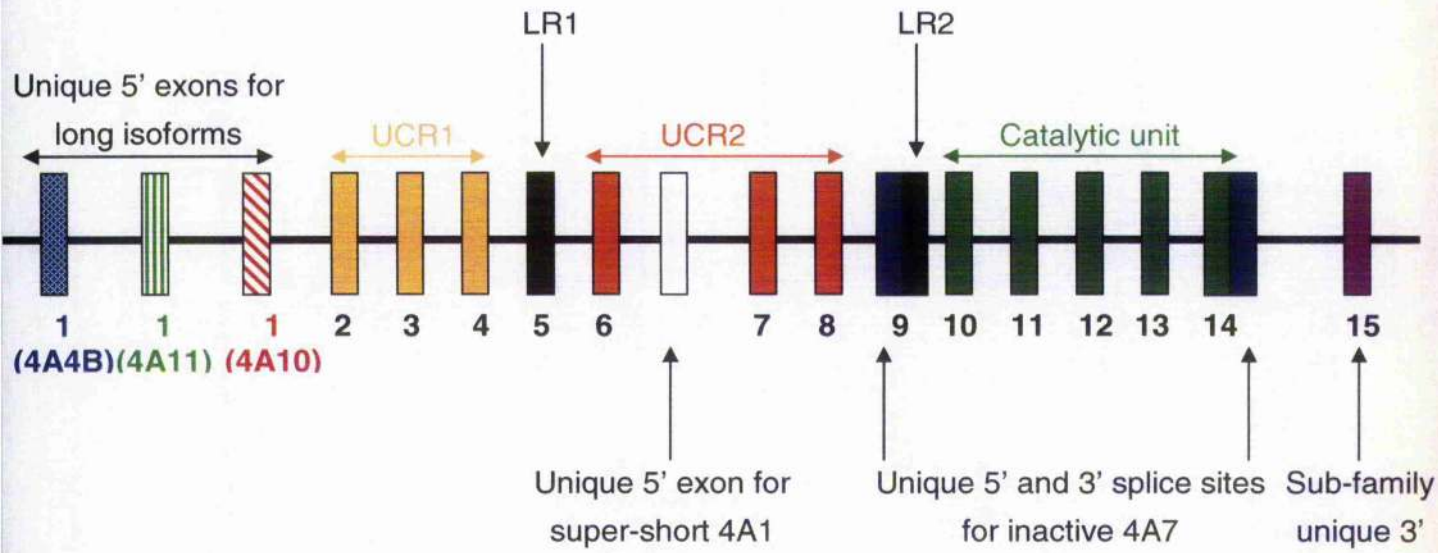
LR1
LR2
Unique 5' exons for long isoforms
UCR1
UCR2
Catalytic unit
1 1 1 2 3 4 5 6 7 8 9 10 11 12 13 14 15
(4A4B) (4A11) (4A10)
Unique 5' exon for super-short 4A1
Unique 5' and 3' splice sites for inactive 4A7
Sub-family unique 3'

(b)

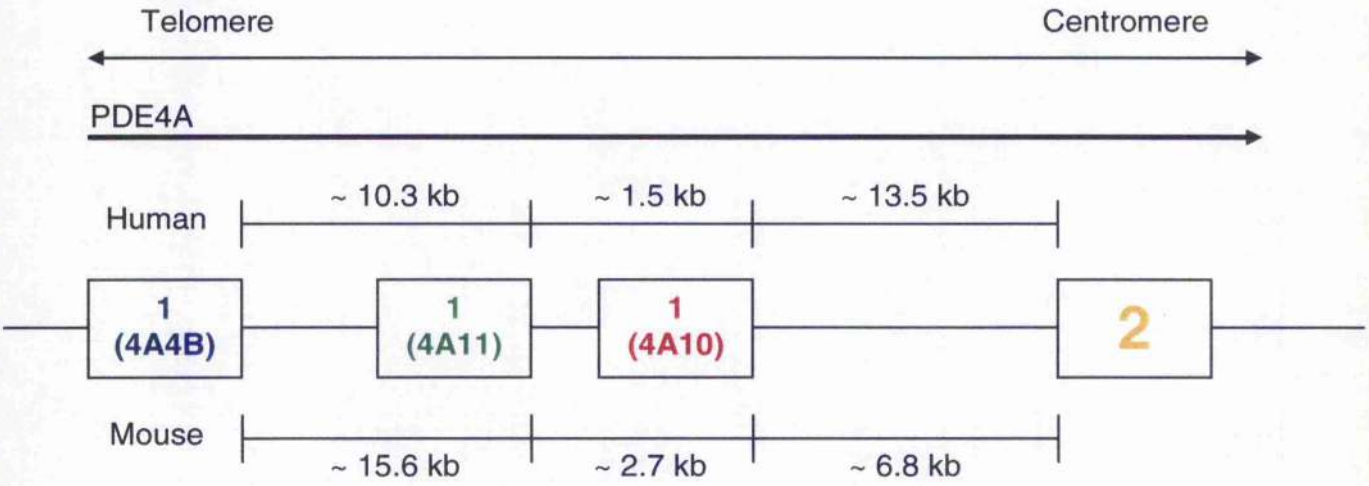
Telomere
Centromere
PDE4A
Human
~ 10.3 kb
~ 1.5 kb
~ 13.5 kb
1 (4A4B)
1 (4A11)
1 (4A10)
2
Mouse
~ 15.6 kb
~ 2.7 kb
~ 6.8 kb

Figure 3.1 – Schematic representation of the PDE4A gene structure.

(a) shows the coding exons (boxes) of the active PDE4A enzyme and the non-coding introns (horizontal lines, black). The unique 5' exons for the long isoforms PDE4A4B (hashed, blue), PDE4A11 (hashed, green) and PDE4A10 (hashed, red) are shown and encode the unique N-terminal regions. The unique 5' exon for the super-short PDE4A1 isoform (white) is embedded between exons 6 and 7 resulting in the expression of an active enzyme lacking UCR1 (yellow) and containing a truncated UCR2 module (orange). The linker regions (black), LR1 and LR2, are encoded by exons 5 and 9 respectively. The unique 5' and 3' exons for the catalytically inactive PDE4A7 enzyme are also shown (blue). Exons 10-14 (green) encode the catalytic unit and exon 15 (purple) the sub-family unique C-terminal region. (b) shows the organisation of the unique 5' exons (or exon 1) for the three human PDE4A long isoforms and their orientation 5' – 3' telomere to centromere on chromosome 19p13.2.

```
Consensus  MAR-RGLGRIPELQLAAFP-AAA-AEDEAFLPEPPAPRAPR

Human      MARPRGLGRIPELQLVAFPVAVA*AEDEAFLPEPLAPRAPR
Mouse      MAR*RGWGRIPEPCAAAFPEAVA**EDDAFLPGPPTVSAFL
Rat        MAR*RGCGRIPEPRAAAFPEAAA**EDDAFLPGPASVSAFF
Bat        MARQRGLGCIPELQLAAFPAAAAAAEDEAFLPEPPAPRAPR
Pig        -----SLGRIPELQLVAFPAAAT**EDEAFLPEPPAPRAPR

Consensus  --RSPPSSPVFFASPSPTLRRRLRLLRGSFQD-GRQAWAG--

Human      RPRSPPSSPVFFASPSPTFRRRLRLLR*SCQDLGRQAWAGAG
Mouse      SSTT**********PMPY*RR*LRLFRGSVQDWGRQAWAG**
Rat        SSTP**********PTPY*RR*LRLFRGGIQDWGRQAWAG**
Bat        WLRSPPSSPVFFASPSPTLRRRLRLLR*SFQDFGRQAWAG**
Pig        RPRSPPSSPVFFASPSPTLRRRLRLLR*SFQDFSRPAWAG**
```

Figure 3.2 – Sequence alignments of the predicted amino acid sequences encoded by the PDE4A11 unique 5' exon in various species.

Alignment shows human (GenBank accession number AY618547), mouse (GenBank accession numbers AC027154 and AC073749), rat (GenBank accession number AC115140), bat (GenBank accession number AC148813) and pig predicted sequences. Conserved residues are highlighted (red). The predicted consensus sequence for the unique PDE4A11 N-terminal region is also shown (underlined, blue).

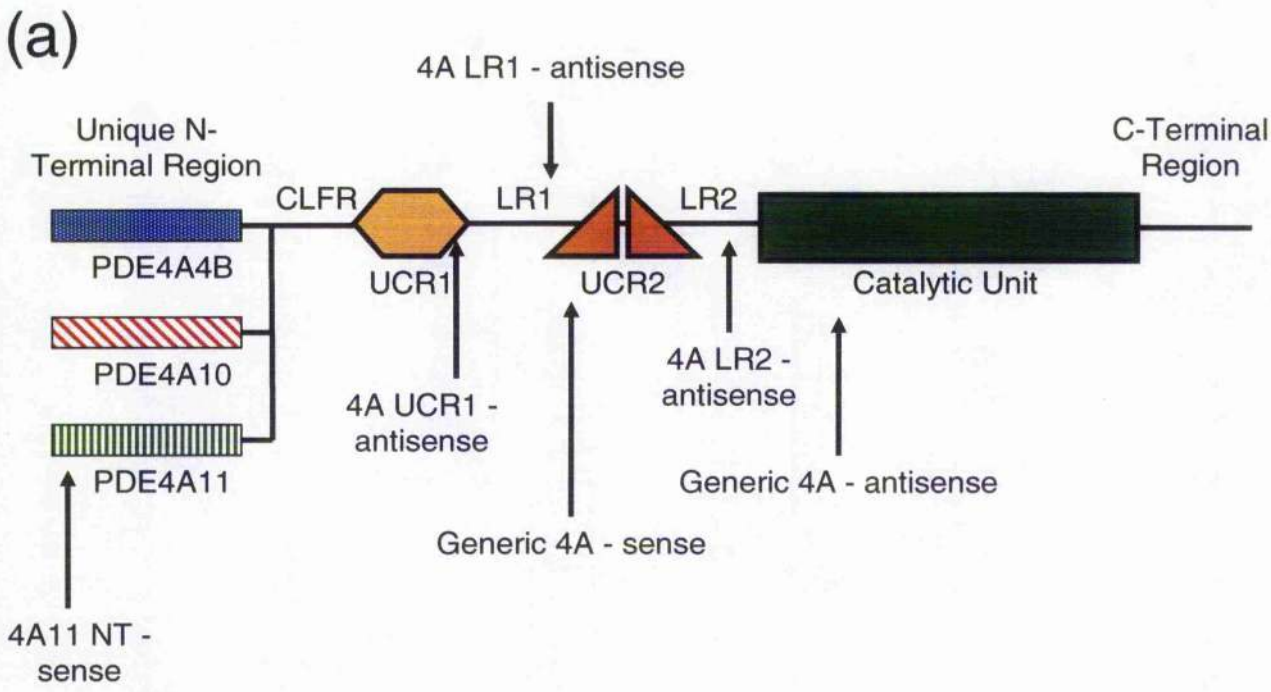
(a)
4A LR1 - antisense
Unique N-Terminal Region
C-Terminal Region
CLFR
LR1
LR2
PDE4A4B
UCR1
UCR2
Catalytic Unit
PDE4A10
4A LR2 - antisense
4A UCR1 - antisense
PDE4A11
Generic 4A - antisense
Generic 4A - sense
4A11 NT - sense

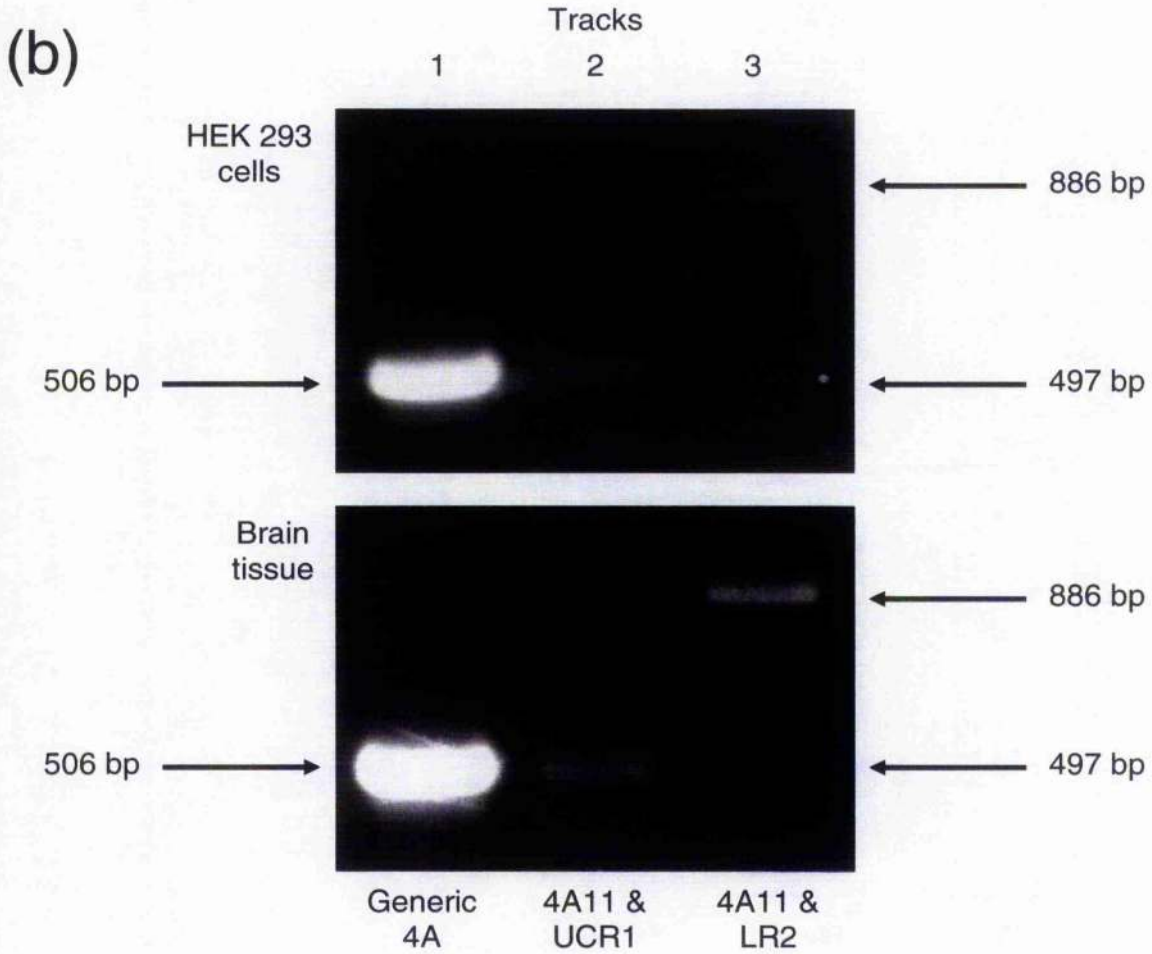
(b)
Tracks
1
2
3
HEK 293 cells
886 bp
506 bp
497 bp
Brain tissue
886 bp
506 bp
497 bp
Generic 4A
4A11 & UCR1
4A11 & LR2

Figure 3.3 – Schematic representation of the modular structure of PDE4A enzymes and authentication of PDE4A11 by RT-PCR.

(a) is a schematic representation of the key regions of a full length PDE4A enzyme. The unique N-terminal regions are shown for PDE4A4B (hashed, blue) (GenBank accession number L20965), PDE4A10 (hashed, red) (GenBank accession number AF110461) and PDE4A11 (hashed, green) (GenBank accession number AY618547). Note the common long form region (CLFR) located between the unique N-terminal region and UCR1 regulatory module. Also shown is the position for the primers used for RT-PCR. The generic PDE4A primers were designed to anneal to regions common to all PDE4A long isoforms, i.e. the UCR2 regulatory module and the catalytic unit. Assuming the PDE4A11 ATG start codon in the open reading frame is assigned nucleotides 1, 2 and 3 respectively then the 4A11 NT sense primer anneals at nucleotides 1 – 25, the UCR1 anti-sense primer anneals at nucleotides 471 – 497, and the 4A LR2 anti-sense primer anneals at nucleotides 859 – 886. The sequences of the primers and the primer pairs used for each RT-PCR are shown in Table 2.3 on Page 70 of Chapter 2, Materials and Methods. (b), shows the identification of PDE4A11 as an authentic PDE4A long isoform by RT-PCR from mRNA isolated from HEK293 cells (top panel) and brain tissue (bottom panel). In both figures, track 1 shows the RT-PCR products generated using the generic PDE4A sense and anti-sense primers. These were designed to amplify a 506bp product from the common UCR2 region to the catalytic unit. Tracks 2 and 3 show the RT-PCR products using the PDE4A11 N-terminal sense primer with either the 4A UCR1 anti-sense primer or the 4A LR2 anti-sense primer. These were designed to amplify products of 497bp and 886bp respectively. These data are from experiments done once.

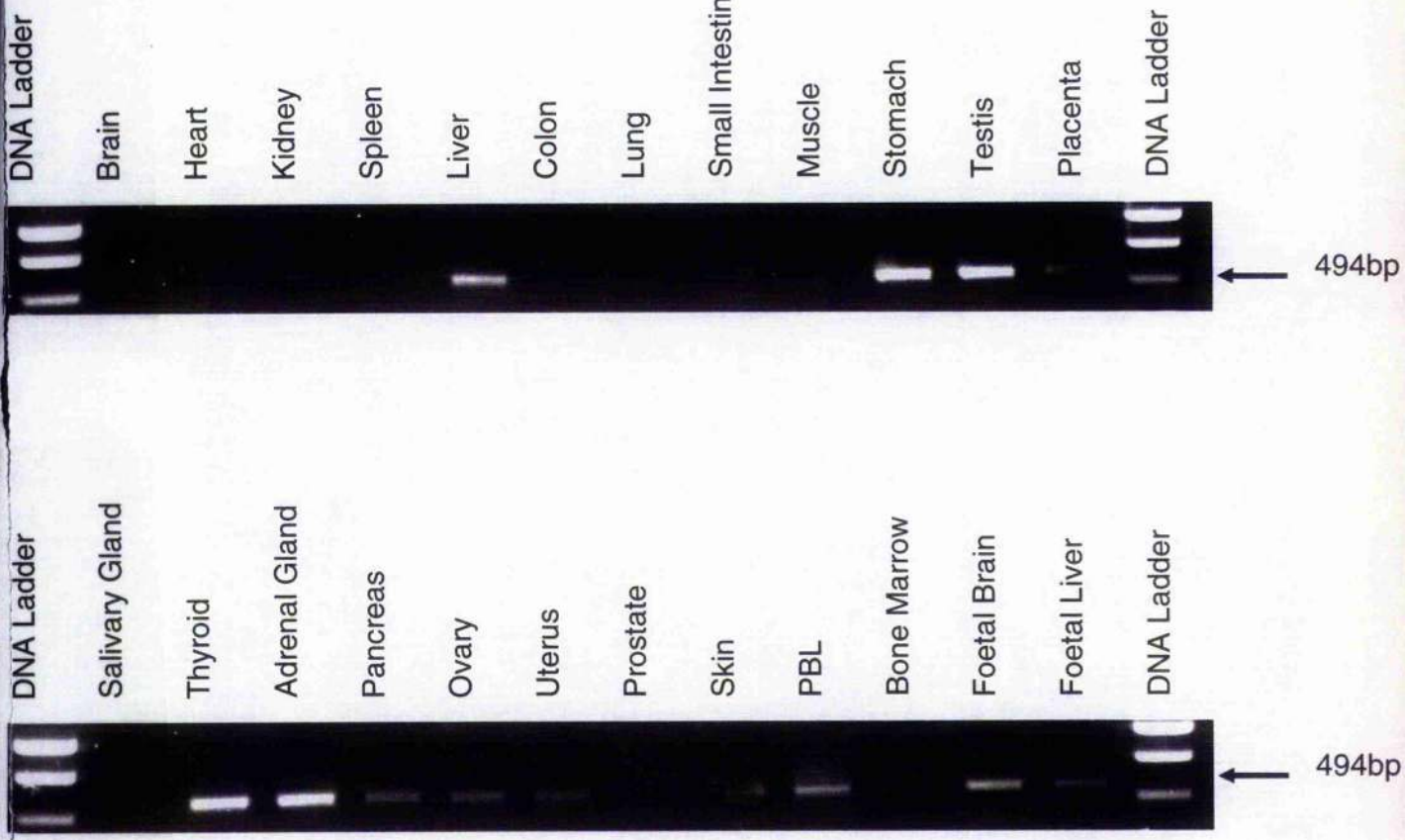
DNA Ladder
Brain
Heart
Kidney
Spleen
Liver
Colon
Lung
Small Intestine
Muscle
Stomach
Testis
Placenta
DNA Ladder
494bp
DNA Ladder
Salivary Gland
Thyroid
Adrenal Gland
Pancreas
Ovary
Uterus
Prostate
Skin
PBL
Bone Marrow
Foetal Brain
Foetal Liver
DNA Ladder
494bp

Figure 3.4 – Expression profile of PDE4A11 by PCR using a cDNA panel derived from various human tissues.

cDNA derived from various human tissues was used to assess the distribution of transcripts for PDE4A11. PCR was undertaken using the 4A11 NT sense primer (nucleotides 33 – 50) and the 4A LR1 anti-sense primer (nucleotides 507 – 527). The annealing positions of these primers are presented in Figure 3.3(a). These primers were designed to amplify a 494bp product. These data are representative of experiments done twice.

(a)

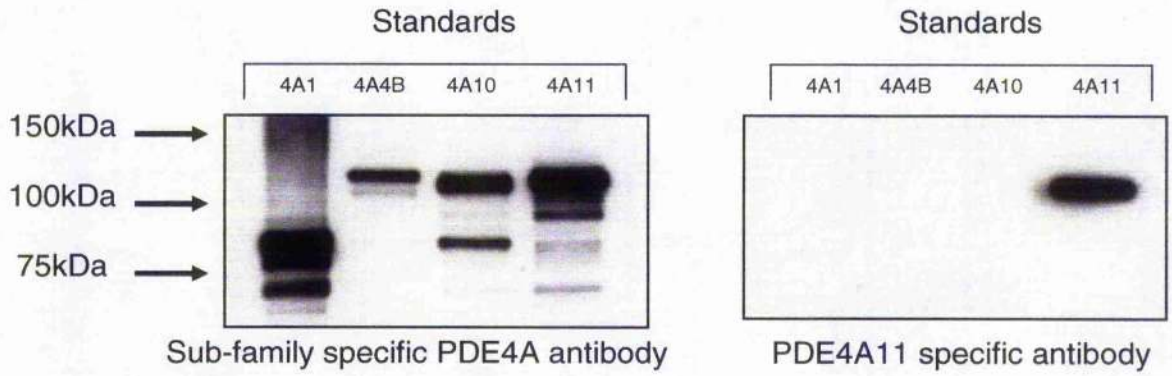
Standards
4A1
4A4B
4A10
4A11
150kDa
100kDa
75kDa
Sub-family specific PDE4A antibody
Standards
4A1
4A4B
4A10
4A11
PDE4A11 specific antibody

(b)

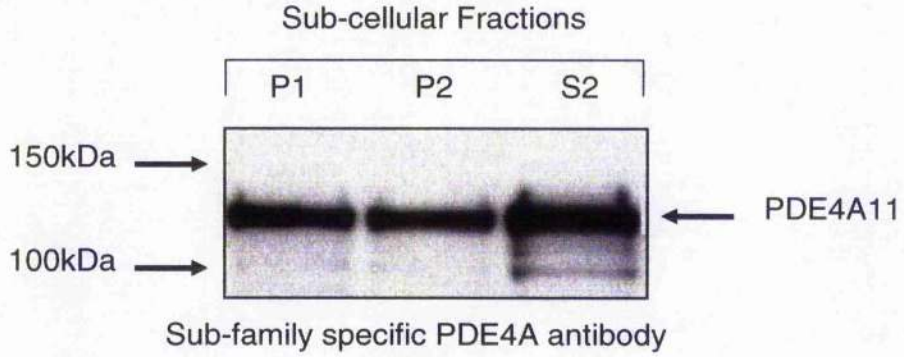
Sub-cellular Fractions
P1
P2
S2
150kDa
100kDa
PDE4A11
Sub-family specific PDE4A antibody

(c)

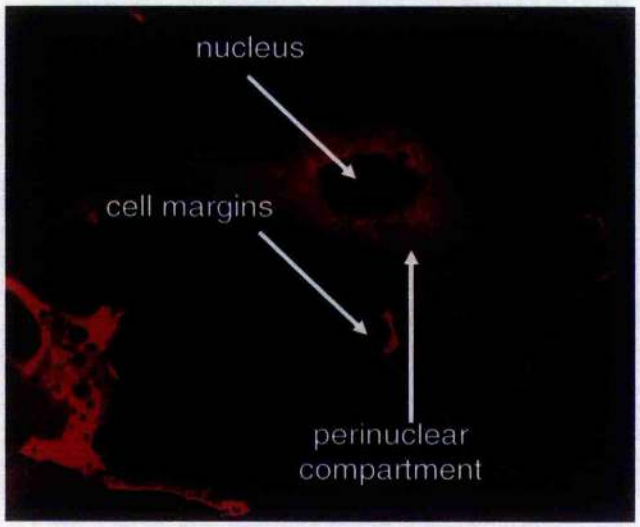
nucleus
cell margins
perinuclear
compartment

Figure 3.5 – Expression of recombinant PDE4A11 in COS7 cells.

(a), left panel, shows a Western blot of whole cell lysate from COS7 cells that had been transfected with a plasmid allowing mammalian expression of human PDE4A1, PDE4A4B, PDE4A10 or the novel PDE4A11. In these cells immuno-reactive bands at approximately 85kDa (PDE4A1) and 125kDa (PDE4A4B, PDE4A10 and PDE4A11) were identified using a specific anti-serum that detects the conserved C-terminal region of all active PDE4A isoforms. (a), right panel, shows the same Western blot re-probed with an anti-serum specific to the unique N-terminal region of PDE4A11. This detects a single, 125-kDa protein in the lane containing cell lysate over-expressing human PDE4A11. (b), shows the distribution of PDE4A11 when transiently over-expressed in COS7 cells. COS7 cells were transfected to transiently express PDE4A11 before sub-cellular fractionation. This method, described previously [McPhee et al., 1995], separates the total cellular matter into the soluble, cytosolic cellular components (high-speed supernatant or S2), the plasma membrane and internal organelles (high-speed pellet or P2), and intact cells and other cellular debris (low-speed pellet or P1). Table 3.1 shows the quantification of the distribution of all the active human PDE4A isoforms over-expressed in COS7 cells. (c), shows laser-scanning confocal microscopy analysis of the PDE4A11 distribution in COS7 cells. COS7 cells were transfected to express PDE4A11 and then visualised immunologically using the PDE4A C-terminal specific anti-serum to evaluate the localisation of this novel isoform. All data shown are examples of experiments done at least three times with different cellular transfections.

Sub-cellular Fraction	PDE4A1*	PDE4A4B*	PDE4A10*	PDE4A11
P1	22 +/- 6	19 +/- 4	7 +/- 4	30 +/- 3
P2	63 +/- 8	26 +/- 3	10 +/- 7	27 +/- 4
S2	15 +/- 5	55 +/- 5	83 +/- 7	43 +/- 3

Table 3.1 – Distribution of PDE4A isoforms in COS7 cells.

COS7 cells were transfected to transiently express each isoform before sub-cellular fractionation into high-speed supernatant (S2), high-speed pellet (P2), and low-speed pellet (P1). The distribution of each isoform was determined by quantitative immuno-blotting and is expressed as a percentage of the total cellular expression. *Data here for the distribution of PDE4A1 [Sullivan et al., 1998], PDE4A4B [McPhee et al., 1999] and PDE4A10 [Rena et al., 2001] as reported previously. These data are given as means +/- standard deviation for at least three different transfections and experiments.

(a)

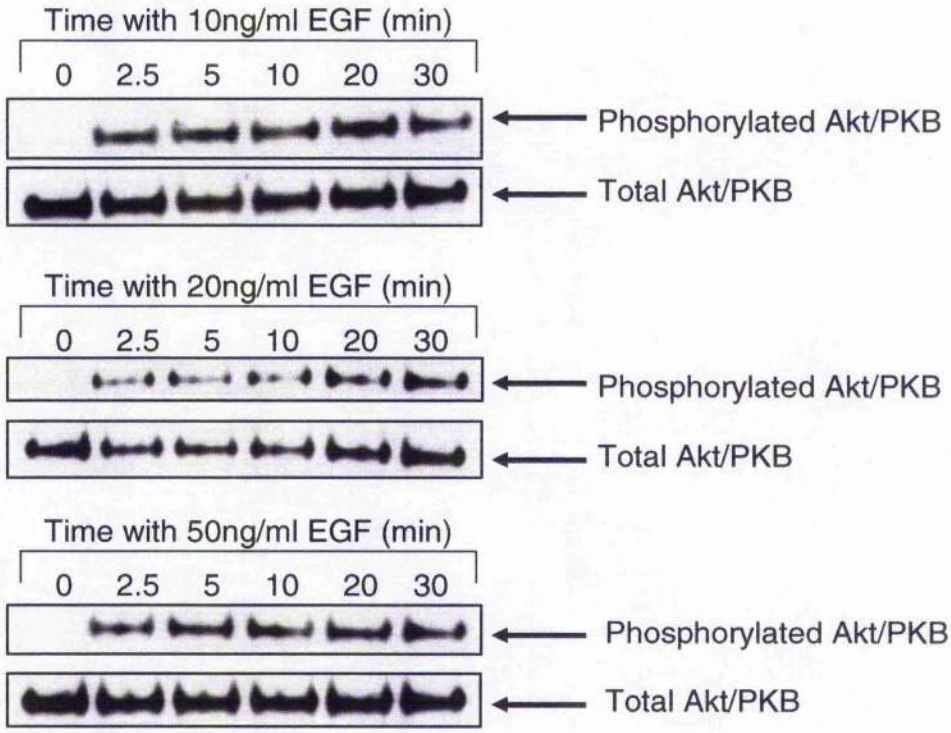
Time with 10ng/ml EGF (min)
0 2.5 5 10 20 30
Phosphorylated Akt/PKB
Total Akt/PKB
Time with 20ng/ml EGF (min)
0 2.5 5 10 20 30
Phosphorylated Akt/PKB
Total Akt/PKB
Time with 50ng/ml EGF (min)
0 2.5 5 10 20 30
Phosphorylated Akt/PKB
Total Akt/PKB

(b)

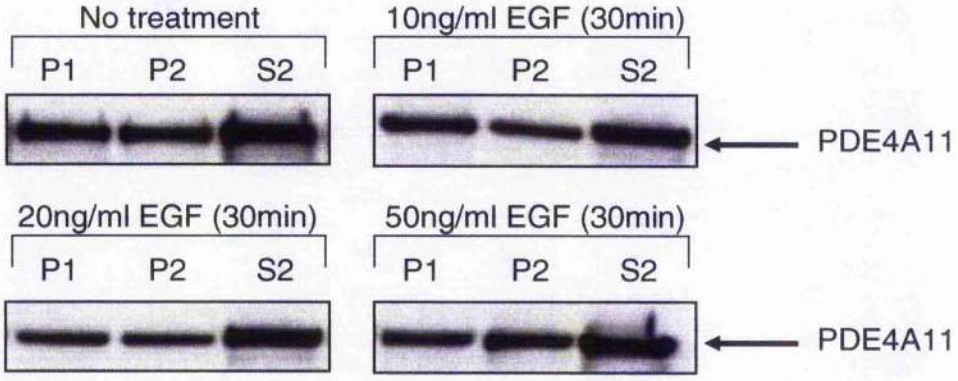
No treatment
P1 P2 S2
10ng/ml EGF (30min)
P1 P2 S2
PDE4A11
20ng/ml EGF (30min)
P1 P2 S2
50ng/ml EGF (30min)
P1 P2 S2
PDE4A11

(c)

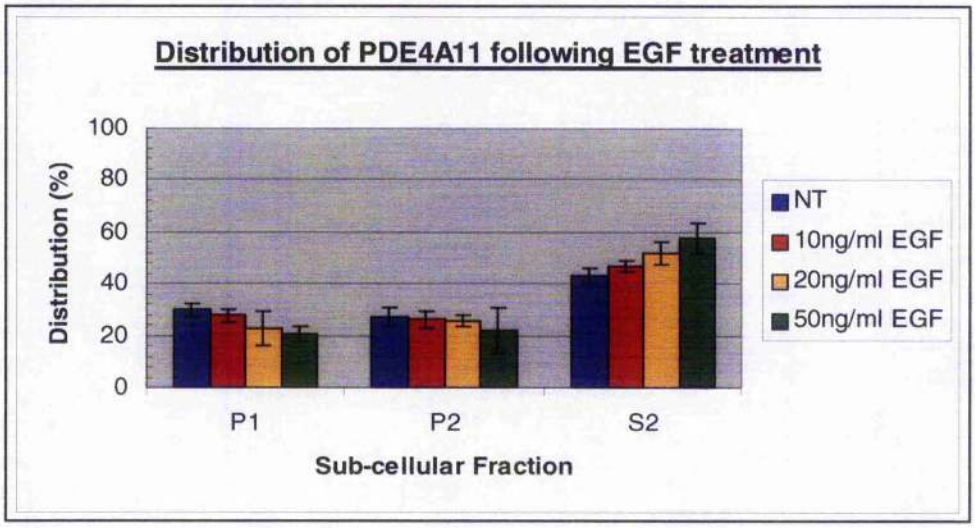
Distribution of PDE4A11 following EGF treatment
Distribution (%)
100
80
60
40
20
0
P1
P2
S2
Sub-cellular Fraction
NT
10ng/ml EGF
20ng/ml EGF
50ng/ml EGF

Figure 3.6 – PDE4A11 translocation to the plasma membrane of COS7 cells following stimulation with EGF.

(a), top panels, are Western blots showing the endogenous activation time course of Akt (Protein Kinase B; PKB) in COS7 cells following treatment with EGF, at various increasing concentrations (10, 20 and 50ng/ml), between 0 and 30min. The activation of Akt was detected using a phospho-specific anti-serum to one of the phosphorylation sites required for Akt activation. (a), bottom panels, are Western blots showing the total endogenous expression levels of Akt in COS7 cells and also functions as loading controls for the activation time courses. PDE4A11 was transiently expressed in COS7 cells. The cells were stimulated with the various concentrations of EGF for 30min. The cells were then harvested and sub-cellular fractions produced by centrifugation. This method, described previously [McPhee et al., 1995], separates the total cellular matter into the soluble, cytosolic cellular components (high-speed supernatant or S2), the plasma membrane and internal organelles (high-speed pellet or P2), and intact cells and other cellular debris (low-speed pellet or P1). (b), shows Western blots probed with the C-terminal PDE4A-specific anti-serum to evaluate the effect of increasing EGF concentrations on the sub-cellular distribution of PDE4A11 in COS7 cells. (c), is the quantification of these Western blots to reflect any change in the COS7 cellular distribution of PDE4A11 within each sub-cellular fraction (total PDE4A11 expression equals 100%). All data shown are either representative Western blots of three separate transfections and sub-cellular fractionations, or mean quantification data +/- standard deviation of the three separate transfections and sub-cellular fractionations. Two-Sample t-test statistical analysis of the quantification data were undertaken, where $p < 0.05$ indicates a statistically significant difference in the relative PDE4A11 immuno-reactivity within the P2 sub-cellular fraction between untreated and treated cells, as indicated.

(a)

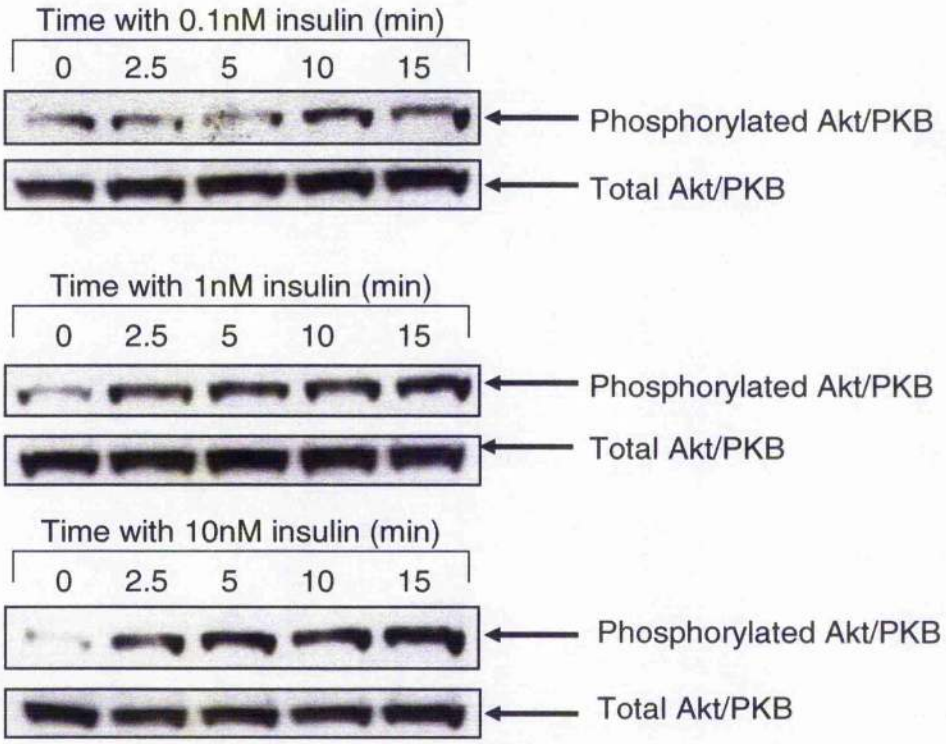
Time with 0.1nM insulin (min)
0 2.5 5 10 15
Phosphorylated Akt/PKB
Total Akt/PKB
Time with 1nM insulin (min)
0 2.5 5 10 15
Phosphorylated Akt/PKB
Total Akt/PKB
Time with 10nM insulin (min)
0 2.5 5 10 15
Phosphorylated Akt/PKB
Total Akt/PKB

(b)

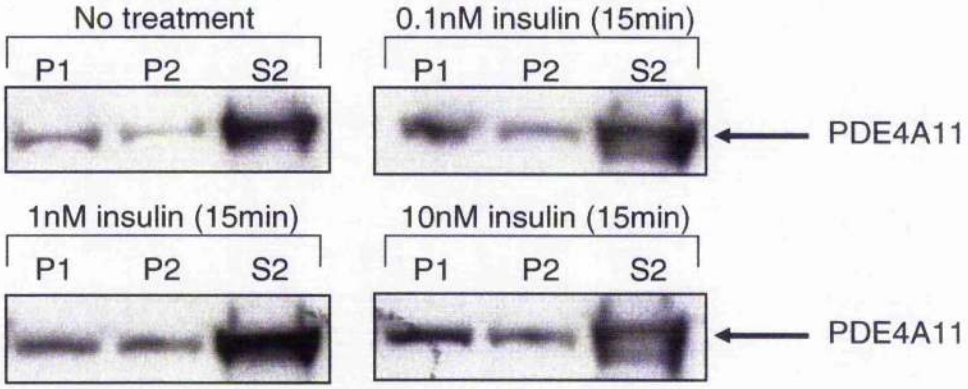
No treatment
P1 P2 S2
0.1nM insulin (15min)
P1 P2 S2
PDE4A11
1nM insulin (15min)
P1 P2 S2
10nM insulin (15min)
P1 P2 S2
PDE4A11

(c)

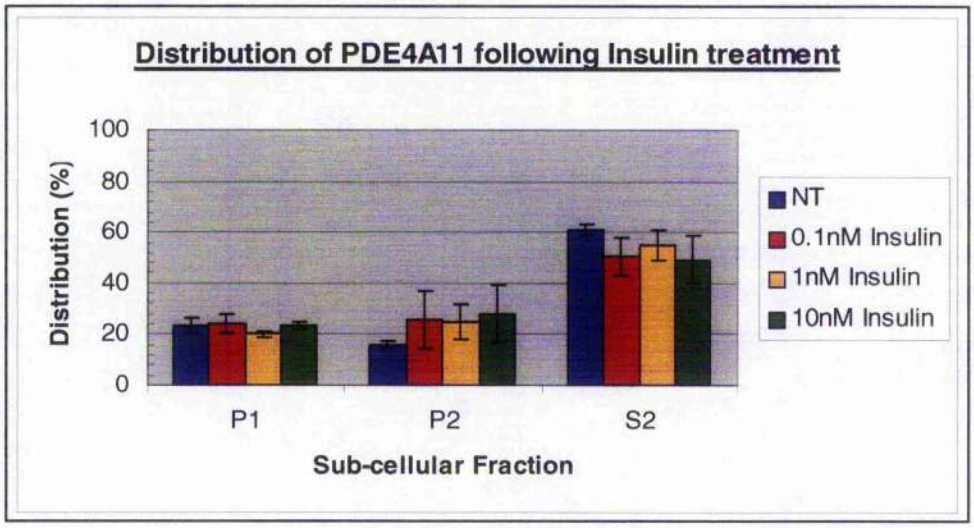
Distribution of PDE4A11 following Insulin treatment
Distribution (%)
100
80
60
40
20
0
P1
P2
S2
Sub-cellular Fraction
NT
0.1nM Insulin
1nM Insulin
10nM Insulin

Figure 3.7 – PDE4A11 translocation to the plasma membrane of HEK293 cells following stimulation with insulin.

(a), top panels, are Western blots of the endogenous activation time course of Akt (Protein Kinase B; PKB) in HEK293 cells following treatment with insulin, at increasing concentrations (0.1, 1 and 10nM), between 0 and 15min. The activation of Akt was detected using a phospho-specific anti-serum to one of the phosphorylation sites required for Akt activation. (a), bottom panels, are Western blots representing the total endogenous expression levels of Akt in HEK293 cells and also functions as loading controls for the Akt activation time courses. PDE4A11 was transiently expressed in HEK293 cells. The cells were stimulated with the increasing concentrations of insulin for 15min. The cells were harvested and sub-cellular fractionated as described previously [McPhee et al., 1995]. (b), shows Western blots probed with the C-terminal PDE4A-specific anti-serum to evaluate the effect of increasing insulin concentrations on the sub-cellular distribution of PDE4A11 in HEK293 cells. (c), is the quantification of these Western blots to assess any change in the HEK293 cellular distribution of PDE4A11 within each sub-cellular fraction (total PDE4A11 expression equals 100%). All data shown are either representative Western blots of two separate transfections and sub-cellular fractionations. Mean quantification data of the Western blots +/- standard deviation are representative of the two separate transfections and sub-cellular fractionations. Two-Sample t-test statistical analysis of the quantification data were undertaken, where $p < 0.05$ indicates a statistically significant difference in the relative PDE4A11 immuno-reactivity within the P2 sub-cellular fraction between untreated and treated cells, as indicated.

First-generation PDE4 inhibitors

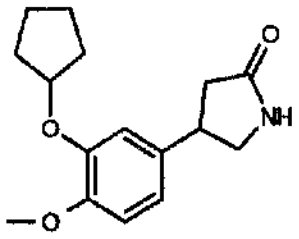

Rolipram

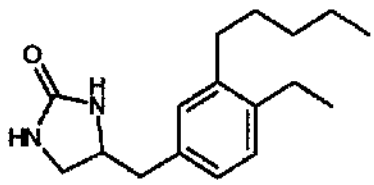

Ro 20-1724

Second-generation PDE4

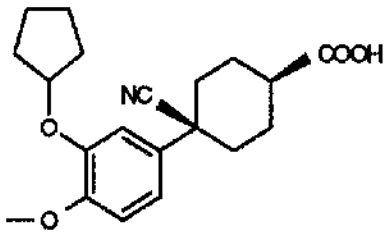

Ariflo (Cilomilast)

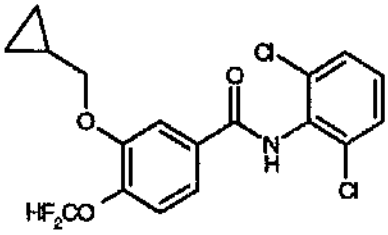

Roflumilast

Xanthine derivative PDE4 inhibitor

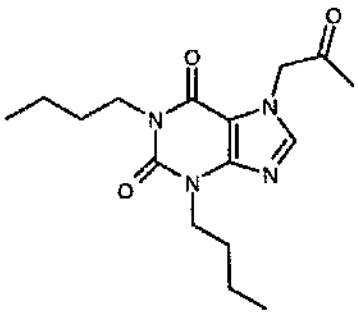

Denbufylline

Figure 3.8 – Chemical structures of the common PDE4 inhibitors.

Structures taken from Houslay et al., 2005.

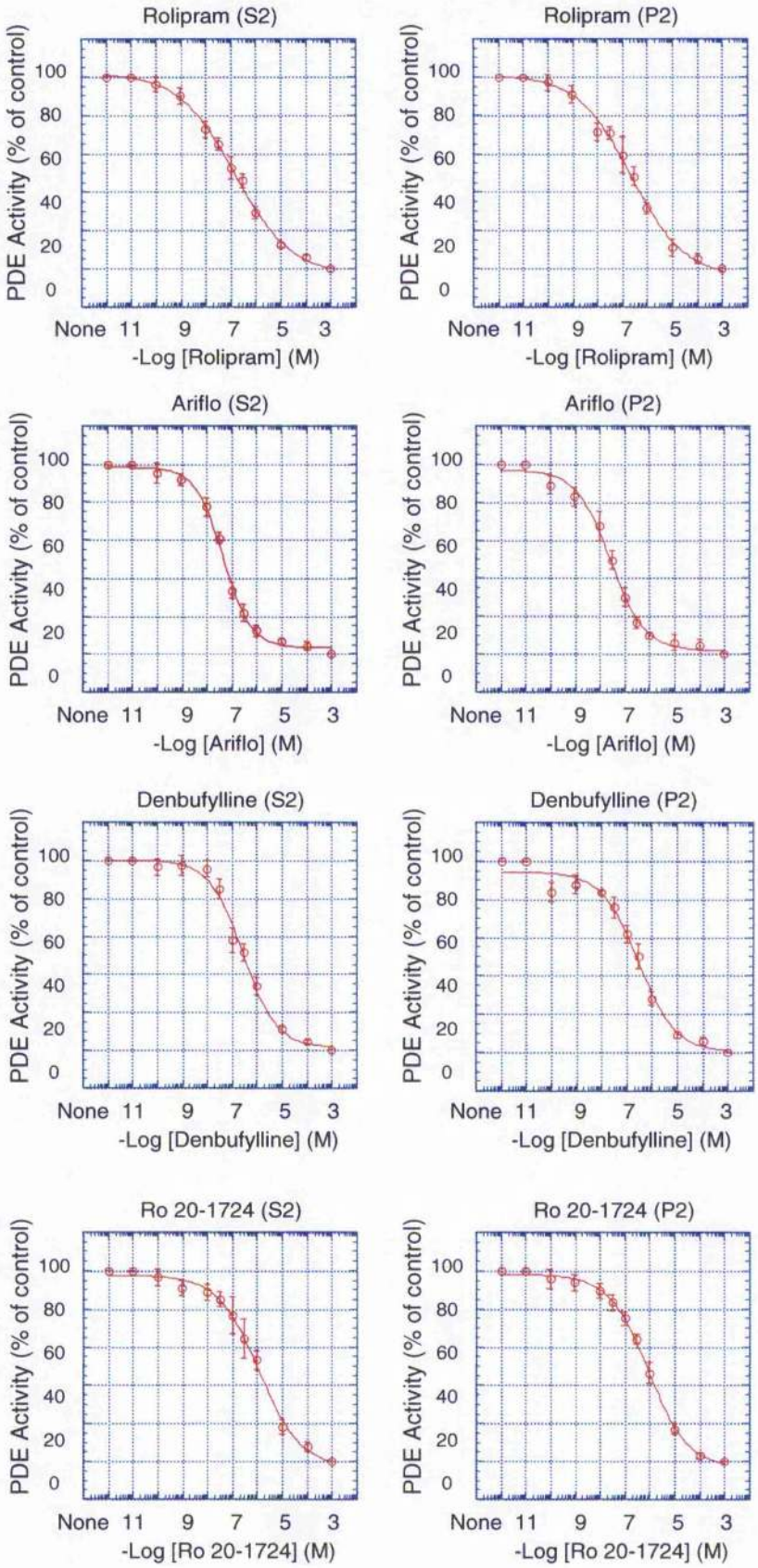
Rolipram (S2)
Rolipram (P2)
Ariflo (S2)
Ariflo (P2)
Denbufylline (S2)
Denbufylline (P2)
Ro 20-1724 (S2)
Ro 20-1724 (P2)
PDE Activity (% of control)
0
20
40
60
80
100
None 11 9 7 5 3
-Log [Rolipram] (M)
-Log [Ariflo] (M)
-Log [Denbufylline] (M)
-Log [Ro 20-1724] (M)

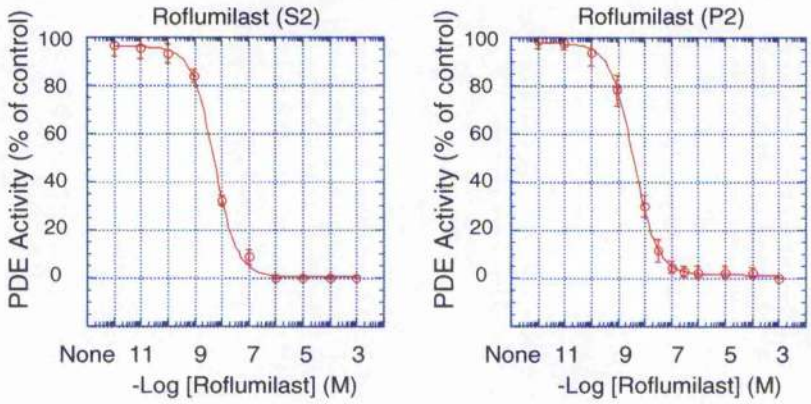
Roflumilast (S2)
PDE Activity (% of control)
100
80
60
40
20
0
None 11 9 7 5 3
-Log [Roflumilast] (M)
Roflumilast (P2)
PDE Activity (% of control)
100
80
60
40
20
0
None 11 9 7 5 3
-Log [Roflumilast] (M)

Figure 3.9 – Inhibition of PDE4A11 by selective PDE4 inhibitors.

COS7 cells were transfected to transiently express each isoform before sub-cellular fractionation into high-speed supernatant (S2) and high-speed pellet (P2). PDE4 activity assays were done using 1μM cAMP as substrate against a range of inhibitor concentrations, as indicated. The data presented here are mean values +/- standard deviation of three separate transfections, sub-cellular fractionations and activity assays. The determinations of the respective IC_{50} values for each inhibitor are shown in Table 3.2.

Inhibitor	PDE4A4B (S2)	PDE4A4B (P2)	PDE4A10 (S2)	PDE4A11 (S2)	PDE4A11 (P2)
Rolipram	1.31 +/- 0.08	0.26 +/- 0.09	0.13 +/- 0.03	0.72 +/- 0.08	0.66 +/- 0.12
Ariflo	0.061 +/- 0.007	0.059 +/- 0.004	0.064 +/- 0.009	0.034 +/- 0.005	0.034 +/- 0.005
Denbufylline	0.56 +/- 0.30	0.46 +/- 0.20	0.59 +/- 0.17	0.25 +/- 0.06	0.31 +/- 0.04
Ro 20-1724	2.93 +/- 1.16	2.90 +/- 0.10	1.24 +/- 0.07	0.99 +/- 0.11	0.91 +/- 0.07
Roflumilast	0.0090 +/- 0.0016	0.0025 +/- 0.0009	0.0041 +/- 0.0008	0.0048 +/- 0.0004	0.0039 +/- 0.0002

Table 3.2 – IC_{50} values for inhibition of PDE4A11 by PDE4 selective inhibitors.

COS7 cells were transfected to transiently express each isoform before sub-cellular fractionation into high-speed supernatant (S2) and high-speed pellet (P2). Assays were done using 1μM cAMP as substrate against a range of inhibitor concentrations as indicated in Figure 3.7. Data is only shown for PDE4A10 expressed in the high-speed supernatant fraction (S2), as the majority (approximately 83%) of this isoform is soluble [Rena et al., 2001], as shown in Table 3.1. These data are given as IC_{50} values in micro-molar (μM) concentrations and are mean values +/- the standard deviation from three separate transfections, sub-cellular fractionations and activity assays.

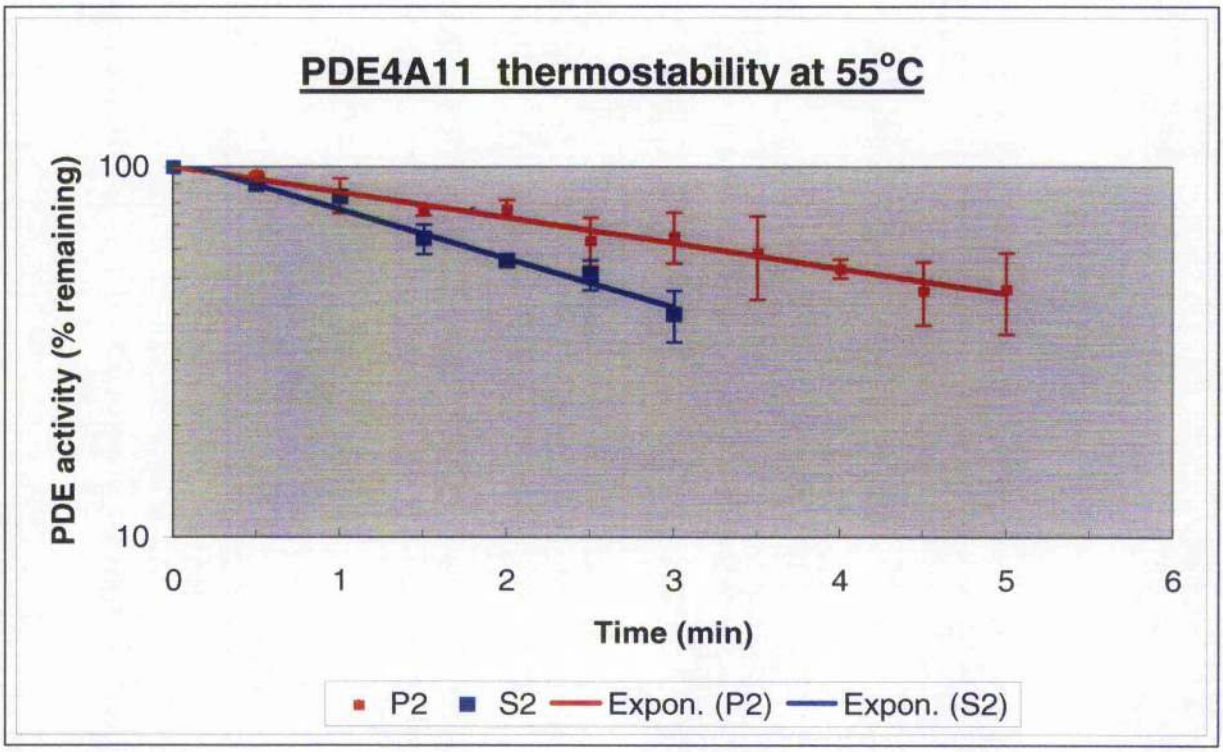
PDE4A11 thermostability at 55°C
PDE activity (% remaining)
100
10
0
1
2
3
4
5
6
Time (min)
P2
S2
Expon. (P2)
Expon. (S2)

Figure 3.10 – Thermo-stability of PDE4A11.

Recombinant PDE4A11 was transiently expressed in COS7 cells before fractionation of the cells into high-speed supernatant (S2; blue) and high-speed pellet (P2; red). Fractions were incubated at 55°C for the indicated times and then assayed for PDE4 activity using 1µM cAMP as substrate. The log% residual activity was calculated and plotted as a function of increasing time. The half-life ($t_{1/2}$) was determined as the time at which 50% of the total PDE4 activity at time zero remained. Data shown are from three separate experiments using fractions from three separate transfections and are expressed as mean values +/- standard deviation. Two-Sample t-Test statistical analysis of the determined half-life values for thermo-stability was undertaken, where $p < 0.05$ indicates a statistically significant difference between PDE4A11 sub-cellular fractions.

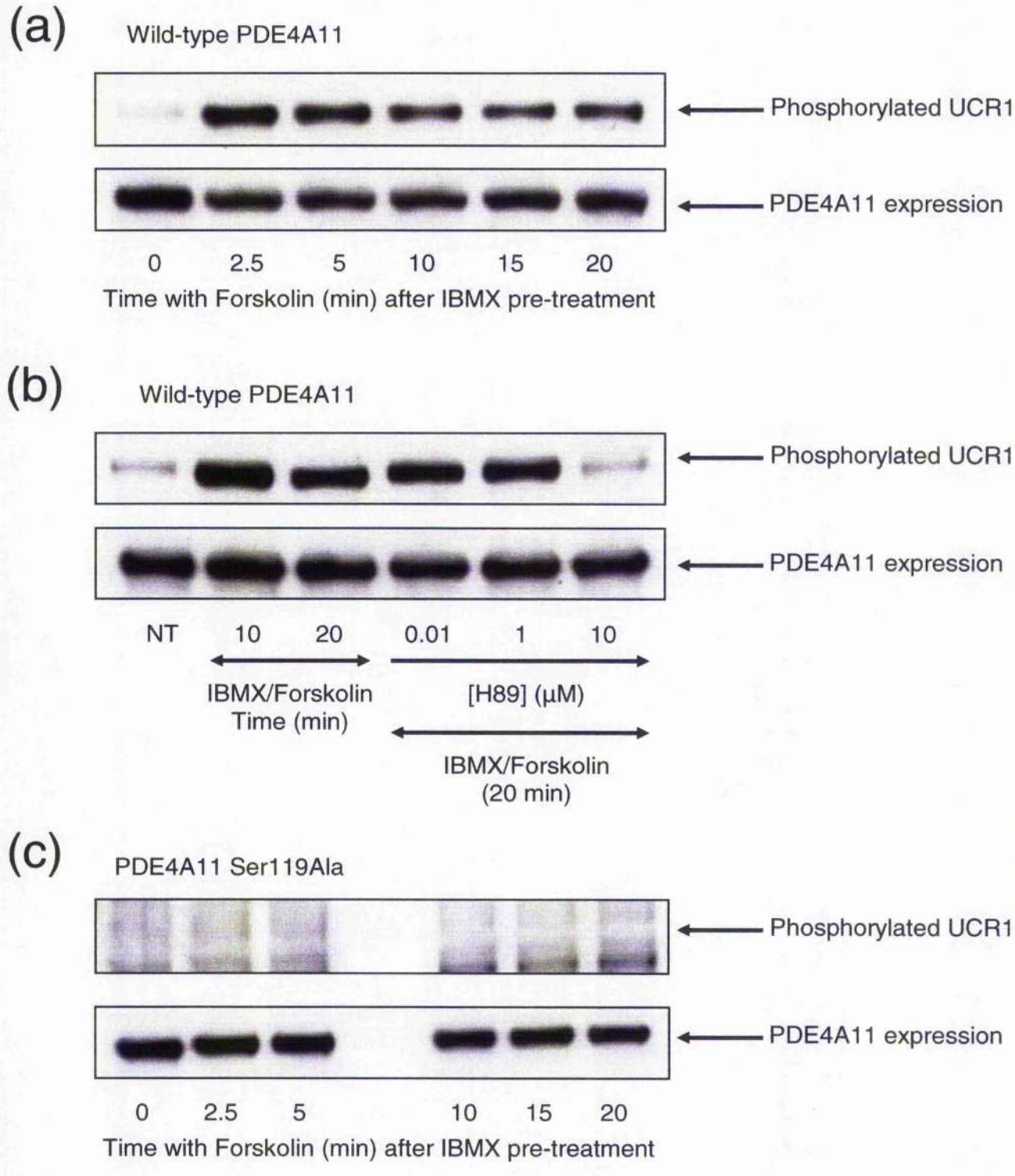
(a)
Wild-type PDE4A11
Phosphorylated UCR1
PDE4A11 expression
0 2.5 5 10 15 20
Time with Forskolin (min) after IBMX pre-treatment
(b)
Wild-type PDE4A11
Phosphorylated UCR1
PDE4A11 expression
NT 10 20 0.01 1 10
IBMX/Forskolin
Time (min)
[H89] (μM)
IBMX/Forskolin
(20 min)
(c)
PDE4A11 Ser119Ala
Phosphorylated UCR1
PDE4A11 expression
0 2.5 5 10 15 20
Time with Forskolin (min) after IBMX pre-treatment

(d)

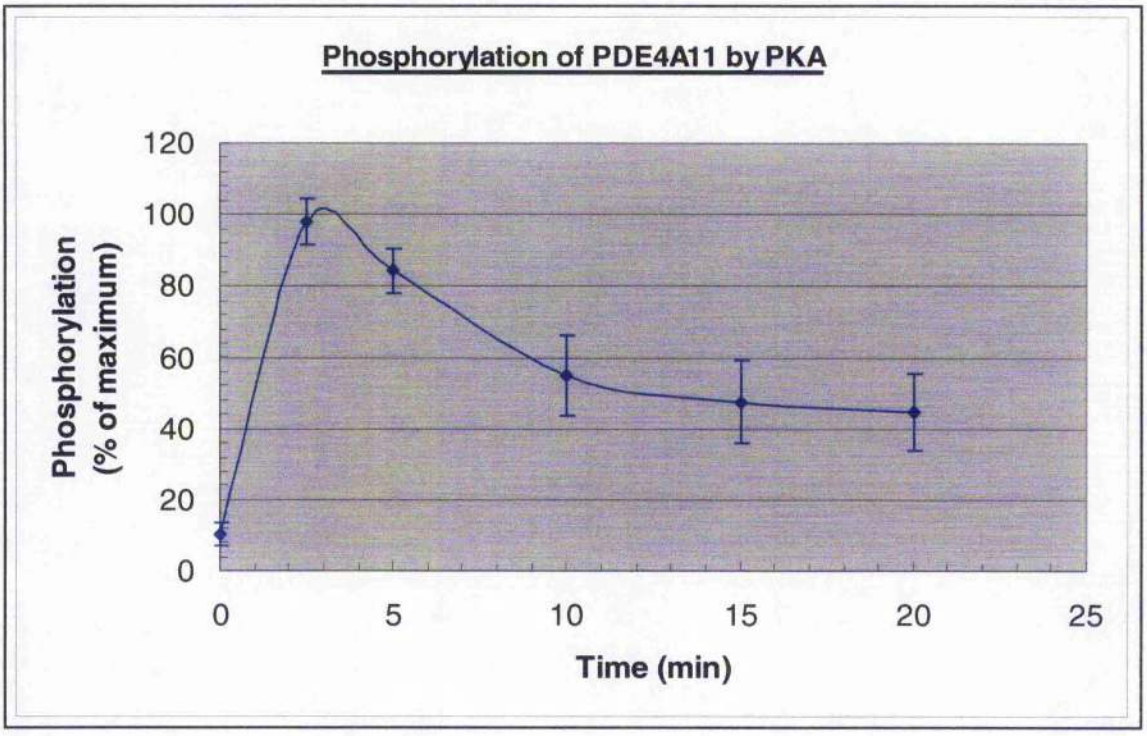
Phosphorylation of PDE4A11 by PKA
Phosphorylation (% of maximum)
120
100
80
60
40
20
0
0
5
10
15
20
25
Time (min)

(e)

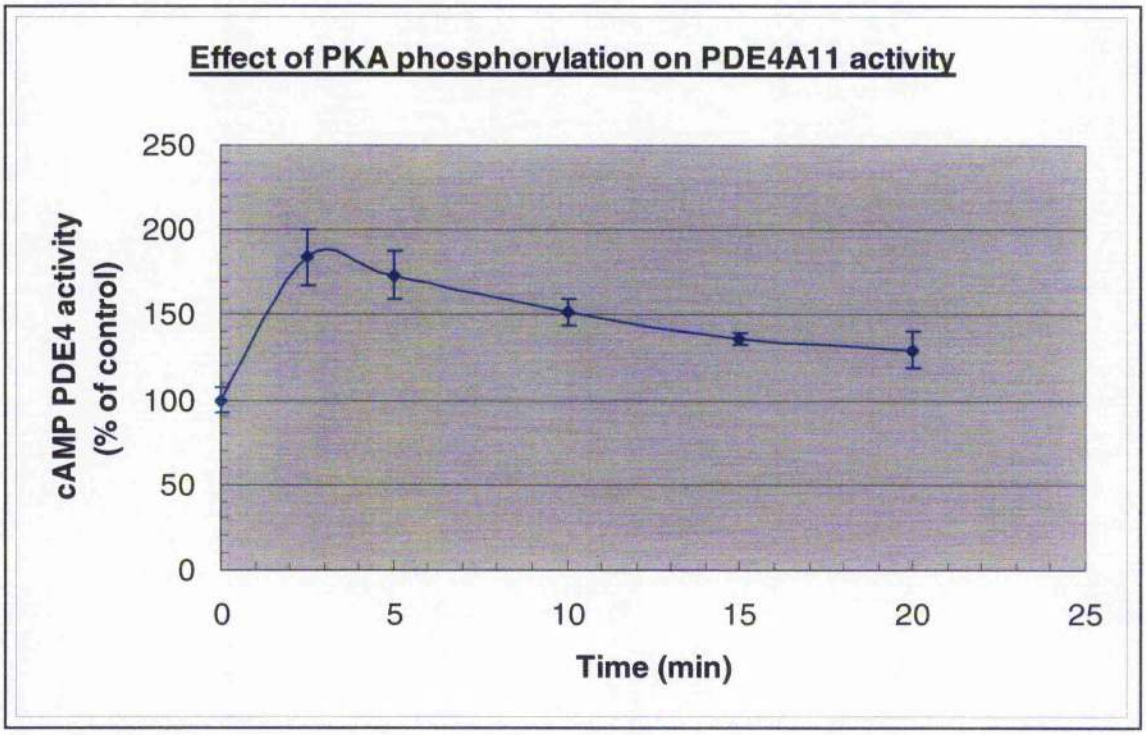
Effect of PKA phosphorylation on PDE4A11 activity
cAMP PDE4 activity (% of control)
250
200
150
100
50
0
0
5
10
15
20
25
Time (min)

Figure 3.11 – Phosphorylation and activation of PDE4A11 by PKA.

COS7 cells were transfected to transiently express human PDE4A11. The transfected cells were pre-treated for 10min with the non-specific PDE inhibitor IBMX (100µM) before challenge, 0–20min, with the adenylyl cyclase activator forskolin (100µM). (a), top panel, is a Western blot probed with a specific anti-serum to the PKA phosphorylated serine residue in within the UCR1 regulatory module (herein referred to as phospho-UCR1) (a), bottom panel, shows the same Western blot re-probed with the PDE4A C-terminal specific anti-serum to provide both loading and PDE4A11 expression controls. (b), top panel, is a Western blot probed with the phospho-UCR1 anti-serum. COS7 cells over-expressing PDE4A11 were pre-treated as above with IBMX and challenged with forskolin for 10 and 20min. This 20-min forskolin challenge was repeated in the presence of increasing concentrations of the PKA inhibitor H89 (0.1, 1 and 10µM). (b), bottom panel, shows the same Western blot re-probed with the PDE4A C-terminal specific anti-serum to provide both loading and PDE4A11 expression controls. The plasmid encoding wild type human PDE4A11 was engineered to express PDE4A11 with the target phosphorylation Ser-119-Ala. The PKA phosphorylation time course described above was repeated with COS7 cells transfected to transiently express the mutant form. (c), top panel, is a Western blot probed with the phospho-UCR1 anti-serum and, bottom panel, is the same Western blot re-probed with the PDE4A C-terminal specific anti-serum to provide both loading and PDE4A11 expression controls. (d), shows the densitometry of the Western blots showing the PKA phosphorylation time course of PDE4A11. These data are expressed as a percentage of the maximum phosphorylation, where the phospho-UCR1 densitometry is corrected for PDE4A11 expression. (e), shows the effect of the PKA phosphorylation on PDE4A11 catalytic activity. Assays were done using 1µM cAMP as substrate with COS7 cell lysates expressing equal immuno-reactive amounts of PDE4A11, as determined by the quantification of PDE4A11 expression. All data shown are either representative Western blots of three separate transfections and experiments, or mean data +/- standard deviation of three separate transfections and experiments.

(a)

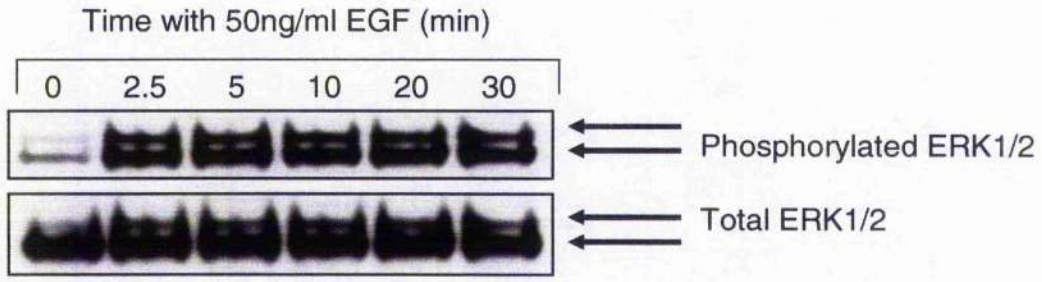
Time with 50ng/ml EGF (min)
0
2.5
5
10
20
30
Phosphorylated ERK1/2
Total ERK1/2

(b)


No treatment
EGF
EGF + U0126
Control
IP
Control
IP
Control
IP
Phosphorylated PDE4A11
PDE4A11 immuno-precipitated

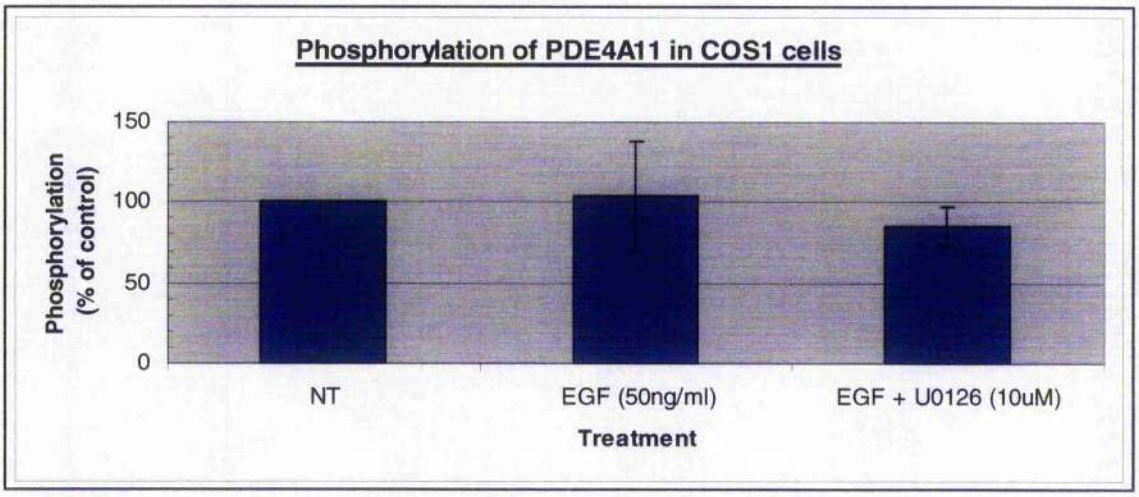
Phosphorylation of PDE4A11 in COS1 cells
Phosphorylation (% of control)
150
100
50
0
NT
EGF (50ng/ml)
EGF + U0126 (10uM)
Treatment

(c)

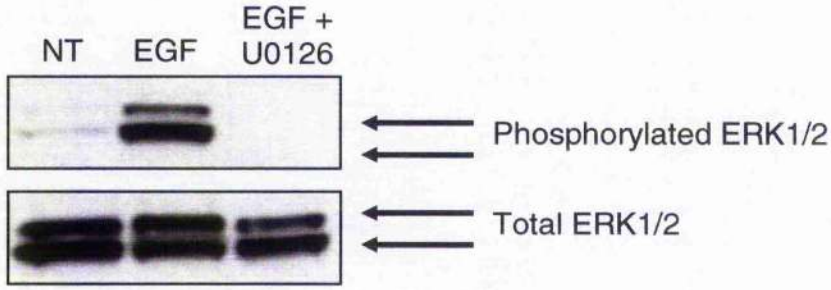
NT
EGF
EGF + U0126
Phosphorylated ERK1/2
Total ERK1/2

Figure 3.12 – Phosphorylation of PDE4A11 in COS1 cells following stimulation with EGF.

COS1 cells were transfected to over-express PDE4A11 and the cells were stimulated with EGF (50ng/ml) for up to 30min. (a), top panel, is a Western blot showing an EGF time course (0-30min) of endogenous ERK1/2 activation in COS1 cells. ERK1/2 activation was detected using a phospho-specific anti-serum to the phosphorylation sites required for activation. (a), bottom panel, is a Western blot showing the total, endogenous levels of ERK1/2. COS1 cells were transfected to transiently express PDE4A11. The transfected cells were grown in phosphate-free media radio-labelled with [^{32}P]-orthophosphate. The cells were retained as either untreated, stimulated with EGF for 30min alone or EGF in the presence of the MEK inhibitor, U0126 (10μM). The cells were harvested and PDE4A11 was immuno-precipitated using the C-terminal PDE4A-specific anti-serum conjugated to Protein G agarose resin. Protein G agarose resin was used alone as an immuno-precipitation control. The immuno-precipitated proteins were separated by SDS-PAGE and transferred to a nitrocellulose membrane where the radioactive proteins were resolved using phosphor image screen technology. (b), top panel, is a phosphor screen image of the phosphorylation status of PDE4A11 following immuno-precipitation from (un)treated whole cell lysates. (b), bottom panel, is a Western blot showing the relative immuno-reactive amounts of PDE4A11 extracted from the cell lysate by immuno-precipitation. The level of phosphorylation was quantified and corrected for the relative level of PDE4A11 immuno-precipitated. (b), graph, quantifies the level of PDE4A11 phosphorylation, in comparison to no treatment (100%), following EGF stimulation of COS1 cells. Also shown is the quantification of the effect of ERK1/2 inhibition by U0126 on PDE4A11 phosphorylation. (c), top panel, is a Western blot showing the activation and inhibition of ERK1/2, as detected using the phospho-specific anti-serum, and (c), bottom panel, shows the total level of endogenous ERK1/2 expression in the COS1 cell lysates. All data shown are either representative phosphor screen images or Western blots of three separate transfections and experiments, or mean data +/- standard deviation of the three separate transfections and experiments. Paired t-test

statistical analysis of the quantified phosphorylation data were undertaken, where $p < 0.05$ indicates a statistically significant difference in the level of wild type PDE4A11 phosphorylation between untreated and treated cells, as indicated.

(a)

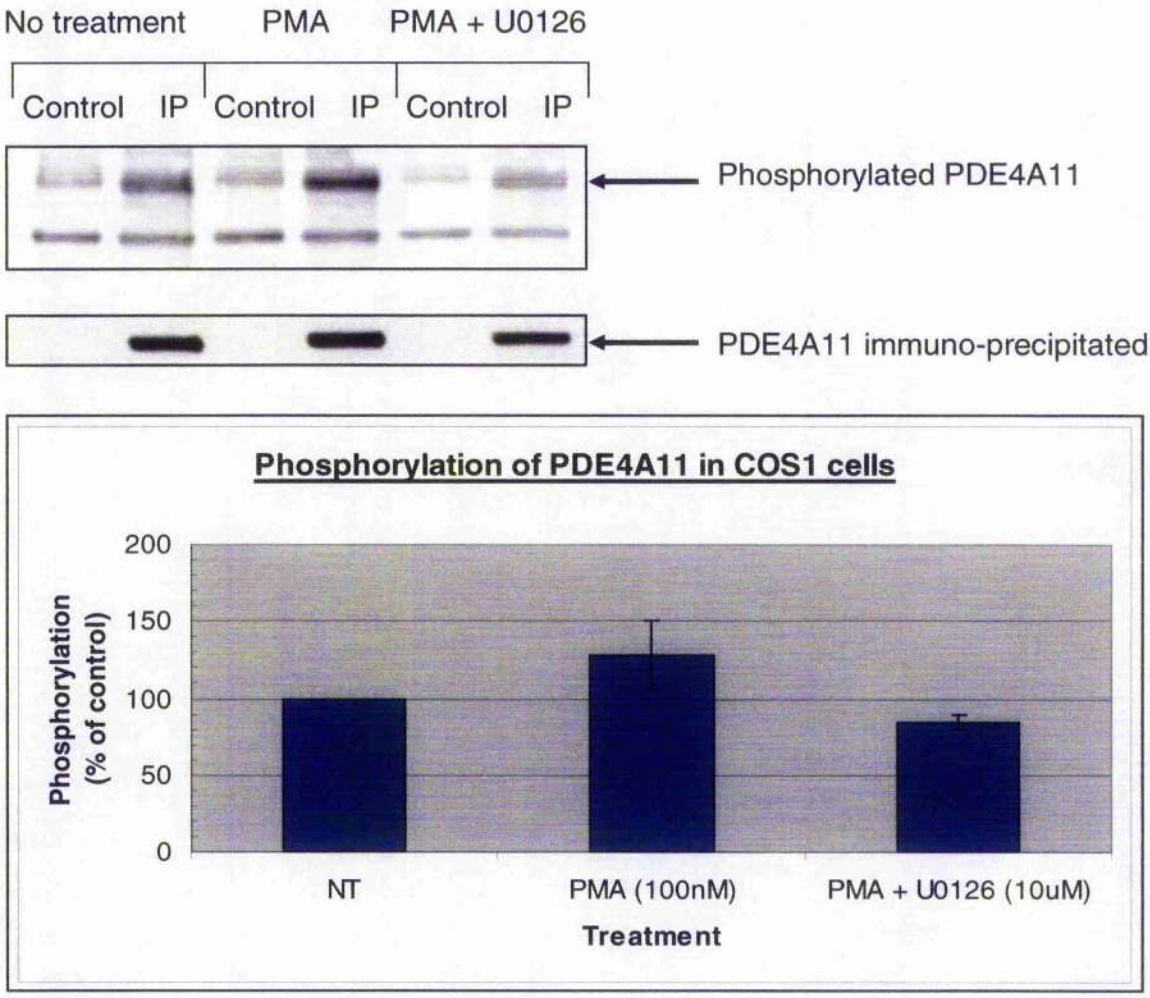
No treatment
PMA
PMA + U0126
Control
IP
Control
IP
Control
IP
Phosphorylated PDE4A11
PDE4A11 immuno-precipitated
Phosphorylation of PDE4A11 in COS1 cells
Phosphorylation (% of control)
200
150
100
50
0
NT
PMA (100nM)
PMA + U0126 (10uM)
Treatment

(b)

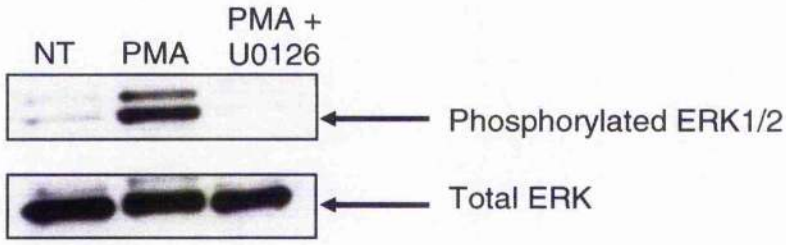
NT
PMA
PMA + U0126
Phosphorylated ERK1/2
Total ERK

Figure 3.13 – Phosphorylation of PDE4A11 in COS1 cells following stimulation with phorbal 12-myristate 13-acetate (PMA).

COS1 cells were transfected to over-express PDE4A11 and stimulated with PMA (100nM) for 20min. The transfected cells were grown in phosphate-free media with phosphate re-introduced by the addition of [^{32}P]-orthophosphate. The cells were stimulated with PMA for 20min alone and in the presence of the MEK inhibitor, U0126 (10μM). The cells were harvested and PDE4A11 was immuno-precipitated using the C-terminal PDE4A-specific anti-serum conjugated to Protein G agarose resin. Protein G agarose resin was used alone as an immuno-precipitation control. The immuno-precipitated proteins were separated by SDS-PAGE and transferred to a nitrocellulose membrane where the radioactive proteins were resolved using phosphor image screen technology. (a), top panel, is a phosphor screen image of the phosphorylation level of PDE4A11 following immuno-precipitation from (un)treated cell lysates. (a), bottom panel, is a Western blot showing the relative immuno-reactive amounts of PDE4A11 extracted from the cell lysate by immuno-precipitation. (a), graph, quantifies any change in PDE4A11 phosphorylation in COS1 cells, compared to no treatment (100%), following PMA stimulation. Similarly, the effect of ERK1/2 inhibition by U0126 on PDE4A11 phosphorylation is also quantified. (b), top panel, shows the activation and inhibition of ERK1/2, as detected using the phospho-specific anti-serum to the phosphorylation sites required for activation. The level of phosphorylation was quantified and corrected for the immuno-reactive level of PDE4A11 immuno-precipitated. (b), bottom panel, shows the total level of endogenous ERK1/2 expression in the COS1 whole cell lysates. All phosphor screen images and Western blots are representative of two separate transfections and experiments. Mean quantification data +/- standard deviation are also the products of the two separate transfections and experiments. Paired t-test statistical analysis of the quantified phosphorylation data were undertaken, where $p < 0.05$ indicates a statistically significant difference in the level of wild type PDE4A11 phosphorylation between untreated and treated cells, as indicated.

(a)

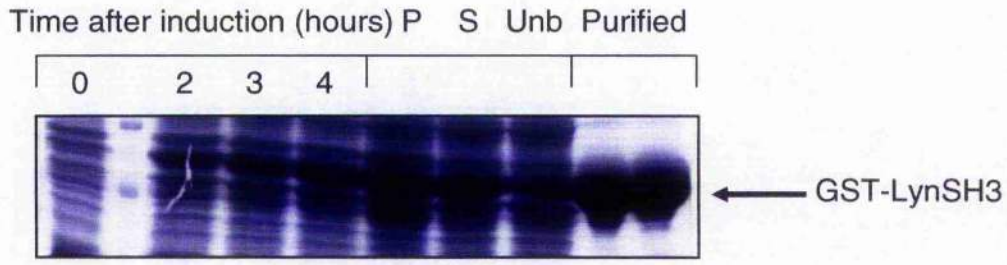
Time after induction (hours) P S Unb Purified
0 2 3 4
GST-LynSH3

(b)

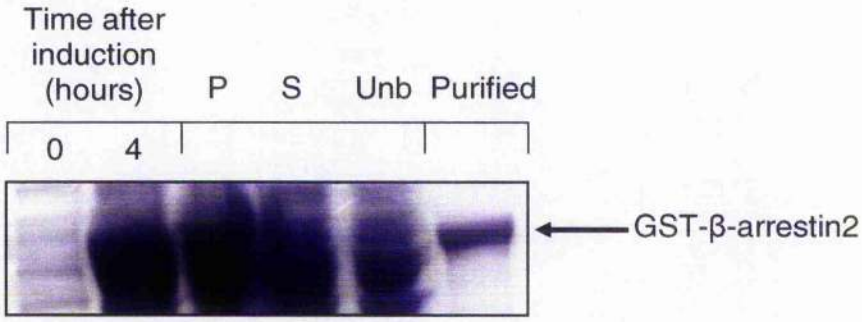
Time after induction (hours)
P S Unb Purified
0 4
GST-β-arrestin2

Figure 3.14 – *E.coli* expression and purification of recombinant GST-tagged LynSH3 and GST-tagged β-arrestin2.

Coomassie® staining of SDS polyacrylamide gels showing the *E.coli* expression of recombinant Gluathione-S-Transferase (GST) fusion proteins. The proteins expressed were the SH3 domain of the tyrosyl kinase Lyn (LynSH3), panel (a), and the signalling scaffold protein β-arrestin2, panel (b). Briefly, competent *E.coli* BL21 pLysS (DE3) cells were transformed with pGEX plasmids encoding either GST-LynSH3 or GST-β-arrestin2. Expression of the proteins was induced with 0.2mM Isopropyl-β-D-thiogalactopyranoside (IPTG) for 4h at 30°C. The cells were collected, re-suspended in lysis buffer and subjected to sonication to produce total cell extract (P). The soluble proteins were isolated by centrifugation (S). The expressed recombinant GST fusion proteins were purified using glutathione sepharose resin and eluted using excess glutathione (10mM). Fractions of the GST fusion proteins remained unbound to the glutathione sepharose resin (Unb) whereas a significant proportion bound could be purified to a single band as detectable by Coomassie® staining of the SDS polyacrylamide gels (Purified). These gels represent the single successful expression experiment undertaken for both proteins in *E.coli*.

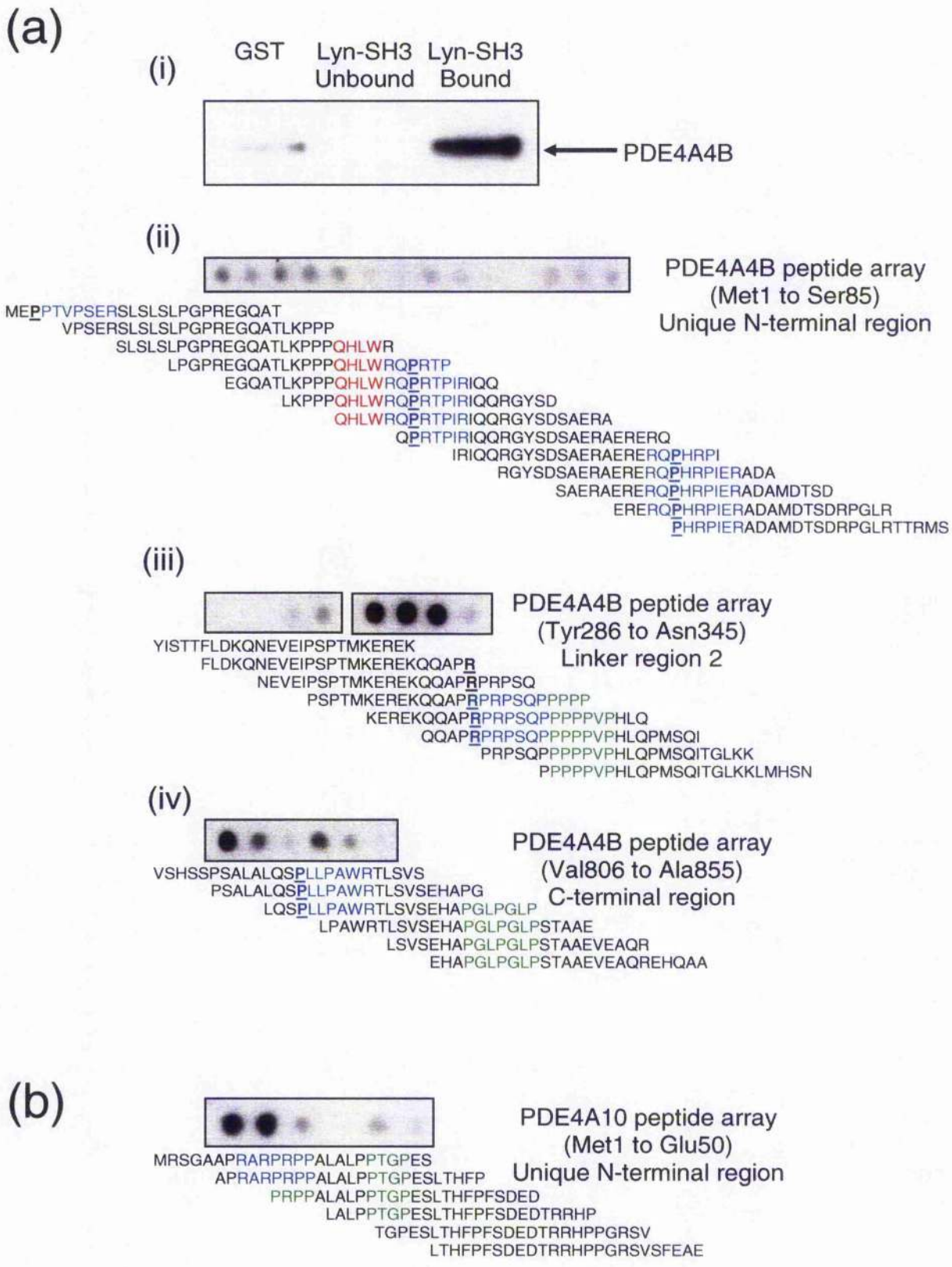
(a)
(i)
GST
Lyn-SH3 Unbound
Lyn-SH3 Bound
PDE4A4B
(ii)
PDE4A4B peptide array
(Met1 to Ser85)
Unique N-terminal region
MEPPTVPSERSLSLSLPGPREGQAT
VPSERSLSLSLPGPREGQATLKPPP
SLSLSLPGPREGQATLKPPPQHLWR
LPGPREGQATLKPPPQHLWRQPRTP
EGQATLKPPPQHLWRQPRTPIRIQQ
LKPPPQHLWRQPRTPIRIQQRGYSD
QHLWRQPRTPIRIQQRGYSDSAERA
QPRTPIRIQQRGYSDSAERAERERQ
IRIQQRGYSDSAERAERERQPHRPI
RGYSDSAERAERERQPHRPIERADA
SAERAERERQPHRPIERADAMDTSD
ERERQPHRPIERADAMDTSDRPGLR
PHRPIERADAMDTSDRPGLRTTRMS
(iii)
PDE4A4B peptide array
(Tyr286 to Asn345)
Linker region 2
YISTTFLDKQNEVEIPSPTMKEREK
FLDKQNEVEIPSPTMKEREKQQAPR
NEVEIPSPTMKEREKQQAPRPRPSQ
PSPTMKEREKQQAPRPRPSQPPPPP
KEREKQQAPRPRPSQPPPPPVPHLQ
QQAPRPRPSQPPPPPVPHLQPMSQI
PRPSQPPPPPVPHLQPMSQITGLKK
PPPPPVPHLQPMSQITGLKKLMHSN
(iv)
PDE4A4B peptide array
(Val806 to Ala855)
C-terminal region
VSHSSPSALALQSPLLPAWRTLSVS
PSALALQSPLLPAWRTLSVSEHAPG
LQSPLLPAWRTLSVSEHAPGLPGLP
LPAWRTLSVSEHAPGLPGLPSTAAE
LSVSEHAPGLPGLPSTAAEVEAQR
EHAPGLPGLPSTAAEVEAQREHQAA
(b)
PDE4A10 peptide array
(Met1 to Glu50)
Unique N-terminal region
MRSGAAPRARPRPPALALPPTGPES
APRARPRPPALALPPTGPESLTHFP
PRPPALALPPTGPESLTHFPFSDED
LALPPTGPESLTHFPFSDEDTRRHP
TGPESLTHFPFSDEDTRRHPPGRSV
LTHFPFSDEDTRRHPPGRSVSFEAE

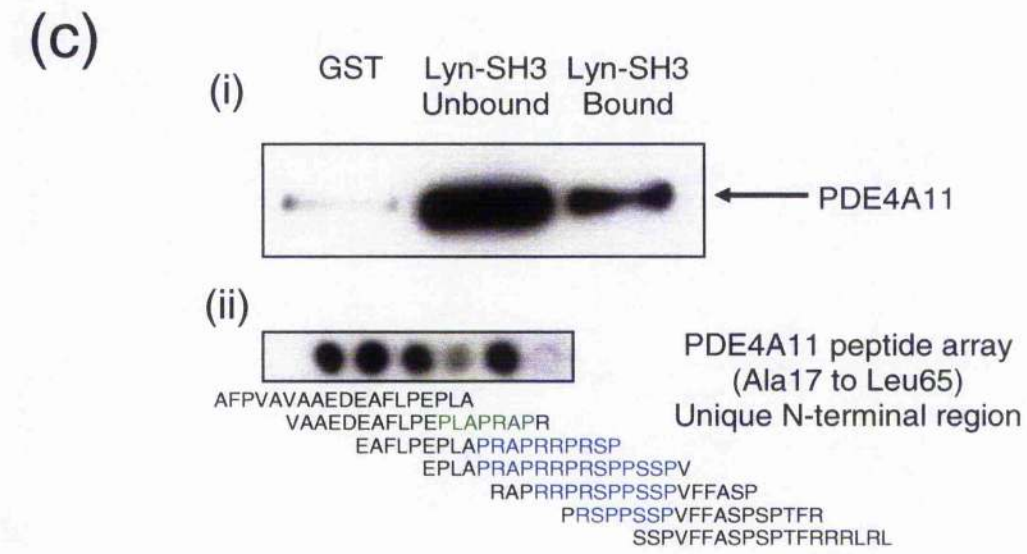
(c)
(i)
GST
Lyn-SH3 Unbound
Lyn-SH3 Bound
PDE4A11
(ii)
PDE4A11 peptide array
(Ala17 to Leu65)
Unique N-terminal region
AFPVAVAAEDEAFLPEPLA
VAAEDEAFLPEPLAPRAPR
EAFLPEPLAPRAPRRPRSP
EPLAPRAPRRPRSPPSSPV
RAPRRPRSPPSSPVFFASP
PRSPPSSPVFFASPSPTFR
SSPVFFASPSPTFRRRLRL

Figure 3.15 – Interaction of PDE4A long isoforms with the SH3 domain of the Src tyrosyl kinase, Lyn.

Pull-down assays were used to probe the interaction of the purified GST-LynSH3, immobilised on glutathione sepharose resin, with COS7 cell lysate expressing equal immuno-reactive amounts of either PDE4A4B or PDE4A11, as determined using the C-terminal PDE4A-specific anti-serum. (a), panel (i), and (c), panel (i), shows the interactions of GST-LynSH3 with PDE4A4B or PDE4A11 respectively (Lyn-SH3 Bound). As a control, the pull-down of PDE4A4B or PDE4A11 with GST alone was compared (GST). To directly compare the interaction of PDE4A4B and PDE4A11 with GST-LynSH3, the cell lysate following the pull-down assay was also probed for PDE4A using the C-terminal PDE4A-specific anti-serum (Lyn-SH3 Unbound). This analysis was undertaken as described previously for PDE4A4B [McPhee et al., 1999] and PDE4A10 [Rena et al., 2001]. (a), panels (ii) – (iv), map the interaction sites of GST-LynSH3 on full-length PDE4A4B using peptide array technology. Briefly, the entire PDE4A4B peptide sequence was synthesised on a membrane and the membrane incubated with the purified GST-LynSH3. The membrane was then essentially treated as a Western blot and probed for GST-LynSH3 binding using a GST-specific anti-serum. (b), and (c), panel (ii), shows similar peptide array analysis of the GST-LynSH3 binding sites on the unique N-terminal and UCR1 of PDE4A10 and PDE4A11 respectively. All Western blots shown are representative of the results obtained from three separate experiments. The peptide array interaction data are from experiments done once.

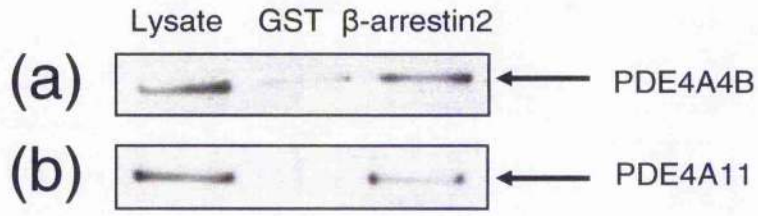
Lysate
GST
β-arrestin2
(a)
PDE4A4B
(b)
PDE4A11

Figure 3.16 – Interaction of PDE4A4B and PDE4A11 with the β-arrestin2 signalling scaffold protein.

Pull-down assays were used to probe the interaction of the purified GST-β-arrestin2, immobilised on glutathione sepharose resin, with COS7 cell lysate expressing equal immuno-reactive amounts of either PDE4A4B or PDE4A11, as determined using the C-terminal PDE4A-specific anti-serum. (a) and (b) show the interactions of GST-β-arrestin2 with PDE4A4B or PDE4A11 respectively. As a control, the pull-down of PDE4A4B or PDE4A11 with GST alone was compared (GST). All Western blots shown are representative of the results obtained from three separate experiments.

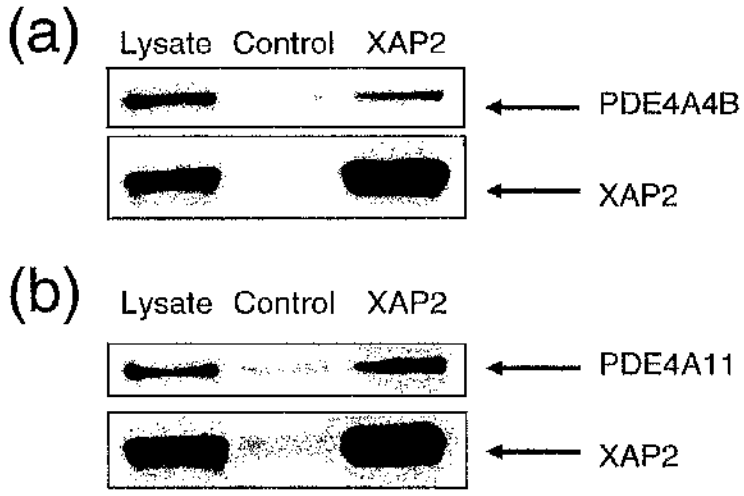
(a)
Lysate
Control
XAP2
PDE4A4B
XAP2
(b)
Lysate
Control
XAP2
PDE4A11
XAP2

Figure 3.17 – Interaction of PDE4A4B and PDE4A11 with the Immunophilin XAP2.

COS7 cells co-expressing untagged PDE4A4B or PDE4A11, and FLAG-tagged XAP2 were harvested. The FLAG-tagged XAP2 was immuno-purified using anti-FLAG agarose. The interaction of PDE4A4B or PDE4A11 with XAP2 was detected by probing the immuno-purified protein complexes with the C-terminal PDE4A-specific anti-serum. (a), top panel, shows the expression of PDE4A4B in COS7 cell lysate and the interaction of PDE4A4B with XAP2 following immuno-precipitation. As a control, anti-vsv agarose was used to determine the level of PDE4A4B non-specific interactions. (a), bottom panel, shows the immuno-reactive amounts of FLAG-tagged XAP2 expressed in COS7 cells, interacting with anti-vsv agarose, and immuno-precipitated respectively. (b), top panel, shows the interaction between PDE4A11 and XAP2. Similarly, anti-vsv agarose was used as the control. (b), bottom panel, shows the immuno-precipitation of XAP2 and the initial expression in COS7 cells. As before, non-specific immuno-precipitation of FLAG-tagged XAP2 was assessed in the control lane. All Western blots shown are representative of the results obtained from three separate experiments.

3.3 Discussion

cAMP signalling is the classical paradigm of the second messenger, participating in intra-cellular signal transduction pathways through a plethora of signalling molecules, allowing the cell to tailor specific responses to particular extra-cellular stimuli [Houslay and Milligan, 1997]. Intra-cellular cAMP is not homogeneously distributed within cells but exists in functionally relevant locals [Zaccolo and Pozzan, 2002 and Mongillo et al., 2004]. Numerous isoforms of both adenylyl cyclases and cAMP-specific PDE4s are responsible for the production and degradation of cAMP [Sunahara and Taussig, 2002 and Zhang et al., 2005]. The relationship between these enzymes provides the dynamic control of intra-cellular cAMP concentration [Houslay and Milligan, 1997 and Willoughby and Cooper, 2005]. There are now over twenty isoforms of PDE4 enzymes, some of which have been recently identified, and these primarily differ in their N-terminal region, which is responsible for intra-cellular targeting [Houslay et al., 1998, Shepherd et al., 2003, Wallace et al., 2005 and Richter et al., 2005]. Each isoform must play a distinct role in generating cAMP compartmentalisation within cells in which they are expressed, and herein lays the rationale for such an abundance of PDE4 isoforms.

The presence of a third novel PDE4A long isoform was indicated from the sequencing and analysis of the PDE4A gene locus [Sullivan et al., 1998]. This highlighted a putative PDE4A exon located between the exons for PDE4A4B and PDE4A10, which is now known as the exon encoding the third long isoform, PDE4A11 (Figure 3.1a). The position of this exon was sufficiently distant from the upstream PDE4A4B encoding exon that the intronic sequence could theoretically support the interaction of DNA transcription complexes (Figure 3.1b). Analysis, in a luciferase reporter assay, of the 1kb region immediately preceding the ATG start codon, and deletions therein, identified the first 250bp as the functional promoter region for PDE4A11, with the second 250bp negatively impacting promoter activity, indicating a possible level of transcription repression [Wallace et al., 2005].

The promoter regions of some PDE4 isoforms contain a CRE, which conforms to the general consensus sequence 5'-TGACGTCA-3' [Mayr and Montminy, 2001, Rena et al., 2001 and Le Jeune et al., 2002]. The promoter regions of these PDE4s also contain Stimulating protein 1 (Sp1) binding sites, which are typical of genes that do not contain a TATA box [Le Jeune, 2002, Rena et al., 2001]. Sp1 binding sites are generally located within GC-rich regions. The first 250bp region responsible for PDE4A11 promoter activity boasts up to six putative Sp1 binding sites, together with a number of binding sites for other transcription factors [Wallace et al., 2005]. Taken together these data indicates that the sequence immediately upstream of the PDE4A11 ATG start codon is sufficient for driving protein expression.

The unique N-terminal region of PDE4A11, encoded by the novel exon, is comprised of 81 amino acids that are substantially conserved across species including mouse, rat, bat and pig (Figure 3.2). In mouse and rat, the amino acid sequences are only 66 residues in length compared to the protein encoded by the human gene. In fact, only 50% of the human residues are conserved in rodents. The bat and pig PDE4A11 N-terminal sequences are approximately 77 amino acids in length and 80% of these are conserved with the human form. It will be interesting to ascertain whether the rat homologue of PDE4A11 has strikingly different properties because of sequence divergence at either extremity of the protein.

RT-PCR utilising primers to the unique N-terminal region of PDE4A11, and across splice junctions to the PDE4A common regions, was a simple method of authenticating the existence of the PDE4A11 isoform. This allowed the detection of PDE4A11 transcripts in HEK293 cells and in an abundance of human tissues (Figure 3.3b and 3.4). PDE4A isoforms are known to be differentially expressed in many immune and inflammatory cells [Barber et al., 2004, Shepherd et al., 2004, Abrahamsen, et al., 2004]. PDE4A11 provides the major PDE4A transcript level in immune and inflammatory cells, and also in bronchial epithelia and bronchial smooth muscle, with the level of PDE4A4B transcripts generally in lowest abundance throughout [Wallace et al., 2005]. It is possible that this could be due to the reduced promoter activity

of PDE4A4B compared to PDE4A10 and PDE4A11 [Wallace et al., 2005]. Subsequently to these studies, a PDE4A11 specific anti-serum was successfully generated (Figure 3.5a) and in a future study should be used to immunologically assess the endogenous distribution of PDE4A11 in many cell types, because invariably transcript levels do not accurately reflect protein expression.

Transient over-expression of PDE4A isoforms in mammalian cells shows distinct intra-cellular localisation per isoform (Table 3.1). PDE4A1 is predominantly membrane-bound, and this interaction is mediated through a novel helix-hinge-helix domain, known as TAPAS-1, which binds PA in phospho-lipid bi-layer of membranous structures [Smith et al., 1996 and Baillie et al., 2002]. PDE4A4B is can localise as both a soluble cytosolic and membrane-bound protein [Huston et al., 1996]. On the other hand, PDE4A10 is predominantly a soluble protein located within the cytosol of the cell with minor association with cellular organelles [Rena et al., 2001]. How do similar structures exhibit such diverse intra-cellular localisations? The point of structural divergence of PDE4A isoforms, coupled with the differential inclusion of the UCR regulatory modules, is their unique N-terminal regions, and these confer their sub-cellular targeting [Beard et al., 2002 and Houslay and Adams, 2003]. From sub-cellular fractionation experiments a soluble and particulate component of PDE4A11 was identified (Figure 3.5b). These data should always be interpreted with caution, as cellular disruption may result in PDE4A11 release from particulate structures, biasing the intra-cellular distribution profiles. Yet, if this were indeed the case, it is likely that a significantly greater proportion of PDE4A1 and PDE4A10 would be released to the cytosolic compartment of the cell when their intra-cellular distribution were assessed in a similar manner. Visualisation of PDE4A11 intra-cellular localisation using the human PDE4A C-terminal antibody conjugated to a fluorescent probe and laser-scanning confocal microscopy of the intact cell, we see that PDE4A11 cannot traverse the nuclear membrane, but is widely distributed across the peri-nuclear region and can associate distinctly in membrane ruffles at the cell margins (Figure 3.5c).

Analysis of the N-terminal region of PDE4A11 revealed a possible PIP3-binding PH domain. PH domains can bind with moderate or high affinity with phospho-inositides (PI), which are integral components of the lipid bi-layer of the plasma membrane. PIP2 is formed from PI by the action of PI-4K and PI-5K. The generation of PIP3 from PIP2 is catalysed by PI-3K. Therefore, it was hypothesised that N-terminal PDE4A11 binding of PIP3, the region responsible for the intra-cellular targeting of PDE4s, may cause the translocation of PDE4A11 from the cytosolic compartment of the cell to the plasma membrane [Chen et al., 2003]. Furthermore, PDE4A11 could be recruited to the appropriate location in the cell through an interaction with the SH3 domain of PI-3K and the putative SH3 binding domain within the unique N-terminal region (Figure 3.15c). In cells over-expressing PDE4A11 no such translocation or re-distribution was concluded (Figures 3.6 and 3.7). Similarly, in real-time laser-scanning confocal microscopy no redistribution of PDE4A11 was observed on stimulating PI-3K activity [E. Huston and M.D. Houslay, unpublished observations]. However, it is possible that the extensive over-expression may conceal a translocation mediated in cells where endogenous levels of PDE4A11 are immunologically detectable. Therefore, these experiments should be replicated in cells where endogenous expression can be detected with the novel PDE4A11 anti-serum. If these putative interactions were true, it could reveal the pertinent region of PDE4A11 that is responsible for its distinct peri-nuclear distribution and it localisation within membrane ruffles. In fact, PI-3K activity and the activation of the small G-protein Rac, are pre-requisites for membrane ruffle formation [Doughman et al., 2003 and Jaffe and Hall, 2005]. Furthermore, in neuronal cells, it has been observed that cAMP activation of PKA prevents the subsequent phosphorylation of PKB/Akt indicating a reduction in the activity of PI-3K [Leemhuis et al., 2004]. Therefore, it is possible that PDE4A11 is recruited to the plasma membrane ruffles through PIP3 binding and may exclusively control the cAMP concentrations in the vicinity of PI-3K, regulating its activity.

Rolipram is the archetypal PDE4-selective inhibitor. In cells chronically treated with rolipram, over-expressing a GFP chimera of PDE4A4B, results in a severe redistribution into accretion foci [Terry et al., 2003]. It is proposed

that the mechanism through which this occurs is a consequence of PDE4A4B conformational changes [Terry et al., 2003]. Thus, one would not expect PDE4A10 or PDE4A11 to form such accretion foci as they are not subject to conformational changes as sensed by differential rolipram inhibition (Figure 3.9 and Table 3.2). This is indeed the case with PDE4A10 and PDE4A11, and serves to provide credence to PDE4A10 and PDE4A11 not able to form distinct PDE4 conformers and that the formation of foci is an intrinsic property of PDE4A4B [Wallace et al., 2005].

PDE4 enzymes are being investigated as potential drug targets and the inhibition of PDE4 activity may provide considerable therapeutic benefits in a number of disease states including asthma, COPD and rheumatoid arthritis [Burnouf and Pruniaux, 2002 and Giembycz, 2002]. As such, there are many PDE4-selective inhibitors available (Figure 3.8). Here I note that PDE4A11 is concentration-dependently inhibited by rolipram, Ariflo®, denbufylline, Ro 20-1724 and roflumilast (Figure 3.9). Roflumilast is by far the most potent PDE4 inhibitor across all PDE4A isoforms, 150-fold more potent than the conventional PDE4 inhibitor rolipram (Table 3.2). As a membrane-bound protein PDE4A11 does not indicate any level of conformational change, as sensed by an increase in sensitivity to inhibition by rolipram nor does it extend to any adjustment in kinetic profile with respect to K_m or V_{max}. This phenomenon does not translate to PDE4A10, leaving PDE4A4B as the only PDE4A isoform to be subject to conformational change [Huston et al., 1996 and McPhee et al., 1999].

The interaction with SH3 domain containing proteins, such as the tyrosyl kinase Lyn, with LR2 of PDE4A4B is able to induce the associated conformational change. Indeed, inhibition of cytosolic PDE4A4B in the presence of Lyn-SH3 results in a comparable IC_{50} value for that of the particulate form [McPhee et al., 1999]. Previous data have indicated that both the N-terminal and LR2 binding sites for Lyn-SH3 are responsible for instigating the conformational change on the catalytic unit [McPhee et al., 1999]. Therefore, it was conceived that the lack of SH3 binding domains within the N-terminal region of PDE4A10 and PDE4A11 resulted in reduced

affinity for Lyn-SH3 therefore preventing these isoforms from undergoing conformational change [Rena et al., 2001 and Wallace et al., 2005]. However, exploiting peptide array technology has indicated that PDE4A10 and PDE4A11 do contain SH3 binding domains within their unique N-terminal region (Figure 3.15). Furthermore, the interaction of Lyn-SH3 with full length PDE4A4B indicates that the contribution of binding within the unique N-terminal region is insignificant compared to other sites within the protein. The interaction site for the SH3 domain of Lyn on PDE4A4B lies between Lys-306 and Arg-340 within LR2 and this region incorporates a class I SH3 binding motif from Arg-315 to Pro-321, immediately followed by an extensive core motif proline-rich region ending at Pro-327. These data co-relate closely with the previously published data indicating the same region by deletion analysis [McPhee et al., 1999]. A second site within the sub-family specific C-terminal region was also identified. This region incorporates the previously identified Pro-819 as the initiating proline residue of a putative class I SH3 binding motif [McPhee et al., 1999]. This is at variance with the published data that postulates Pro-3, Pro-37 and Pro-61 as initiating SH3 domain binding through distinct class I, class II and overlapping class I & II SH3 binding motifs respectively [McPhee et al., 1999]. The binding site for PDE4A10 was formerly assigned as the PDE4A common LR2, whereby deletion of this region ablated any interaction with Lyn-SH3 [Rena et al., 2001]. A class I SH3 binding domain, commencing at Arg-8, is present within this PDE4A10 region together with a putative core motif at Pro-20. Removal of the first three amino acids of the class I consensus sequence, leaving a simple core motif, ablated the interaction of Lyn-SH3. Likewise, the unique N-terminal of PDE4A11 is also able to bind Lyn-SH3. Within this region there are core SH3 binding motifs from Pro-33 with multiple, over-lapping class I and class II SH3 binding consensus motifs from Pro-36, which are likely to support Lyn-SH3 binding. To accurately map the critical residues for SH3 domain interactions with PDE4A long isoforms scanning alanine substitution peptide array analyses through the interacting regions are required, as described previously for the competing β-arrestin and RACK1 interactions with PDE4D5 [Bolger et al., 2006]. Therefore, it is entirely possible that the primary site of interaction of Lyn-SH3 with PDE4A long isoforms differ in such a way that they confer

distinct functional changes upon the catalytic unit. Lyn-SH3 preferentially interacts, with high affinity through, the LR2 of PDE4A4B eliciting profound conformational changes upon the catalytic unit. Conversely, PDE4A10 and PDE4A11 interact with Lyn-SH3, with lower affinity, through their unique N-terminal binding sites and this is sufficient to prevent Lyn-SH3 interaction with LR2 and the accompanying conformational change in catalytic function. Elucidation of full-length PDE4 crystal structures, perhaps in complex with Lyn-SH3, as has been achieved with cAMP analogues and PDE inhibitors, will be key to identifying this mechanism [Lee et al., 2002 , Sung et al., 2003 and Xu et al., 2004].

In spite of this, some conformational alteration between the particulate and cytosolic forms of PDE4A11 is implied from thermal stability experiments. These basic experiments show particulate PDE4A11 as being structurally more stable than the cytosolic form (Figure 3.10). A simple explanation of this is the stabilisation of the particulate form through protein interactions. Intriguingly, this is different for both PDE4A4B and PDE4A10, which show the cytosolic form as the more stable species with the particulate form in a conformation that makes it susceptible to denaturation [Rena et al., 2001]. PDE4A4B and PDE4A10 have superior thermal stability profiles than PDE4A11, in either sub-cellular location.

In the case of PDE4D3, PKA phosphorylation of Ser-54, contained within a UCR1 Arg-Arg-Glu-Ser-Phe consensus motif in all PDE4 long isoforms, translates to an increase in catalytic activity and a conformational change that is indicated by dual affinity for rolipram [Sette and Conti, 1996, Hoffman et al., 1998 and MacKenzie et al., 2002]. At present, PDE4D3 is the only isoform to exhibit distinct kinetics of inhibition by rolipram and it is widely accepted that this effect is not replicated in PDE4A long isoforms [MacKenzie et al., 2002]. PDE4A11 is phosphorylated and activated by PKA at Ser-119 within UCR1, an effect ablated by pre-treatment with the PKA inhibitor, H89 (Figure 3.11).

Analysis of the PDE4A11 unique N-terminal region indicates the presence of a putative ERK1 phosphorylation site at Ser-48, accompanied by an appropriately positioned possible docking domain further towards the N-terminal of the enzyme. Additionally, a potential GSK-3 site positioned four residues towards the N-terminal of the ERK1 site could further phosphorylate PDE4A11, where ERK1 primes for GSK-3 [Biondi and Nebreda, 2003 and Doble and Woodgett, 2003]. The phosphorylation efficiency of GSK-3 is enhanced up to 100-fold, if a priming phosphorylation is available. Furthermore, the phosphorylation of this site has the potential to allow 14-3-3 proteins to interact, indicating a prospective role for PDE4A11 in cell cycle regulation and apoptosis. No effect on PDE4A11 phosphorylation was observed with EGF (Figure 3.12). Therefore, it was hypothesised that EGF stimulation of ERK1/2 activity may disguise the potential ERK1/GSK-3 phosphorylation of PDE4A11 through the activation of the PI-3K signalling pathway. Although EGF elicits a substantial activation of ERK, the same concentration also induces a robust activation of PKB/Akt (Figure 3.6a), which directly inhibits the kinase activity of GSK-3 [Biondi and Nebreda, 2003 and Doble and Woodgett, 2003]. PMA directly activates ERK1/2 without affecting GSK-3 activity. Unfortunately, phosphorylation of PDE4A11 through the PMA activation of ERK1 also proved inconclusive (Figure 3.13). These experiments should be repeated in vitro, in the isolation of other signalling components to ultimately determine whether this phosphorylation is evident. However, the putative ERK1 docking domain does not contain the paired basic residues that form part of the KIM located approximately three to six residues downstream of the Leu-Xaa-Leu (LXL) motif and concomitantly also lacks the Phe-Gln-Phe (FQF) motif shown to be essential for the ERK2 phosphorylation of PDE4D isoforms [MacKenzie et al., 2000 and Sharrocks et al., 2000]. A novel phosphorylation of the unique N-terminal region of PDE4A11 will give much needed insight into its intra-cellular targeting, the regulation of its catalytic activity and the signal transduction pathways in which this particular isoform plays a crucial role.

A pertinent way of delivering protein to particular locations within the cell is through the interaction of scaffold or adaptor proteins. This is of

particular relevance in the delivery of PDE4D5 to the β_2-adrenoceptor and its function in the desensitisation and internalisation of the receptor [Perry et al., 2002 and Lynch et al., 2005]. PDE4 enzymes interact with the scaffold protein β-arrestin through a conserved binding region with the catalytic unit and an exclusive binding site within the unique N-terminal of PDE4D5, directing specificity of interaction [Bolger et al., 2003 and Bolger et al., 2006]. On this basis, PDE4A4B and PDE4A11 are able to interact through the conserved binding site located within the PDE4 catalytic unit (Figure 3.16).

A similar exclusive interaction has been determined for the rat PDE4A5 isoform with the immunophilin XAP2 [Bolger et al., 2003]. As with the interaction of PDE4 isoforms with β-arrestin, a common binding site is available through the Glu-Glu-Leu-Asp motif within UCR2, coupled with a functionally relevant interaction within the N-terminal domain of PDE4A5. These two regions both bind XAP2, but only the unique N-terminal interaction confers the inhibitory effect on PDE4A5 activity. Thus, one might expect all PDE4 isoforms containing a complete UCR2 domain to interact with XAP2, where functionally these interactions may not necessarily translate into any alteration in catalytic activity. However, yeast-2-hybrid data confirms that PDE4A5 specifically interacts with XAP2, suggesting that the N-terminal region elicits a conformational change within the regulatory modules, gating the UCR2 domain for further binding. Indeed, there is a precedent for such regulation through widespread appreciation of the UCR modules interacting with each other and in addition these regions provide the point of PDE4 enzyme dimerisation [Beard et al., 2000 and Richter and Conti, 2004]. PDE4A4B is the human homologue of rat PDE4A5 and as such contains both binding sites for XAP2. Therefore, it is able to interact with XAP2 in co-immuno-precipitation experiments (Figure 3.17a). Interestingly, PDE4A11 is also able to interact with XAP2, with similar affinity, indicating that XAP2 probably binds at a second site in PDE4A11, in additional to the common UCR2 domain, and in so doing allows the presentation of both interaction domains (Figure 3.17b).

Completing our knowledge of the diverse range of PDE4 isoforms expressed in all cell types can we only begin to elucidate their functional role in cellular signalling pathways. In this chapter, I have identified and extensively characterised the novel PDE4A11 isoform. In doing so, I have identified the subtle differences between this protein and the other PDE4A long isoforms, with respect to our current knowledge. PDE4A11 is kinetically identical to the other PDE4A long isoforms and its unique N-terminal region confers its intra-cellular distribution profile. Like all PDE4 long isoforms it is activated by PKA and is able to bind many proteins assigned as interacting partners to PDE4 enzymes. However, it is not subject to cleavage by caspase-3. PDE4A11 is not able to form distinct PDE4 conformers as indicated by both differential rolipram inhibition and the formation of accretion foci, although differences in thermal stability may indicate a degree of conformational shift between the membrane and cytosolic species. Further investigations into modifications, by phosphorylation and/or protein interactions is required to elucidate novel functions for this isoform. PDE4A11 is abundantly expressed across many human tissues and is the major transcript provider in immune and inflammatory cells. Consequently PDE4A11 may be of physiologic and therapeutic significance for selective PDE4 inhibition or knockdown using siRNA.

Chapter 4 MAPKAPK2 phosphorylation of PDE4A5

4.1 Introduction

4.1.1 Mitogen-Activated Protein Kinases

Mitogen-activated protein kinases (MAPKs) form phosphorylation cascades that control a variety of cellular functions including the immune and inflammatory response, gene regulation and cell differentiation, proliferation and apoptosis [Kyriakis and Avruch, 2001, Pearson et al., 2001 and Dong et al., 2002]. This diverse range of cellular functions alludes to the involvement of MAPK signalling in many disease states, including asthma and COPD, rheumatoid arthritis, cardiac hypertrophy and cancer [Cowan and Storey, 2003]. This super-family of protein kinases consists of three members; extra-cellular signal-regulated protein kinase (ERK), c-Jun N-terminal kinase (JNK) and p38 MAPK [Cowan and Storey, 2003]. A detailed list of the isoforms, alternative nomenclature, physiological substrates and function are described in Table 4.1. Activation of a cell surface receptor by growth factors and cytokines initiates these phosphorylation relay cascades through the step-wise phosphorylation-induced conformational change and activation of a series of at least three MAPKs. Following receptor stimulation, the MAP kinase kinase kinases (MAPKKKs) are recruited, and it is at this stage where a high degree of cross talk occurs between the three cascades. The Raf isoforms for the downstream activation of ERK1/2 are the most commonly studied MAPKKKs, which are recruited to the plasma membrane by the GTPase, Ras [Daum et al., 1994 and Kolch, 2005]. MAPKKK phosphorylation and activation of the downstream MAP kinase kinases (MAPKKs) induces the dual phosphorylation and activation of the MAP kinases (MAPK). MAPK kinase phosphorylation occurs at a serine or threonine residue and a tyrosine residue within the consensus motif [Ser/Thr]-Xaa-Tyr. It is at this level where greatest specificity is conferred across the three signalling pathways [Cowan

and Storey, 2003]. The intermediate amino acid residue (Xaa) within this phosphorylation motif controls the specificity of kinase activation, where the presence of glutamate confers ERK, proline confers JNK, and glycine confers p38 MAPK [Hommes et al., 2003]. Signalling specificity through ERK is achieved by MAPKK1 and MAPKK2, and via JNK through MAPKK4 and MAPKK7 [Dong et al., 2002]. p38 MAPK is directly activated through MAPKK3 and MAPKK6 [Dong et al., 2002]. Cross talk occurs between the JNK and p38 MAPK pathways through MAPKK4, which is able to activate both downstream MAPKs [Ho et al., 2003]. MAPKs direct the incorporation of phosphate groups at specific serine and threonine residues contained within a minimal consensus motif, and in some cases the presence of additional docking sites are required for target protein specificity [Tanoue et al., 2000, Sharrocks et al., 2000, Tanoue and Nishida, 2003 and Biondi and Nebreda, 2003]. Target proteins for phosphorylation by MAPKs are wide and varied, and include further downstream protein kinases within the same cascade and other protein kinases participating in alternative pathways [Houslay and Kolch, 2000]. Similarly, signalling enzymes such as PDE4s, scaffold and adaptor proteins such as β-arrestins, and the modulation of gene expression through the phosphorylation of transcription factors, are also targets for MAPKs [Lefkowitz and Shenoy, 2005].

4.1.2 p38 Mitogen-Activated Protein Kinase

The p38 MAPK signalling cascade is a key signal transduction pathway involved in the control of cellular immune, inflammatory and stress responses [Tibbles and Woodgett, 1999, Dong et al., 2002 and Hommes et al., 2003]. There are four isoforms of p38 MAPK encoded by four distinct genes, as shown in Table 4.1, which show cell type specific patterns of endogenous expression [Kyriakis and Avruch, 2001 and Hommes et al., 2003]. The α and β isoforms are ubiquitously expressed, with the α isoform predominating in immune and inflammatory cells. The γ (skeletal muscle) and δ (lungs, kidneys, testis, pancreas, and small intestine) isoforms have a more restricted expression pattern, as indicated in parenthesis.

4.1.2.1 Activation and Inhibition of p38 MAPK

p38 MAPKs are activated by a variety of extra-cellular stimuli such as growth factors, ultra-violet light, ionising radiation, oxidative stress, osmotic shock, and cytokines, as shown in Figure 4.1 [Cowan and Storey, 2003, Dent et al., 2003, Dodeller and Schulze-Koops, 2006 and Xu et al., 2006]. The activation of this 38kDa protein kinase occurs through the direct phosphorylation by upstream kinases such as MAPKK3, MAPKK4 and MAPKK6, the regulation of which is poorly understood. All isoforms are activated by MAPKK6 whereas MAPKK3 only activates the α and β isoforms. These kinases phosphorylate p38 MAPK at two residues essential for kinase activity, namely Thr-180 and Tyr-182, with specificity for p38 MAPK driven by Gly-181. Anisomycin, Figure 4.5, is a protein synthesis inhibitor and a commonly used agent that can initiate a robust activation of p38 MAPK activity in many cells through synergistic stimulation of Rac and Cdc42, as shown in Figure 4.1 [Cahill et al., 1996 and Uhlik et al., 2003]. Similarly shown in Figure 4.1 is the activation of p38 MAPK by TNFα through the recruitment of intra-cellular scaffold signalling proteins to the TNF receptor. Plasma membrane recruitment of these proteins, specifically TRAF2, facilitates the activation of apoptosis signal-regulating kinase (ASK), of which MAPKK6 is a substrate [Ichijo et al., 1997, Nishitoh et al., 1998, and Yuasa et al., 1998]. Selective inhibition of p38 MAPK activity can be achieved with the cytokine-suppressive anti-inflammatory drug and specific p38 MAPK inhibitor, SB203580, Figure 4.5, which directly competes at the ATP binding site [Cuenda et al., 1995, Young et al., 1997, Davies et al., 2000 and Guo et al., 2003]. SB203580 is specific for p38α and p38β due to the presence of the conserved Thr-106, His-107, Leu-108 binding pocket and therefore has no effect on the activity of p38γ or p38δ, or the other MAPKS, ERK and JNK [Cuenda et al., 1995 and Guo et al., 2003].

4.1.2.2 Downstream Effectors of p38 MAPK

The substrates or downstream effectors of p38 MAPK include other protein kinases such as mitogen-activated protein kinase-activated protein

kinase 2 and 3 (MAPKAPK2 and 3), p38-regulated/activated protein kinase (PRAK), MAPK signal-integrating kinases (MNKs), and mitogen- and stress-activated protein kinases (MSKs) [Stokoe et al., 1992, McLaughlin et al., 1996, Fukunaga and Hunter, 1997, New et al., 1998 and Deak et al., 1998]. p38 MAPKs can directly, or indirectly via downstream protein kinases, phosphorylate cytosolic proteins, such as phospholipase A_2, heat shock protein 25/27 (HSP25/27) and 5-lipoxygenase, plus numerous transcription factors, including serum response factor, CREB, c-Jun, activating transcription factor 2 (ATF2), nuclear factor of activated T-cells (NFAT), nuclear factor-κB (NF-κB) and signal transducers and activators of transcription (STAT) [Nahas et al., 1996, Guay et al., 1997, Tibbles and Woodgett, 1999, Heidenreich et al., 1999, Werz et al., 2000, Delghandi et al., 2005 and Dodeller and Schulze-Koops, 2006]. Recent work using fibroblasts derived from p38α knock-out mice has indicated that p38 MAPK can actually control the expression level of its downstream kinase MAPKAPK2, where knock-in of p38α rescues MAPKAPK2 expression [Sudo et al., 2005]. Conversely, in osteoblasts, the activation of ERK1/2 drives MAPKAPK2 synthesis [San Miguel et al., 2005].

MAPKAPK2 is a downstream protein kinase of p38 MAPK and is composed of an N-terminal regulatory domain and a C-terminal kinase domain [Stokoe et al., 1992, Ben-Levy et al., 1995 and Meng et al., 2002]. It is encoded by one gene that is subject to 3' mRNA splicing resulting in the differential inclusion of both a nuclear localisation signal (NLS) and a nuclear export signal (NES), giving rise to isoforms with marginally different molecular weights of 60kDa and 53kDa respectively [Stokoe et al., 1992 and Kervinen et al., 2006]. The 53kDa MAPKAPK2 gene product is rare and entirely cytosolic. Its phosphorylation and activation by p38α/β MAPK allows it to phosphorylate cytosolic target proteins (see below). p38α/β MAPK can translocate to the nucleus, where it activates the 60kDa MAPKAPK2 gene product through phosphorylation at critical residues, namely Thr-25, followed co-operatively by Thr-222, which is located within the activation loop, Ser-272, and Thr-334, which is positioned between the N- and C-terminal domains and relieves an auto-inhibitory constraint [Rouse et al., 1994, Freshney et al., 1994, and Ben-Levy et al., 1995]. The nuclear phosphorylation and activation of MAPKAPK2

masks the NLS and exposes the NES resulting in its expulsion from the nucleus [Ben-Levy et al., 1998 and Meng et al., 2002]. Down-regulation of MAPKAPK2 activity occurs through de-phosphorylation by the serine/threonine protein phosphatase 2A (PP2A) [Stokoe et al., 1992].

Prior to its exclusion from the nucleus, MAPKAPK2 can directly phosphorylate the transcription factors, SRF and, to a lesser extent CREB [Tan et al., 1996 and Heidenreich et al., 1999]. It is now becoming clear that a major role for MAPKAPK2 is the control of gene expression at the post-transcriptional level [Dodeller and Schulze-Koops, 2006]. MAPKAPK2 phosphorylation of mRNA binding proteins, such as tristetraprolin (TTP) and heterogeneous nuclear ribonucleoprotein A0 (hnRNP A0), confers stabilisation of the AU-rich elements (ARE) in the 3' un-translated region of mRNA transcripts, thereby stimulating gene expression of cytokines such as TNFα, IL-6 and IL-8, and enzymes such as urokinase plasminogen activator and cyclo-oxygenase-2 [Winzen et al., 1999, Rousseau et al., 2002 and Gaestel, 2006].

The p38 MAPK-MAPKAPK2 pathway also has a key role to play in the regulation of the cell cycle [Gaestel, 2006]. p53 is a tumour suppressor gene that is activated upon cell damage and prevents G_1/S-phase transition and initiates the apoptosis mechanism. Phosphorylation and activation of p53 occurs directly via p38 MAPK. Conversely downstream activation of MAPKAPK2 targets p53 for degradation through the phosphorylation-induced activation of the ubiquitin ligase, HDM2 [Weber et al., 2005]. MAPKAPK2 also controls the PP activity of Cdc25B, which is a crucial component of the G_2/M cell cycle checkpoint [Gaestel, 2006].

In the cytosol MAPKAPK2 can phosphorylate cytosolic target proteins such as HSP25/27, 5-lipoxygenase, and neurite outgrowth inhibitor protein (Nogo-B) [Stokoe et al., 1992, Guay et al., 1997, Larsen et al., 1997, Werz et al., 2000, Rousseau et al., 2005]. HSP25/27 can function as a chaperone or scaffold protein, and is an important regulatory component in F-actin accumulation and microfilament structural stabilisation of the cytoskeleton

[Guay et al., 1997]. Furthermore, the phosphorylation of HSP27 by MAPKAPK2 appears to play a fundamental role in regulating cell motility, and this may indicate a potential role in cancer cell metastasis [Xu et al., 2006]. The MAPKAPK2 phosphorylation and activation of 5-lipoxygenase, in the presence of arachidonic acid, may underlie a proportion of the pro-inflammatory effects of MAPKAPK2 signalling pathway [Werz et al., 2000 and Werz et al., 2002]. More recently, MAPKAPK2 phosphorylation of Nogo-B was described but the functional significance of this phosphorylation has still to be elucidated [Rousseau et al., 2005].

PRAK or MAPKAPK5 is a 50kDa protein kinase with 20-30% homology with other MAPKs [New et al., 1998 and Gaestel, 2006]. It is activated by p38α/β MAPK phosphorylation at Thr-182. Of note, p38δ MAPK can phosphorylate at a different site but cannot activate PRAK. RNA transcripts for PRAK have been detected in human tissues and many commonly used human cell lines, confirming the authenticity of the protein kinase. As with MAPKAPK2, PRAK efficiently phosphorylates HSP25/27.

MNKs, of which there are two isoforms, MNK1 and MNK2, are serine/threonine protein kinases activated through the MAPK signalling pathways and have sequence similarities to the MAPKAPKs [Fukunaga and Hunter, 1997 and Waskiewicz et al., 1997]. Phosphorylation of MNK1 by ERK1/2 and p38 MAPKs, but not JNKs, induces kinase activation and this activation indicates another point of convergence of these two pathways and further supports evidence of signalling cross talk. ERK1/2 phosphorylates MNK1 at Thr-344, the equivalent residue to Thr-334 in MAPKAPK2. Activation of MNK1 also requires Thr-197 and Thr-202 [Waskiewicz et al., 1997]. Activation of the p38 MAPK pathway by anisomycin and pro-inflammatory cytokines such as TNFα and IL-1 also activate MNK1, an effect ablated by co-incubation with SB202190, a derivative of SB203580 [Young et al., 1997]. However, there are likely to be multiple sites for activation with Thr-344 directing specificity for ERK1/2 and a second site directing specificity for p38 MAPK. MNK1 phosphorylates the RNA 5' cap binding protein

eukaryotic translation initiation factor 4E (eIF-4E) at Ser-209 to modulate RNA translation [Waskiewicz et al., 1999].

A second group of downstream protein kinases that facilitates the convergence of the ERK1/2 and p38 MAPK signalling cascades are the MSKs [Deak et al., 1998]. There are two isoforms of MSK, namely MSK1 and MSK2, of which MSK1 is the most extensively studied. MSK1 is a nuclear protein kinase and accordingly, the major physiological substrate for MSK1, but not MSK2, is CREB [Deak et al., 1998 and Delghandi et al., 2005]. MSKs can also phosphorylate other transcription factors including ATF1, NK-κB and STAT [Dodeller and Schulze-Koops, 2006]. MSKs also target histone H3 for phosphorylation, inducing chromatin remodelling and the modulation of gene expression [Kyriakis and Avruch, 2001].

4.1.2.3 p38 MAPK in the Immune and Inflammatory Response

The activation of p38 MAPK plays a central role in the regulation of the immune and inflammatory response. It is involved in the regulation of PBL adhesion to the vascular endothelial cells, diapedisis or cell migration through the cell-cell junctions of the vascular endothelium, the production of super-oxide (O_2^-) and ROS via phosphorylation of p47-*phox*, assembly and activation of NADPH oxidase, and release of proteinases such as elastase and metalloproteinases that degrade the cell matrix and compromise tissue integrity [Herlaar and Brown, 1999].

TNFα and IL-1 are expressed in a variety of immune and inflammatory cells including monocytes and macrophages. Specific inhibition of p38 MAPK activity with SB203580 attenuates their expression [Lee et al., 1994]. Using SB203580 also attenuated the cell type specific expression of IL-6 and IL-10 (anti-inflammatory cytokine) as well as IL-1 and TNFα, corroborating the early studies [Guo et al., 2003]. Therefore, p38 MAPK must play a fundamental role in the regulation of the immune and inflammatory response. In support of this, MAPKAPK2$^{(-/-)}$ mice, when exposed to bacterial LPS to induce endotoxic shock or sepsis, showed increased survival coupled with near ablation of

TNFα expression [Kotlyarov et al., 1999]. Cytokines can also activate the p38 MAPK pathway in cells in which they are expressed and thus have the ability to regulate their own expression in an autocrine manner, e.g. TNFα and IFNγ.

Activation of the T-cell receptor (TCR) and CD28 by antigen-presenting cells (APC) elicits the proliferation and differentiation of CD4+ T-cells to either T-helper type 1 (Th1) or T-helper type 2 (Th2) cell lineage. Th1 cells mediate autoimmune disorders whereas Th2 cells mediate allergic inflammation. The balance of Th1 and Th2 cells is thought to be critical in the pathogenesis many disease states where excessive Th1 cells may cause chronic inflammation, e.g. in rheumatoid arthritis, and where Th2 cells are believed to underlie airway hyper-sensitivity in asthma [Bertrand, 2000 and Hart, 2001]. Each cell type is characterised by the expression of specific cytokines. Cytokines such as IL-12 and IL-18 activate p38 MAPK in Th1 cells and phosphorylate STAT4 and ATF2 inducing interferon-γ (IFNγ) gene expression [Dodeller and Schulze-Koops, 2006]. Inhibition of IL-12 stimulated p38 MAPK activity in these cells attenuates IFNγ gene expression and subsequently the level of the pro-inflammatory response [Rincon et al., 1998]. Additionally, activation of p38 MAPK can occur through IFN signalling indicating further autocrine regulation of cytokine expression [Platanias, 2003]. Th1 cells predominantly express IFNγ, which has anti-viral activity, activates phagocytic killing and activates natural killer cell cytotoxicity through TNFα production. The endogenous expression of IL-4 and IL-5 is also controlled by TCR-induced p38 MAPK activity in Th2 cells [Dodeller and Schulze-Koops, 2006]. Th2 cells express IL-4 and IL-5, which induces IgE production from B-cells and promotes eosinophil and mast cell immune responses [Hart, 2001].

The activation of p38 MAPK in many cells plays a fundamental role in the expression of pro-inflammatory cytokines and subsequent activation of the immune and inflammatory response. As such, modulation of p38 MAPK activity through specific inhibition of p38 MAPK isoforms, specifically p38α, or its downstream protein kinases, such as MAPKAPK2, may be of benefit in the treatment of both autoimmune and inflammatory disease [Herlaar and Brown, 1999 and Saklatvala, 2004]. Indeed, p38 MAPK inhibition with SB203580 in

many animal models of inflammatory disease have shown reduced pro-inflammatory cytokine expression and PBL recruitment [Badger et al., 1996]. Unfortunately, serious CNS side effects and hepatic toxicity have hampered the progress of p38 MAPK inhibitors [Herlaar and Brown, 1999 and Saklatvala, 2004].

4.1.3 Phosphorylation of PDE4 Enzymes

PDE4 enzymes are subject to phosphorylation and catalytic activity regulation by PKA [Sette et al., 1994, Sette and Conti, 1996, Laliberté et al., 2002 and MacKenzie et al., 2002], ERK1/2 [Lenhard et al., 1996, Hoffmann et al., 1998, Hoffmann et al., 1999, Baillie et al., 2000, MacKenzie et al., 2000 and Baillie et al., 2001], and a hitherto unknown protein kinase involved in the PI-3K signalling pathway [MacKenzie et al., 1998]. These phosphorylation events are discussed in some detail in Section 1.7.5.

As discussed above, the p38 MAPK plays a fundamental role in the immune and inflammatory response. The aim of this chapter was to identify whether PDE4 enzymes could be phosphorylated and regulated through activation of the p38 MAPK pathway and elucidate the functional significance of the integration of cross talk between p38 MAPK and cAMP signalling.

MAPK Isoform	Alternative Name	Substrates	Cell Response
ERK1	p44 MAPK	PDE4B, PDE4C, PDE4D, p47-*phox*, MAPKAPK1 ($p90^{rsk}$), MNK, MSK, Elk1	Cell proliferation Cell differentiation Cell survival
ERK2	p42 MAPK	PDE4B, PDE4C, PDE4D, p47-*phox*, MAPKAPK1 ($p90^{rsk}$), MNK, MSK, Elk1	
ERK3α	p63 MAPK	MNK, MSK	
ERK3β	Human ERK3		
ERK4	ERK1b		
ERK5			
ERK7			
JNK1	SAPKγ	c-Jun, JunD, ATF2, Elk1, Myc	Cell apoptosis Inflammation Tumourigenesis
JNK2	SAPKα		
JNK3	SAPKβ		
p38α	CSBP, SAPK2a, MPK2, RK, Mxi2	p47-*phox*, PLA_2, MAPKAPK2/3, PRAK, MNK, MSK, c-Jun, ATF2, NFAT, MEF2A/C, STAT4, SRF	Cell motility Cell apoptosis Chromatin remodelling Cytoskeletal reorganisation
p38β	p38-2, $p38\beta_2$, SAPK2b		
p38γ	ERK6, SAPK3	ATF2, Sap1	
p38δ	SAPK4		

Table 4.1 – The MAPK isoforms, alternative nomenclature, known substrates and cell response.

For description of abbreviations the reader is referred to the List of Abbreviations. Note that MAPKAPK1 ($p90^{rsk}$) is structurally unrelated to MAPKAPK2/3.

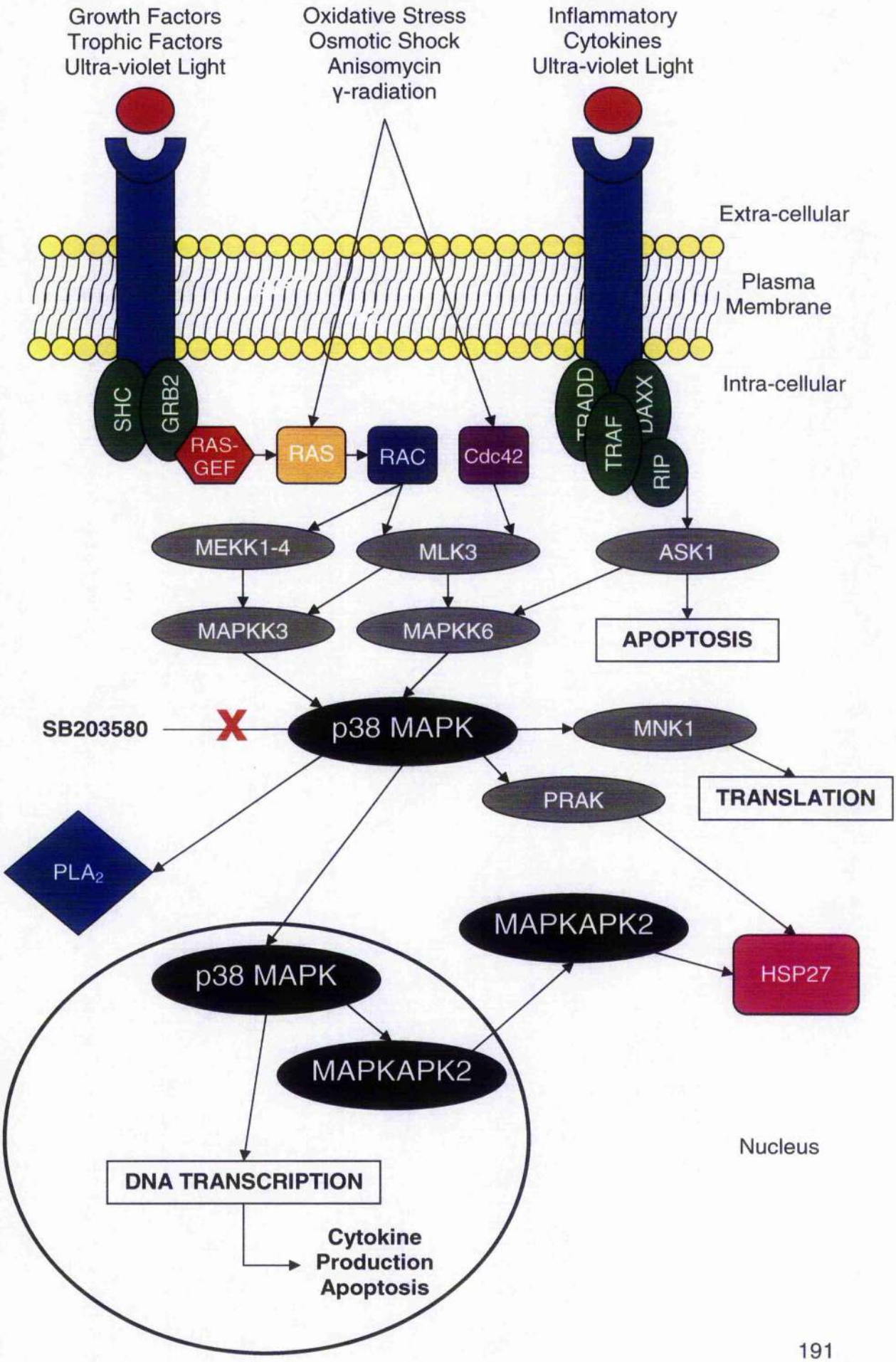
Growth Factors
Trophic Factors
Ultra-violet Light
Oxidative Stress
Osmotic Shock
Anisomycin
γ-radiation
Inflammatory
Cytokines
Ultra-violet Light
Extra-cellular
Plasma Membrane
Intra-cellular
SHC
GRB2
RAS-GEF
RAS
RAC
Cdc42
TRADD
TRAF
DAXX
RIP
MEKK1-4
MLK3
ASK1
MAPKK3
MAPKK6
APOPTOSIS
SB203580
p38 MAPK
MNK1
TRANSLATION
PRAK
PLA2
MAPKAPK2
HSP27
p38 MAPK
MAPKAPK2
Nucleus
DNA TRANSCRIPTION
Cytokine
Production
Apoptosis

Figure 4.1 – Schematic representation of the p38 MAPK signalling pathway.

4.2 Results

Analysis of the PDE4A5 primary structure revealed two serine residues within the UCR1 module that conform to the putative MAPKAPK2 phosphorylation consensus motif, Ø-Xaa-Arg-Xaa-Xaa-Ser-Ø, where Ø are hydrophobic amino acids [Stokoe et al., 1993 and Rousseau et al., 2005]. The putative target residues were Ser-147, within the motif Leu-Tyr-Arg-Ser-Asp-Ser-Asp, and Ser-161, within the motif Val-Ser-Arg-Ser-Ser-Ser-Val. Unpublished work from the Houslay laboratory postulated that a purified MBP fusion protein of PDE4A5, generated by expression in *E.coli*, could be phosphorylated in vitro by recombinant MAPKAPK2. In contrast, little phosphorylation was evident in comparable studies done on MBP fusions of PDE4B1 and PDE4D3 [E.V. Hill and M.D. Houslay, unpublished observations]. Also preliminary studies by E.V. Hill have shown that incubation of purified PDE4A5 with a lysate from anisomycin-treated cells, to activate p38 MAPK, induced a marked phosphorylation of PDE4A5 when [^{32}P]-ATP was added to the incubation. Lysates from cells treated additionally with the specific p38 MAPK inhibitor, SB203580, were ineffective. In these experiments a proportion of residual phosphorylation was identified in the no treatment control. Furthermore, in pull down assays and co-immuno-precipitation experiments MAPKAPK2 was shown to be able to interact directly with PDE4A5 [F. McCallum and M.D. Houslay, unpublished observations]. In addition, transfection of a Ser-147-Asp mutant of PDE4A5, designed to mimic the theoretical phosphorylated protein, showed altered intra-cellular distribution versus wild type [F. McCallum and M.D. Houslay, unpublished observations].

Analysis of the PDE4A5 amino acid sequence using the ScanSite consensus motif scanning database (http://scansite.mit.edu.cgi-bin/motifscan_seq) on high stringency, also identified two putative p38 MAPK phosphorylation motifs within the catalytic unit of PDE4A5, namely Thr-437 and Thr-776. The identified regions of PDE4A5 potentially susceptible to phosphorylation by MAPKAPK2 or p38 MAPK are shown in Figure 4.2.

4.2.1 In Vitro Phosphorylation of PDE4A5 by MAPKAPK2 and/or p38

In order to determine whether PDE4A5 was able to be phosphorylated directly by either p38 MAPK, or its downstream effector kinase MAPKAPK2, it was expressed and purified as a N-terminal MBP fusion protein in *E.coli*, as shown in Figure 4.3. Full-length PDE4 enzymes are notoriously difficult to express as a soluble protein in *E.coli* and require the addition of a sizeable soluble fusion protein tag, such as MBP. However, I managed to express MBP-PDE4A5 as a moderately soluble protein and purified it to a final concentration of approximately 0.5mg/ml. In addition to the native enzyme, mutant versions were also expressed and purified in *E.coli*. These were generated by site-directed mutagenesis (serine or threonine to alanine) of the indicated putative phosphorylation sites for MAPKAPK2 and p38 MAPK. These mutants could be expressed and purified on a similar scale to the wild type enzyme (data not shown).

In an in vitro phosphorylation assay I showed that PDE4A5 was phosphorylated by purified recombinant forms of both MAPKAPK2 (Figure 4.4(a)) and p38 MAPK (Figure 4.4(b)). Mutation of Ser-147 to alanine, the site identified by former laboratory colleagues, significantly reduced the level of phosphorylation to 40% +/- 2%, compared to the phosphorylation of wild type, which was set at 100% ($p < 0.05$). Conversely, mutation of Ser-161 to alanine had no effect on the phosphorylation status of PDE4A5, 90% +/- 2% compared to the wild type at 100% ($p > 0.05$).

Wild type PDE4A5 was also potentially phosphorylated by p38 MAPK. With the level of wild type phosphorylation set at 100%, the level of phosphorylation of the Thr-437 to alanine mutant was determined at 121% +/- 4% ($p > 0.05$) and was comparable to the level of phosphorylation of the Thr-776 to alanine mutant at 90% +/- 17% ($p > 0.05$). As described, mutation to alanine of either of the identified putative threonine target residues showed no reduction in phosphorylation efficiency. These data indicated that either these

sites were not the p38 MAPK phosphorylation targets, or alternatively, these could be non-specific in vitro phosphorylation assay events.

4.2.2 In Vivo Phosphorylation of PDE4A5 by p38 MAPK-dependent pathway

As with all in vitro phosphorylation assays, the data was approached with caution because these experiments were undertaken in isolation, normally with supra-physiological protein kinase concentrations. Therefore, artificial and indiscriminate phosphorylation of target proteins may have occurred. From Section 4.2.1, it was concluded that PDE4A5 was a substrate for MAPKAPK2, and furthermore the data indicates Ser-147 as the target residue for MAPKAPK2 phosphorylation. Whether PDE4A5 is a true substrate for p38 MAPK remains to be elucidated as Thr-437-Ala and Thr-776-Ala mutants of the potential sites did not attenuate the phosphorylation. However, it was pertinent to elucidate whether the MAPKAPK2 phosphorylation was able to occur in a bone fide cell signalling system, where all components were present in their natural environment.

To achieve this, COS1 and HEK293 cells were assessed for p38 MAPK and MAPKAPK2 activation following treatment with anisomycin, which initiates a robust activation of p38 MAPK, and also after treatment with the inflammatory cytokine, TNFα. Figure 4.6(a) shows that endogenous p38 MAPK activity in COS1 cells was low in the basal state, and that anisomycin initiated a robust and time-dependent activation of p38 MAPK, as indicated by dual phosphorylation of p38 MAPK at Thr-180 and Tyr-182. The activation of p38 MAPK reached a maximum in approximately 20min and was sustained for up to 60min. Activation of p38 MAPK caused a concomitant activation of MAPKAPK2, as indicated in Figure 4.6(b) by phosphorylation at Thr-334. MAPKAPK2 was also activated in a time-dependent manner, was fully activated at 30min, and sustained up to at least 60min post-stimulation. HEK293 cells had relatively low, but immunologically detectable, basal p38 MAPK and MAPKAPK2 activity, as shown in Figure 4.7. Although TNFα was

able to initiate a rapid activation of p38 MAPK activity after 5min, the downstream activation of MAPKAPK2 over time-zero was less convincing than that observed with the anisomycin treatment of COS1 cells. On this basis, anisomycin activation of the p38 MAPK cell-signalling pathway in COS1 cells was selected for the in vivo phosphorylation experiments.

COS1 cells were grown in phosphate-free growth media and transfected to transiently over-express VSV-tagged PDE4A5. The cell media was supplemented with [^{32}P]-orthophosphate and the cells were then either retained untreated, treated with anisomycin, or treated with anisomycin plus the p38 MAPK inhibitor, SB203580. PDE4A5 was immuno-precipitated and assessed for [^{32}P] incorporation as a marker of protein phosphorylation.

VSV-tagged PDE4A5 was exclusively immuno-precipitated with the VSV monoclonal antibody conjugated to Protein G agarose, as shown in Figure 4.8(a), bottom panel. Therefore, PDE4A5 in Figure 4.8(a), top panel, was easily distinguishable from a non-specific protein interaction at a slightly higher molecular weight, which was isolated with the Protein G agarose alone control immuno-precipitation. In untreated cells, residual phosphorylation of PDE4A5 was detected and, for quantification purposes, this control level was described as 100%. Figure 4.8(b) shows no detection of basal p38 MAPK or MAPKAPK2 activity in unstimulated cells. However, a marked increase in the intensity of PDE4A5 [^{32}P]-orthophosphate incorporation was measured, Figure 4.8(a), on activation of both p38 MAPK and MAPKAPK2 with anisomycin, Figure 4.8(b), first and third panels.

When the activation of both p38 MAPK and MAPKAPK2 was prevented by SB203580 the increase in phosphorylation of PDE4A5 was attenuated to near control state, as shown in Figure 4.8(a). The significant increase in PDE4A5 phosphorylation following anisomycin action was quantified at 172% +/- 8% ($p < 0.01$), whilst the level of phosphorylation was reduced, but still significantly elevated over the control, to 124% +/- 4% ($p < 0.01$) in the presence of SB203580.

Such p38 MAPK-dependent phosphorylation of PDE4A5 was also seen using other stimuli to activate the p38 MAPK pathway, including H_2O_2, to induce cellular oxidative stress, and NaCl, to induce cellular osmotic stress [E.V. Hill and M.D. Houslay, unpublished observations].

In order to gain preliminary insight into the site of PDE4A5 subject to phosphorylation following anisomycin treatment of COS1 cells, two truncates, which removed the significant amino acids that comprise the unique N-terminal (Met-1 to Thr-134) and the N-terminal plus UCR1 (Met-1 to Val-196), of PDE4A5, which have been described previously by others [Beard et al., 2002], were evaluated. These untagged PDE4A5 constructs were immuno-precipitated using a rat PDE4A C-terminal specific anti-serum. Although PDE4A5 was clearly immuno-precipitated, Figure 4.9(a) and Figure 4.10(a), bottom panels, these truncated forms of PDE4A5 migrated with a non-specific, phosphorylated protein of similar molecular weight.

The p38 MAPK-dependent phosphorylation of PDE4A5, less the unique N-terminal region, occurred as per the full-length enzyme, with an increase in phosphorylation to approximately 164% over the no treatment control, as shown in Figure 4.9(a). Protection from phosphorylation was afforded by SB203580, where the phosphorylation level was quantified at approximately 120%. In this experiment the level of basal p38 MAPK activity was markedly increased prior to anisomycin stimulation of p38 MAPK and may have played a role in preventing complete ablation of activity with SB203580. However, Figure 4.10 revealed that removal of both the N-terminal and UCR1 domains resulted in the prevention of anisomycin-induced PDE4A5 phosphorylation, with the level of phosphorylation determined at 88% +/- 35% ($p > 0.05$) with anisomycin and 82% +/- 11% ($p > 0.05$) with prior SB203580 treatment, compared to the control level of 100%. Basal p38 MAPK activity was notably lower than previously measured, i.e. Figure 4.10(b) compared to Figure 4.9(b), top panels of each. These data indicates that the p38 MAPK-dependent phosphorylation occurred within UCR1, the region with the putative phosphorylation sites for MAPKAPK2, and that had previously

been identified as providing the phosphorylation target in the experiments of Figure 4.4(a).

Site-directed mutagenesis of either Ser-147 to alanine or Ser-161 to alanine did not impact either expression in COS1 cells or catalytic activity of PDE4A5 (data not shown). Treatment of cells expressing the Ser-147 to alanine mutant of PDE4A5 demonstrated no significant increase in the level of phosphorylation following anisomycin treatment (109% +/- 9%; $p > 0.05$) nor did the pre-incubation of SB203580 prior to anisomycin addition alter this (93% +/- 10%; $p > 0.05$), as shown in Figure 4.11(a). On the other hand, the Ser-161 to alanine mutant of PDE4A5 was phosphorylated in the same manner as the wild type, Figure 4.8(a), and N-terminal truncate, Figure 4.9(a), with an increase in phosphorylation to 189% +/- 28% ($p > 0.05$), Figure 4.12(a), compared to the 100% control level. SB203580 ameliorated, on average, any effect induced by anisomycin to 97% +/- 64% ($p > 0.05$). A reproducible activation of p38 MAPK was achieved at comparable levels in both cases, as shown in Figure 4.11(b) and Figure 4.12(b), top panels.

Taken together, the above data lead to the hypothesis that MAPKAPK2 and not p38 MAPK caused the phosphorylation of PDE4A5. In order to address this I used small interfering RNA (siRNA) to knockdown endogenous MAPKAPK2 expression in order to determine whether this prevented the phosphorylation of wild type PDE4A5. siRNA specific for MAPKAPK2 was transfected into COS1 cells and MAPKAPK2 expression monitored over a 72h period, as shown in Figure 4.13(a). This figure confirmed that MAPKAPK2 was expressed in COS1 cells at endogenous levels sufficient for immunological detection. The use of non-targeting or control siRNA indicated that any knockdown of expression was target protein specific and not a global effect of siRNA transfection, as shown in Figure 4.13(a), middle panel. MAPKAPK2 siRNA prevented expression of the endogenous kinase, as detected by standard Western immuno-blotting in Figure 4.13(c), bottom panel, with minimal MAPKAPK2 expression 24h after transfection, and complete ablation of expression at 48-72h. Figure 4.13(b), bottom panel, and Figure 4.13(c) confirmed that co-transfection of VSV-PDE4A5 and

MAPKAPK2 siRNA had no effect on either the level of PDE4A5 expression and immuno-precipitation, the level of endogenous p38 MAPK expression and activation, or the siRNA knockdown efficiency of MAPKAPK2 expression. The level of phosphorylation of PDE4A5, following anisomycin treatment in COS1 cells, with complete knockdown of MAPKAPK2 expression, showed no significant change from the unchallenged control, quantified in Figure 4.13(b), graph, at 95% +/- 15% ($p > 0.05$). These data imply that PDE4A5 was phosphorylated by MAPKAPK2, a downstream substrate of p38 MAPK, at Ser-147 within its UCR1 regulatory module. Control siRNA allowed the MAPKAPK2 phosphorylation of PDE4A5 to progress as per the wild type (data not shown).

4.2.3 Functional Effects of PDE4A5 Phosphorylation

As has been discussed extensively in Section 1.7.5 and Section 3.2.5, PDE4 enzymes are subject to activity regulation by both PKA and ERK1/2 phosphorylation [Houslay, 2001]. The common UCR1 domain of all PDE4 long isoforms contains a single PKA phosphorylation target residue, the phosphorylation of which induces up to a 2-fold increase in PDE4 activity dependent upon the long isoform target [Sette and Conti, 1996, Hoffman et al., 1998, MacKenzie et al., 2002 and Manganiello, 2002]. However, only in the case of PDE4D3 can PKA phosphorylation induce a conformational change in catalytic unit that leads to an increase in the sensitivity to inhibition by rolipram. PDE4A isoforms are not subject to regulation by ERK2 phosphorylation of the catalytic unit as they lack the phosphorylation consensus site, but they do contain the required docking domains [Baillie et al., 2000]. In PDE4 isoforms, excluding the PDE4A gene family, ERK2 phosphorylation exerts an activation of short isoforms and an inhibition of long isoforms [Lenhard et al., 1996, Hoffman et al., 1999, MacKenzie et al., 2000 and Houslay and Adams, 2003]. The inhibitory effect of ERK2 action is overcome by the PKA activating phosphorylation [Houslay and Kolch, 2000 and Baillie et al., 2001]. A third activating phosphorylation event on PDE4A4B/PDE4A5, where the kinase responsible has not been assigned,

occurs through the stimulation of the PI-3K pathway, an effect that is sensitive to both wortmannin and rapamycin, indicating the involvement of a PI-3K downstream effector protein kinase [MacKenzie et al., 1998 and MacKenzie and Houslay, 2000].

4.2.3.1 Enzymatic Activity of PDE4A5

Described above are three examples of protein kinase phosphorylation of PDE4 isoforms that confers regulation of PDE activity. In COS7 cells the UCR1 regulatory module of PDE4A5 was phosphorylated by active PKA, and was detected using an anti-serum specific for the phosphorylated residue, as described previously [Bolger et al., 2003]. Similarly in COS1 cells, the activation of PKA was instigated, through ablation of global PDE-mediated cAMP degradation, with the non-specific PDE inhibitor, IBMX. Subsequent treatment with the adenylyl cyclase activator, forskolin, induced a time-dependent increase in PDE4A5 PKA phosphorylation, to a maximum and persistent response after 10-20min, as shown in Figure 4.14(a), top panel. This was quantified, as a function of PDE4A5 expression (Figure 4.14(a), bottom panel) in Figure 4.14(b). On the basis of optimal PKA phosphorylation being 100%, the time-zero PKA phosphorylation of PDE4A5 was determined at 18% +/- 4% of the peak response. Figure 4.14(c) showed that the time course of PDE4A5 PKA phosphorylation accurately translated to a robust activation of PDE4A5, as expected. In the native state PDE4A5 activity was considered to 100%. Mirroring the phosphorylation time course, the activity of PDE4A5 increased to a plateau at 10min, where the activity was calculated to be some 219% +/- 11%, above the control. The activation was maintained up to 20min at a equivalent level of some 223% +/- 6%.

I successfully generated an anti-serum specific to the MAPKAPK2 phosphorylated Ser-147 of PDE4A5 and this facilitated the resolution of the phosphorylation time course, and in addition confirmed the identity of the phosphorylation target residue. Indeed, Figure 4.15(a), and the quantification of this figure, Figure 4.15(b), showed that PDE4A5 was phosphorylated at Ser-147 in a time-dependent manner with anisomycin. The residual

phosphorylation of PDE4A5, also observed with the in vivo phosphorylation experiments, Figure 4.8(a), was mirrored, with immunological detection of phosphorylation at time-zero, calculated as being 28% +/- 4% of the peak response. The phosphorylation progressed in a near linear fashion to 20min before tailing off and reaching saturation at 30-60min post-stimulation. Unlike PKA phosphorylation, the time-dependent MAPKAPK2 phosphorylation of PDE4A5 had negligible effect on enzymatic activity with the activity 93% +/- 7%, versus the 100% control activity after 30min. Further confirmation of having correctly identified the target residue was achieved when phosphorylation of Ser-147 was not detected in cells transfected to express the alanine mutant, as shown in Figure 4.15(d). To eliminate the possibility of antibody irregularity, a non-specific band of a 37kDa was consistently detected with this antibody, irrespective of the PDE4A5 construct expressed (data not shown).

PDE4A5 was capable of being phosphorylated by PKA, following phosphorylation by MAPKAPK2, as shown in Figure 4.16(a). Quantification of the PDE4A5 PKA phosphorylation, succeeding MAPKAPK2 phosphorylation, offered a potential modification in the phosphorylation profile. An initial burst of PKA phosphorylation is observed at 1min, as shown in Figure 4.16(b), which is followed by a more restrained linear increase to the 20-minute maximum response. Comparison with Figure 4.14(b) showed solitary PKA phosphorylation to have a more incremental increase to the maximal response post-stimulation. The overall reduction in phosphorylation efficiency translates to a 50% inhibition of PKA-mediated PDE4A5 activation. The maximum activation following a 20-minute treatment with the adenylyl cyclase activator, forskolin reached 156% +/- 8%, as shown in Figure 4.16(c), compared to a PKA alone activation, above the 100% control level, of 223% +/- 6%, in Figure 4.14(c).

PKA phosphorylation of long PDE4 isoforms results in stimulation of enzyme activity, but substantial disparity exits as to whether this translates to an increase in the sensitivity to inhibition by rolipram [Hoffman et al., 1998, Laliberté et al., 2002 and MacKenzie et al., 2002]. To elucidate whether the

phosphorylation of PDE4A5 at Ser-147 had an effect on the conformational status of the catalytic unit, concentration response curves to rolipram were generated and the IC_{50} values were determined for both the wild type and the Ser-147 to aspartate mutant that I generated as a potential phospho-mimetic, as shown in Figure 4.17. Rolipram inhibited both forms of PDE4A5 in concentration-dependent fashion. The IC_{50} value for rolipram inhibition of wild type PDE4A5 was 1.1μM +/- 0.3μM, whereas the Ser-147-Asp mutant showed a small reduction in sensitivity with an IC_{50} value of 2.1μM +/- 0.4μM.

4.2.3.2 Intra-cellular Distribution of PDE4A5

The intra-cellular distribution of PDE4A5, following sub-cellular fractionation, was found to be completely cytosolic in COS1 cells with no immunological detection within the particulate fractions, as shown in Figure 4.18(a). This contradicts the published literature, which shows PDE4A5 to be of both particulate and cytosolic distribution [Huston et al., 2000]. Phosphorylation of PDE4A5, via the anisomycin activation of MAPKAPK2, did not alter this cellular localisation profile. Confocal microscopy analysis of PDE4A5, Figure 4.18(b), all panels, showed it to be localised at the perinuclear region around the nuclear membrane and at distinct regions of the plasma membrane, when transiently over-expressed in COS1 cells. Furthermore, this intra-cellular distribution of PDE4A5, over-expressed in both live and fixed COS1 cells, showed no change in distribution on anisomycin treatment using analogous time and concentrations to induce protein phosphorylation.

4.2.3.3 PDE4A5 Protein Interactions

4.2.3.3.1 β-arrestin

In Chapter 3, Figure 3.16, it was concluded that PDE4A4B, the human homologue of PDE4A5, was able to interact with the scaffold protein, β-arrestin. It is widely appreciated that β-arrestin preferentially interacts with PDE4D5, but PDE4A isoforms can interact via a PDE4 common interaction

site within the catalytic unit [Perry et al., 2002, Bolger et al., 2003 and Bolger et al., 2006]. The interaction is discussed extensively in Section 1.7.6.6.

Figure 4.19(a) was in accordance with Figure 3.16, and showed that PDE4A5 interacted effectively with β-arrestin, following immuno-precipitation and immuno-probing for PDE4A5, when both proteins were co-expressed in COS1 cells. Cell lysates expressing PDE4A5 alone showed no interaction with the FLAG agarose used to immuno-precipitate β-arrestin, indicating the absence of non-specific interactions, as shown in Figure 4.19(c). Cell lysates expressing both proteins were then pre-treated with anisomycin to instigate MAPKAPK2 phosphorylation, and IBMX plus forskolin to instigate PKA phosphorylation, or both for dual phosphorylation of PDE4A5. Figure 4.19(b) quantified the level of interaction, and in each case the relative amount of PDE4A5 interacting with β-arrestin was 134% following treatment with anisomycin alone, 112% following treatment with IBMX and forskolin, and 127% with anisomycin pre-treatment followed by IBMX and forskolin.

4.2.3.3.2 Immunophilin XAP2

The C-terminal component containing the TPR domains of XAP2 interacts specifically with human PDE4A4B and rat PDE4A5 through a unique interaction sequence located within the N-terminal region of the enzyme together with an additional, recognisable TPR binding site within the UCR2 region, common to all PDE4 isoforms [Bolger et al., 2003]. The interaction is discussed fully in Section 1.7.6.3.

PDE4A5 and XAP2 were co-expressed in COS1 cells and the interaction in untreated cells was confirmed by co-immuno-precipitation, as shown in Figure 4.20(a). Figure 4.20(a) aimed to determine whether this interaction was modulated, following PDE4A5 phosphorylation by MAPKAPK2, PKA or both kinases simultaneously. In each case equal immuno-reactive amounts of PDE4A5 and XAP2 were co-expressed, coupled with comparable levels of XAP2 immuno-precipitation. Quantification of the immuno-reactive level of PDE4A5 co-immuno-precipitated with XAP2

revealed a 50% +/- 9% ($p < 0.001$) significant reduction of XAP2 binding to PDE4A5 following PDE4A5 phosphorylation by MAPKAPK2, Figure 4.20(b). This reduction in interaction was reverted to control, at 99% +/- 7% ($p > 0.05$) upon co-challenge of cells with SB203580.

It was also noted that XAP2 was not phosphorylated in cells via activation of the p38 MAPK signalling pathway with anisomycin [E.V. Hill and M.D. Houslay, unpublished observation]. Conversely, phosphorylation of PDE4A5 by PKA had no effect on the efficiency of interaction at 84% +/- 14% ($p > 0.05$) compared to the 100% control.

Simultaneous MAPKAPK2 and PKA phosphorylation of PDE4A5, stimulated by pre-treatment with anisomycin followed by IBMX and forskolin, showed a similar significant reduction in XAP2 binding to PDE4A5 when compared with anisomycin alone, with the interaction some 54% +/- 5% ($p < 0.05$) of the control. This further confirmed that PKA phosphorylation of PDE4A5 plays no role in modulating the PDE4A5-XAP2 interaction. Furthermore, PKA phosphorylation of PDE4A5 does not influence the ability of MAPKAPK2 phosphorylation to attenuate the interaction of PDE4A5 and XAP2.

Cell lysates expressing PDE4A5 alone showed no interaction with the FLAG agarose used to immuno-precipitate XAP2, indicating the absence of non-specific interactions, as shown in Figure 4.20(c).

4.2.3.3.3 Action of Caspase-3

PDE4A5 contains a caspase-3 cleavage motif at Asp-69 to Asp-72. Cleavage at this site by caspase-3 results in the intra-cellular re-distribution of PDE4A5 and loss of the SH3 binding domains required for interaction with tyrosyl kinases, such as Lyn [Huston et al., 2000].

The ability of recombinant, active caspase-3 to cleave equal immuno-reactive amounts of PDE4A5 wild type and PDE4A5 after being MAPKAPK2

phosphorylated, and both the Ser-147-Asp and Ser-147-Ala mutants were assessed in vitro. In all instances, PDE4A5 was cleaved by caspase-3, as indicated by the detection of two immuno-reactive bands, of 110kDa and 100kDa respectively, with the rat C-terminal specific anti-serum. The PDE4A5 Ser-147-Asp and Ser-147-Ala mutants were cleaved more efficiently by caspase-3, as indicated by the conversion of nearly all available PDE4A5 to the lower molecular weight product (100kDa).

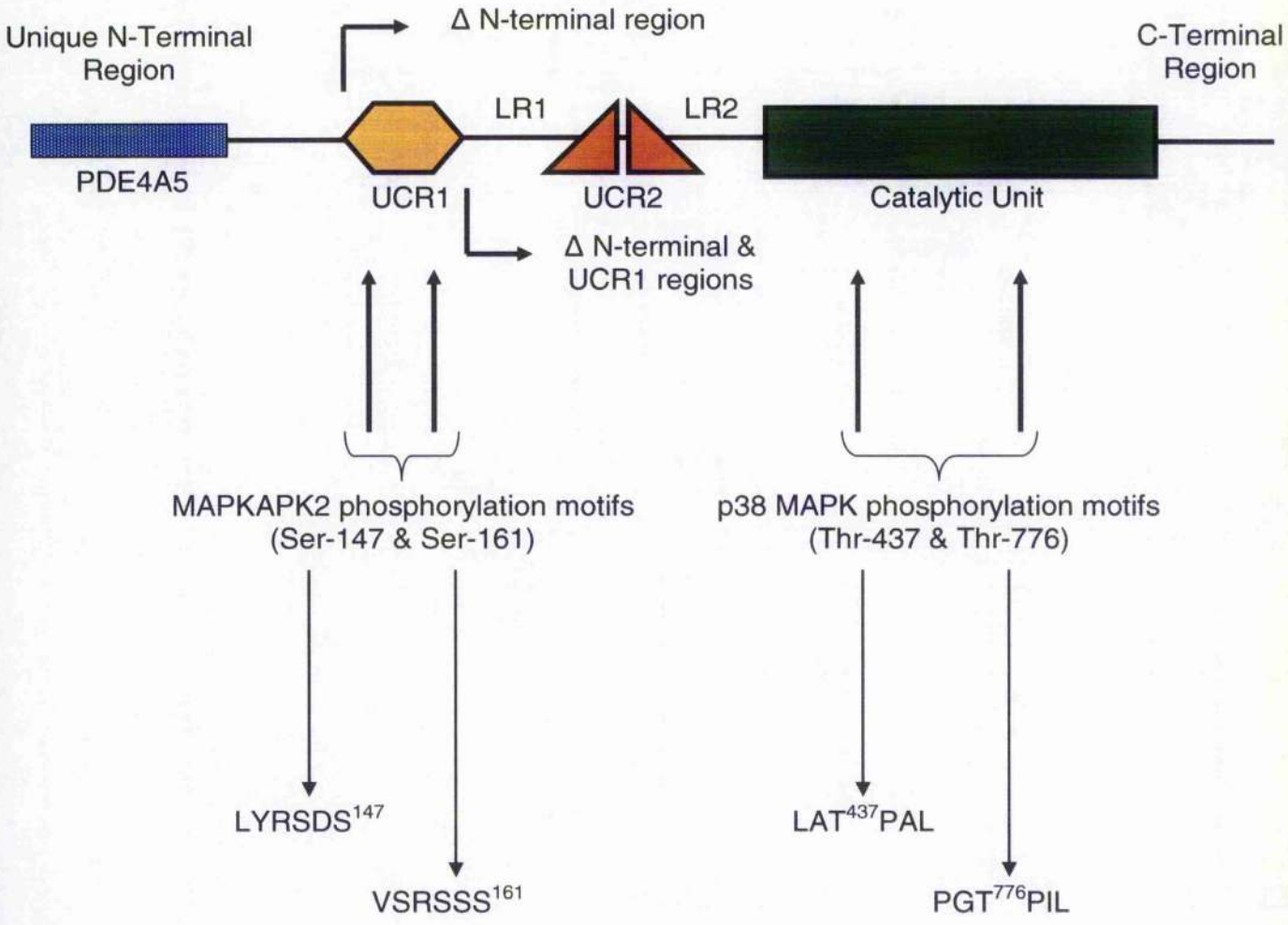
Unique N-Terminal Region
Δ N-terminal region
C-Terminal Region
LR1
LR2
PDE4A5
UCR1
UCR2
Catalytic Unit
Δ N-terminal & UCR1 regions
MAPKAPK2 phosphorylation motifs (Ser-147 & Ser-161)
p38 MAPK phosphorylation motifs (Thr-437 & Thr-776)
LYRSDS147
VSRSSS161
LAT437PAL
PGT776PIL

Figure 4.2 – Truncation and phosphorylation site mutants of rat PDE4A5.

The schematic shows the two positions at which PDE4A5 N-terminal truncations were engineered and also putative MAPKAPK2 and p38 MAPK phosphorylation sites on long PDE4A isoforms. Plasmids were generated encoding rat PDE4A5 less the entire N-terminal region (Δ N-terminal region truncated at Ser-135) and less the entire N-terminal and UCR1 regions (Δ N-terminal & UCR1 regions truncated at Pro-197). Also shown are the putative phosphorylation residues contained within either MAPKAPK2 phosphorylation motifs (Ser-147 and Ser-161) within UCR1 or p38 MAPK phosphorylation motifs (Thr-437 and Thr-776) located within the catalytic unit. These residues were subjected to site directed mutagenesis with nucleotide codons for the serine or threonine amino acids altered to code for alanine in all instances respectively.

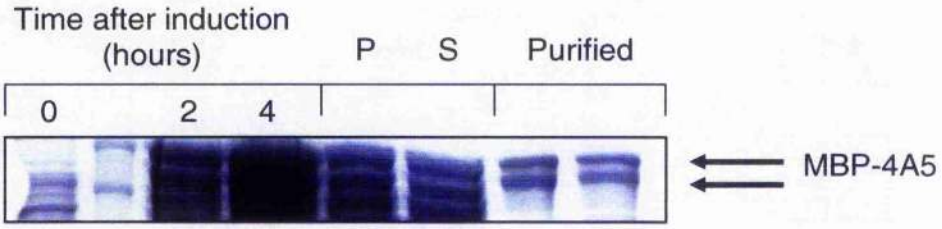
Time after induction
(hours)
P
S
Purified
0
2
4
MBP-4A5

Figure 4.3 – *E.coli* expression and purification of recombinant MBP-tagged rat PDE4A5.

Coomassie® staining of SDS polyacrylamide gels showing the *E.coli* expression of full-length recombinant rat PDE4A5 as a fusion with maltose binding protein (MBP). Briefly, competent *E.coli* BL21 pLysS (DE3) cells were transformed with pMAL plasmids encoding MBP-PDE4A5. Expression of the protein was induced with 0.2mM IPTG for 4h at 30°C. The cells were collected, re-suspended in lysis buffer and subjected to sonication to produce total cell extract (P). The soluble proteins were isolated by centrifugation (S). The expressed recombinant MBP fusion protein was purified using amylose resin and eluted using excess maltose (10mM). The MBP fusion protein could be purified to two bands as detectable by Coomassie® staining of the SDS-PAGE (Purified). These gels are representative of numerous successful expression experiments undertaken to produce PDE4A5 wild type and various single serine or threonine to alanine mutants in *E.coli*.

(a)

(i)

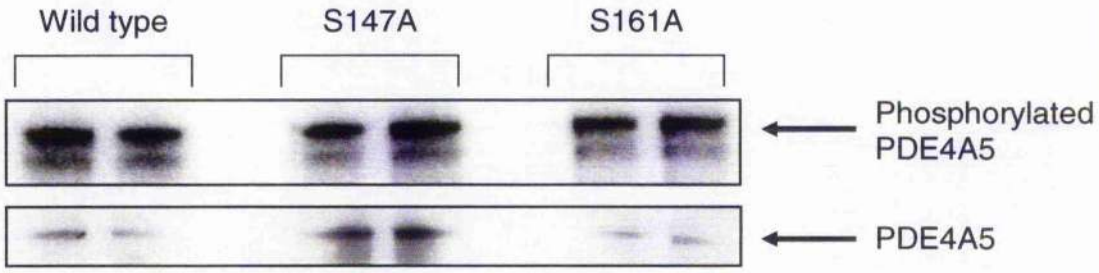
Wild type
S147A
S161A
Phosphorylated PDE4A5
PDE4A5

(ii)

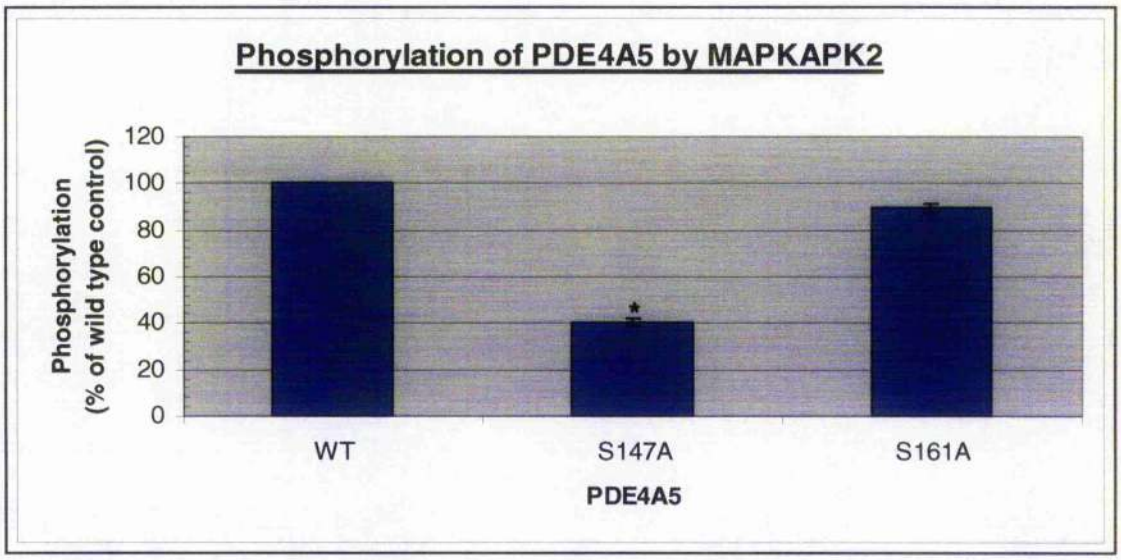
Phosphorylation of PDE4A5 by MAPKAPK2
Phosphorylation (% of wild type control)
120
100
80
60
40
20
0
*
WT
S147A
S161A
PDE4A5

(b)

(i)

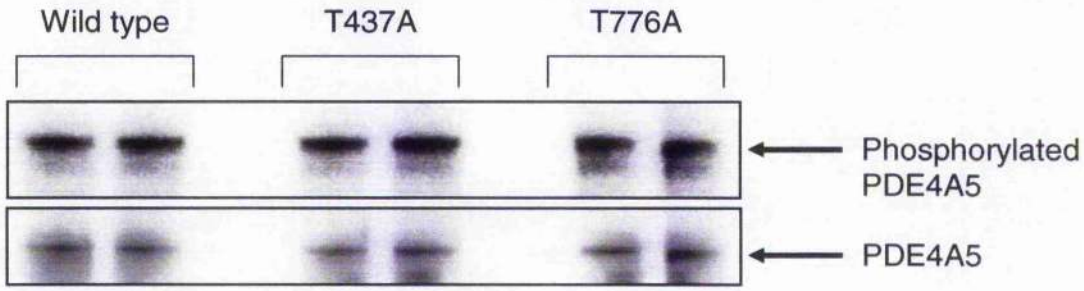
Wild type
T437A
T776A
Phosphorylated PDE4A5
PDE4A5

(ii)

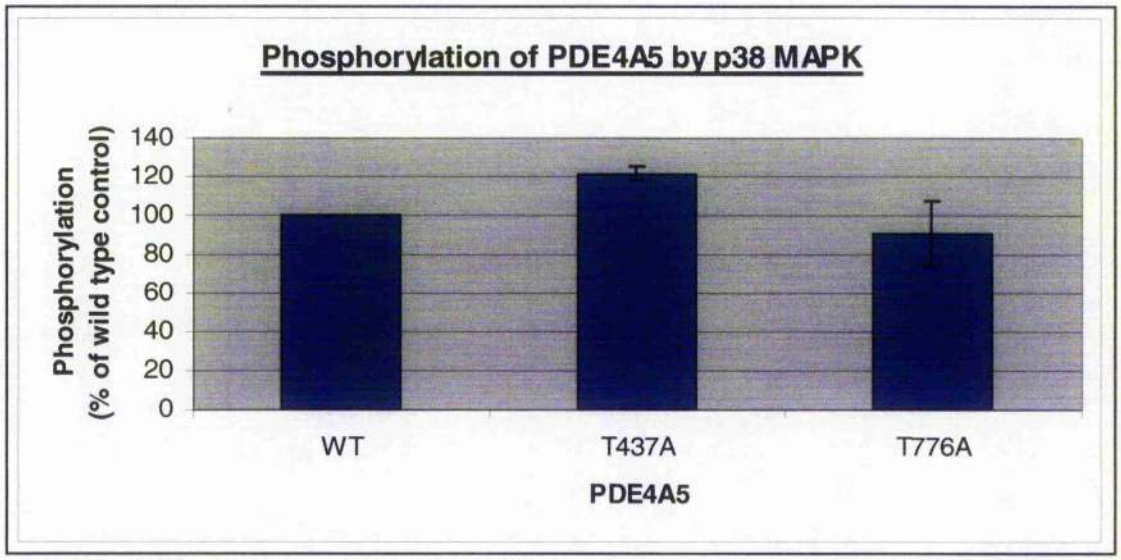
Phosphorylation of PDE4A5 by p38 MAPK
Phosphorylation (% of wild type control)
140
120
100
80
60
40
20
0
WT
T437A
T776A
PDE4A5

Figure 4.4 – In vitro phosphorylation of wild type PDE4A5 and putative phosphorylation site mutants with recombinant MAPKAPK2 or p38 MAPK.

The phosphorylation of rat PDE4A5 (wild type, Ser-147-Ala and Ser-161-Ala) by recombinant MAPKAPK2 and rat PDE4A5 (wild type, Thr-437-Ala and Thr-776-Ala) by recombinant p38 MAPK were carried out in vitro. Briefly, purified rat MBP-PDE4A5 wild type, or mutants, were incubated with either MAPKAPK2 or p38 MAPK and [^{32}P]-ATP for 10min at 30°C. The phosphorylated MBP-PDE4A5 proteins were separated by SDS-PAGE and transferred to a nitrocellulose membrane. The radioactive nitrocellulose membrane was exposed in close proximity to a storage phosphor image screen for at least 3 hours and developed using a high-resolution laser scanner. (a) (i), top panel, is a scanned storage phosphor screen image showing PDE4A5 (wild type, Ser-147-Ala and Ser-161-Ala) phosphorylation by recombinant MAPKAPK2. (a) (i), bottom panel, is a Western blot of the radioactive nitrocellulose membrane, probed using a rat PDE4A C-terminal specific anti-serum, showing the relative immuno-reactive amounts of PDE4A5 in each assay. (a) (ii), displays the quantification of PDE4A5 phosphorylation as a function of the immuno-reactive PDE4A5 in each assay. Similarly, (b) (i), top panel, is a scanned storage phosphor screen image showing PDE4A5 (wild type, Thr-437-Ala and Thr-776-Ala) phosphorylation by recombinant p38 MAPK. (b) (i), bottom panel, is a Western blot of the radioactive nitrocellulose membrane, probed using a rat PDE4A C-terminal specific anti-serum, showing the relative immuno-reactive amounts of PDE4A5 in each assay. (b) (ii), shows the quantification of the phosphorylation as a function of the immuno-reactive PDE4A5 in each assay. All scanned storage phosphor screen images and Western blots are representative of in vitro phosphorylation assays done three times. The quantification of the phosphorylation experiments are expressed as mean values +/- standard deviations of the three separate experiments. Paired t-test statistical analysis of the quantified phosphorylation data were undertaken, where $p < 0.05$ indicates statistical significant difference in the level of phosphorylation between wild type and mutant forms of PDE4A5.

Anisomycin

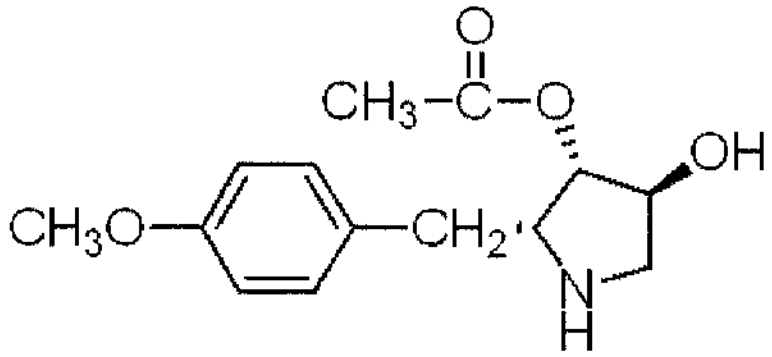

SB203580

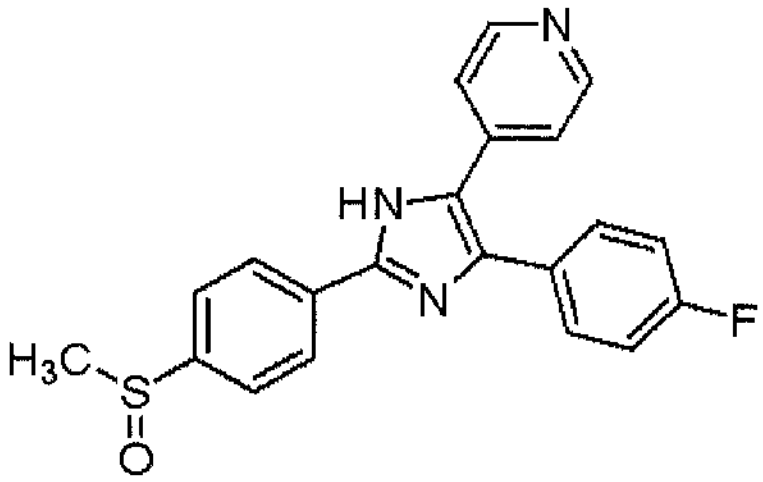

Figure 4.5 Chemical structures of anisomycin and SB203580.

(a)

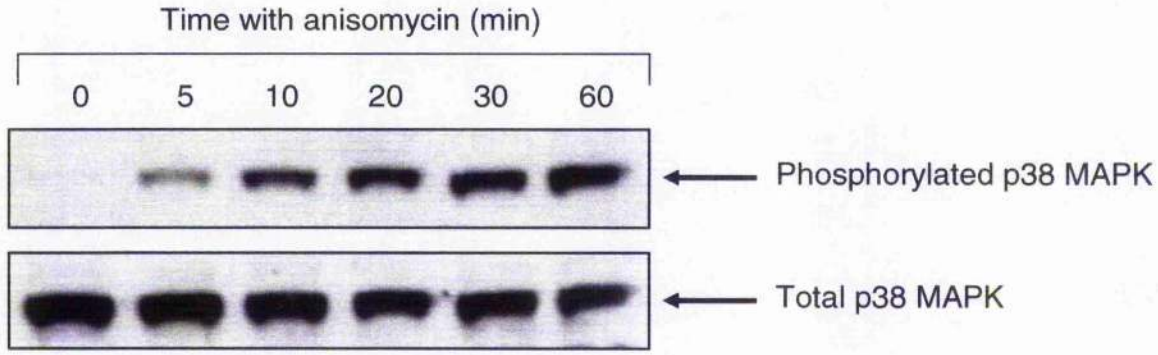
Time with anisomycin (min)
0
5
10
20
30
60
Phosphorylated p38 MAPK
Total p38 MAPK

(b)

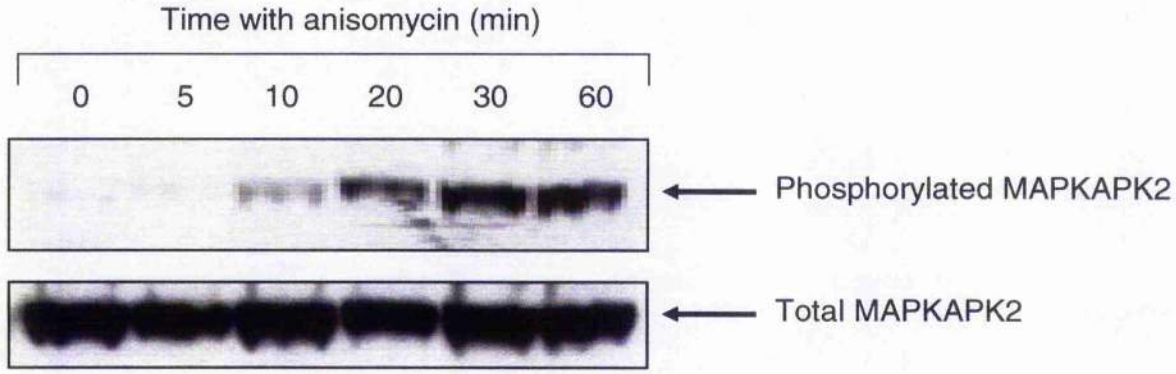
Time with anisomycin (min)
0
5
10
20
30
60
Phosphorylated MAPKAPK2
Total MAPKAPK2

Figure 4.6 – Anisomycin time course of p38 MAPK and MAPKAPK2 activation in COS1 cells.

COS1 cells were treated with anisomycin (10µg/ml) at the indicated time points (0-60min). Total cell extract was produced and the lysates immuno-probed with anti-sera specific for the respective kinase activation. (a), top panel, is a Western blot probed with anti-sera able to detect endogenous levels of the dual phosphorylated (Thr-180 and Tyr-182), and activated, p38 MAPK. (a), bottom panel, is the same Western blot re-probed with an anti-serum to detect total endogenous p38 MAPK. (b), top panel, is a Western blot of phosphorylated, and activated, MAPKAPK2, as indicated by the detection of the mono phosphorylated (Thr-334) form. (b), bottom panel, is the same Western blot re-probed for total endogenous MAPKAPK2, using a specific anti-serum. All Western blots are representative blots of at least three separate experiments.

(a)

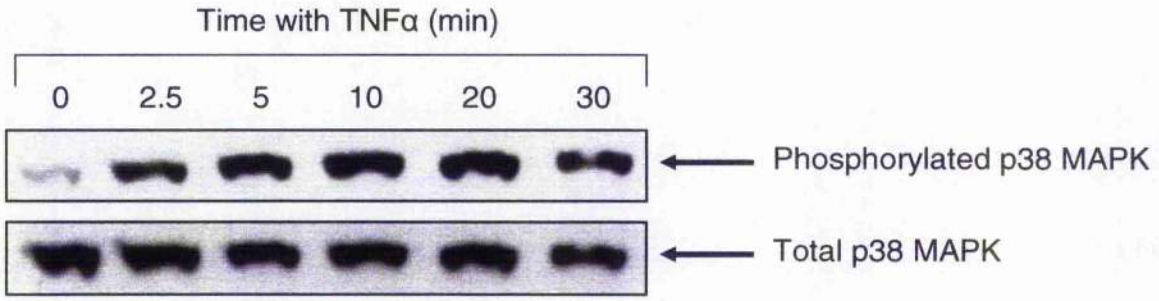
Time with TNFα (min)
0
2.5
5
10
20
30
Phosphorylated p38 MAPK
Total p38 MAPK

(b)

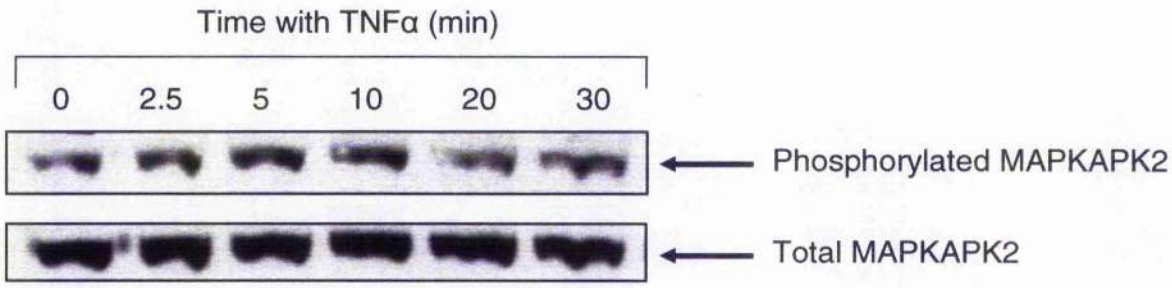
Time with TNFα (min)
0
2.5
5
10
20
30
Phosphorylated MAPKAPK2
Total MAPKAPK2

Figure 4.7 – Activation of p38 MAPK and MAPKAPK2 with TNFα in HEK293 cells.

HEK293 cells were treated with TNFα (10ng/ml) at the indicated time points (0-30min). Total cell extract was produced and the lysates immuno-probed with anti-sera specific for the respective kinase activation. (a), top panel, is a Western blot probed with anti-sera able to detect endogenous levels of the dual phosphorylated (Thr-180 and Tyr-182) and activated p38 MAPK. (a), bottom panel, is the same Western blot re-probed with an anti-serum to detect total endogenous p38 MAPK. (b), top panel, is a Western blot of phosphorylated and activated MAPKAPK2, as indicated by the detection of the mono phosphorylated (Thr-334) form. (b), bottom panel, is the same Western blot re-probed for total endogenous MAPKAPK2, using a specific anti-serum. All Western blots are representative blots of at least three separate experiments.

(a)

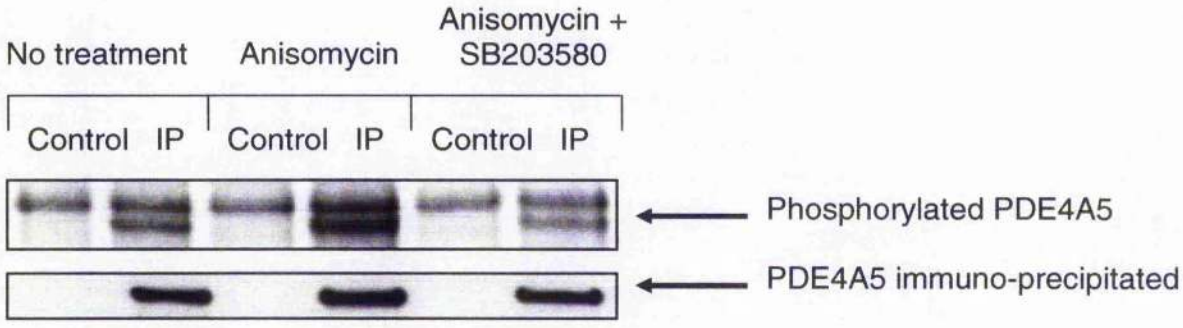
No treatment
Anisomycin
Anisomycin + SB203580
Control IP
Control IP
Control IP
Phosphorylated PDE4A5
PDE4A5 immuno-precipitated

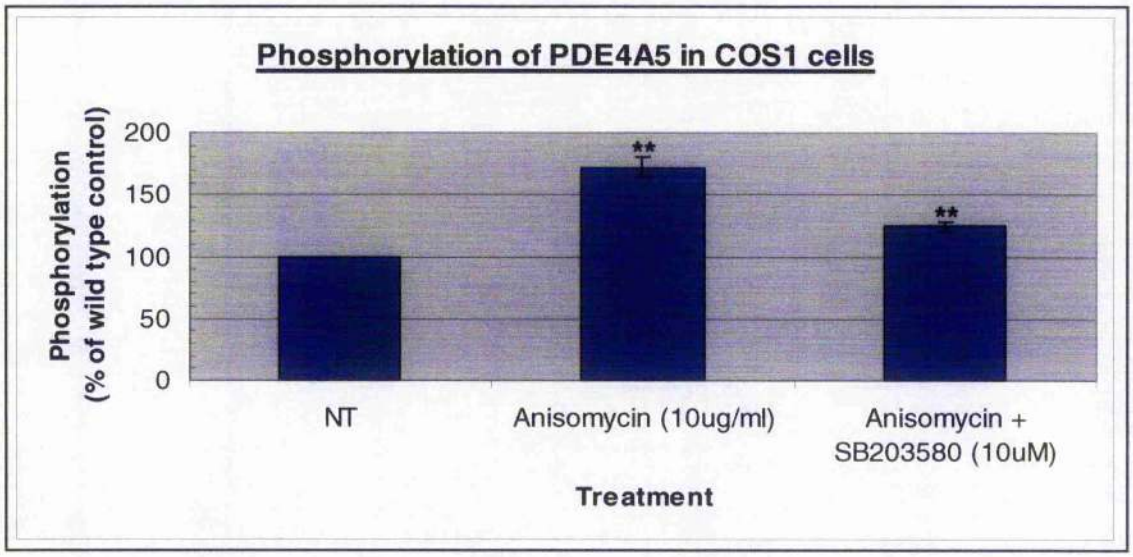
Phosphorylation of PDE4A5 in COS1 cells
Phosphorylation (% of wild type control)
200
150
100
50
0
**
**
NT
Anisomycin (10ug/ml)
Anisomycin + SB203580 (10uM)
Treatment

(b)

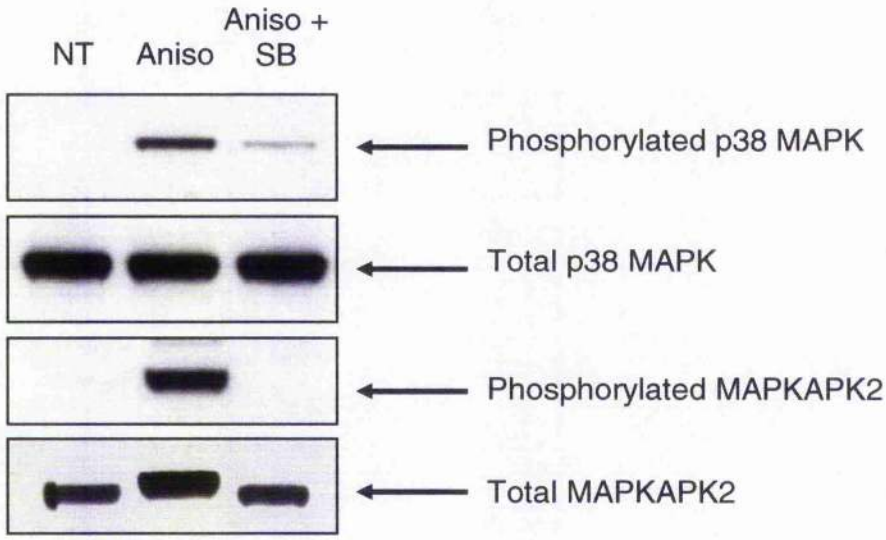
NT
Aniso
Aniso + SB
Phosphorylated p38 MAPK
Total p38 MAPK
Phosphorylated MAPKAPK2
Total MAPKAPK2

Figure 4.8 – In vivo phosphorylation of rat PDE4A5 wild type in COS1 cells stimulated with anisomycin.

COS1 cells were transfected with a plasmid encoding vsv-PDE4A5 for transient over-expression. The cells were grown in phosphate-free cell media that was supplemented with [^{32}P]-orthophosphate overnight. The cells were treated with anisomycin (10µg/ml) for 60min, to activate the p38 MAPK phosphorylation cascade, or anisomycin plus the p38 MAPK inhibitor SB203580 (10µM) for 60min respectively. Total cell lysate was produced. PDE4A5-vsv was immuno-precipitated using an anti-vsv antibody conjugated to Protein G agarose with un-conjugated Protein G agarose used as a control immuno-precipitation. The immuno-precipitated proteins were separated by SDS-PAGE and transferred to a nitrocellulose membrane where the radioactive proteins were resolved using phosphor image screen technology. (a), top panel, is a scanned phosphor image screen of the phosphorylated PDE4A5 immuno-precipitated following treatment with anisomycin plus or minus SB203580. (a), bottom panel, is a Western blot of the same nitrocellulose membrane probed with the anti-vsv antibody to determine the relative immuno-precipitation of PDE4A5 from the three samples. (a), graph, quantifies the change in phosphorylation of PDE4A5 following activation of the p38 MAPK signalling cascade relative to the no treatment control (100%). These data account for the relative immuno-reactive amounts of PDE4A5 isolated by immuno-precipitation. (b), are Western blots of total cell lysate immuno-probed for both p38 MAPK and MAPKAPK2 activation together with the corresponding total cellular expression of both kinases. All scanned phosphor image screens and Western blots are representative of at least three separate transfections and experiments. The quantification data are expressed as the mean percentage change in phosphorylation over the control +/- standard deviation of at least three separate transfections and experiments. Paired t-test statistical analysis of the quantified phosphorylation data were undertaken, where $p < 0.05$ indicates a statistically significant difference in the level of wild type PDE4A5 phosphorylation between untreated and treated cells, as indicated.

(a)

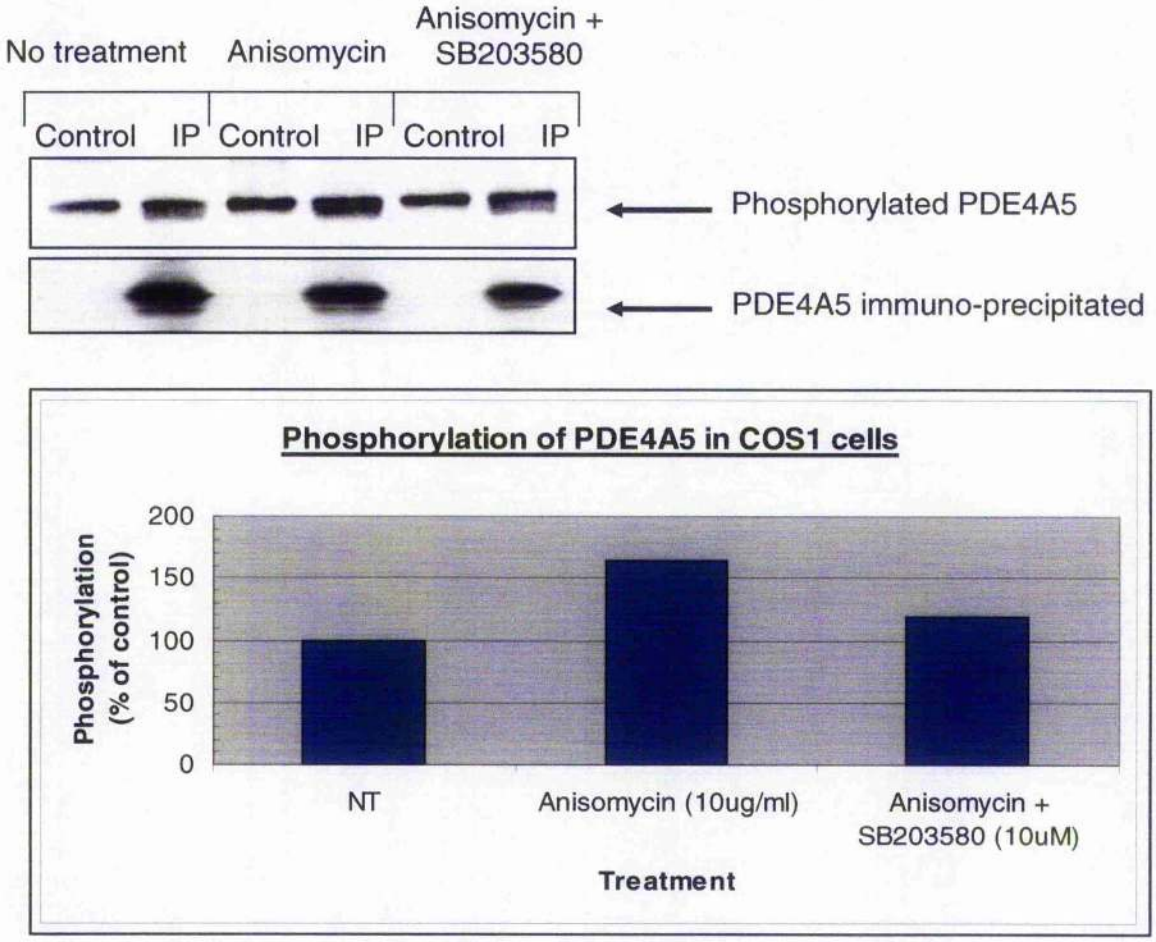
No treatment
Anisomycin
Anisomycin + SB203580
Control
IP
Control
IP
Control
IP
Phosphorylated PDE4A5
PDE4A5 immuno-precipitated
Phosphorylation of PDE4A5 in COS1 cells
Phosphorylation (% of control)
200
150
100
50
0
NT
Anisomycin (10ug/ml)
Anisomycin + SB203580 (10uM)
Treatment

(b)

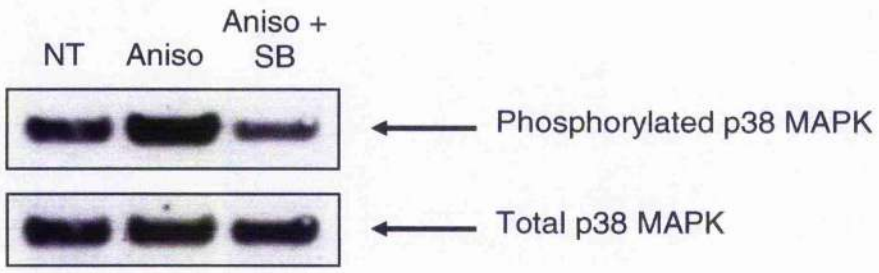
NT
Aniso
Aniso + SB
Phosphorylated p38 MAPK
Total p38 MAPK

Figure 4.9 – In vivo phosphorylation of rat PDE4A5, less the entire N-terminal region, in COS1 cells stimulated with anisomycin.

COS1 cells were transfected to express the truncated rat PDE4A5, amino acids Ser-135 to Ala-844 inclusive. The cells were grown in phosphate-free cell media that was supplemented with [^{32}P]-orthophosphate overnight and then treated with anisomycin (10µg/ml) for 60min or anisomycin plus SB203580 (10µM) for 60min each respectively. Total cell lysate was produced. PDE4A5-Δ N-terminal was immuno-precipitated using an anti-serum specific to the C-terminal region of rat PDE4A isoforms. This antibody was conjugated to Protein G agarose with un-conjugated Protein G agarose used as a control immuno-precipitation. The immuno-precipitated proteins were separated by SDS-PAGE and transferred to a nitrocellulose membrane where the radioactive proteins were resolved using phosphor image screen technology. (a), top panel, is a scanned phosphor image screen of the phosphorylated PDE4A5-Δ N-terminal, immuno-precipitated following treatment with anisomycin plus or minus SB203580. (a), bottom panel, is a Western blot of the same nitrocellulose membrane probed with the specific rat PDE4A antibody to determine the relative PDE4A5 immuno-precipitation for the three treatment samples. (a), graph, shows the quantification of the change in the phosphorylation state of PDE4A5-Δ N-terminal protein following activation of the p38 MAPK signalling cascade relative to the no treatment control (100%). These quantifications take into account the relative immuno-reactive amounts of PDE4A5-Δ N-terminal isolated by immuno-precipitation. (b), are Western blots of total cell lysate immuno-probed for p38 MAPK activation together with the corresponding total cellular expression. All scanned phosphor image screens and Western blots are of a preliminary experiment of one transfection. The quantification data are expressed as the percentage change in phosphorylation over the control of this one experiment.

(a)

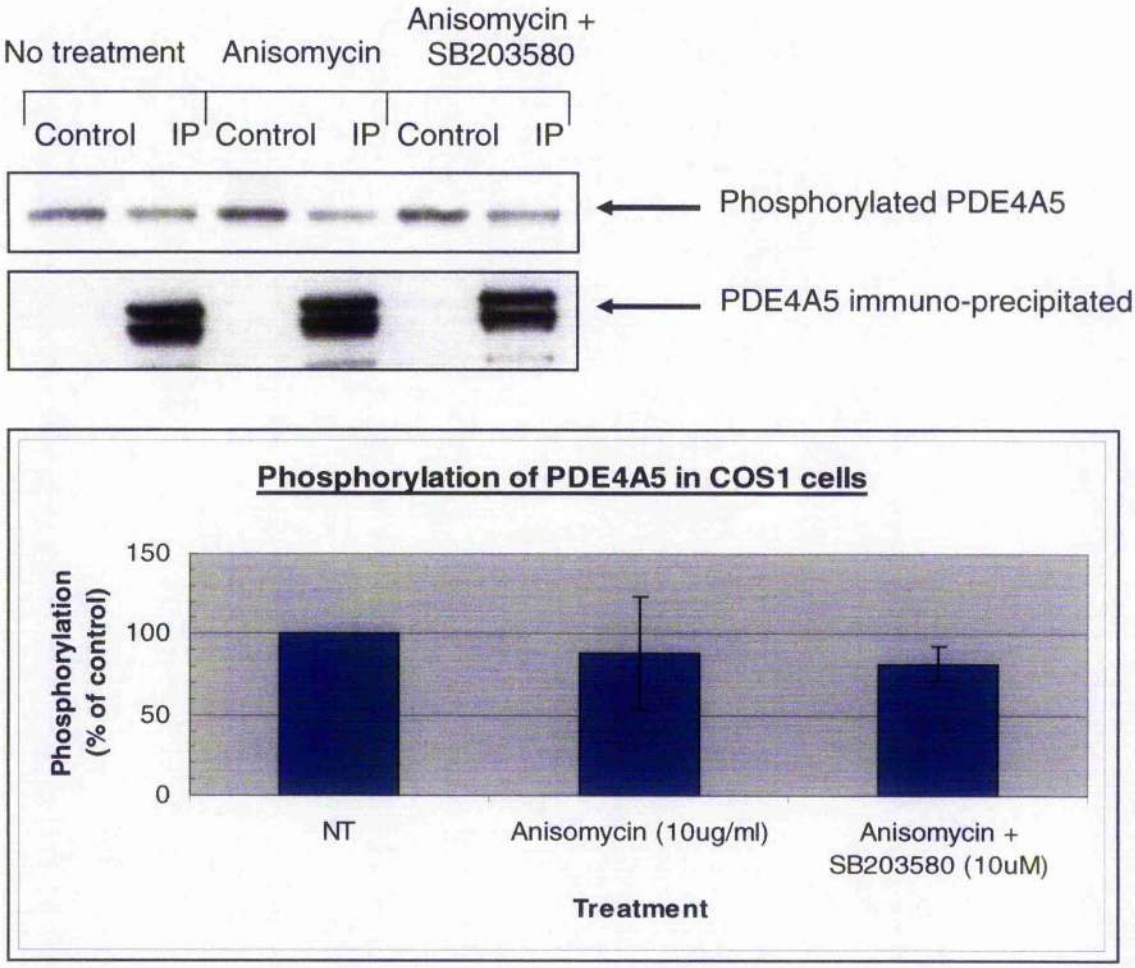
No treatment
Anisomycin
Anisomycin + SB203580
Control
IP
Control
IP
Control
IP
Phosphorylated PDE4A5
PDE4A5 immuno-precipitated
Phosphorylation of PDE4A5 in COS1 cells
Phosphorylation (% of control)
150
100
50
0
NT
Anisomycin (10ug/ml)
Anisomycin + SB203580 (10uM)
Treatment

(b)

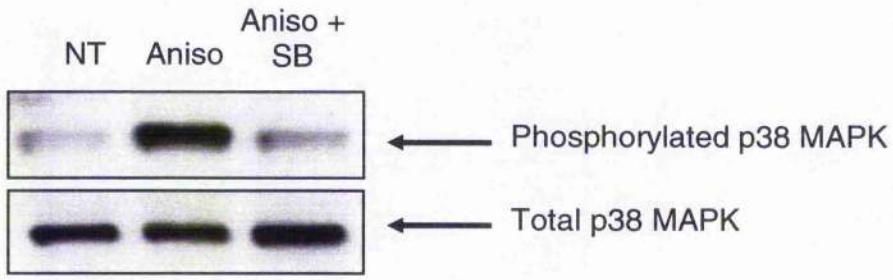
NT
Aniso
Aniso + SB
Phosphorylated p38 MAPK
Total p38 MAPK

Figure 4.10 – In vivo phosphorylation of truncated rat PDE4A5, less the N-terminal and UCR1 region, in COS1 cells stimulated with anisomycin.

COS1 cells were transfected to transiently over-express Pro-197 to Ala-844 of PDE4A5. The cells were grown in phosphate-free cell media, which was supplemented with [^{32}P]-orthophosphate 24h prior to cell treatments. Activation of the p38 MAPK signalling pathway was initiated with anisomycin (10µg/ml) for 60min. The cells were also treated with anisomycin plus the p38 MAPK inhibitor, SB203580 (10µM) for 60min each respectively. Total cell lysate was produced and PDE4A5-Δ N-terminal and UCR1 was immuno-precipitated using an anti-serum specific to the C-terminal region of all rat PDE4A isoforms. Again, this antibody was conjugated to Protein G agarose with the control immuno-precipitation un-conjugated Protein G agarose. The immuno-precipitated proteins were separated by SDS-PAGE and transferred to a nitrocellulose membrane where the radioactive proteins were resolved using phosphor image screen technology. (a), top panel, is a scanned phosphor image screen of the phosphorylated PDE4A5-Δ N-terminal and UCR1, immuno-precipitated following treatment with anisomycin plus or minus SB203580. (a), bottom panel, is a Western blot of the same nitrocellulose membrane probed with the C-terminal specific rat PDE4A antibody to determine the relative PDE4A5 immuno-precipitation in the three treatment cell extracts. (a), graph, shows the quantification of the change in the phosphorylation state of the PDE4A5-Δ N-terminal and UCR1 protein following activation of the p38 MAPK signalling pathway compared to the no treatment control (100%). These quantifications take into account the relative immuno-reactive amounts of PDE4A5-Δ N-terminal and UCR1 isolated by immuno-precipitation. (b), are Western blots of total cell lysate immuno-probed for both p38 MAPK activation and total p38 MAPK cellular expression. All scanned phosphor image screens and Western blots are typical of separate transfections and experiments undertaken twice. The quantification data, representative of the change in phosphorylation as a function of PDE4A5-Δ N-terminal and UCR1 immuno-precipitated, are mean values +/- standard deviation of the two experiments. Paired t-test statistical analysis of the quantified phosphorylation data were undertaken, where $p < 0.05$

indicates a statistically significant difference in the level of truncated PDE4A5 phosphorylation between untreated and treated cells, as indicated.

(a)

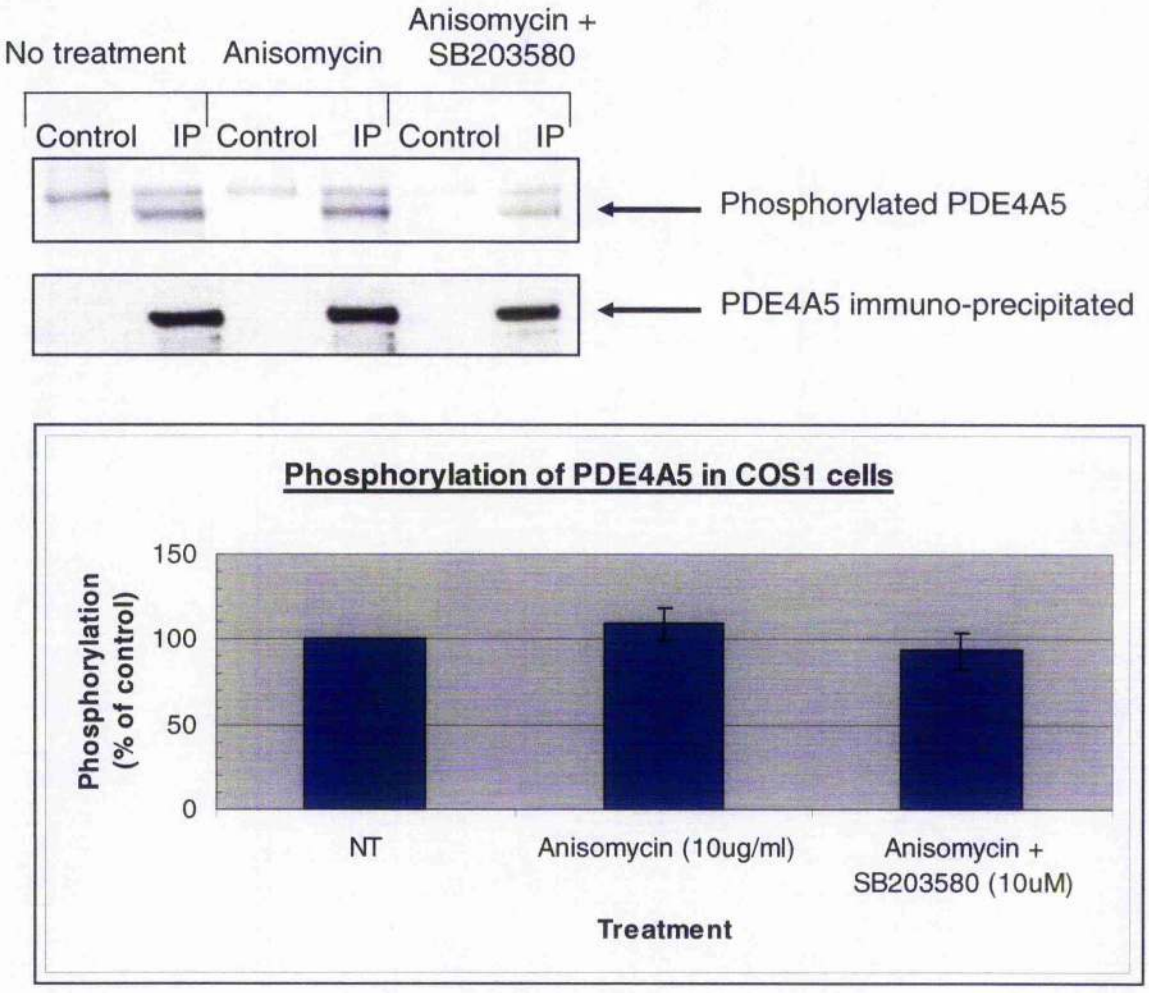
No treatment
Anisomycin
Anisomycin + SB203580
Control
IP
Control
IP
Control
IP
Phosphorylated PDE4A5
PDE4A5 immuno-precipitated
Phosphorylation of PDE4A5 in COS1 cells
Phosphorylation (% of control)
150
100
50
0
NT
Anisomycin (10ug/ml)
Anisomycin + SB203580 (10uM)
Treatment

(b)

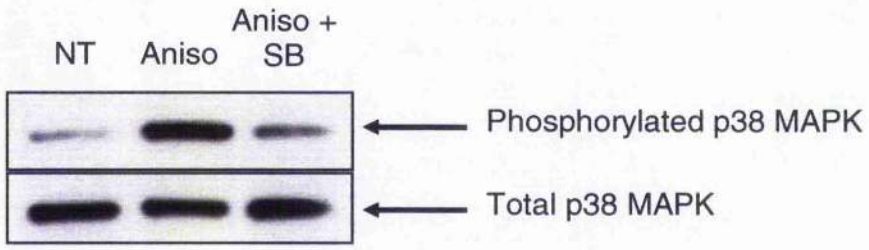
NT
Aniso
Aniso + SB
Phosphorylated p38 MAPK
Total p38 MAPK

Figure 4.11 – In vivo phosphorylation of rat PDE4A5 Ser-147-Ala in COS1 cells stimulated with anisomycin.

The vsv-tagged rat PDE4A5-Ser-147-Ala protein was transiently expressed in COS1 cells. The cells were grown in phosphate-free cell media that was supplemented with [^{32}P]-orthophosphate at least 24h prior to cell treatment. The cells were treated with anisomycin (10µg/ml for 60min) or anisomycin plus SB203580 (10µM for 60min). PDE4A5-Ser-147-Ala-vsv was immuno-precipitated from total cell lysate using an anti-vsv monoclonal antibody conjugated to Protein G agarose. Un-conjugated Protein G agarose was used as the control immuno-precipitation. The immuno-precipitated proteins were separated by SDS-PAGE and transferred to a nitrocellulose membrane where the radioactive proteins were resolved using phosphor image screen technology. (a), top panel, is a laser scanned phosphor image screen of the phosphorylated PDE4A5-Ser-147-Ala-vsv immuno-precipitated following treatment with anisomycin plus or minus SB203580. (a), bottom panel, is a Western blot of the same nitrocellulose membrane probed with the anti-vsv monoclonal antibody to determine the relative PDE4A5 immuno-precipitation from the three cell lysates. (a), graph, displays the quantification of the change in phosphorylation of PDE4A5-Ser-147-Ala-vsv following activation of the p38 MAPK signalling cascade against the no treatment control (100%). These data take into account the relative immuno-reactive amounts of PDE4A5-Ser-147-Ala-vsv isolated by immuno-precipitation. (b), are Western blots of total cell lysate immuno-probed for p38 MAPK activation together with the corresponding total cellular expression of the kinase. All scanned phosphor image screens and Western blots are representative of at least four separate transfections and experiments. These quantification data are expressed as the mean percentage change in phosphorylation over the no treatment control +/- standard deviation of the four separate experiments. Paired t-test statistical analysis of the quantified phosphorylation data were undertaken, where $p < 0.05$ indicates a statistically significant difference in the level of PDE4A5 Ser-147-Ala phosphorylation between untreated and treated cells, as indicated.

(a)

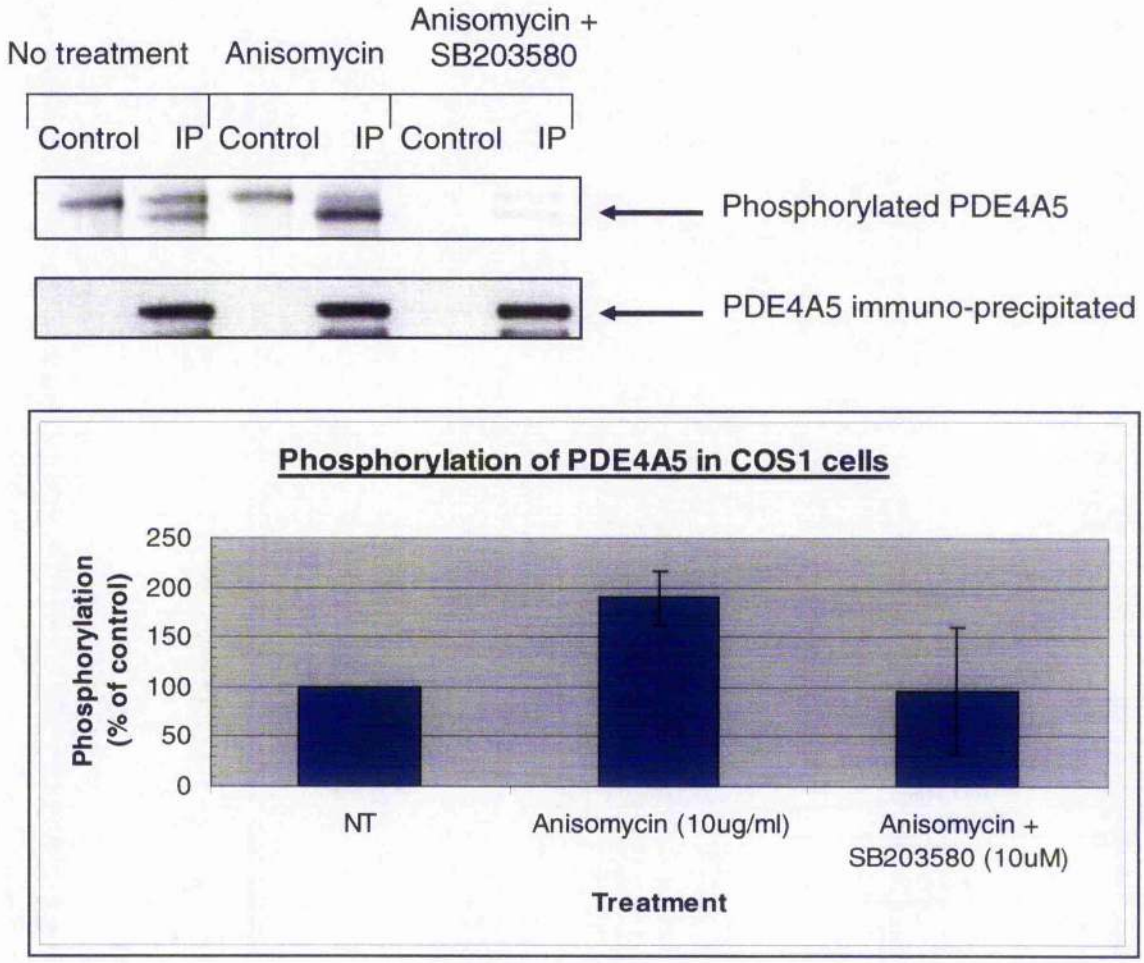
No treatment
Anisomycin
Anisomycin + SB203580
Control
IP
Control
IP
Control
IP
Phosphorylated PDE4A5
PDE4A5 immuno-precipitated
Phosphorylation of PDE4A5 in COS1 cells
Phosphorylation (% of control)
250
200
150
100
50
0
NT
Anisomycin (10ug/ml)
Anisomycin + SB203580 (10uM)
Treatment

(b)

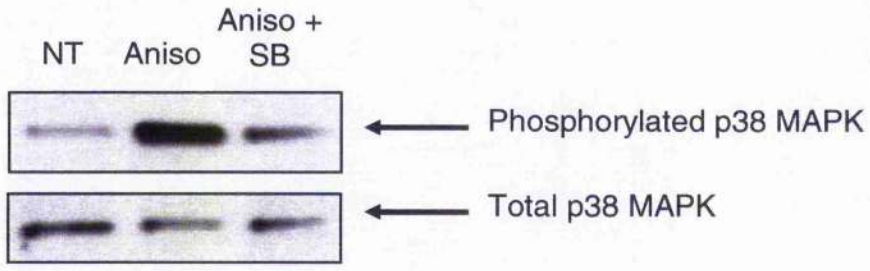
NT
Aniso
Aniso + SB
Phosphorylated p38 MAPK
Total p38 MAPK

Figure 4.12 – In vivo phosphorylation of rat PDE4A5 Ser-161-Ala in COS1 cells stimulated with anisomycin.

The vsv-tagged PDE4A5-Ser-161-Ala protein was transiently expressed in COS1 cells. The cells were grown in phosphate-free cell media that was supplemented with [^{32}P]-orthophosphate at least 24h prior to cell treatment. The cells were treated with anisomycin (10µg/ml for 60min) or anisomycin plus SB203580 (10µM for 60min). PDE4A5-Ser-161-Ala-vsv was immuno-precipitated from total cell lysate using an anti-vsv monoclonal antibody conjugated to Protein G agarose. Un-conjugated Protein G agarose was used as the immuno-precipitation control. The immuno-precipitated proteins were separated by SDS-PAGE and transferred to a nitrocellulose membrane where the radioactive proteins were resolved using phosphor image screen technology. (a), top panel, is a laser scanned phosphor image screen of the phosphorylated PDE4A5-Ser-161-Ala-vsv immuno-precipitated following treatment with anisomycin plus or minus SB203580. (a), bottom panel, is a Western blot of the same nitrocellulose membrane probed with the anti-vsv monoclonal antibody to determine the relative PDE4A5 immuno-precipitation from the three cell lysates. (a), graph, displays the quantification of the change in the phosphorylation state of PDE4A5-Ser-161-Ala-vsv following activation of the p38 MAPK signalling cascade compared to the no treatment control (100%). These data take into account the relative immuno-reactive amounts of PDE4A5-Ser-161-Ala-vsv isolated by immuno-precipitation. (b), are Western blots of total cell lysate immuno-probed for both p38 MAPK activation and the corresponding total cellular expression of the kinase. All scanned phosphor image screens and Western blots are representative of two separate transfections and experiments. These quantification data are expressed as the mean percentage change in phosphorylation over the no treatment control +/- standard deviation of the two separate experiments. Paired t-test statistical analysis of the quantified phosphorylation data were undertaken, where $p < 0.05$ indicates a statistically significant difference in the level of PDE4A5 Ser-161-Ala phosphorylation between untreated and treated cells, as indicated.

(a)

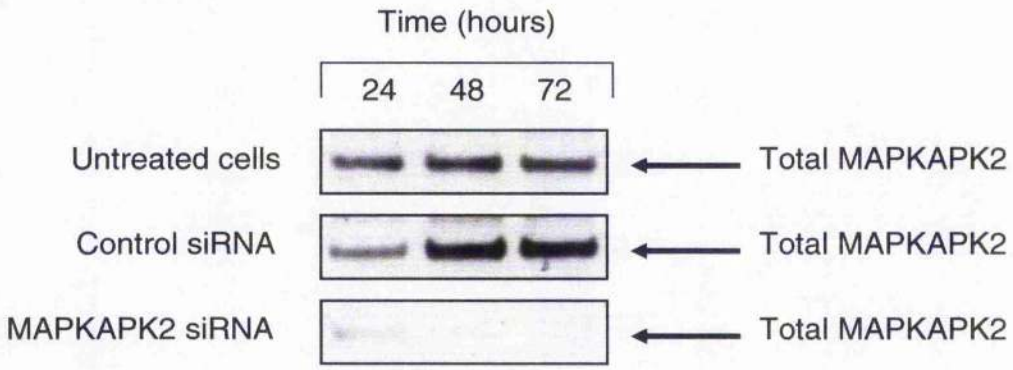
Time (hours)
24
48
72
Untreated cells
Control siRNA
MAPKAPK2 siRNA
Total MAPKAPK2
Total MAPKAPK2
Total MAPKAPK2

(b)

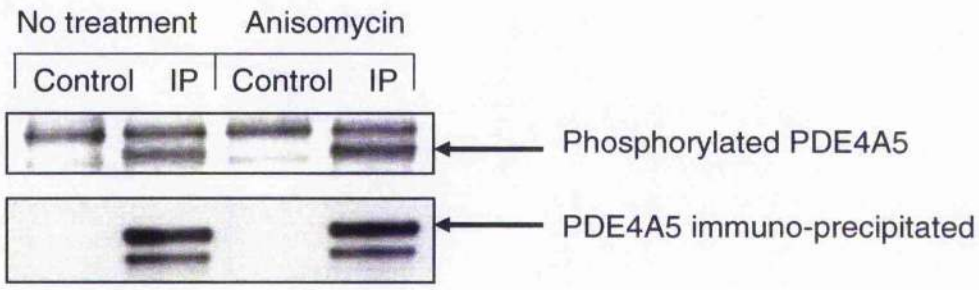
No treatment
Anisomycin
Control
IP
Control
IP
Phosphorylated PDE4A5
PDE4A5 immuno-precipitated

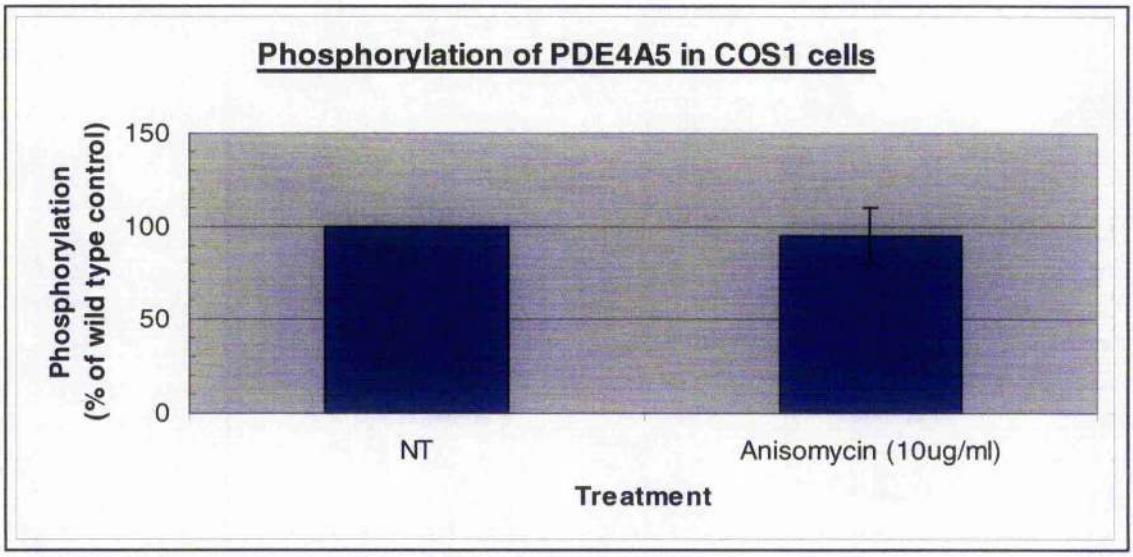
Phosphorylation of PDE4A5 in COS1 cells
Phosphorylation (% of wild type control)
150
100
50
0
NT
Anisomycin (10ug/ml)
Treatment

(c)

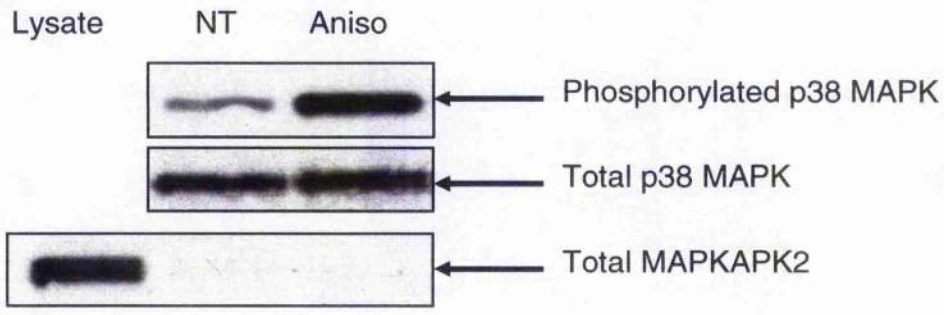
Lysate
NT
Aniso
Phosphorylated p38 MAPK
Total p38 MAPK
Total MAPKAPK2

Figure 4.13 – In vivo anisomycin-induced phosphorylation of rat PDE4A5 in COS1 cells with siRNA to eliminate endogenous MAPKAPK2.

A time course of siRNA knockdown of MAPKAPK2 was undertaken in COS1 cells and the total cell lysates were immuno-probed for endogenous MAPKAPK2 expression. COS1 cells were optimally co-transfected with MAPKAPK2 siRNA and wild type vsv-PDE4A5. The cells were grown in phosphate-free cell media supplemented with [^{32}P]-orthophosphate 24h prior to anisomycin (10µg/ml for 60min) cell treatment. PDE4A5-vsv was immuno-precipitated from cell lysate using an anti-vsv antibody conjugated to Protein G agarose. Un-conjugated Protein G agarose was used as the immuno-precipitation control. The immuno-precipitated proteins were separated by SDS-PAGE, transferred to a nitrocellulose membrane and the radioactive proteins resolved using phosphor image screen technology. (a), top panel, is a Western blot of endogenous MAPKAPK2 expression in COS1 cells. (a), middle panel, shows a Western blot of endogenous MAPKAPK2 expression in COS1 cells transfected with a non-targeting siRNA. (a), bottom panel, is a Western blot of endogenous MAPKAPK2 expression in COS1 cells following transfection with MAPKAPK2 specific siRNA. (b), top panel, is a laser scanned phosphor image screen of the phosphorylated PDE4A5-vsv immuno-precipitated following anisomycin treatment. (b), bottom panel, is a Western blot of the same membrane probed with the anti-vsv antibody to determine the relative PDE4A5 immuno-precipitation from the cell lysates. (b), graph, displays the quantification of the phosphorylation state of PDE4A5-vsv, in cells with no expression of MAPKAPK2, following p38 MAPK activation. These data incorporate the relative immuno-reactive amounts of PDE4A5-vsv isolated by immuno-precipitation. (c), are Western blots of cell lysate immuno-probed for p38 MAPK activation together with total cellular expression of p38 MAPK and MAPKAPK2. All scanned phosphor image screens and Western blots are representative of three separate transfections and experiments. These quantification data are expressed as the mean percentage change in phosphorylation of at least three separate transfections and experiments over the no treatment control +/- standard deviation. Paired t-test statistical analysis of the quantified phosphorylation data were

undertaken, where $p < 0.05$ indicates a statistically significant difference in the level of PDE4A5 wild type phosphorylation between untreated and treated cells, as indicated.

(a)

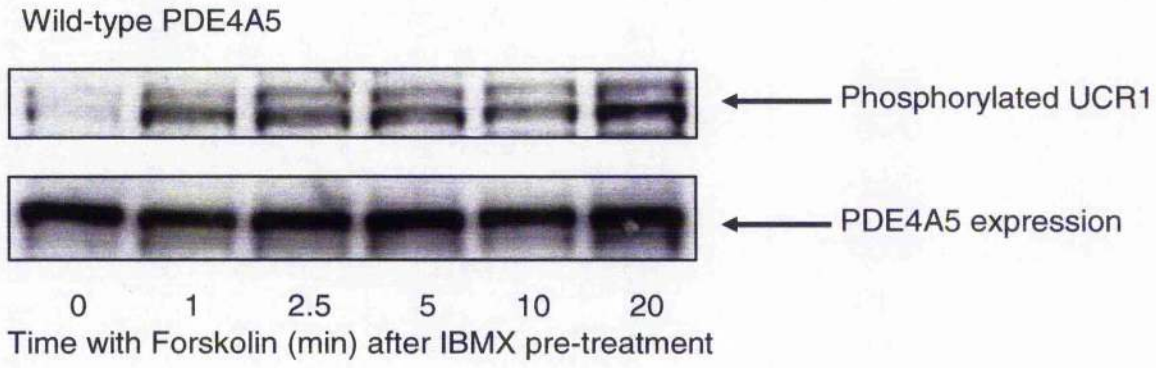
Wild-type PDE4A5
Phosphorylated UCR1
PDE4A5 expression
0
1
2.5
5
10
20
Time with Forskolin (min) after IBMX pre-treatment

(b)

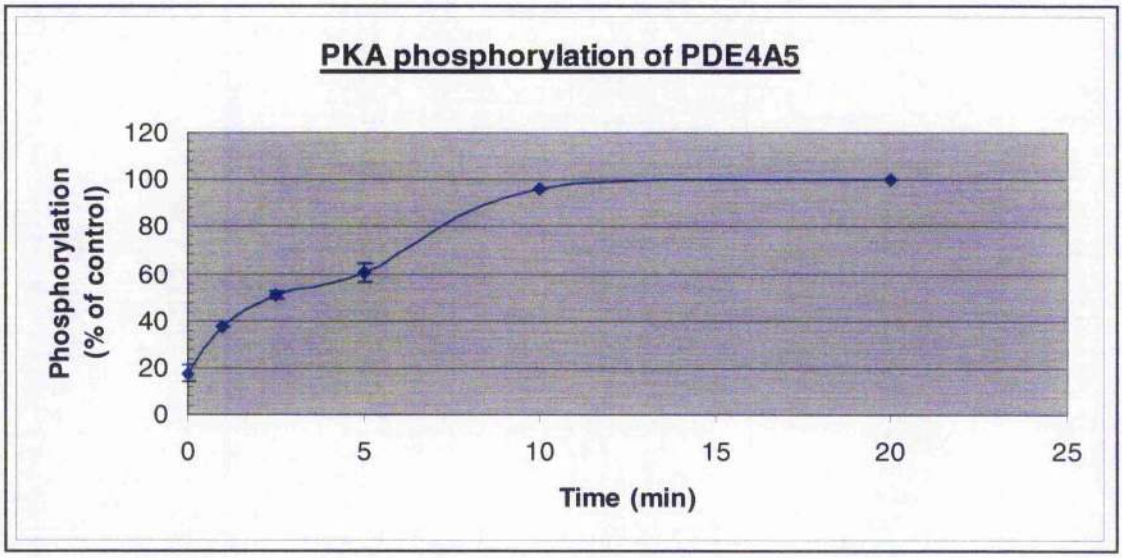
PKA phosphorylation of PDE4A5
Phosphorylation (% of control)
120
100
80
60
40
20
0
0
5
10
15
20
25
Time (min)

(c)

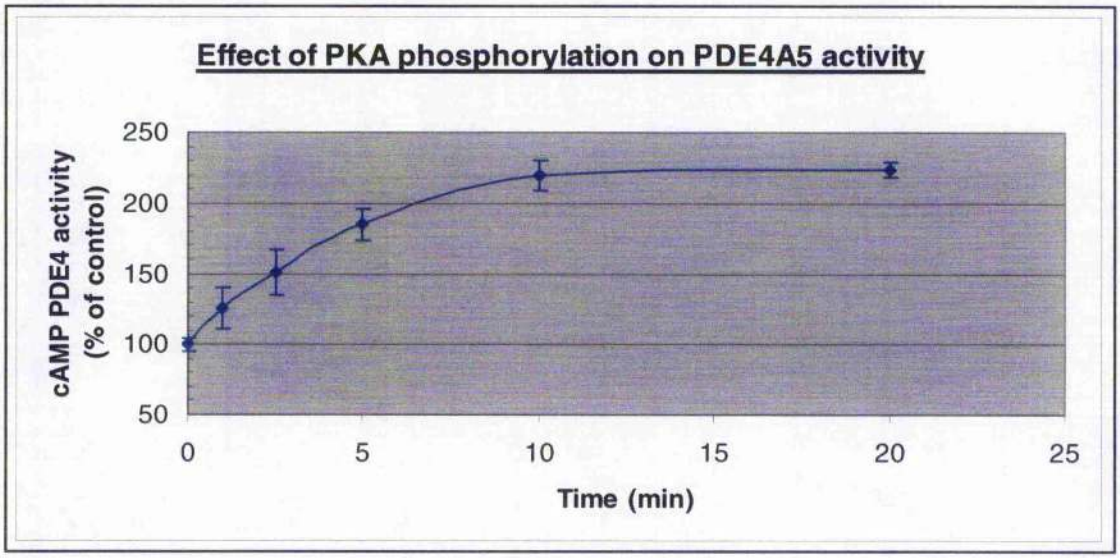
Effect of PKA phosphorylation on PDE4A5 activity
cAMP PDE4 activity (% of control)
250
200
150
100
50
0
5
10
15
20
25
Time (min)

Figure 4.14 – Phosphorylation and activation of rat PDE4A5 by PKA.

COS1 cells were transfected to transiently express wild type rat PDE4A5. The transfected cells were pre-treated for 10min with the non-specific PDE inhibitor, IBMX (100μM) before challenge, 0-20min, with the adenylyl cyclase activator, forskolin (100μM). (a), top panel, is a Western blot probed with the phospho-UCR1 specific anti-serum to the PKA phosphorylated serine (S*) residue within the RRES*F consensus motif [MacKenzie et al., 2002]. (a), bottom panel, shows the same Western blot re-probed with a rat PDE4A C-terminal specific anti-serum to provide both loading and PDE4A5 expression controls. (b), shows the densitometry of the phospho-UCR1 time course, corrected for PDE4A5 expression. (c), shows the effect of the PKA phosphorylation on PDE4A5 enzymatic activity. Assays were done using 1μM cAMP as substrate with COS1 cell lysates expressing equal immuno-reactive amounts of PDE4A5, as determined by the quantification of PDE4A5 expression. All data shown are either representative Western blots of three separate transfections and experiments, or mean data +/- standard deviation of the three separate transfections and experiments.

(a)

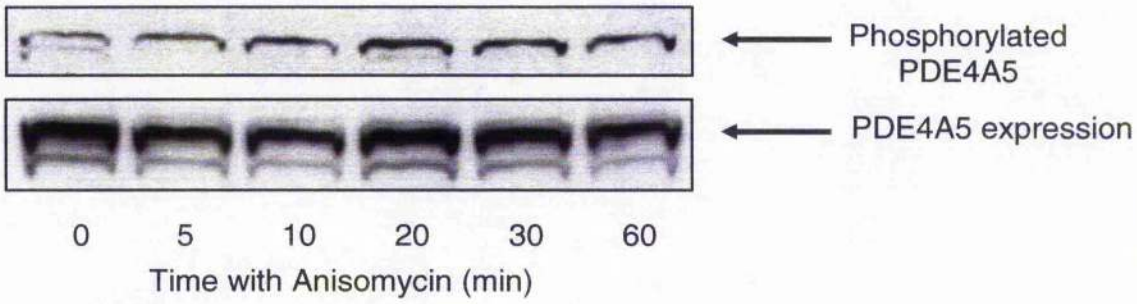
Wild-type PDE4A5
Phosphorylated PDE4A5
PDE4A5 expression
0
5
10
20
30
60
Time with Anisomycin (min)

(b)

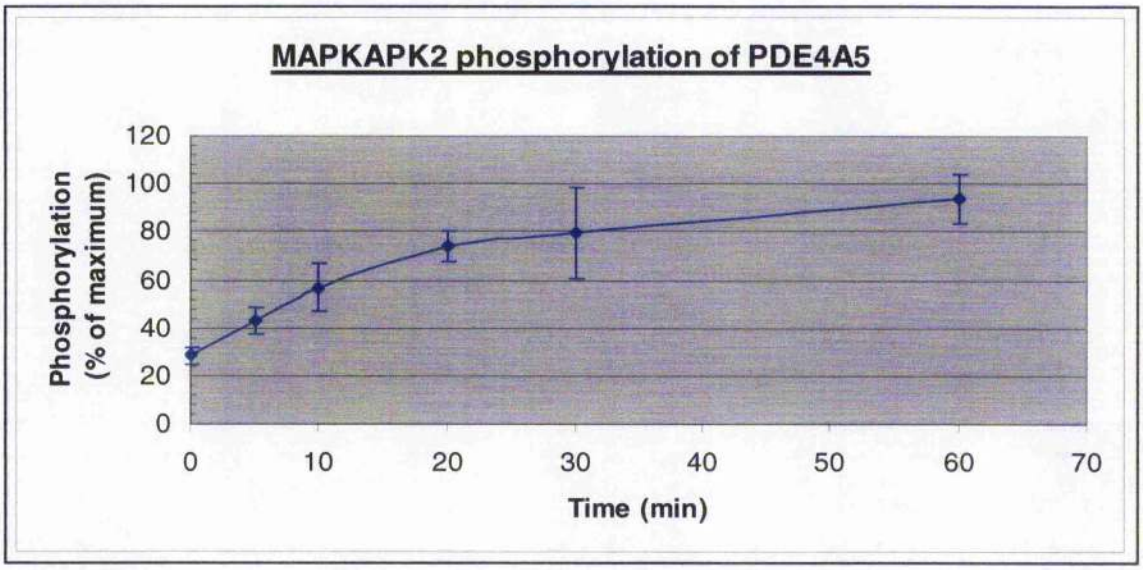
MAPKAPK2 phosphorylation of PDE4A5
Phosphorylation (% of maximum)
120
100
80
60
40
20
0
0
10
20
30
40
50
60
70
Time (min)

(c)

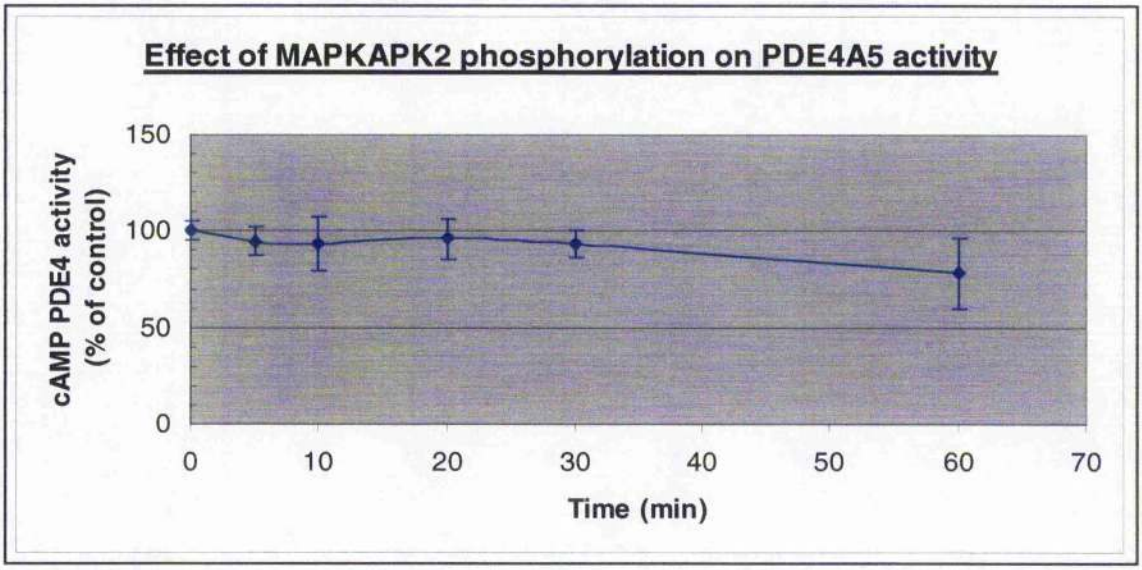
Effect of MAPKAPK2 phosphorylation on PDE4A5 activity
cAMP PDE4 activity (% of control)
150
100
50
0
0
10
20
30
40
50
60
70
Time (min)

(d)


PDE4A5 S147A
Phosphorylated PDE4A5
PDE4A5 expression
0
5
10
20
30
60
Time with Anisomycin (min)

Figure 4.15 – Phosphorylation of rat PDE4A5 by MAPKAPK2 and activity analysis.

COS1 cells were transfected to transiently express rat PDE4A5. The transfected cells were treated for up to 60min with anisomycin (10µg/ml). (a), top panel, is a Western blot probed with a novel, specific anti-serum to the MAPKAPK2 phosphorylated serine (S*) residue in the LYRSDS* consensus motif within the UCR1 regulatory module. (a), bottom panel, shows the same Western blot re-probed with a rat PDE4A C-terminal specific anti-serum to provide both loading and PDE4A5 expression controls. (b), quantifies the MAPKAPK2 phosphorylation time course of PDE4A5 by determining the densitometry of the immuno-reactive bands detected with both the novel phosphorylation anti-serum and the anti-serum for PDE4A5 total cellular expression. These were expressed as a percentage of the maximum phosphorylation to expression ratio. (c), shows the effect of the MAPKAPK2 phosphorylation on PDE4A5 wild type catalytic activity. Assays were done using 1µM cAMP as substrate with COS1 cell lysates expressing equal immuno-reactive amounts of PDE4A5, as determined by the quantification of PDE4A5 expression. (d), top panel, is a Western blot of total COS1 cell lysate transfected with rat PDE4A5-Ser-147-Ala and probed with the novel anti-serum specific to the MAPKAPK2 phosphorylated target Ser-147. (d), bottom panel, is the associated PDE4A5-Ser-147-Ala loading and expression control detected using the rat PDE4A C-terminal specific antibody. All data shown are either representative Western blots of three separate transfections and experiments, or are mean data +/- standard deviation of the three separate transfections and experiments.

(a)

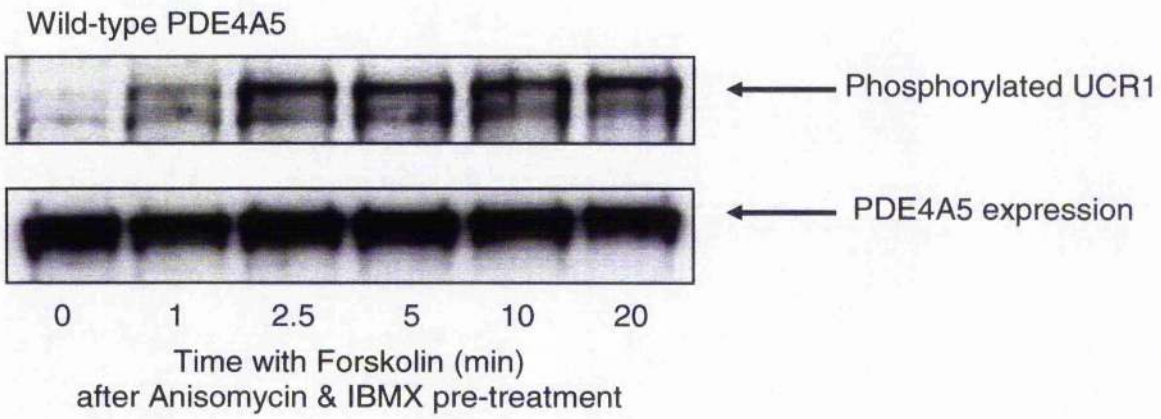
Wild-type PDE4A5
Phosphorylated UCR1
PDE4A5 expression
0
1
2.5
5
10
20
Time with Forskolin (min)
after Anisomycin & IBMX pre-treatment

(b)

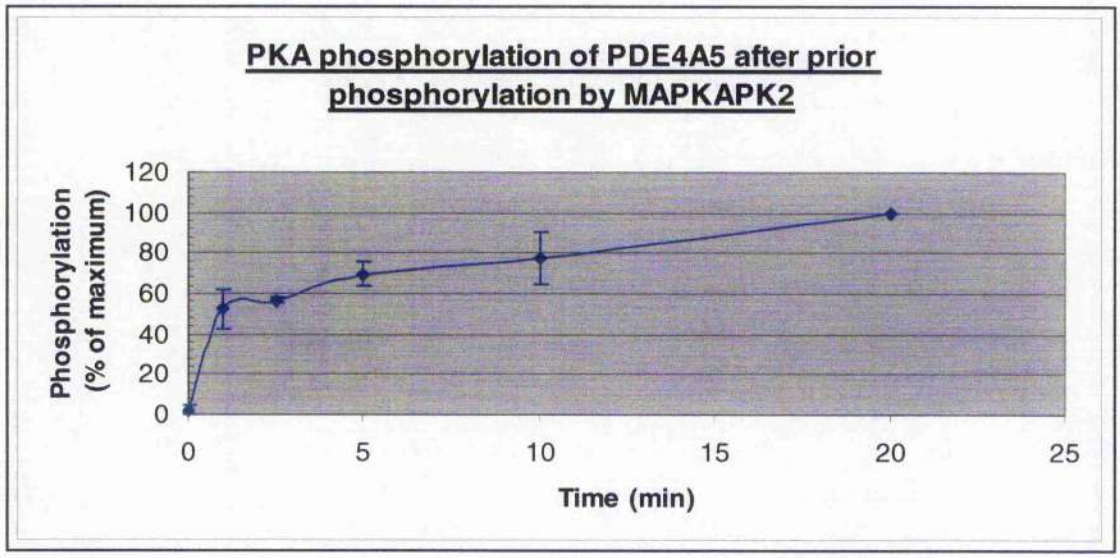
PKA phosphorylation of PDE4A5 after prior phosphorylation by MAPKAPK2
Phosphorylation (% of maximum)
120
100
80
60
40
20
0
0
5
10
15
20
25
Time (min)

(c)

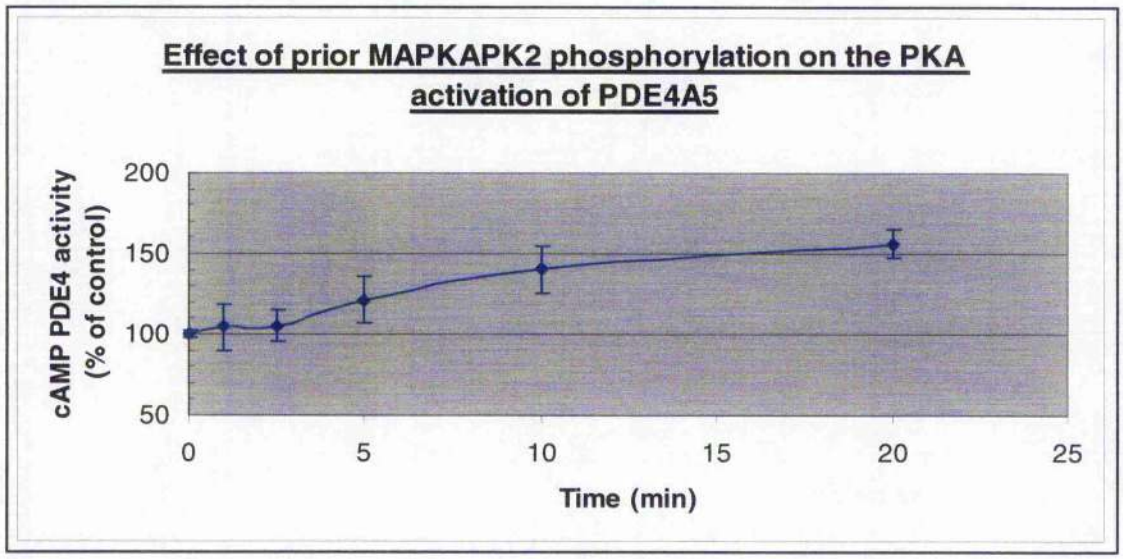
Effect of prior MAPKAPK2 phosphorylation on the PKA activation of PDE4A5
cAMP PDE4 activity (% of control)
200
150
100
50
0
5
10
15
20
25
Time (min)

Figure 4.16 – Dual phosphorylation of PDE4A5 by MAPKAPK2 and PKA.

COS1 cells were transfected to transiently express PDE4A5. Cells were pre-treated with anisomycin (10µg/ml) for 30min and then IBMX (100µM) for 10min. The cells were then challenged with forskolin (100µM) for 0-20min, as indicated. (a), top panel, is a Western blot probed with the phospho-UCR1 anti-serum to the PKA phosphorylated serine within the RRES*F consensus motif of all long PDE4 isoforms [MacKenzie et al., 2002]. (a), bottom panel, is the same Western blot re-probed for PDE4A5 expression using an anti-serum specific to the unique C-terminal region of rat PDE4A isoforms and also acts as loading controls. (b), illustrates the quantification of the PKA phosphorylation corrected for the total PDE4A5 expression. This is presented as a percentage of the maximum phosphorylation. (c), shows the effect of the dual MAPKAPK2 and PKA phosphorylation on PDE4A5 enzymatic activity. Assays were done using 1µM cAMP as substrate with COS1 cell lysates expressing equal immuno-reactive amounts of PDE4A5, as determined by the quantification of PDE4A5 expression. All data shown are either representative Western blots of two separate transfections and experiments, or are mean data +/- standard deviation of the two separate transfections and experiments.

(a)

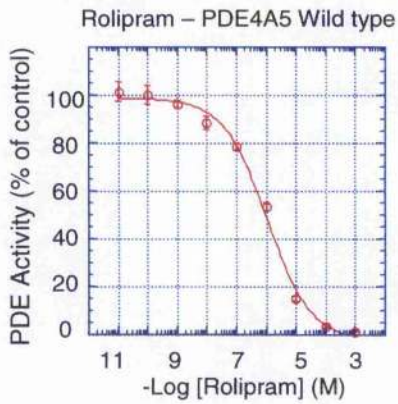
Rolipram – PDE4A5 Wild type
PDE Activity (% of control)
100
80
60
40
20
0
11
9
7
5
3
-Log [Rolipram] (M)

(b)

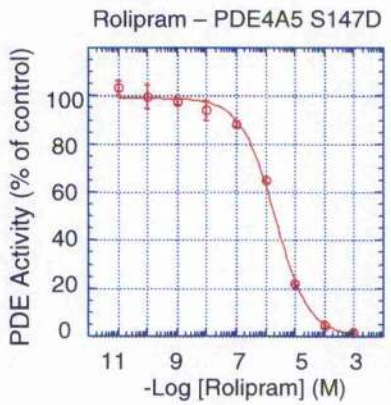
Rolipram – PDE4A5 S147D
PDE Activity (% of control)
100
80
60
40
20
0
11
9
7
5
3
-Log [Rolipram] (M)

Figure 4.17 – Rolipram inhibition of PDE4A5 wild type or PDE4A5 Ser-147-Asp.

COS1 cells were transfected to transiently express wild type PDE4A5 or PDE4A5 Ser-147-Asp before sub-cellular fractionation into high-speed supernatant (S2). PDE4 activity assays were done using 1μM cAMP as substrate against a range of rolipram concentrations, as indicated. The data presented here are mean values +/- standard deviation of three separate transfections and sub-cellular fractionations. The determinations of the respective IC_{50} values for each inhibitor are shown in Table 4.1.

Inhibitor	PDE4A5 Wild type (S2)	PDE4A5 Ser147Asp (S2)
Rolipram	1.10 +/- 0.28	2.13 +/- 0.36

Table 4.2 – Rolipram inhibition of PDE4A5 wild type or PDE4A5 Ser-147-Asp.

COS1 cells were transfected to transiently express each isoform before sub-cellular fractionation into high-speed supernatant (S2). Assays were done using 1μM cAMP as substrate against a range of inhibitor concentrations as indicated in Figure 4.17. These data are given as IC_{50} values in micro-molar (μM) concentrations and are mean values +/- the standard deviation from three separate transfections.

(a)

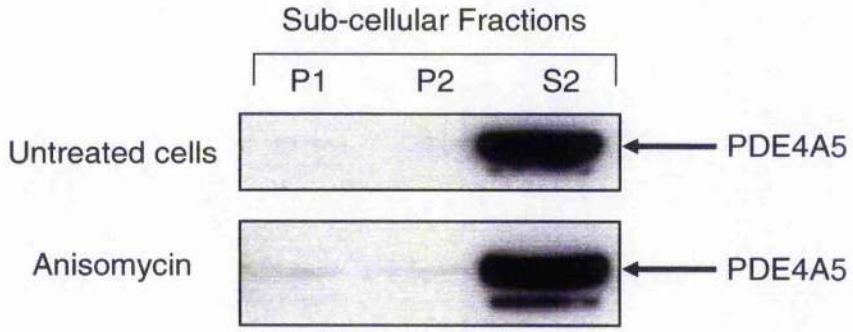
Sub-cellular Fractions
P1
P2
S2
Untreated cells
PDE4A5
Anisomycin
PDE4A5

(b)

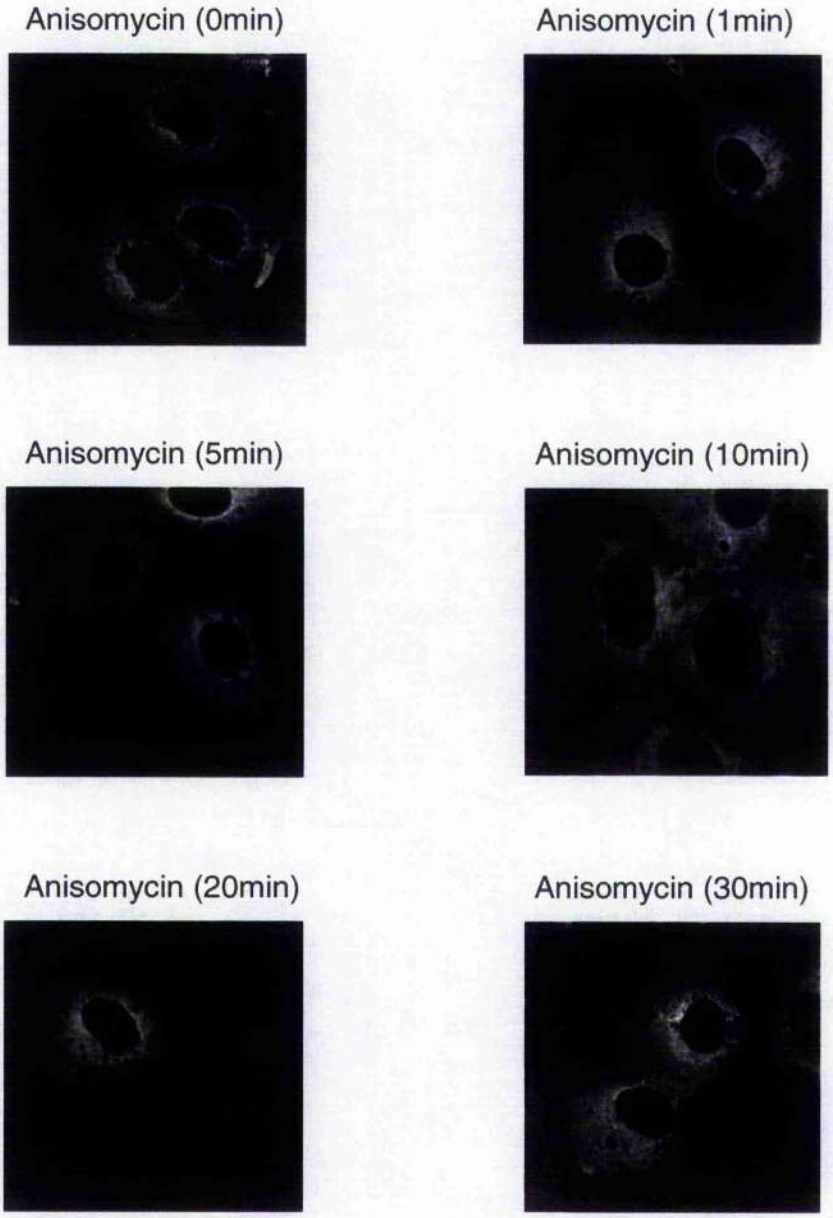
Anisomycin (0min)
Anisomycin (1min)
Anisomycin (5min)
Anisomycin (10min)
Anisomycin (20min)
Anisomycin (30min)

Figure 4.18 – Distribution of native PDE4A5 and MAPKAPK2 phosphorylated PDE4A5 in COS1 cells.

(a), top panel, shows a Western blot of the distribution of wild type PDE4A5 when transiently over-expressed in untreated COS1 cells. (a), bottom panel, shows a Western blot of the distribution of wild type PDE4A5 following treatment with anisomycin (10µg/ml for 60min). COS1 cells were harvested and subjected to sub-cellular fractionation producing the high-speed supernatant (S2), the high-speed pellet (P2), and the low-speed pellet (P1) as described previously [McPhee et al., 1999]. (b), shows laser-scanning confocal microscopy analysis of PDE4A5 distribution in COS1 cells with anisomycin treatment (10µg/ml) at the indicated times. COS1 cells were transfected to express PDE4A5 and then visualised immunologically using the rat PDE4A C-terminal specific anti-serum to evaluate any change in PDE4A5 localisation compared to the time zero control. All data are examples of experiments done at least three times with different transfections.

(a)

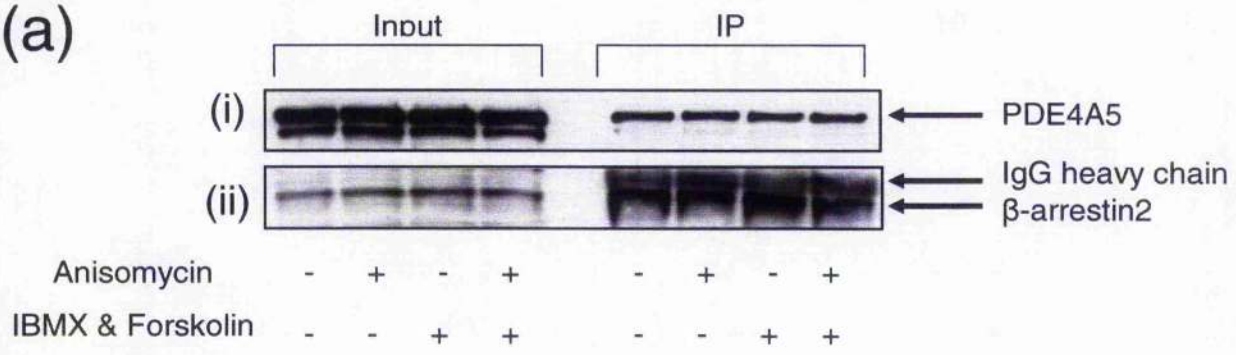
Input
IP
(i)
(ii)
PDE4A5
IgG heavy chain
β-arrestin2
Anisomycin - + - + - + - +
IBMX & Forskolin - - + + - - + +

(b)

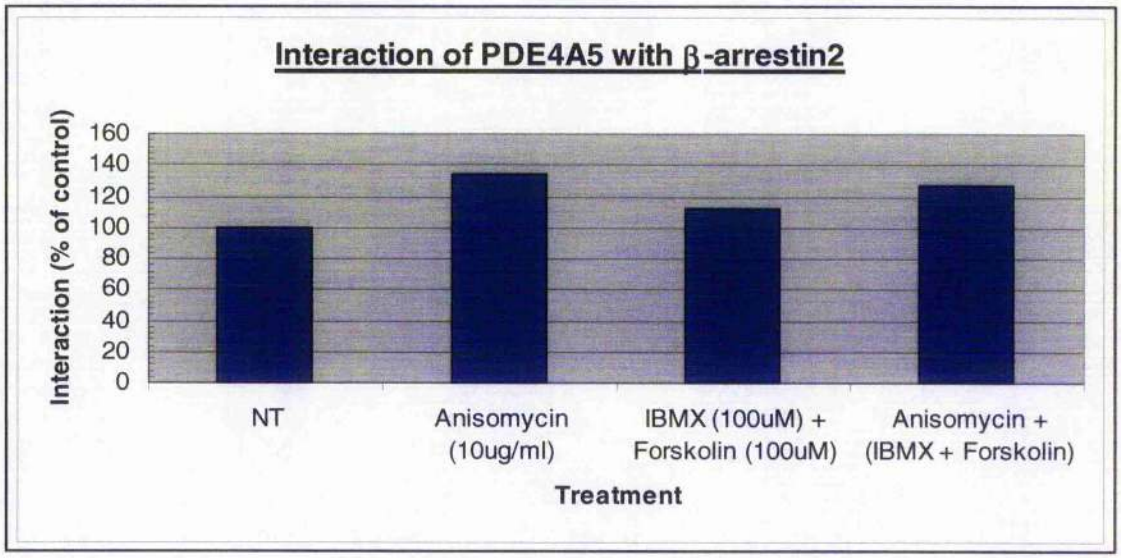
Interaction of PDE4A5 with β-arrestin2
Interaction (% of control)
160
140
120
100
80
60
40
20
0
NT
Anisomycin (10ug/ml)
IBMX (100uM) + Forskolin (100uM)
Anisomycin + (IBMX + Forskolin)
Treatment

(c)

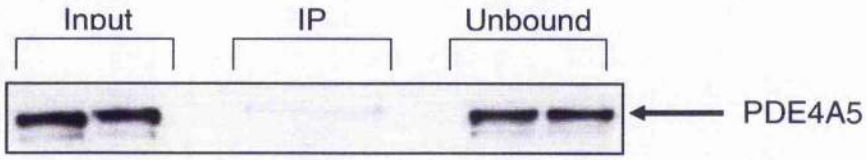
Input
IP
Unbound
PDE4A5

Figure 4.19 – MAPKAPK2 phosphorylation of PDE4A5 and the interaction with the scaffold protein β-arrestin2.

COS1 cells were co-transfected to transiently express both vsv-tagged PDE4A5 and FLAG-tagged β-arrestin2. The transfected cells were either retained as control cells or treated with anisomycin (10μg/ml for 60 minutes), IBMX and forskolin (100μM for 10min respectively) or both treatments together. Total cell lysate was produced and β-arrestin2, and its associated proteins, was immuno-precipitated using FLAG agarose. The immuno-precipitated proteins were separated by SDS-PAGE and immuno-probed for possible PDE4A5-β-arrestin2 interaction using a specific anti-serum to the unique C-terminal region of rat PDE4A isoforms. (a) (i), is a Western blot showing the relative immuno-reactive amounts of PDE4A5 expressed in each cell lysate prior to immuno-precipitation and the immuno-reactive amounts interacting with β-arrestin2 following co-immuno-precipitation. (a) (ii), is a Western blot showing the relative immuno-reactive amounts of β-arrestin2 expressed in each cell lysate and the relative immuno-reactive amounts immuno-precipitated using FLAG agarose. (b), presents the quantification of the Western blots assessing the effect of the MAPKAPK2 and/or PKA phosphorylation of PDE4A5 upon the interaction with β-arrestin2. Quantification of the immuno-precipitation corrects for the expression of both proteins in the initial cell extract and for immuno-precipitation efficiency. (c), is a Western blot of a control FLAG agarose immuno-precipitation using COS1 cell lysate singularly transfected with vsv-tagged PDE4A5. All Western blots are representative of transfections and experiments undertaken at least three times and quantification data is expressed as mean values +/- standard deviation of at least three separate transfections and experiments.

(a)

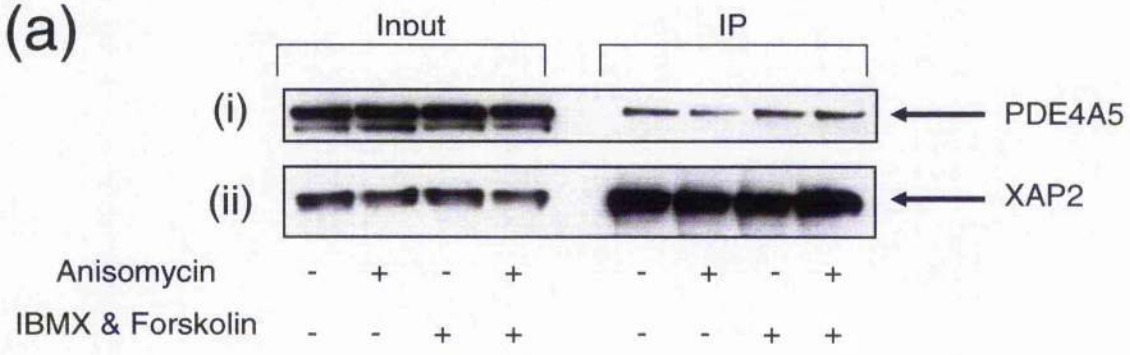
Input
IP
(i)
PDE4A5
(ii)
XAP2
Anisomycin - + - + - + - +
IBMX & Forskolin - - + + - - + +

(b)

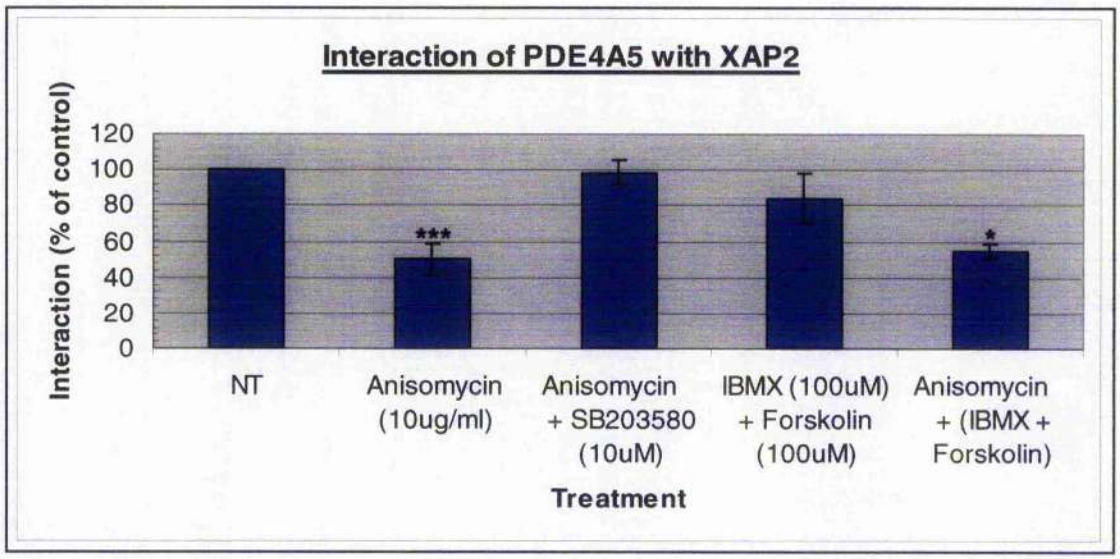
Interaction of PDE4A5 with XAP2
Interaction (% of control)
120
100
80
60
40
20
0
***
*
NT
Anisomycin (10ug/ml)
Anisomycin + SB203580 (10uM)
IBMX (100uM) + Forskolin (100uM)
Anisomycin + (IBMX + Forskolin)
Treatment

(c)

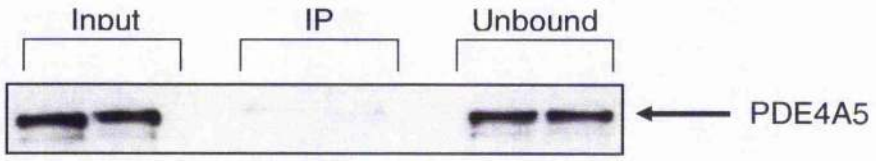
Input
IP
Unbound
PDE4A5

Figure 4.20 – MAPKAPK2 phosphorylation of PDE4A5 and the interaction with the immuno-philin XAP2.

COS1 cells were co-transfected to transiently express both vsv-tagged PDE4A5 and FLAG-tagged XAP2. The transfected cells were either retained as control cells or treated with anisomycin (10µg/ml for 60min), IBMX and forskolin (100µM for 10min respectively) or both treatments together. Total cell lysate was produced and XAP2, and its associated proteins, were immuno-precipitated using FLAG agarose. The immuno-precipitated proteins were separated by SDS-PAGE and immuno-probed for possible PDE4A5-XAP2 interaction using a specific anti-serum to the unique C-terminal region of rat PDE4A isoforms. (a) (i), is a Western blot showing the relative immuno-reactive amounts of PDE4A5 expressed in each cell lysate prior to immuno-precipitation and the immuno-reactive amounts interacting with XAP2 following co-immuno-precipitation. (a) (ii), is a Western blot showing the relative immuno-reactive amounts of XAP2 expressed in each cell lysate and the relative immuno-reactive amounts immuno-precipitated using FLAG agarose. (b), presents the quantification of the Western blots assessing the effect of the MAPKAPK2 and/or PKA phosphorylation of PDE4A5 upon the interaction with XAP2. Quantification of the immuno-precipitation corrects for the expression of both proteins in the initial cell extract and for immuno-precipitation efficiency. (c), is a Western blot of a control FLAG agarose immuno-precipitation using COS1 cell lysate singularly transfected with vsv-tagged PDE4A5. All Western blots are representative of transfections and experiments undertaken at least three times and quantification data is expressed as mean values +/- standard deviation of at least three separate transfections and experiments. Paired t-test statistical analysis of the quantified co-immuno-precipitation data were undertaken, where $p < 0.05$ indicates a statistically significant difference in the level of PDE4A5 co-immuno-precipitated with XAP2 between native and treated cells, as indicated.

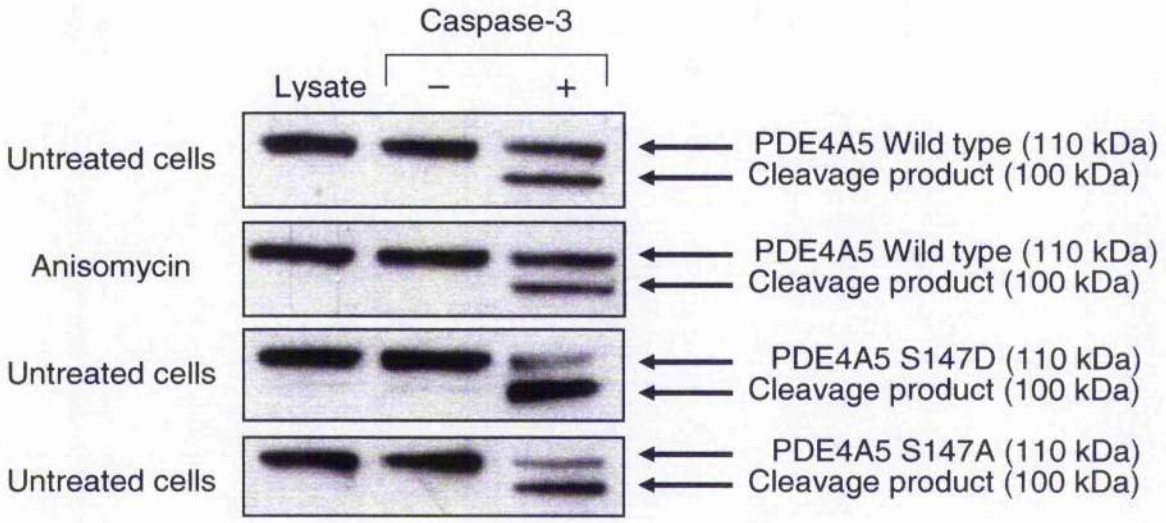
Caspase-3
Lysate
–
+
Untreated cells
Anisomycin
Untreated cells
Untreated cells
PDE4A5 Wild type (110 kDa)
Cleavage product (100 kDa)
PDE4A5 Wild type (110 kDa)
Cleavage product (100 kDa)
PDE4A5 S147D (110 kDa)
Cleavage product (100 kDa)
PDE4A5 S147A (110 kDa)
Cleavage product (100 kDa)

Figure 4.21 – Cleavage of wild type and MAPKAPK2 phosphorylated PDE4A5 by recombinant caspase-3.

Total cellular lysates from COS1 cells transiently expressing PDE4A5 (wild type; no treatment, wild type; anisomycin treated, Ser-147-Asp mutant or Ser-147-Ala mutant) were incubated in the presence of recombinant caspase-3 for 2h at 37°C. All panels are Western blots of COS1 cell lysate expressing PDE4A5 and probed with a specific anti-serum to the unique C-terminal region of rat PDE4A isoforms to detect both full length (~110 kDa) and caspase-3 cleaved species (~100 kDa) [Huston et al., 2000]. All Western blots are representative of transfections and experiments undertaken at least three times.

4.3 Discussion

The p38 MAPK phosphorylation cascade plays a fundamental role in regulating the immune and inflammatory response to infection and tissue injury [Herlaar and Brown, 1999 and Dong et al., 2002]. p38 MAPK activity regulates cell adhesion and migration, cytokine expression, and function of many immune and inflammatory cells including monocytes, macrophages, mast cells and T-lymphocytes [Guo et al., 2003]. Therefore, it has been proposed that inhibition of p38 MAPK activity may be of potential therapeutic benefit in disease states characterised by excessive immune or inflammatory reactions, such as asthma, COPD, rheumatoid arthritis and psoriasis [Herlaar and Brown, 1999 and Saklatvala, 2004].

Early work from the Houslay laboratory has indicated potential signalling cross talk between the p38 MAPK signalling cascade and the regulation of intra-cellular cAMP concentrations [MacKenzie and Houslay, 2000]. This work concluded for the first time that IFNγ, a pro-inflammatory cytokine, could activate monocytic p38 MAPK activity and that the activation was attenuated by rolipram inhibition of PDE4 activity. However, in contrast to these data, cAMP has been shown to activate p38 MAPK in FRTL-5 rat thyroid cells in a PKA- and Rac1-dependent manner indicating cell-type specific signalling patterns [Pomerance et al., 2000].

These effects are consistent with the plethora of data that implicates both PDE4 [Souness et al., 1999, Jin and Conti, 2002, Houslay et al., 2005 and Zhang et al., 2005] and p38 MAPK inhibition as potential means of attenuating pro-inflammatory cytokine production and the overall inflammatory response.

Scanning the primary amino acid sequence of PDE4A5, utilising the ScanSite database (http://scansite.mit.edu/cgi-bin/motifscan_seq) on medium stringency, predicted two putative p38 MAPK phosphorylation sites at Thr-437 and Thr-776 (Figure 4.2). Scanning the PDE4A5 primary amino acid

sequence for the MAPKAPK2 phosphorylation consensus sequence, Ø-Xaa-Arg-Xaa-Xaa-**Ser***-Ø where Ø represents a hydrophobic amino acid, revealed two potential MAPKAPK2 phosphorylation sites, namely Ser-147 and Ser-161 (Figure 4.2). Ser-161 (Val-Ser-Arg-Ser-Ser-**Ser***-Val) is surrounded by optimal residues for MAPKAPK2 phosphorylation whereas the Ser-147 (Leu-Tyr-Arg-Ser-Asp-**Ser***-Asp) contains a less favourable N-terminal hydrophobic leucine residue and a C-terminal aspartic acid residue [Rousseau et al., 2005]. Discrepancy exists however for the requirement of the C-terminal hydrophobic residue and therefore both Ser-147 and Ser-161 are possible MAPKAPK2 phosphorylation target sites based on our current knowledge [Stokoe et al., 1993]. Furthermore, in the case of Nogo-2, a recently identified MAPKAPK2 substrate, optimal consensus motifs were not required for phosphorylation to occur [Rousseau et al., 2005]. Analysis of the consensus motifs for MAPKAPK2 phosphorylation on two well-established substrates, HSP27 and 5-lipoxygenase, permits the presence of a leucine residue at the position n – 5 from the target serine [Werz et al., 2000].

In vitro phosphorylation of a recombinant MBP fusion protein of PDE4A5 (Figure 4.3) with recombinant, active MAPKAPK2 or p38 MAPK provided initial evidence that PDE4A5 was a potential substrate for both kinases (Figure 4.4). These initial experiments alluded to PDE4A5 being phosphorylated at Ser-147 by MAPKAPK2. Additional sites may also be available because the level of phosphorylation was not completely ablated with the Ser-147-Ala mutant form of PDE4A5. However, as with all in vitro protein kinase phosphorylation assays there is a propensity for background or indiscriminate phosphorylation to occur [Berwick and Tavaré, 2004]. To reconcile whether this was the case a time course of in vitro phosphorylation coupled with a positive, i.e. HSP27 or 5-lipoxygenase, and a negative control, i.e. MBP, needs to be undertaken. Furthermore, it is possible that MBP itself is a target for both MAPKAPK2 and p38 MAPK.

Activation of p38 MAPK in most cells can be induced with anisomycin, which acts synergistically with growth factors through stimulation of the G-proteins, Rac and Cdc42 (Figures 4.1 and 4.6) [Cahill et al., 1996 and Uhlik et

al., 2003]. The delayed onset of MAPKAPK2 activation with anisomycin was noted and this is indicative of its location downstream of p38 MAPK in the phosphorylation cascade. The pro-inflammatory cytokine TNFα is a potent and rapid activator of p38 MAPK and MAPKAPK2 via the TNF receptor, recruitment of TRAF2, and activation of ASK (Figures 4.1 and 4.7) [Ichijo et al., 1997 and Nishitoh et al., 1998]. Anisomycin was used to stimulate p38 MAPK activity in COS1 cells over-expressing PDE4A5, with the aim of confirming any physiological effects with TNFα-treated cells expressing immuno-logically detectable levels of endogenous PDE4A5.

PDE4A5 was phosphorylated in vivo in a p38 MAPK-dependent manner, as indicated following anisomycin treatment and co-incubation with the specific p38 MAPK inhibitor, SB203580 (Figure 4.8) [Cuenda et al., 1995, Young et al., 1997, Davies et al., 2000 and Guo et al., 2003]. These data identified PDE4A5 as a substrate of p38 MAPK or a p38 MAPK-dependent protein kinase. Of intrigue was the immuno-precipitation of a phosphorylated band of a marginally higher molecular weight to PDE4A5. This protein was also immuno-precipitated with Protein G agarose beads alone and was not detected following Western immuno-blotting with the VSV monoclonal antibody used to assess PDE4A5 immuno-precipitation efficiency. PDE4A5 (110kDa) is subject to cleavage by caspase-3 at Asp-69 within the Asp-Ala-Val-Asp motif located within the unique N-terminal region [Huston et al., 2000]. Cleavage results in the production of a truncated PDE4A5 species of approximately 100kDa. If indeed the doublet was indicative of native and cleaved PDE4A5 then an immuno-reactive doublet would have been revealed on the Western blot, as PDE4A5 is in fusion with VSV at the C-terminal. Furthermore, the unidentified protein in the control immuno-precipitation does not appear to be subject to p38 MAPK-dependent phosphorylation.

Utilising N-terminal truncations of PDE4A5 [Beard et al., 2002], it was concluded that the UCR1 module was subject to phosphorylation via activation of the p38 MAPK signalling pathway (Figures 4.9 and 4.10). Relating these data to the initial phosphorylation motif scanning and preliminary in vitro phosphorylation data implied that MAPKAPK2 was

responsible for mediating the p38 MAPK-dependent phosphorylation. Site-directed mutagenesis of Ser-147-Ala and Ser-161-Ala within the MAPKAPK2 consensus motifs identified Ser-147 as the sole target for PDE4A5 phosphorylation (Figures 4.11 and 4.12). Generation of a phospho-specific anti-serum further confirmed Ser-147 as the target phosphorylation residue and, as expected, anisomycin induced a time-dependent increase in the level of phosphorylation at this site (Figure 4.15). The anti-serum also identified a level of basal phosphorylation at Ser-147, which was ablated on alanine mutation.

Small interfering RNA (siRNA) is a very powerful tool used to elucidate the functional significance of cell signalling enzymes, kinases and scaffold proteins. siRNAs are targeted 19-25 nucleotides that specifically knockdown endogenous protein expression in mammalian cells [Banan and Puri, 2004 and Jones et al., 2004]. They do this by incorporating into RNA-induced silencing complexes, which bind to mRNA transcripts through complementary base pair interactions. This targets the mRNA for degradation, resulting in the ablation of protein expression. MAPKAPK2 siRNA completely ablated endogenous expression in COS1 cells [San Miguel et al., 2005]. Phosphorylation of PDE4A5 was completely ablated in MAPKAPK2 deficient COS1 cells and therefore identified MAPKAPK2 as the relevant protein kinase downstream of p38 MAPK.

Proving that proteins are authentic substrates for specific protein kinases is extremely difficult given the promiscuous nature of in vitro phosphorylation assays, and the complexity and integration of cell signalling pathways. To address such concerns certain criteria should be satisfied en-route to formally identifying protein kinase substrates [Berwick and Tavaré, 2004]. These criteria include (1) the recombinant in vitro phosphorylation of the proposed substrate and reduction of phosphorylation using site-specific alanine mutant(s) (Figure 4.4), (2) proving that the phosphorylation can occur in intact cells to a stimuli that activates the protein kinase in a stimulus and concentration-dependent time course (Figures 4.6, 4.8 and 4.15), (3) matching the phosphorylation site in vivo to the phosphorylation site in vitro

(Figures 4.4, 4.11 and 4.15) and (4) ablating, or at least attenuating, the phosphorylation using specific inhibitors or siRNA knockdown of protein kinase expression (Figures 4.8 and 4.13) [Berwick and Tavaré, 2004]. As PDE4A5 satisfies each of these criteria for MAPKAPK2 phosphorylation, I conclude that PDE4A5 is a bone fide substrate of MAPKAPK2 in cells, with phosphorylation occurring at a single serine residue (Ser-147).

The phosphorylation of PDE4 enzymes by a cAMP-dependent protein kinase, now known to as PKA, was first shown in thyroid FRTL-5 cells on stimulation with TSH [Sette et al., 1994]. Further work identified a conserved single serine residue (Ser-54 of PDE4D3) within the UCR1 module as the phosphorylation target and the enzyme activation it conferred [Sette and Conti, 1996, Hoffman et al., 1998 and MacKenzie et al., 2002]. These data provided the first evidence that these domains participate in the regulation of catalytic activity, and therefore must interact in some way. PKA phosphorylation is proposed to relieve an inhibitory constraint conferred upon the catalytic machinery by UCR2 via disruption of the intra-molecular interactions between the UCR1 and UCR2 regulatory domains [Lim et al., 1999 and Beard et al., 2000]. The resolution of the crystal structure of the N-terminal region and UCR domains of full-length PDE4 isoforms will provide much needed insight into the mechanism through which these domains regulate the catalytic unit and how PKA phosphorylation impacts on such regulation.

As previously described, PDE4A5 enzyme activity is markedly enhanced following PKA phosphorylation (Figure 4.14) [MacKenzie et al., 2002 and Bolger et al., 2003]. However, MAPKAPK2 phosphorylation of PDE4A5 exerts no functional effect upon catalytic activity (Figure 4.15). Because of UCR1 conservation across the PDE4 gene families, one would expect MAPKAPK2 to phosphorylate all PDE4 long isoforms. PDE4 isoforms differ by virtue of their unique N-terminal regions and their sub-family specific LR1, LR2 and C-terminal regions [Houslay, 2001 and Houslay et al., 2005]. Therefore, although PDE4A5 phosphorylation by MAPKAPK2 does not exert functional consequences upon catalytic activity, other long isoforms may

behave differently, by virtue of their unique properties. For example, the PDE4D3 long isoform is phosphorylated by PKA, but this is the only isoform where it confers both activation of catalytic activity and increased sensitivity to rolipram inhibition [Hoffmann et al., 1998]. Phosphorylation of other long isoforms across all gene families facilitates a similar activation but displays no altered rolipram inhibition profile to the native form [MacKenzie et al., 2002]. Utilising a Ser-147-Asp phospho-mimetic shows that MAPKAPK2 phosphorylation does not alter PDE4A5 sensitivity to rolipram inhibition (Figure 4.17).

Adding credence to isoform specific modifications conferred upon phosphorylation and/or protein interactions, PDE4A4B is the only isoform susceptible to conformational switching, as sensed by altered rolipram inhibition, on interaction with the SH3 domain of the tyrosyl kinase Lyn [McPhee et al., 1999]. It is also the only isoform to form accretion foci in cells following chronic rolipram treatment [Terry et al., 2003]. Thus, long isoforms for the PDE4B, PDE4C and PDE4D gene families should be assessed for functional attributes conferred upon MAPKAPK2 phosphorylation, including enzyme activity and rolipram inhibition.

The phosphorylation site for MAPKAPK2 is located some n + 7 residues upstream of the target PKA phosphorylation site at Ser-140. It was hypothesised that phosphorylation by MAPKAKP2 may not confer a functional effect in isolation but may play a role in controlling the PKA activation state of PDE4A5. This was indeed the case where MAPKAPK2 phosphorylation delayed both the onset and amplitude of PKA activation (Figure 4.16). A similar effect was noted upon interaction of PDE4A5 with XAP2 [Bolger et al., 2003]. This also delayed the onset and amplitude of PKA-mediated PDE4A5 activation and was attributed to two possible mechanisms; (1) the interaction of XAP2 with the unique N-terminal region and UCR2 or (2) the disruptions of the UCR1-UCR2 intra-molecular interaction, where both interdict the availability of the PKA phosphorylation motif. Therefore, one can infer that MAPKAPK2 phosphorylation of PDE4A5 may modulate the PKA-mediated activation in a similar vain, as it hinders XAP2 binding (Figure 4.20) and also

delays the onset and amplitude of PKA phosphorylation. Therefore, in cells where the p38 MAPK-MAPKAPK2 signalling pathway is active, activation of PKA in a negative feedback system to control local cAMP concentrations will be attenuated due to active MAPKAPK2.

In T-lymphocytes PDE4A isoforms can interact with AKAP1, AKAP3 and AKAP8 [Asirvatham et al., 2004]. In bovine spermatozoa PDE4A5 has been specifically targeted for interaction with AKAP3 [Bajpai et al., 2006]. Thus, the delayed onset and amplitude of PKA activation of PDE4A5 may be mediated by attenuation of AKAP interactions with PDE4A5 following MAPKAPK2 phosphorylation. Mapping of potential AKAPs and their binding sites on PDE4A5 will give insight into whether such modulation of interaction is possible. There is a precedent for such phosphorylation-induced modification of PDE4-AKAP interactions, where the PKA phosphorylation state of Ser-13 within the N-terminal region of PDE4D3 enhances its affinity for binding AKAP6 [Carlisle Michel et al., 2004]. One would advocate experiments in T-lymphocytes, where endogenous levels of PDE4A5 and specifically AKAP1 and AKAP8 can be immunologically detected, to assess their interaction following activation of the p38 MAPK phosphorylation cascade [Asirvatham et al., 2004]. Furthermore, given the comparable intra-cellular distribution of these AKAPs and PDE4A5, e.g. at the perinuclear region, raises the possibility of their co-localisation (Figure 4.18) [McPhee et al., 1995, Huston et al., 2000, Beard et al., 2002 and Asirvatham et al., 2004].

The unique N-terminal region of PDE4A5 has also been shown to mediate multiple interactions with partner proteins. These include SH3 domain-containing proteins, such as Lyn tyrosyl kinase, susceptibility for binding and cleavage by caspase-3, and interaction with scaffold and adaptor proteins such as β-arrestin and XAP2 [McPhee et al., 1999, Huston et al., 2000, Beard et al., 2002, Bolger et al., 2003 and Wallace et al., 2005]. Many of these interactions are supported at additional sites within the regulatory and catalytic domains.

MAPKAPK2 can also bind SH3 domains through its proline-rich N-terminal region [Ben-Levy et al., 1995]. The Abl tyrosyl kinase has been identified as a partner protein of MAPKAPK2 and this may imply the requirement of SH3 domain-containing proteins to control its intra-cellular localisation. Additionally, SH3 domain-containing proteins may act as a scaffold protein to recruit PDE4A isoforms in vivo and impart specificity to the phosphorylation, as only PDE4A isoforms and the unique N-terminal region of PDE4D4 can interact with SH3 domain-containing proteins and thus will not be able to recruit MAPKAPK2 [McPhee et al., 1999 and Beard et al., 1999]. However, the positive phosphorylation of the N-terminal truncated form of PDE4A5 potentially eliminates such a possibility of using the N-terminal SH3 binding region and given the other proline-rich region located within the C-terminal region of PDE4A4B are not conserved to provide additional or compensatory binding regions (Figures 3.15 and 4.9) [McPhee et al., 1999]. Furthermore, the Abl tyrosyl kinase interacts poorly with PDE4A4B adding power to the argument against SH3-mediated bridging interactions [McPhee et al., 1999].

MAPKAPK2 phosphorylation of PDE4A5 does not alter PDE4A5 susceptibility for caspase-3 cleavage (Figure 4.21). PDE4A5 cleavage by caspase-3 disrupts both interactions with SH3 domain-containing proteins and its intra-cellular targeting [Beard et al., 1999 and Huston et al., 2000]. Therefore, it is unlikely that MAPKAPK2 phosphorylation will disrupt N-terminal SH3 domain interactions as this would result in alterations to its intra-cellular targeting in a manner analogous to either progressive N-terminal truncation or caspase-3 cleavage (Figure 4.18(b)) [Huston et al., 2000 and Beard et al., 2002].

Analysis of PDE4A5 intra-cellular localisation by laser-scanning confocal microscopy identified PDE4A5 expression to predominate at a distinct perinuclear localisation with a proportion located at the cell margins, as previously identified [Beard et al., 2002]. No effect on intra-cellular localisation was mediated with anisomycin following sub-cellular fractionation or laser-scanning confocal microscopy (Figure 4.18). A note of caution; there

are limitations to analysing the intra-cellular localisation profile of any protein when over-expressed due to the saturation of anchor sites and that different anchors are present at different concentrations in different cells. Also, sub-cellular fractionation is a crude means of evaluating intra-cellular distribution because reversible or weak protein interactions can be released upon cell breakage and this is likely to underlie the absence of PDE4A5 in the particulate fractions, as described previously [McPhee et al., 1995 and Beard et al., 2002]. Assessment of the intra-cellular distribution of MAPKAPK2 will also determine whether MAPKAPK2 and PDE4A5 exist in the same sub-cellular location in the basal state, or whether activation is required to release MAPKAPK2 from the nucleus and direct it towards a PDE4A5-containing sub-cellular location. Furthermore, it would be advantageous to confirm that PDE4A5 can be co-immuno-precipitated with MAPKAPK2 and identify further proteins involved in the complex, such as members of the Src tyrosyl kinases, which may be significant in kinase docking [Ben-Levy et al., 1995 and McPhee et al., 1999].

Adaptation of the structure of the actin cytoskeleton regulates a variety of cellular processes including migration, chemotaxis, adhesion and phagocytosis [Ibarra et al., 2005]. Activation of the p38 MAPK-MAPKAPK2 pathway results in the phosphorylation of HSP27, actin polymerisation and accumulation, thereby contributing to the maintenance of the microfilament network [Guay et al., 1997]. Wiskott-Aldrich syndrome protein verprolin homologous-1 (WAVE-1) is a scaffold protein also involved in the regulation of the actin cytoskeleton [Soderling and Scott, 2006]. It recruits the actin-related protein 2/3 (Arp2/3) complex, which catalyses the formation of actin polymers and branching. Arp2/3 is a target for MAPKAPK2 and may be involved in its regulation [Singh et al., 2003]. The N-terminal WAVE homology domain of the WAVE-1 scaffold protein supports numerous protein interactions including HSPC300, Abi2 (Abl-interacting protein 2), Nap1 (Nck-associated protein), and Sra1 (specifically Rac-associated protein 1) [Soderling and Scott, 2006]. Active Rac1-GTP regulates WAVE-1 through recruitment of Sra1. It is also able to the recruit the Abl tyrosyl kinase through SH3 domain interactions with the proline-rich region of WAVE-1 and this interaction may facilitate the

recruitment of MAPKAPK2 and the phosphorylation of Arp2/3 complex [Ben-Levy et al., 1995, Westphal et al., 2000 and Singh et al., 2003]. Furthermore, WAVE-1, but not WAVE-2 or WAVE-3, is able to function as an AKAP, binding the RII sub-units of PKA [Westphal et al., 2000]. Indeed the RII binding site is hypothesised to compete with actin for binding and therefore may be subject to regulation by actin concentration [Taskén and Aandahl, 2004]. Therefore, it would be interesting to ascertain whether PDE4A5 was part of this complex. If so, the reduction in onset and amplitude of PDE4A5 PKA phosphorylation and activation, as a result of MAPKAPK2 phosphorylation (Figure 4.16), could be indicative of enhanced actin binding and disruption of PKA interactions with WAVE-1. Given the evidence that Rac1 activity can also be regulated by cAMP and PKA in a variety of cells, PDE4 recruitment may participate in the regulation of the actin cytoskeleton [Pomerance et al., 2000, Waschke et al., 2004 and Pelletier et al., 2005].

The interaction of PDE4 enzymes with the scaffold protein β-arrestin2 occurs at a conserved site within the catalytic unit, with preference for PDE4D5 facilitated through a second site located within the unique N-terminal region [Perry et al., 2002, Bolger et al., 2003 and Bolger et al., 2006]. In Chapter 3, Figure 3.16, it was confirmed that PDE4A4B, the human homologue of PDE4A5, and also PDE4A11, could interact with β-arrestin2 [Wallace et al., 2005]. Consistent with these data is the confirmation that this interaction extends to PDE4A5 (Figure 4.19). Furthermore, it was concluded that conformational changes conferred upon the catalytic unit following UCR1 phosphorylation of PDE4A5 by PKA or MAPKAPK2 do not affect its ability to interact with β-arrestin2 (Figure 4.19).

PDE4D5 is the preferential and functionally relevant PDE4 isoform that interacts with β-arrestin2 and is responsible for the recruitment of PDE4 activity to the GRK phosphorylated β_2-adrenoceptor, resulting in the attenuation of local PKA activity and blockade of G_s to G_i switching [Perry et al., 2002, Lynch et al., 2005, and Li et al., 2006]. Whether MAPKAPK2 affects the ability of the PDE4D5 isoform to interact with β-arrestin2 given the

additional binding sites within the unique N-terminal region remains to be elucidated [Bolger et al., 2003 and Bolger et al., 2006].

Modulation of PDE4 activity upon protein interaction with the unique N-terminal region of PDE4A5 has been observed with XAP2. XAP2 or AIP is an immunophilin-like protein that interacts and confers a specific partial, non-competitive inhibitory effect on PDE4A5 [Bolger et al., 2003]. This interaction was attenuated upon MAPKAPK2 phosphorylation of PDE4A5 and restored upon co-incubation with SB203580 (Figure 4.20). Furthermore, XAP2 itself was not subject to phosphorylation by a p38 MAPK-dependent protein kinase, indicating that this effect is dependent upon PDE4A5 phosphorylation [E.V. Hill and M.D. Houslay, unpublished observation]. The functional interaction site for XAP2 binding on PDE4A5 is predominantly the unique N-terminal region with additional binding supported by UCR2 [Bolger et al., 2003]. As discussed above, it is likely that the MAPKAPK2 phosphorylation of PDE4A5 induces structural reorganisation of the intra-molecular interactions between the unique N-terminal and regulatory domains, which not only precludes the accessibility of the PKA phosphorylation site but also one, or both, of the XAP2 interaction sites. Relief of the XAP2 inhibitory constraint upon PDE4A5 will no doubt contribute to altered cAMP signalling responses in cellular locations where these interactions occur. Future experiments should be performed to prove PDE4A5 activity modulation can occur following MAPKAPK2 phosphorylation and partial release of XAP2-mediated inhibition of PDE4A5 catalytic activity.

However, one caveat to this interaction in the intact cell may be the requirement for XAP2 release from the nucleus. In undisclosed work, I have shown that over-expression of PDE4A5 and XAP2 in COS7 cells shows divergent patterns of localisation, with XAP2 predominantly nuclear and PDE4A5 located in the perinuclear regions of the cell. Sequence analysis of XAP2 indicates that it contains no NLS and was reliant on secondary interacting proteins to confer nuclear localisation [Kashuba et al., 2000].

XAP2 controls both the stability and cytoplasmic cellular localisation of the AhR and therefore negatively regulates AhR-mediated gene expression [Meyer and Perdew, 1999, Lees et al., 2003 Ramadoss et al., 2004 and Pollenz and Dougherty, 2005]. Activation of the lung AhRs by pollutants, such as dioxin (TCDD) and poly-aromatic hydrocarbons present in cigarette smoke, increases neutrophil recruitment and the onset of the excessive inflammatory response, a characteristic of COPD [Martinez et al., 2002 and Teske et al., 2005]. Enhanced neutrophil recruitment is likely to be mediated, in part, by the generation of IL-8 and LTB_4 [Harlaar and Brown, 1999]. Interestingly, TCDD can also induce the expression of MAPKAPK2 in lung epithelial cells [Martinez et al., 2002]. Therefore, activation of the AhR may be important in the pathogenesis of inflammatory lung disease.

Human airway smooth muscle cells express peroxisome proliferator-activated receptor (PPAR) α and γ sub-types, which are ligand-activated nuclear hormone receptors [Patel et al., 2003]. XAP2 is a critical component of the PPARα gene transcription complex, and functions to repress gene transcription in hepatocytes [Sumamasekera et al., 2003]. Similarly, PPARα activation inhibits pro-inflammatory mediator gene expression in smooth muscle cells and this may be due to the repressive action of XAP2 [Staels et al., 1998 and Delerive et al., 1999]. This indicates a further role for XAP2 in asthma and COPD, as it would function to attenuate both inflammatory mediator gene expression and cAMP degradation in smooth muscle cells.

PDE4 inhibition coupled with the elevation of cAMP levels is well established to promote anti-inflammatory effects in cells [Souness et al., 2000 and Houslay et al., 2005]. The exact mechanisms as to how cAMP modulates inflammatory cell function are only beginning to be understood. PDE4 inhibition reduces TNFα pro-inflammatory cytokine production and enhances IL-10 anti-inflammatory cytokine production, the expression of which, are dependent upon p38 MAPK activity [Guo et al., 2003 and Houslay et al., 2005]. Similarly, the expression of adhesion molecules, the de-granulation of neutrophils and eosinophils and the activation of T-cells can all be inhibited by both PDE4 and p38 MAPK inhibition [Teixeira et al., 1997, Herlaar and Brown,

1999, Pryzwansky and Madden, 2003, Ariga et al., 2004, Abrahamsen et al., 2004 and Jones et al., 2005]. Excessive mucus production is also a characteristic of COPD and clearance is controlled by the PKA activation state of the CFTR [Houslay et al., 2005]. Additionally, in smokers with and without COPD, PDE4A4B and PDE4B2 expression is induced [Barber et al., 2004].

The partial inhibition of PDE4A4B/PDE4A5 activity on interaction with XAP2 assigns it as an isoform-specific inhibitor of PDE4A4B/PDE4A5 activity [Bolger et al., 2003]. PDE4A11, the major mRNA transcript in immune and inflammatory cells, also interacts with XAP2 but whether this interaction translates similar functional consequences remains to be elucidated (Figure 3.17) [Wallace et al., 2005]. Therefore, one would expect XAP2 to adapt PDE4A4B/PDE4A5, and possibly PDE4A11, activity in specific compartments of the cell in which both proteins are present. Additionally, activation of the p38 MAPK-MAPKAPK2 pathway in the inflammatory response would promote the expression of pro-inflammatory mediators while simultaneously relieving the XAP2 inhibitory constraint placed upon the phosphorylated PDE4A isoform. This would allow the degradation of local cAMP concentrations potentiating pro-inflammatory cell function.

There is evidence for MAPKAPK2 in the activation of the E3 ubiquitin ligase, HDM2, which is responsible for the degradation of the tumour suppressor, p53 [Weber et al., 2005]. Is it possible that PDE4 isoforms could be targeted for degradation via ubiquitination and the interaction with XAP2 enhances their cellular stability in an analogous manner to the AhR? [Lees et al., 2003]. If this were true, it is then possible that both PDE4A4B/PDE4A5 and ubiquitin ligase phosphorylation facilitates the reduction of PDE4-XAP2 binding with a concomitant increase in PDE4 ubiquitin ligase-mediated degradation.

As discussed above, XAP2 has also been identified as being an important component in the repression of PPARα gene transcription in hepatocytes, which regulates fatty acid oxidation, O_2^- and ROS generation, enlargement of the liver through both an increase in cell size and cell

proliferation [Sumamasekera et al., 2003]. Furthermore, it has been established that mutations in XAP2 confers susceptibility to pituitary adenomas [Vierimaa et al., 2006]. Taken together these data are consistent with the role of XAP2 as a tumour suppressor. Survivin is a member of the inhibitor of apoptosis family that functions to regulate cell division and protect cells from apoptosis [Kang and Altieri, 2006]. In contrast to the tumour suppressor function of XAP2, the XAP2 stabilising interaction preventing survivin degradation reveals a role for XAP2 as anti-apoptotic, and will function in this instance to promote the survival of cancerous cells.

In certain types of cancer, the up-regulation of PDE4 expression has been described [Smith et al., 2005]. This is consistent with notion of cAMP as anti-proliferative agent, promoting cell cycle arrest and apoptosis [Schmitt and Stork, 2001, Balmanno et al., 2003 and Zambon et al., 2005]. Consistent with the role for XAP2 as tumour suppressor is its ability to specifically inhibit PDE4A5 activity [Bolger et al., 2003 and Fleming et al., 2004]. Given that p38 MAPK regulates cell apoptosis and MAPKAPK2 regulates cell motility and potentially cancer cell metastasis, therapeutic targeting of the p38 MAPK-MAPKAPK2 signalling pathway might be of benefit in some cancers [Platanias, 2003 and Xu et al., 2006].

In summary, PDE4A5 is a genuine substrate for MAPKAPK2 phosphorylation at Ser-147 within the UCR1 regulatory domain. This phosphorylation delays the onset and amplitude of PKA-mediated activation of PDE4A5 while relieving the propensity for the potential inhibitory interaction with XAP2. The endogenous PDE4A5 phosphorylation by MAPKAPK2 using a physiologically relevant stimulus remains important to confirm. Similarly, whether MAPKAPK2 can phosphorylate other PDE4 isoforms across all gene families and confer isoform-specific functional attributes remains to be elucidated and may reveal important PDE4 modifications. Nevertheless, this phosphorylation event provides further evidence of the integration of the cAMP and p38 MAPK signalling systems.

Chapter 5 NADPH Oxidase, cAMP signalling and PDE4A isoforms

5.1 Introduction

5.1.1 Super-oxide and Reactive Oxygen Species

The production of reactive oxygen species (ROS), such as hydrogen peroxide and hypochlorite from super-oxide (O_2^-) during oxidative stress can result in the attack of many key biological molecules such as enzymes, membrane lipids and DNA, and can ultimately lead to cell death [Hayes and McLellan, 1999]. Oxidative stress occurs when the excessive production of these highly reactive species outweighs their control by enzymes such as super-oxide dismutase (SOD), catalase, and the anti-oxidants such as ascorbic acid, glutathione and α-tocopherol.

Oxidative stress underlies the pathogenesis of many disease states including respiratory and inflammatory diseases such as asthma and COPD and neuro-degenerative diseases such as motor neurone disease. Much research has focussed upon cardiovascular conditions such as cardiac hypertrophy and heart failure [Li et al., 2002 and Murdoch et al., 2006]. Indeed, the treatment of cardiac myocytes with anti-oxidants can reduce the level of cardiac hypertrophy and O_2^- production induced by angiotensin II [Nakamura, et al., 1998 and Nakagami et al., 2003].

The attenuation or ablation of O_2^- and ROS production, for example in chronic granulomatous disease (CGD), results in a reduced immune response coupled with increased bacterial infection [Vignais, 2003]. For that reason, the production of O_2^- and ROS is required in the innate immune response where polymorphonuclear blood leukocytes (PBLs) engulf, kill and digest invading microorganisms, through a process known as oxidative or respiratory

burst. Respiratory burst is generally coupled with the release of proteases via cellular de-granulation of secretory vesicles [Larson et al., 2005].

Aside from their role as microbicidal agents, O_2^- and ROS are now implicated in cellular signalling transduction cascades, through the action of protein kinases, protein phosphatases and control of gene transcription [Groemping and Rittinger, 2005].

The production of O_2^- and ROS in immune and inflammatory cells occurs through the reduced nicotinamide adenine di-nucleotide phosphate (NADPH) oxidase enzyme, which can exist in three states: rest, primed and activated [Sheppard et al., 2005]. Tight control of this enzyme state is essential in maintaining individual cellular function and whole tissue integrity [Babior, 1999]. It is also worth noting here that the production of O_2^- and ROS is not confined to PBLs, and homologues of the core components, known as Nox (NADPH oxidase) proteins, have been identified in a wide variety of tissues including the heart, thyroid, kidney, lung, pancreas, liver, colon, intestine, placenta, testis and uterus [Bokoch and Knaus, 2003]. However, these proteins may have a different mechanism of action, as the activation of Nox proteins with stimuli that initiates a robust activation of the NADPH oxidase enzyme in phagocytic cells is inconsistent in non-phagocytic cells.

5.1.2 NADPH Oxidase

5.1.2.1 Membrane Components

The phagocytic NADPH oxidase enzyme is a hetero-heptameric enzyme that contains a membrane-bound glycoprotein, flavocytochrome b_{558} [Vignais, 2002]. This is composed of a 1:1 stoichiometry of gp91-*phox* (where *phox* stands for phagocyte oxidase) and p22-*phox*, together with the Rap1A G-protein, two haem groups, and a flavin adenine di-nucleotide (FAD).

The gp91-*phox* subunit is composed of an intra-cellular N-terminal tail, followed by six trans-membrane α-helices, the extra-cellular loops two and three contain the three asparagine residues for N-linked glycosylation, and a C-terminal tail responsible for NADPH and FAD binding [Groemping and Rittinger, 2005]. The molecular weight of gp91-*phox* from its primary amino acid sequence is 65kDa, which rises to 91kDa following post-translational glycosylation. NADPH transfers electrons to the FAD, which subsequently transfers the electrons to the O_2 carrying haem groups, resulting in its reduction to O_2^-. Both the FAD, removal of which ablates the production of O_2^-, and the haem groups are responsible for the transfer of electrons across the plasma membrane [Sheppard et al., 2005]. However, inconsistency exists with respect to the role of the haem groups as an electron carrier due to rate limiting kinetics of haem reduction [Babior, 1999].

p22-*phox* is a three trans-membrane α-helical protein of 21kDa with sequence homology for core and classical SH3 binding motifs at its intra-cellular C-terminal tail, which mediate protein-protein interactions, specifically with the cytosolic subunit p47-*phox* [Groemping and Rittinger, 2005].

There is no consensus of opinion regarding the requirement for Rap1A in NADPH oxidase activation [Sheppard et al., 2005]. Rap1A can be co-immuno-precipitated with the flavocytochrome b_{558} in resting cells indicating that Rap1A is a constitutively membrane-bound protein [Babior, 1999]. However, a second mechanism is proposed where Rap1A is a cytosolic protein that migrates to the plasma membrane on phosphorylation by PKC and conversely this migration is inhibited by PKA phosphorylation [Vignais, 2002]. The GDP/GTP-bound state of Rap1A influences the affinity with which it interacts with the flavocytochrome b_{558}, where the GTP-bound Rap1A interacts with greater affinity than the GDP-bound form. Stimulation of neutrophils with platelet-activating factor (PAF) or N-formyl-Met-Leu-Phe (fMLP), a tri-peptide secreted by bacterial cells, increases the proportion of GTP-bound Rap1A at the neutrophil membrane [Zwartkruis and Bos, 1999].

In resting cells 15% of the flavocytochrome b_{558} are present at the plasma membrane, with the remaining 85% at the membrane of cytosolic secretory vesicles or granules [Sheppard et al., 2005]. Enzyme priming and activation, through a plethora of stimuli, results in secretory vesicle membrane fusion and the delivery of the full cytochrome b_{558} complement to the plasma membrane.

5.1.2.2 Cytosolic Components

In the resting state p47-*phox* exists auto-inhibited with the intra-molecular binding of the tandem SH3 domains to a polybasic region at the C-terminal [Groemping et al., 2003, Yuzawa et al., 2004 and Durand et al., 2006]. p47-*phox* is subject to extensive phosphorylation, in comparison to the related p67- and p40-*phox* cytosolic subunits. These phosphorylation events have been assigned to a plethora of protein kinases including PI-3K and PKB/Akt, PKC (β, δ, and ζ isoforms only), Src tyrosyl kinase, p21-activated kinase, and the mitogen-activated protein kinases (MAPKs), p38 and ERK1/2 [El Benna et al., 1996, Lopes, et al., 1999, Hoyal et al., 2003, Brown et al., 2004, Chowdhury et al., 2005, Lin et al., 2005, Martyn et al., 2005 and Dang et al., 2006]. The treatment of phagocytic cells with PMA initiates a direct PKC phosphorylation and robust translocation of p47-*phox* to the plasma membrane [Inanami et al., 1998]. Indeed, p47-*phox* has the potential to be sequentially phosphorylated at up to eleven serine residues, namely 303, 304, 310, 315, 320, 328, 345, 348, 359, 370, and 379 within the SH3 domain-containing region [Groemping and Rittinger, 2005]. Preferential phosphorylation of p47-*phox* at Ser-359 and Ser-370 is necessary for translocation, although contradicting data exists, before further phosphorylation occurs at Ser-303 and Ser-304 to complete the activation step [Johnson et al., 1998, Hoyal et al., 2003 and Massenet et al., 2005]. What is widely accepted though is the pre-requisite phosphorylation of Ser-379 for the translocation of p47-*phox* and the activation of the NADPH oxidase enzyme [Inanami et al., 1998, Babior, 1999, Massenet et al., 2005 and Mitzuki et al., 2005]. The phosphorylation of p47-*phox*, by many of the aforementioned protein kinases, unmasks the PX domain, the SH3 domains,

and the polybasic and proline-rich regions. The availability of both SH3 domains, although preference is observed for domain A situated between residues 159 and 214, facilitates the interaction with the core Pro-Xaa-Xaa-Pro SH3 interaction motif within the C-terminal tail of p22-*phox* at the plasma membrane [Vignais, 2002]. The N-terminal *phox* (PX) domain stabilises direct membrane association through the binding of phospho-inositides (PI) [Wientjes et al., 2001 and Zhan et al., 2004].

p67-*phox* is a 60kDa protein composed of up to four N-terminal TPR domains, required for the competing interaction with either Rac2 or Cdc42, where differential binding confers either activation or inhibition on NADPH oxidase activity [Lapouge et al., 2000]. The C-terminal of p67-*phox* is composed of two SH3 domains, surrounding a *phox* and Bem1 (PB1) domain, which is a site for high affinity (K_d = 7nM) heterodimerisation with the PB1 domain of p40-*phox* [Groemping and Rittinger, 2005]. The region between the TPR and SH3 domains, i.e. amino acids 199-210, is absolutely essential for forming the active enzyme at the plasma membrane through gp91-*phox* binding, and may also play a role in binding NADPH [Babior, 1999, and Bokoch and Knaus, 2003]. Phosphorylation of p67-*phox* by either p38 MAPK or ERK1/2 may also play a fundamental role in membrane translocation, implying that a possible p67-*phox* conformational change is required to relieve an inhibitory constraint, similar to that described for p47-*phox* [Brown et al., 2004, Groemping and Rittinger, 2005 and Lin et al., 2005]. p67-*phox* and p40-*phox* exist together in the cytosol of the cell and translocation to the plasma membrane occurs in a p47-*phox*-dependent fashion [Sheppard et al., 2005].

The final cytosolic *phox* protein is a 39kDa protein called p40-*phox*, which is composed of an N-terminal PX domain for interaction with the plasma membrane, an SH3 domain for possible interaction with the proline-rich region of p47-*phox* and a C-terminal PB1 domain [Wientjes et al., 2001, Groemping and Rittinger, 2005 and Sheppard et al., 2005]. As mentioned above, p40-*phox* is associated with p67-*phox* in the resting state and this occurs through the dimerisation of the PB1 domains. p40-*phox* is also basally

phosphorylated by PKC at Thr-154 and Ser-315 [Vignais, 2002]. p40-*phox* is a stimulatory subunit directly enhancing the membrane translocation of p67-*phox* and indirectly enhancing p47-*phox* translocation via p67-*phox* [Kuribayashi et al., 2002]. Unfortunately, p40-*phox* is the least well studied and characterised of the three cytosolic *phox* proteins so little information exists around its regulation.

Translocation of GTP-bound Rac2 to the flavocytochrome b_{558}, or certainly to the plasma membrane through prenylation, is also a pre-requisite for NADPH oxidase activation [Sheppard et al., 2005]. Rac2 associates with Rho GDP dissociation inhibitor in the cytosol and translocation to the plasma membrane occurs on dissociation of Rho GDP dissociation inhibitor, where it interacts with high affinity with p67-*phox* [Lapouge et al., 2000 and Bokoch and Knaus, 2003]. Cdc42 acts as a competitive inhibitor for Rac2 and attenuates the production of O_2^- and ROS by the NADPH oxidase enzyme.

5.1.3 cAMP Signalling

cAMP is known for its anti-inflammatory properties and there is an abundance of data to support the notion of PDE4 inhibitors as anti-inflammatory agents [Souness et al., 1999, Giembycz, 2002, Houslay et al., 2005 and Zhang et al., 2005]. The generation of O_2^- and ROS underpins a fundamental part of the inflammatory response. Various studies have implicated an increase in intra-cellular cAMP concentrations, with the concomitant activation of PKA, in attenuating the production of O_2^- and ROS [Bengis-Garber and Gruener, 1996 and Lin et al., 2005]. No functional role for the direct PKA phosphorylation of the NADPH oxidase *phox* proteins has been identified [Babior, 1999]. PDE4 inhibitors can attenuate the generation of O_2^- and ROS in immune and inflammatory cells, and also regulate the expression of the NADPH oxidase *phox* proteins [Hatzelmann and Schudt, 2001 and Jacob et al., 2004]. The *phox* proteins contain SH3 and TPR domains, domains through which PDE4A long isoforms can interact [McPhee et al., 1999 and Bolger et al., 2003]. There is a precedent for cell signalling

enzymes to associate with the *phox* proteins and control NADPH oxidase activation [Shmelzer et al., 2003 and Chowdhury et al., 2005].

Taken together these data implies a potential key role for cAMP signalling, PKA activation and PDE4 inhibition in the generation of O_2^- through the recruitment and regulation of the *phox* proteins. The aim of this chapter was to elucidate an accepted means for cAMP signalling in O_2^- generation through possible PDE4 interactions with the *phox* proteins controlling the direct phosphorylation of the *phox* proteins by PKA, thereby influencing the assembly of the active, membrane-bound NADPH oxidase enzyme complex.

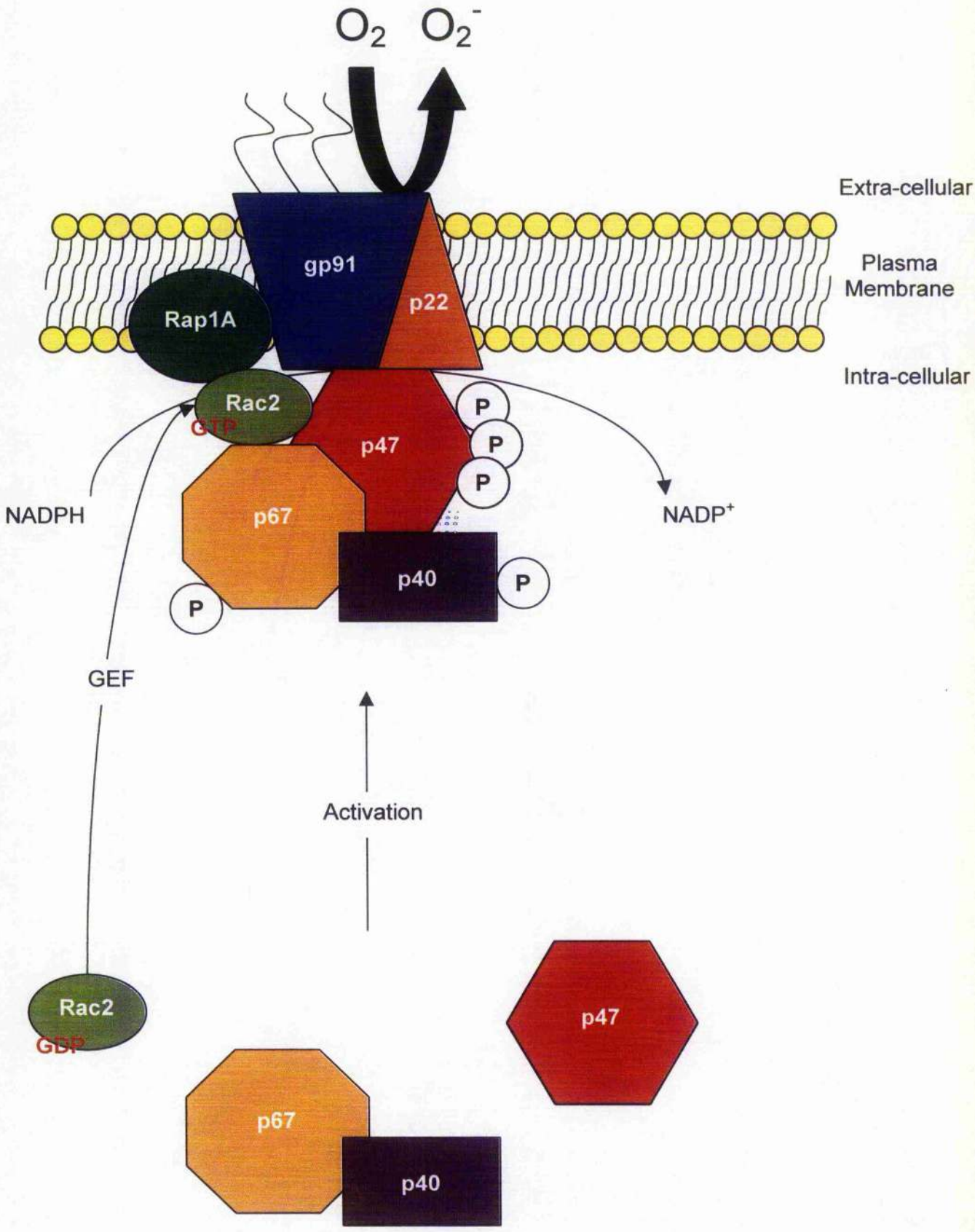
O_2 O_2^-
Extra-cellular
Plasma Membrane
Intra-cellular
gp91
p22
Rap1A
Rac2
GTP
p47
P
P
P
p67
p40
P
P
NADPH
NADP+
GEF
Activation
Rac2
GDP
p47
p67
p40

Figure 5.1 – Schematic representation of the core components of the NADPH oxidase enzyme complex.

5.2 Results

Analysis of the primary amino acid sequence of proteins using the ScanSite protein motif-scanning database (http://scansite.mit.edu./cgi-bin/motifscan_seq) predicts both phosphorylation and secondary structural motifs within any given protein. The amino acid sequences of the p47- and p67-*phox* proteins were analysed using this database to elucidate potential PKA phosphorylation and/or structural motifs that may designate a potential role for their interaction with PDE4 enzymes. ScanSite identified p47-*phox* to consist of a PX domain at the N-terminal of the protein, with two tandem SH3 domains towards the C-terminal. The presence of these SH3 domains indicated a potential interaction with PDE4A isoforms and a precedent for these interactions are well established [McPhee et al., 1999, Rena et al., 2001 and Wallace et al., 2005]. Furthermore, a number of putative PKA consensus motifs were identified at the extreme C-terminal segment of the protein positioned beyond the tandem SH3 domains, namely Ser-304, Ser-320 and Ser-328. Similar analyses of p67-*phox* revealed the presence of up to four N-terminal TPR domains, and a PB module sandwiched between two SH3 domains towards the C-terminal. The presence of further SH3 domains and the additional TPR domains add credence to the possibility of PDE4A interactions where TPR domain interactions with PDE4A enzymes have also been previously described [Bolger et al., 2003]. No putative PKA phosphorylation sites were identified.

5.2.1 PKA Phosphorylation of p47- phox and p67-phox

To determine whether p47-*phox* and p67-*phox* were phosphorylated by PKA in vitro, recombinant GST fusion proteins of both were expressed and purified in *E.coli*, as shown in Figure 5.2. The *phox* proteins were expressed as soluble proteins and the purification on glutathione sepharose resin yielded 8.0mg/ml of GST-p47-*phox* and 4.3mg/ml of GST-p67-*phox*. Truncations of p47-*phox* were also available, specifically the PX domain (amino acids 5-122) and the C-terminal portion containing the SH3 domains

(amino acids 155-390) as fusion proteins with GST. These were also expressed and purified in *E.coli* as per the full-length species to concentrations of 9.1mg/ml for the PX domain and 11.2 mg/ml for the C-terminal region respectively. Furthermore, single serine to alanine mutants of full-length p47-*phox* (Ser-304, Ser-320 and Ser-328) generated by site-directed mutagenesis and showed no impact upon *E.coli* protein expression, solubility, purification or yield.

The purified recombinant *phox* proteins were assayed for PKA phosphorylation in vitro, together with GST as a negative control. Recombinant PKA phosphorylated p47-*phox* but not p67-*phox* or the GST control, as shown in Figure 5.3(a). Moreover in Figure 5.3(a), the truncated forms of p47-*phox* were differentially phosphorylated by PKA, indicating that the phosphorylation sites were contained at the C-terminal end of the protein. This region contains the SH3 domains and the previously identified putative phosphorylation serine residues within the PKA consensus motifs. In an attempt to further define the target residues peptide array technology was utilised, in a radioactive phosphorylation assay, with recombinant PKA. The incorporation of [^{32}P]-ATP to the p47-*phox* peptide array, Figure 5.3(b), transpired within the C-terminal region. One such site occurred between Val-186 and Pro-230 of the first SH3 domain of p47-*phox* and Ser-208 was identified as the probable residue, within the sequence Iso-Pro-Ala-Ser-Phe, as shown in red in Figure 5.3(b), panel (i). The three putative PKA phosphorylation sites at Ser-304, Ser-320 and Ser-328 were also identified as over-lapping phosphorylated sequences, a result of the peptide array synthesising technique where five-residue sequences are removed and added in a step-wise manner for the full length of the protein. Figure 5.3(b), panel (ii), indicated that Ser-304 was contained within the consensus motif Arg-Arg-Ser-Ser-Iso, highlighted in red, Ser-320 within the sequence Lys-Arg-Leu-Ser-Gln, highlighted in blue, and Ser-328 within a consensus sequence Arg-Arg-Asn-Ser-Val, highlighted in green. A further two possible PKA consensus sites, not identified using the ScanSite database, were identified using the peptide array approach. Figure 5.3(b), panel (iii), suggested that Ser-370 (Pro-Arg-Pro-Ser-Ala) in red, and Ser-379 (Asn-Arg-Cys-Ser-Glu) in blue,

were a target residue for PKA phosphorylation. Single alanine mutants of Ser-304, Ser-320 and Ser-328 within full-length p47-*phox* were evaluated in an in-vitro PKA phosphorylation assay, as shown and quantified in Figure 5.3(c). All mutant proteins exhibited a moderate reduction in PKA phosphorylation to 66%, 84% and 69% respectively from the wild type p47-*phox* theoretical control level of 100%.

5.2.2 PDE4 Interaction with p47-phox and p67-phox

The full-length GST fusion proteins of p47- and p67-*phox* were used in pull-down assays to determine whether they were able to directly interact with PDE4A4B, which can bind proteins containing both SH3 and TPR domains, and PDE4A10, known to bind with weaker affinity with SH3 domain containing proteins and theoretically unable to interact with proteins containing TPR domains. Figure 5.4(a) confirmed that PDE4A4B was able to interact directly with both p47- and p67-*phox* proteins whereas PDE4A10 showed specificity for interaction with p47-*phox* and interacted with p67-*phox* at a level comparable to that of the GST alone control. To further probe the interaction of PDE4A long isoforms with p47-*phox*, the full-length peptide array of PDE4A4B was incubated with the recombinant GST fusion protein of p47-*phox*. These data identified a binding site within the UCR2 module and a further three interaction sites within the catalytic unit. Pro-216 to Thr-250 contained the pertinent amino acids responsible for mediating the interaction of p47-*phox*. The three sites within the catalytic unit were mapped to Val-501 to Leu-525, Thr-656 to Glu-685 and Pro-691 to Glu-725.

5.2.3 Translocation of NADPH Oxidase in Cardiac Myocytes

Previous work in rat cardiac myocytes has indicated the existence of compartmentalised cAMP signalling [Zaccolo and Pozzan, 2002, Mongillo et al., 2004 and Zaccolo, 2006]. Rat cardiac myocytes were cultured from isolated rat hearts and the production of whole cell lysates facilitated the immunological detection of PDE4 isoforms from the PDE4A, PDE4B and

PDE4D gene families, as shown in Figure 5.5(a). Significantly, Figure 5.5(a), panel (i), detected the endogenous expression of a long form PDE4A isoform of equivalent molecular weight to the isoforms, PDE4A5 or PDE4A8. Panels (ii) and (iii) of Figure 5.5(a) also identified the expression of two PDE4B isoforms, almost certainly PDE4B2 and PDE4B4, together with significant endogenous expression of the PDE4D long isoform, PDE4D3. Likewise, both p47- and p67-*phox* were also endogenous expressed at appreciable levels indicating the presence of two of the core components of the NADPH oxidase enzyme, as shown in Figure 5.5(b).

To evaluate the translocation of p47-*phox* to the plasma membrane the cells were treated with angiotensin II, a known agonist of NADPH oxidase translocation and activation, leading to the production of O_2^- and ROS [Nakamura, et al., 1998 and Nakagami et al., 2003]. In cultured cardiac myocytes angiotensin II elicited translocation of p47-*phox* to the plasma membrane, as indicated by increased p47-*phox* immuno-reactivity in the P2 fraction of the cells, as shown in Figure 5.6(a). Figure 5.6(b) quantified the magnitude of p47-*phox* translocation, and the effect of various cell treatments to modulate activation of the cAMP signalling system, against the maximum response (100%) with angiotensin II. On this basis, basal p47-*phox* expression at the plasma membrane was some 17% +/- 5% ($p < 0.05$). Angiotensin II in combination with forskolin, to directly activate adenylyl cyclase, or rolipram, to specifically inhibit PDE4 activity, reduced the level of translocation to 54% +/- 2% ($p > 0.05$), and 54% +/-19% ($p > 0.05$), respectively. No effect on the translocation of p47-*phox* was observed with the PDE3 inhibitor, cilostimide in combination with angiotensin II (data not shown). Treatment with angiotensin II and the PKA inhibitor H89 reduced the level of translocation to 63% +/- 11% ($p > 0.05$). A corresponding band shift accompanied this H89-induced reduction in p47-*phox* membrane translocation. Stimulation of cardiac myocytes with angiotensin II, forskolin and rolipram ablated p47-*phox* translocation to plasma membrane, quantified at 13% +/- 13% ($p > 0.05$). The addition of H89 partially rescued this effect to 49% +/- 28% ($p > 0.05$).

(a)

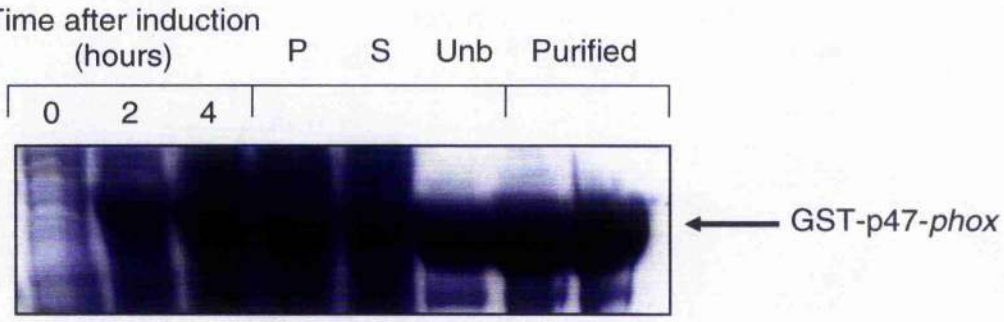
Time after induction
(hours)
P
S
Unb
Purified
0
2
4
GST-p47-phox

(b)

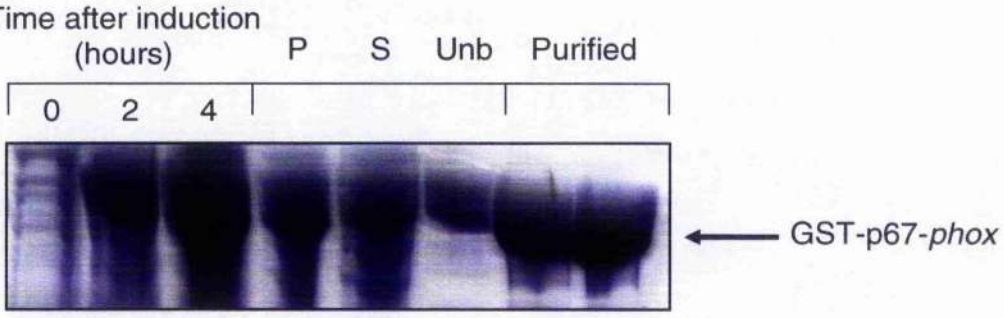
Time after induction
(hours)
P
S
Unb
Purified
0
2
4
GST-p67-phox

Figure 5.2 – *E.coli* expression and purification of recombinant p47-*phox* and p67-*phox*.

(a), shows the expression and purification of GST-p47-*phox* and (b), shows the expression and purification of GST-p67-*phox* in *E.coli*. Briefly, competent *E.coli* BL21 pLysS (DE3) cells were transformed with pGEX plasmids encoding either GST-p47-*phox* or GST-p67-*phox*. Protein expression was induced with 0.2mM IPTG for 4h at 30°C. The cells were collected, re-suspended in lysis buffer and subjected to sonication to produce total cellular extract (P). The soluble proteins were isolated by centrifugation (S). The expressed recombinant GST fusion proteins were purified using glutathione sepharose resin and eluted using excess glutathione (10mM). Fractions of the GST fusion proteins remained unbound to the glutathione sepharose resin (Unb) whereas a significant proportion of bound fusion protein could be purified to a major band as detectable by Coomassie® staining of the SDS polyacrylamide gels (Purified). These gels represent one of many successful expression experiments undertaken to express both proteins as full-length wild type, full-length single site mutants or truncated species in *E.coli*.

(a)

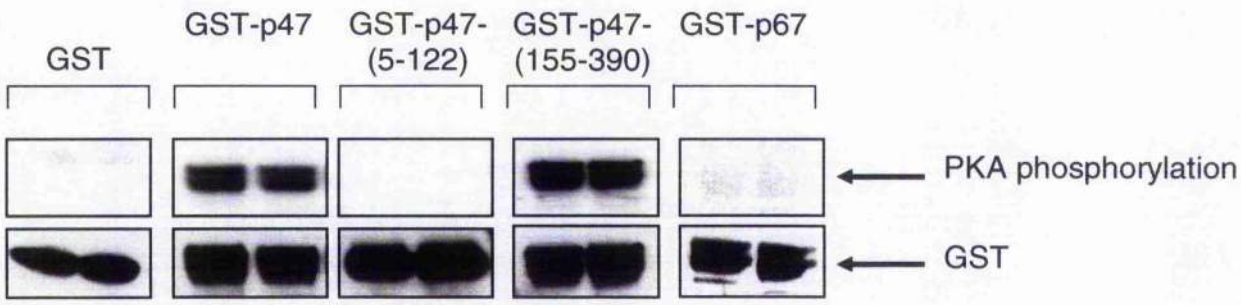

(b)

(i)

VEKSESGWWFCQMKAKRGWIPASFL
SGWWFCQMKAKRGWIPASFLEPLDS
CQMKAKRGWIPASFLEPLDSPDETE
KRGWIPASFLEPLDSPDETEDPEPN
PASFLEPLDSPDETEDPEPNYAGEP

p47-*phox* peptide array
(Val-186 – Pro-230)
SH3 domain 1
Phosphorylation target **Ser-208**

(ii)

QKSGQDVSQAQRQIKRGAPPRRSSI
DVSQAQRQIKRGAPPRRSSIRNAHS
QRQIKRGAPPRRSSIRNAHSIHQRS
RGAPPRRSSIRNAHSIHQRSRKRLS
RRSSIRNAHSIHQRSRKRLSQDAYR
RNAHSIHQRSRKRLSQDAYRRNSVR
IHQRSRKRLSQDAYRRNSVRFLQQR
RKRLSQDAYRRNSVRFLQQRRRQAR
QDAYRRNSVRFLQQRRRQARPGPQS
RNSVRFLQQRRRQARPGPQSPGSPL

p47-*phox* peptide array
(Gln-281 – Leu-350)
C-terminal region
Phosphorylation targets
Ser-304, Ser-320 & Ser-328

(iii)

EEERQTQRSKPQPAVPPRPSADLIL
TQRSKPQPAVPPRPSADLILNRCSE
PQPAVPPRPSADLILNRCSESTKRK
PPRPSADLILNRCSESTKRKLASAV

p47-*phox* peptide array
(Glu-351 – Val-390)
C-terminal region
Phosphorylation targets
Ser-370 & Ser-379

(c)

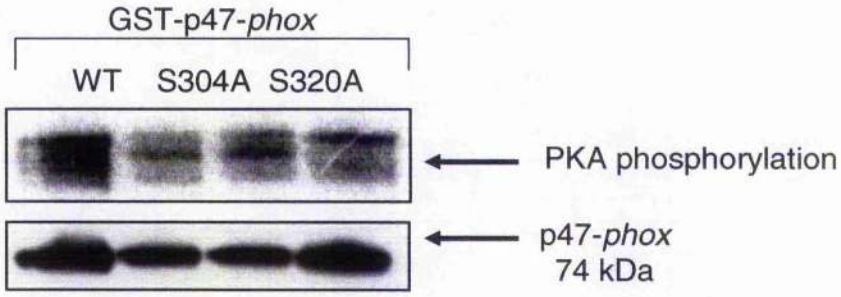
GST-p47-phox
WT
S304A
S320A
PKA phosphorylation
p47-phox
74 kDa

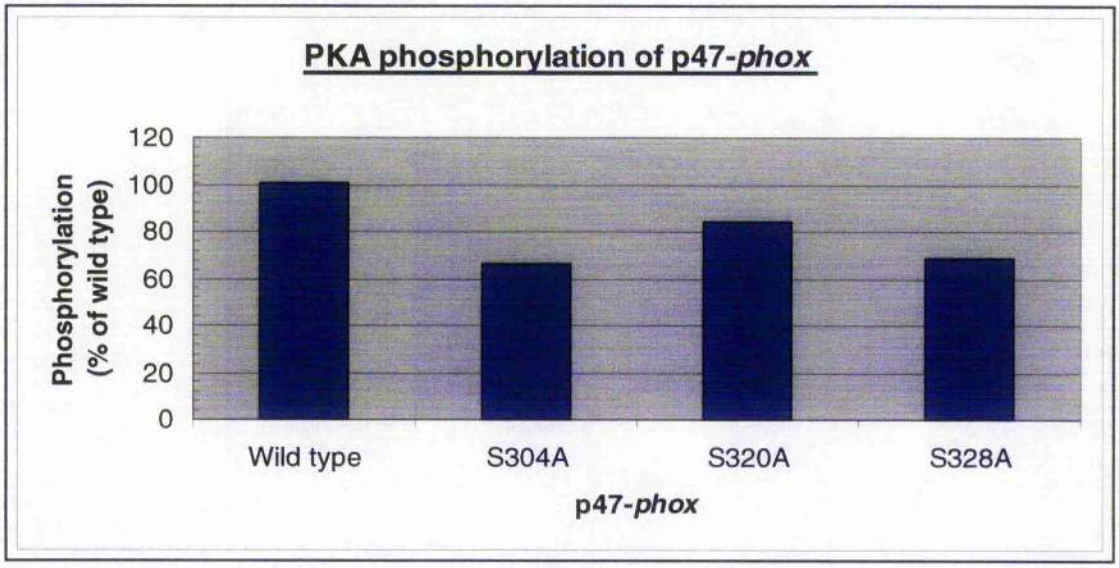
PKA phosphorylation of p47-phox
Phosphorylation (% of wild type)
120
100
80
60
40
20
0
Wild type
S304A
S320A
S328A
p47-phox

Figure 5.3 – Phosphorylation of the p47-*phox* by recombinant PKA.

The in vitro PKA phosphorylation of GST-tagged full-length p47-*phox*, p47-*phox* (amino acids 5-122), p47-*phox* (amino acids 155-390), and full-length p67-*phox* was undertaken. GST was included as a negative control. Purified GST-*phox* proteins were incubated with PKA and [^{32}P]-ATP for 10min at 30°C. The phosphorylated proteins were then separated by SDS-PAGE, transferred to a nitrocellulose membrane, exposed in close proximity to a storage phosphor image screen for 3h, and developed using a high-resolution laser scanner. (a), top panels, are scanned storage phosphor screen images of the PKA phosphorylation of *phox* proteins. (a), bottom panels, are Western blots of the radioactive nitrocellulose membrane, probed using a GST anti-serum showing the relative immuno-reactive amounts of each *phox* protein present in the phosphorylation assays. The scanned storage phosphor screen images and Western blots are representative of in vitro phosphorylation assays of three separate experiments. (b), panels (i)-(iii), is a peptide array of p47-*phox* used to map the phosphorylation target Serine residues in putative PKA consensus motifs. The entire p47-*phox* peptide sequence was synthesised on a membrane and the membrane incubated with PKA and [^{32}P]-ATP for 30min at 30°C. The membrane was exposed in close proximity to a storage phosphor image screen and developed as described above. The p47-*phox* peptide array PKA phosphorylation data are from an experiment done once. (c), top panel, is a scanned storage phosphor screen image showing p47-*phox* (wild type, Ser-304-Ala, Ser-320-Ala and Ser-328-Ala) phosphorylation by recombinant PKA. (c), bottom panel, is a Western blot of the radioactive nitrocellulose membrane, probed using a p47-*phox* specific anti-serum, showing the relative immuno-reactive amounts present in the phosphorylation assays. The scanned storage phosphor screen image and Western blot in (c) are from one experiment. (d), shows the quantification of the p47-*phox* phosphorylation as a function of the immuno-reactive p47-*phox* in each assay. The phosphorylation of the mutant forms of p47-*phox* is calculated relative to that of the wild type control. The quantification of the phosphorylation of p47-*phox* wild type and the serine to alanine mutants are from one experiment.

(a)

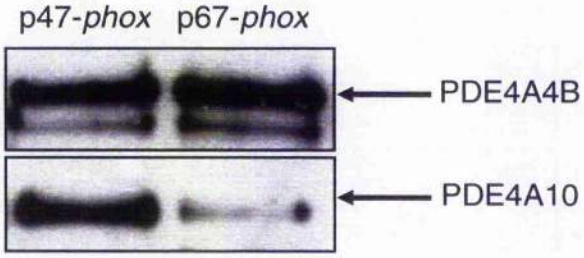

(b)

(i)

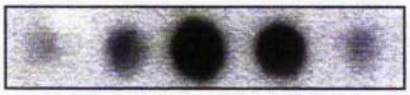

PDE4A4B peptide array
(Leu211 to Ser255)
Upstream conserved region 2

LGGPTPVCKATLSEETCQQLARETL
PVCKATLSEETCQQLARETLEELDW
TLSEETCQQLARETLEELDWCLEQL
TCQQLARETLEELDWCLEQLETMQT
ARETLEELDWCLEQLETMQTYRSVS

(ii)

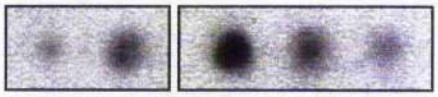

PDE4A4B peptide array
(Glu491 to Lys535)
Catalytic unit

ELALMYNDESVLENHHLAVGFKLLQ
YNDESVLENHHLAVGFKLLQEDNCD
VLENHHLAVGFKLLQEDNCDIFQNL
HLAVGFKLLQEDNCDIFQNLSKRQR
FKLLQEDNCDIFQNLSKRQRQSLRK

(iii)

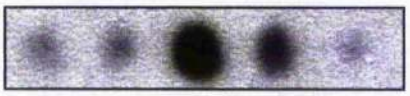

PDE4A4B peptide array
(Iso646 to Pro690)
Catalytic unit

IDYIVHPLWETWADLVHPDAQEILD
HPLWETWADLVHPDAQEILDTLEDN
TWADLVHPDAQEILDTLEDNRDWYY
VHPDAQEILDTLEDNRDWYYSAIRQ
QEILDTLEDNRDWYYSAIRQSPSPP

(iv)

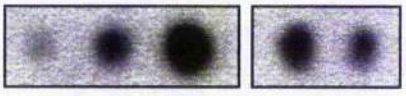

PDE4A4B peptide array
(Ser686 to Ala730)
Catalytic unit

SPSPPPEEESRGPGHPPLPDKFQFE
PEEESRGPGHPPLPDKFQFELTLEE
RGPGHPPLPDKFQFELTLEEEEEEE
PPLPDKFQFELTLEEEEEEEISMAQ
KFQFELTLEEEEEEEISMAQIPCTA

Figure 5.4 – Interaction of p47-*phox* with PDE4A long isoforms.

Pull-down assays were used to probe the interaction of the purified GST-p47-*phox* and GST-p67-*phox*. The *phox* fusion proteins were immobilised on glutathione sepharose resin and incubated with COS7 cell lysate expressing equal immuno-reactive amounts of either PDE4A4B or PDE4A10, determined using the C-terminal PDE4A-specific anti-serum. (a), shows the interaction of GST-p47-*phox* and GST-p67-*phox* with PDE4A4B or PDE4A10 respectively. As a control, the pull-down of PDE4A4B or PDE4A10 with GST alone was compared (an example of PDE4A pull-down with GST alone is shown previously in Figure 3.11). (b), panels (i) – (iv), map the interaction sites of GST-p47-*phox* on full-length PDE4A4B using peptide array technology. Briefly, the entire PDE4A4B peptide sequence was synthesised on a membrane and the membrane incubated with the purified GST-p47-*phox*. The membrane was probed for p47-*phox* interaction using a specific p47-*phox* anti-serum. The Western blots and peptide array interaction data are representative of the results obtained from three separate experiments.

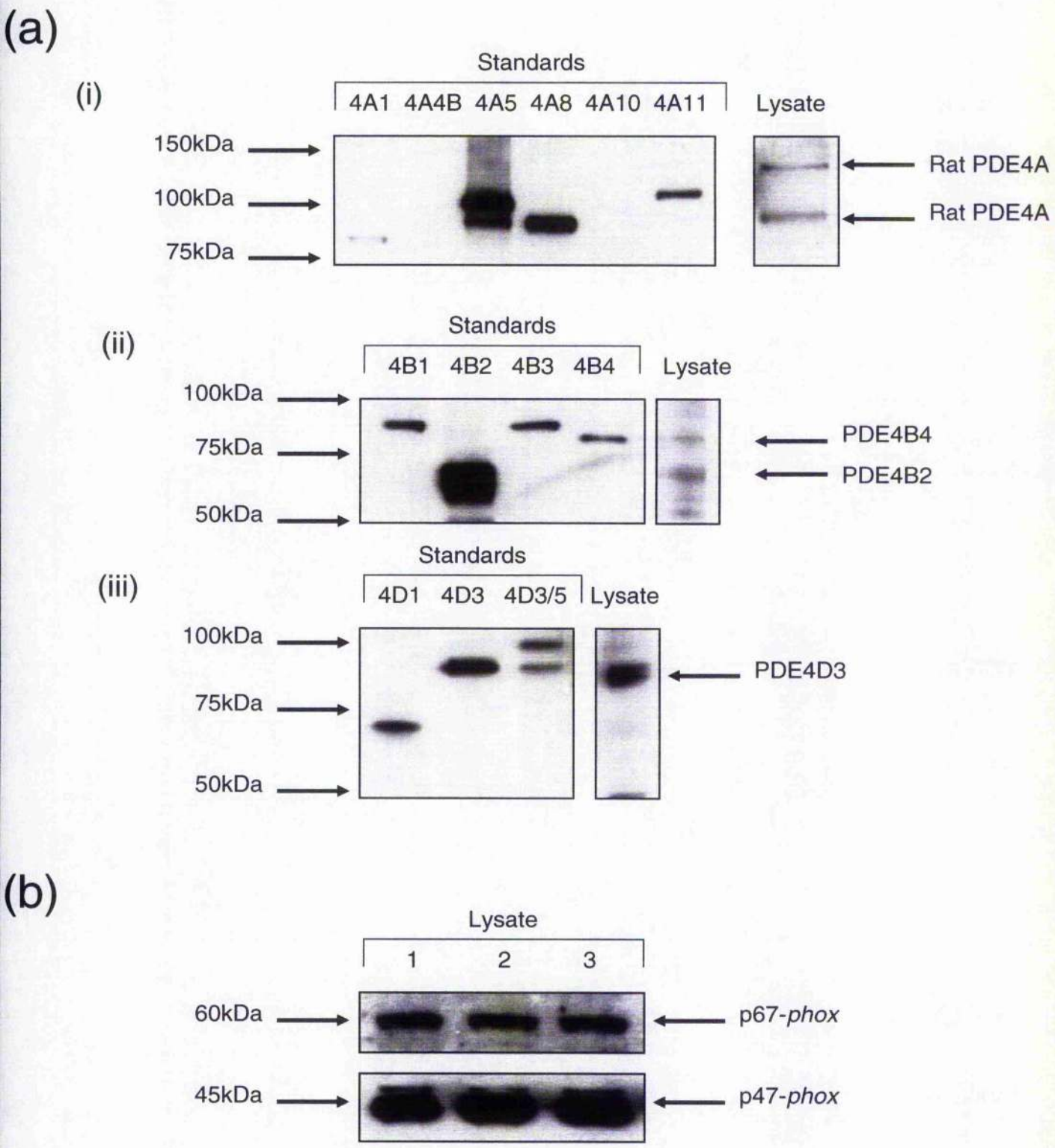
(a)
(i)
Standards
4A1 4A4B 4A5 4A8 4A10 4A11
Lysate
150kDa
100kDa
75kDa
Rat PDE4A
Rat PDE4A
(ii)
Standards
4B1 4B2 4B3 4B4
Lysate
100kDa
75kDa
50kDa
PDE4B4
PDE4B2
(iii)
Standards
4D1 4D3 4D3/5
Lysate
100kDa
75kDa
50kDa
PDE4D3
(b)
Lysate
1 2 3
60kDa
45kDa
p67-phox
p47-phox

Figure 5.5 – Expression profile of endogenous PDE4 isoforms and endogenous p47- and p67-*phox* proteins in rat cardiac myocytes.

Total cell lysate was generated from separately transfected COS7 cells expressing known PDE4 isoforms, as indicated. These were used as PDE4 isoform standards to determine the PDE4 isoform profile of the rat cardiac myocyte cultured cell line. Total cell lysates produced from cultured rat cardiac myocytes were subjected to SDS-PAGE and the endogenous PDE4 profile determined by Western blotting with either the rat PDE4A specific C-terminal anti-serum, (a), panel (i), the PDE4B specific C-terminal anti-serum, (a), panel (ii), or the PDE4D specific C-terminal anti-serum, (a), panel (iii). Panel (b), shows Western blots of the same rat cardiac myocyte cell lysate immuno-probed for endogenous p47-*phox* and endogenous p67-phox using specific anti-sera to both proteins respectively. The Western blots are from screening experiments done once.

(a)

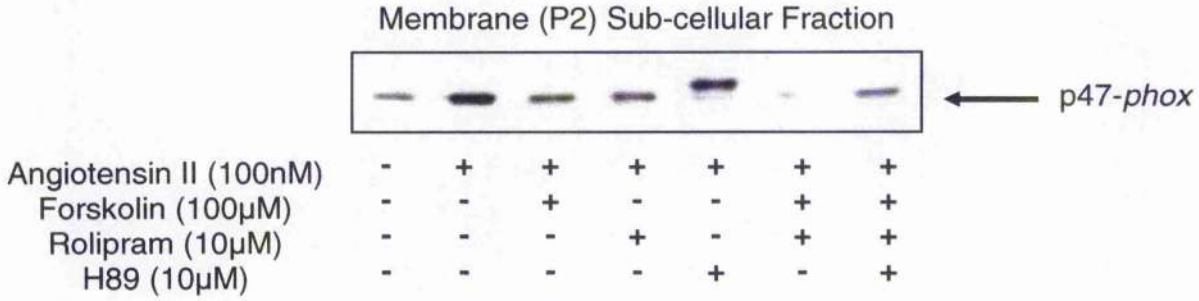
Membrane (P2) Sub-cellular Fraction
p47-phox
Angiotensin II (100nM) - + + + + + +
Forskolin (100μM) - - + - - + +
Rolipram (10μM) - - - + - + +
H89 (10μM) - - - - + - +

(b)

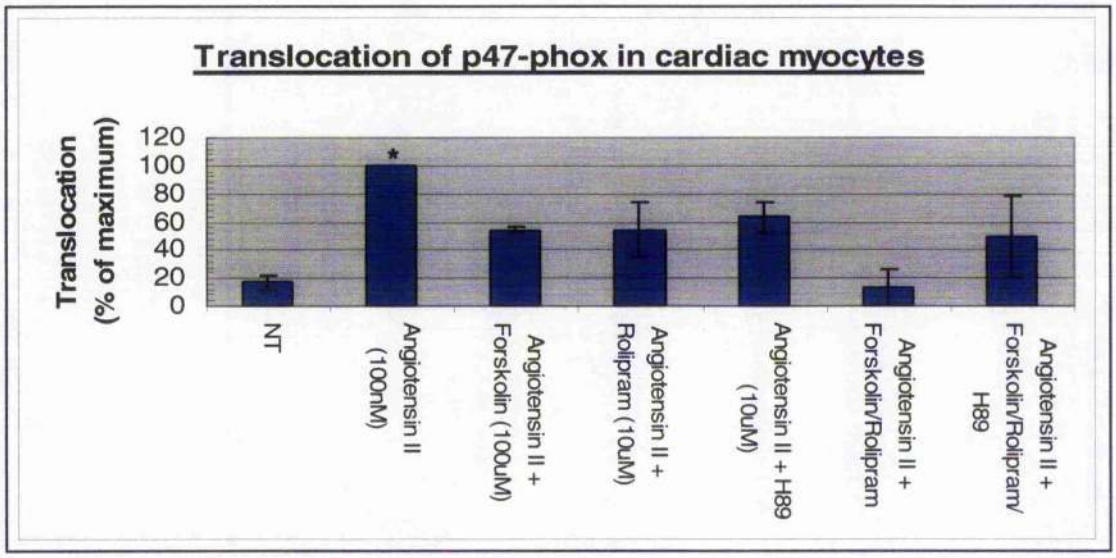
Translocation of p47-phox in cardiac myocytes
Translocation (% of maximum)
120
100
80
60
40
20
0
*
NT
Angiotensin II (100nM)
Angiotensin II + Forskolin (100uM)
Angiotensin II + Rolipram (10uM)
Angiotensin II + H89 (10uM)
Angiotensin II + Forskolin/Rolipram
Angiotensin II + Forskolin/Rolipram/ H89

Figure 5.6 – Plasma membrane translocation of cytosolic p47-*phox* in response to angiotensin II in rat cardiac myocytes.

Cultured rat cardiac myocytes were either retained untreated, treated with angiotensin II alone (100nM for 5 minutes), or pre-treated with combinations of forskolin (100μM for 10 minutes), rolipram (10μM for 10 minutes) and/or H89 (10μM for 10 minutes) prior to angiotensin II. The cells were harvested and sub-cellular fractions produced by centrifugation. This method, described previously [McPhee et al., 1995], separates the total cellular matter into the soluble, cytosolic cellular components (high-speed supernatant or S2), the plasma membrane and internal organelles (high-speed pellet or P2), and intact cells and other cellular debris (low-speed pellet or P1). (a), is a Western blot of the relative immuno-reactive amounts of p47-*phox* at the plasma membrane, following the indicated treatments, as determined by immuno-probing the isolated membrane fractions (P2) with an anti-serum specific to the p47-*phox* protein. (b), quantifies the effect of these treatments and any change in p47-*phox* translocation to the plasma membrane, compared against the maximum p47-*phox* translocation. The Western blot is representative of translocation experiments done three times on different batches of cultured rat cardiac myocytes and the quantification data are expressed as mean values +/- standard deviation from the three separate translocation experiments. Paired t-test statistical analysis of the quantification data were undertaken, where $p < 0.05$ indicates a statistically significant difference in the relative p47-*phox* immuno-reactivity within the P2 sub-cellular fraction between untreated and treated cells, as indicated.

5.3 Discussion

The production of O_2^- and ROS is an important aspect of the innate immune response, providing host defence against invading microorganisms. However, the uncontrolled generation of such species underlies oxidative stress and the onset of a variety of cardiovascular disease states such as cardiac hypertrophy and heart failure [Li et al., 2002 and Murdoch et al., 2006]. Cardiac hypertrophy is characterised by an increase in the size of the heart cells and can be caused by hypertension. Hypertension affects the left ventricle due to chronic pumping against increased arterial pressure. Over time the integrity of the myocardial cells change prompting a decrease in contractile function eventually leading to cardiac failure. In renal hypertension there is an increase in renin release, which is converted to angiotensin I by angiotensinogen, and then to angiotensin II by angiotensin converting enzyme (ACE). Angiotensin II is a potent vasoconstrictor and therefore increases blood pressure, which, in turn, increases the load upon the heart. In cardiac myocytes, angiotensin II can induce the onset of cardiac hypertrophy and this change in cell morphology is mediated, in part, by the production of O_2^- and ROS, and is sensitive to a variety of anti-oxidants [Nakamura, et al., 1998 and Nakagami et al., 2003].

The NADPH oxidase enzyme catalyses the reduction of oxygen (O_2) to O_2^- and enzyme activity is tightly regulated by the extensive phosphorylation of the cytosolic p47-*phox* protein (Figure 5.1) [Groemping and Rittinger, 2005 and Sheppard et al., 2005]. These phosphorylation events occur at the extreme C-terminal region of p47-*phox* and function to relieve an inhibitory constraint [Groemping et al, 2003]. The p40-*phox*/p67-*phox* hetero-dimer is also phosphorylated to a lesser degree, but this is essential, together with the preceding p47-*phox* phosphorylation, for its translocation to the plasma membrane [Vignais, 2002]. The dissociation of Rac2-GDP from the Rho GDP dissociation inhibitor in the cytosol, and the association of Rac2-GTP with the TPR domains of p67-*phox* at the plasma membrane, is also a key event in the activation process [Lapouge et al., 2000]. At the plasma membrane, the now

accessible SH3 domains of the heavily phosphorylated p47-*phox* interact with the proline-rich region of p22-*phox* and directly with the membrane through PI binding to the PX domain [Zhan et al., 2004 and Groemping and Rittinger, 2005]. The proline-rich region of p47-*phox* interacts with the SH3 domains of both p67- and p40-*phox*, with p40-*phox* also utilising its PX domain for additional membrane binding [Wientjes et al., 2001]. p67-*phox* bound to Rac2-GTP and Rap1A interacts directly with both the membrane and the membrane-bound flavocytochrome b_{558} [Babior, 1999, Zwartkruis and Bos, 1999, Lapouge et al., 2000 and Bokoch and Knaus, 2003]. The membrane-bound flavocytochrome b_{558}, specifically the gp91-*phox* subunit, binds NADPH, FAD and the haem groups [Vignais, 2002].

In non-phagocytic cells, such as cardiac myocytes, homologous components of the phagocytic NADPH oxidase enzyme are present including gp91-*phox*, or Nox2 as it is known in non-phagocytic cells [Murdoch et al., 2006]. In isolated rat cardiac myocytes, the endogenous expression of both p47- and p67-*phox* was immunologically detected together with various isoforms from the PDE4A, 4B and 4D gene families (Figure 5.5) [Mongillo et al., 2004]. Stimulation of cardiac myocytes with 100nM angiotensin II initiated a robust translocation of p47-*phox* to the plasma membrane, as indicated by increased immunological detection in the membranous sub-cellular fraction (Figure 5.6). This is in complete agreement with previous work showing that the treatment of cardiac myocytes with the same concentration of angiotensin II induced a significant increase in the production of O_2^- and ROS [Nakamura et al., 1998]. The angiotensin II receptor is a GPCR that couples to G_q and activates both PKC and ERK1/2, protein kinases implicated in p47-*phox* phosphorylation and translocation [Lopes et al., 1999, Liebmann, 2001, Ahn et al., 2004 and Dang et al., 2006]. Furthermore, the angiotensin II receptor also recruits β-arrestin and the recruitment of other protein kinases through β-arrestin interactions, which might play a fundamental role in controlling the p47-*phox* phosphorylation state and translocation [Lefkowitz and Shenoy, 2005]. Forskolin or rolipram attenuated the magnitude of this angiotensin II response on activation of the cAMP-PKA signalling cascade, through either direct activation of adenylyl cyclase or global PDE4 inhibition respectively.

Using both forskolin and rolipram together the synergistic activation of PKA ablated p47-*phox* translocation to the membrane, an effect that was partially rescued by PKA inhibition. From these data it was concluded that enhanced PKA activity might, in part, underlie the mechanism through which PDE4 inhibitors reduce O_2^- and ROS production. Angiotensin II plus the PKA inhibitor H89 also reduced p47-*phox* translocation, an unexpected effect, but accompanying this was a notable band shift indicating a possible increase in the extent of protein phosphorylation. It is possible that this may be a H89 non-specific effect (10μM for endogenous PKA inhibition is considered an excess) inhibiting p47-*phox* phosphorylation resulting in attenuation of plasma membrane translocation [Davies, et al., 2000, Hoyal et al., 2003 and Brown et al., 2004]. Indeed, 10μM can markedly attenuate the activity of p38 MAPK downstream kinases such as MSK1 and MAPKAPK1, and PKB/Akt, with both pathways proposed to be involved in the translocation of p47-*phox* and the activation of NADPH oxidase [Davies, et al., 2000]. However, this simple explanation does not reconcile the band shift and further work is required to determine whether this effect is of functional significance to p47-*phox* protein regulation.

The current and limited information on the role that PKA activation exerts upon the NADPH oxidase enzyme components is conflicting. In neutrophils isolated from the bronchoalveolar lavage (BAL) of rats treated with LPS, O_2^- and ROS production was attenuated on treatment with PDE4 inhibitors [Jacob et al., 2004]. This is consistent with the current knowledge of PDE4 inhibition. However, this mechanism was proposed to occur through the activation of ERK1/2 and not through an increase in intra-cellular cAMP concentrations or the associated activation of PKA phosphorylation or EPAC. Although this study contradicts the proposal here that PKA activation is directly responsible for mediating an inhibitory effect on O_2^- and ROS production, it does provide evidence of kinase activation that is capable of mediating O_2^- and ROS inhibition, which is also in contrast to the current knowledge of NADPH oxidase activation by phosphorylation. The activation of neutrophils measured by both O_2^- production and β_2-integrin expression, using fMLP is inhibited by lysophosphatidylcholine (LPC) through an

accompanying increase in intra-cellular cAMP concentrations and activation of PKA [Lin et al., 2005]. H89 rescued this inhibitory effect, indicating an inhibitory role of PKA phosphorylation and not an EPAC-mediated effect. Furthermore, at the level of p47- and p67-*phox*, their translocations induced by fMLP were inhibited by LPC and rescued by H89. This study corroborates the possibility of a similar mechanism in cardiac myocytes where the direct phosphorylation of p47-*phox* prevents translocation together with p67-*phox*, as it cannot translocate in isolation [Johnson et al., 1998 and Babior, 1999].

The p47-*phox* cytosolic subunit is known to be a substrate for numerous protein kinases that elicit its translocation to the plasma membrane. Utilising recombinant GST fusion proteins of full-length *phox* proteins in an in vitro kinase assay, it was confirmed that p47-*phox*, but not p67-*phox*, was a target for PKA phosphorylation (Figure 5.3). Predictably, the PKA phosphorylation region on p47-*phox* was mapped, using truncated versions of the protein, to the C-terminal, SH3 domain-containing region with no detectable phosphorylation of the N-terminal PX domain. In an attempt to elucidate putative target phosphorylation residues a similar in vitro kinase assay was undertaken using a peptide array of full-length p47-*phox*. This identified six putative phosphorylation sites for PKA, namely Ser-208, Ser-304, Ser-320, Ser-328, Ser-370 and Ser-379. The consensus motif for phosphorylation by PKA is Arg-Arg-Xaa-Ser-Ø, where Ø is a hydrophobic residue. Of the six possible PKA target serine residues identified, Ser-304 and Ser-328 conform to perfect PKA consensus motifs. The first residue of the consensus motif surrounding Ser-370 is a proline, but the remaining residues are of the correct amino acid classification. Ser-320 and Ser-379 contain the core Arg-Xaa-Ser motif but lack the acceptable extreme residues to conform to perfect PKA consensus sites. Perhaps most important, due to its positioning within the first SH3 domain or SH3 domain A, is Ser-208, which contains the correct amino acid complement surrounding the target serine to conform as a PKA target site. A brief attempt to determine the PKA target sites by site-directed serine to alanine mutagenesis of residues 304, 320 and 328 yielded a reduction but not ablation of PKA phosphorylation in each case indicating that further sites are likely to be involved. Thus, mutagenesis of

amino acids 208, 370 and 379 as single alanine mutants, and combinations therein, will allow the delineation of the relative contribution of each putative target serine. It is well established that Ser-304, Ser-320, Ser-328, Ser-370 and Ser-379 are key phosphorylation sites for the relief of the inhibitory constraints placed upon p47-*phox* in the resting state [Groemping and Rittinger, 2005]. Phosphorylation of Ser-303, Ser-304 and Ser-328 are the major sites for mediating high affinity interactions with p22-*phox* following translocation, with Ser-315 and Ser-320 playing relatively minor roles [Groemping et al., 2003]. Thus, one would expect phosphorylation at one, some or all of these five sites to promote a conformational change in p47-*phox* to allow translocation to, and interaction with, the p22-*phox* component of the flavocytochrome b_{558} at the plasma membrane. Of course in the intact cell, lack of phosphorylation at Ser-359 may impact the activation status of p47-*phox* by preventing the sequential phosphorylation at the N-terminal residues thereby impacting translocation efficiency [Johnson et al., 1998, Hoyal et al., 2003 and Massenet et al., 2005]. Alternatively, the preceding phosphorylation events at the aforementioned residues may promote access to SH3 domain A for further PKA phosphorylation at Ser-208. This phosphorylation may attenuate the interaction with the proline-rich region of the p22-*phox*, in a similar manner to PR-39, an anti-microbial peptide, which binds to the SH3 domains and prevents the p22-*phox* interaction [Babior, 1999 and Groemping and Rittinger, 2005]. Indeed, the exposure of the first SH3 domain is sufficient to interact with p22-*phox*, where the second SH3 domain in isolation cannot associate [Groemping et al., 2003]. However, the second SH3 domain must play a co-operative role, forming a so-called "superSH3 domain", in the binding at the plasma membrane, as the affinity is greatest when both are present. Phosphorylation at this site may also prevent the interaction of the PX domain with the first SH3 domain preventing access for lipid-mediated binding at the plasma membrane [Durand et al., 2006]. Of course a point of caution with all in vitro phosphorylation assays is the propensity for indiscriminate phosphorylation to occur. Direct phosphorylation of p47-*phox* may not be involved in the mechanism and simply the phosphorylation of an intermediate substrate in signalling cross talk, e.g. Raf isoforms or Rap1, may prevent the translocation of p47-*phox* and underlie the

inhibitory action of PKA [Houslay and Kolch, 2000]. Therefore, whole cell phosphorylation experiments should be undertaken to determine whether translocation is modified with PKA phosphorylation in vivo. It is possible that a co-transfection to transiently over-express p47-*phox*, and its membrane partner protein p22-*phox*, will be sufficient components for interaction. If so, then single and multiple serines to alanine mutants can be employed to assess the effect of direct PKA phosphorylation upon p47-*phox* interaction with p22-*phox*.

Activation of the β-adrenoceptor in cardiac myocytes controls the strength, duration and frequency of myocardial contraction and is also involved in the onset of cardiac hypertrophy [Zou et al., 1999 and Zaccolo and Pozzan, 2002]. Indeed, in cardiac myocytes cAMP-dependent intra-cellular signalling and the endogenous expression of PDE4 isoforms is highly compartmentalised [Mongillo et al., 2004 and Zaccolo, 2006]. Supporting such compartmentalisation was the identification of PDE4D isoforms as the key PDE4 sub-family in controlling β_2-adrenoceptor signalling in cardiac myocytes, where PDE4D knock-out had no effect on β_1-adrenoceptor signalling, which activates the PKA phosphorylation of L-type Ca^{2+} channels and the ryanodine receptor to control myocardial contraction [Xiang et al., 2005 and Zaccolo, 2006]. Activation of G_sPCRs is also associated with the onset of cardiac hypertrophy [Zou et al., 1999]. On the basis of the data shown in this chapter, this effect is unlikely to mediated through a PKA driven mechanism upon the NADPH oxidase enzyme components as global increases in intra-cellular cAMP concentrations prevent p47-*phox* translocation to the plasma membrane (Figure 5.6). A possible mechanism of an activating phosphorylation conferring p47-*phox* translocation may lie in G_s to G_i, or G_q, switching [Zou et al., 1999 and Lawler et al., 2001]. Compartmentalised β-adrenoceptor signalling may facilitate the activation of ERK1/2 or PKC, by switching to G_i or G_q, thereby activating the NADPH oxidase enzyme via extensive phosphorylation of the p47-*phox*, and p67-*phox* in the case of ERK1/2. Thus, cAMP signal compartmentalisation and the sub-cellular localisation of specific PDE4 isoforms may underlie the differential

effects of stimuli on the activation of the NADPH oxidase enzyme, the production of O_2^- and ROS, and the onset of cardiac hypertrophy.

p47-*phox* and p67-*phox* both contain SH3 and TPR domains, which are known to facilitate interactions with PDE4A isoforms [McPhee et al., 1999 and Bolger et al., 2003]. On this premise, p47- and p67-*phox* might also interact with PDE4A isoforms to allow the temporal and spatial control of cAMP concentrations and subsequent PKA phosphorylation of *phox* proteins. In concert, these interactions could modulate PDE4A activity by inducing a conformational change in the catalytic unit as sensed by increased sensitivity to inhibition by rolipram [McPhee et al., 1999 and Bolger et al., 2003]. In pull-down assays, PDE4A4B was able to interact with both p47- and p67-*phox* whereas, PDE4A10 was only able to interact with p47-*phox* (Figure 5.4). This differential binding indicates isoform specificity of interaction with p67-*phox* and possibly PDE4A gene family specificity for interaction with p47-*phox*. On the basis of the current knowledge of these interactions this is what one would predict. PDE4A4B is known for its interaction with both SH3 and TPR domain-containing proteins whereas, PDE4A10 can interact with SH3 domain-containing proteins but not those with TPR domains as this interaction, in the case of XAP2, was mediated through the unique N-terminal region of PDE4A4B and its homologue PDE4A5 [McPhee et al., 1999, Rena et al., 2001 and Bolger et al., 2003]. To further probe the interaction sites of p47-*phox* on PDE4A4B, the full-length peptide array was utilised (Figure 5.4). All interaction sites were core conserved sequences within the PDE4 family and thus one would expect all PDE4 isoforms to interact with p47-*phox*. The UCR2 interaction site is analogous to that participating in the XAP2 interaction with PDE4A4B/PDE4A5, i.e. Glu-Glu-Leu-Asp [Bolger et al., 2003]. The catalytic binding region identified between Iso-646 and Pro-690 also contains a similar motif, i.e. Glu-Iso-Leu-Asp. This is also the site required for the UCR1-UCR2 intra-molecular interaction and may disrupt PDE4 oligomerisation [Beard et al., 2000, Richter and Conti, 2002 and Richter and Conti, 2004]. It is interesting that p47-*phox* did not interact with the regions required for SH3 domain binding, as described for the SH3 domains of the tyrosyl kinase Lyn, indicating that the SH3 domains are probably not involved

in this interaction. Furthermore, the identification of the region responsible for mediating the XAP2 interactions may indicate competition for p47- and p67-*phox* binding on PDE4A4B/PDE4A5. It would be beneficial to map the interaction sites for p67-*phox* on PDE4A4B using the peptide array technique to identify whether competition for binding is possible. Alanine scanning will elucidate the specific residues involved in mediating these interactions, as has been described previously for the interactions of both β-arrestin and RACK1 with PDE4D5 [Bolger et al., 2006]. The activation state of p47-*phox* may be crucial to its interaction with PDE4 isoforms. Priming or activation of the NADPH oxidase enzyme, i.e. a conformational change induced by p47-*phox* phosphorylation, may be required before further phosphorylation and/or interaction can occur. Similarly, the activation state could drive the specificity of PDE4 interaction. Auto-inhibited p47-*phox* may be able to interact with all PDE4 enzymes, whereas activation and exposure of the SH3 domains may be fundamental in conferring specificity to PDE4A. Endogenous co-immuno-precipitation of both p47- and p67-*phox* with PDE4 enzymes, identified either through Western immuno-blotting or PDE activity assays will allow the identification of interaction specificity in the three NADPH oxidase states; rest, primed and activated [Sheppard et al., 2005]. Therefore, distinct PDE4 isoforms, perhaps from the PDE4A gene family, may be important in the control of NADPH oxidase activity through interactions with the NADPH oxidase *phox* proteins. To elucidate such specificity the use of dominant negative PDE4 isoforms or sub-family specific siRNA techniques could be employed, as described before [Lynch et al., 2005 and McCahill et al., 2005]. Furthermore, with the resolution of the crystal structure of the catalytic unit of PDE4 enzymes and the extensive structural information available with respect to the activation and assembly of the NADPH oxidase enzyme, it would be of interest to model the proposed interaction to determine if an interaction is theoretically viable [Xu et al., 2000 and Groemping and Rittinger, 2005].

Other possible mechanisms that have the potential to be involved in the regulation of O_2^- and ROS production through the PKA phosphorylation of p47-*phox* include the requirement for AKAP-mediated interactions. Indeed, p47-*phox* is able to bind moesin, a member of the ERM (ezrin, radixin and

moesin) family of proteins, through its PX domain and translocation to the plasma membrane through association with F-actin components of the cytoskeleton [Wientjes et al., 2001 and Zhan et al., 2004]. Thus, the activation of ERK1/2 or ERK5 may be inhibitory to p47-*phox* translocation through direct disruption of the cellular cytoskeletal structure [Barros and Marshall, 2005]. Although moesin is not considered to be an AKAP, the associated family member ezrin has been assigned such functionality and may play a role in recruiting PKA [Dransfield et al., 1997 and Sun et al., 2000]. However, WAVE-1 has been assigned AKAP function and it has been shown that it participates in the translocation of p47-*phox* to membrane ruffles in endothelial cells [Westphal et al., 2000 and Wu et al., 2003]. AKAPs may also play a role in the recruitment of protein phosphatases to p47-*phox*, as many studies have implicated the balance between phosphorylation versus de-phosphorylation as being extremely important in controlling p47-*phox* translocation [Bengis-Garber and Gruener, 1996 and Babior, 1999].

The activation of EPAC through cAMP is unlikely to be involved, as the exchange of GDP for GTP on Rap1A will result in the activation of NADPH oxidase activity [Jacob et al., 2004]. However, control of the activation state of Rac2 may underlie part of the inhibitory translocation mechanism conferred upon increases in intra-cellular cAMP levels [Pomerance et al., 2000 and Pelletier et al., 2005].

Further exploration of this mechanism is certainly required. If the activation of the NADPH oxidase enzyme is indeed controlled through the PKA phosphorylation state of p47-*phox* through interactions with distinct PDE4 isoforms, following a specific stimulation within a given cell type, then this would further substantiate the need for cAMP signal compartmentalisation in cardiac myocytes and support the necessity for distinct isoforms of PDE4 enzymes to control functionally distinct cellular processes.

Chapter 6 General Discussion

PDE4-selective inhibitors promote the immuno-suppressive, anti-inflammatory and smooth muscle relaxant properties associated with cAMP, and are being pursued as novel therapeutics for disease states such as asthma, COPD, rheumatoid arthritis and psoriasis [Souness et al., 2000, Burnouf and Pruniaux, 2002, Houslay et al., 2005 and Zhang et al., 2005]. The beneficial effects of PDE4 inhibition are also being exploited for the treatment of CNS disorders including cognitive enhancement, depression, Alzheimer's, Parkinson's and Schizophrenia, as well as cardiovascular diseases such as atherosclerosis, restenosis, pulmonary hypertension and stroke [Maurice et al., 2003, O'Donnell and Zhang, 2004, Houslay et al., 2005, Millar et al., 2005 and Zhang et al., 2005]. cAMP also modulates the expression levels of proteins involved in the regulation of the cell cycle, causing G_1/S-phase cell cycle arrest and apoptosis, indicating the therapeutic potential for PDE4 inhibition in cancer [Schmitt and Stork, 2001, Balmanno et al., 2003 and Zambon et al., 2005]. PDE4 inhibition prevents chemotaxis and cell migration implying a potential role in both inflammatory cell diapedesis and cancer cell metastasis [Kohyama et al., 2002 and Fleming et al., 2004].

However, cAMP concentrations are not controlled by global PDE4 activity but restricted to isoforms, in distinct cAMP micro-domains, expressed on a cell-type specific basis and participating in dedicated signalling systems. Unsurprisingly, collective PDE4 inhibition is associated with severe side effects, a likely consequence of the vast number of physiological and metabolic processes that are regulated by cAMP [Huang et al., 2001 and Zhang et al., 2005]. Therefore, complete knowledge of the plethora of PDE4 isoforms expressed in humans and their regulation is essential, and will allow their selective inhibition, specific gene knockout, siRNA ablation or the use of dominant negative constructs to delineate the physiological requirement for such an array of PDE4 isoforms. In the process, this will allow the identification of beneficial and adverse effects arising from isoform-specific PDE4 inhibition.

Twenty-one human isoforms of the cAMP-specific PDE4 enzyme family have now been characterised and these provide the predominant cAMP-hydrolysing activity in many cells [Houslay, 2001 and Conti et al., 2003]. PDE4 isoforms are widely expressed and distributed on a cell-type specific basis. The unique N-terminal region of each isoform is responsible for its intra-cellular targeting to discrete regions of the cell, in concert with protein kinases, scaffold, anchoring, and adaptor proteins [Houslay and Adams, 2003]. The protein interactions with the unique N-terminal regions of PDE4 isoforms are often stabilised by additional contacts within PDE4 conserved regions. The many established protein interactions and their functional effects upon PDE4 activity are discussed in some detail in Section 1.7.6. PDE4 activity and some protein interactions are regulated by phosphorylation, and these are discussed in Section 1.7.5.

To assess the physiological requirement for multiple PDE4 isoforms it is first essential to ascertain the full complement of enzymes that can be expressed. Accordingly, the first objective of this thesis was to characterise the novel PDE4A11 long isoform, summarising its key distinguishing features in relation to our current knowledge of the PDE4A isoforms, and elucidating the functional significance of its expression. Chapter 3 described the PDE4A11 isoform in detail [Wallace et al., 2005].

PDE4A11 is an authentic PDE4A long isoform. mRNA transcripts were detected in many human tissues (Figure 3.4) and were most striking in liver, stomach, testis, thyroid, adrenal gland, PBLs and foetal brain. Of interest were the low levels of PDE4A11 transcripts in the adult brain. In contrast, PDE4A10 provides abundant transcript levels [Rena et al., 2001 and McPhee et al., 2001], indicating isoform specific changes at different stages of brain development. PDE4A11 is also widely expressed in immune and inflammatory cells, as well as bronchial smooth muscle cells, providing the principal PDE4A transcript [Wallace et al., 2005]. Of course, the presence of PDE4A11 transcripts does not necessarily translate to protein expression. Specific changes in PDE4A isoform expression have already been established during monocyte to macrophage differentiation (up-regulation of

PDE4A10), in monocytes and macrophages in smokers and people diagnosed with COPD (up-regulation of PDE4A4B) and in human pulmonary arterial smooth muscle cells in response to hypoxia (up-regulation of PDE4A10 and PDE4A11) [Shepherd et al., 2004, Barber et al., 2004 and Millen et al., 2006]. Therefore, the identification of endogenous PDE4A11 expression at various tissue developmental stages and during disease progression will develop our understanding of its physiological significance. To facilitate these experiments a specific anti-sera to the unique N-terminal region of PDE4A11 was generated (Figure 3.5).

PDE4A11 is characterised by a unique 81 amino acid N-terminal region that is likely to confer its distinct intra-cellular targeting to membrane ruffles (Figure 3.5). The identification of a putative PIP3 binding PH domain within the unique N-terminal region of PDE4A11 may facilitate its appropriate positioning to participate in cAMP-mediated cell signalling events at ruffled membranes, such as cell motility. This implies a potential role for PDE4A11 in the regulation of inflammatory cell migration or cancer cell metastasis. Furthermore, the activation of PKA attenuates PI-3K activation, as indicated by reduced phosphorylation of PKB/Akt [Leemhuis et al., 2004]. PDE4A11 recruitment may control the cAMP regulation of PI-3K activity and consequently physiologic and metabolic processes such as glucose uptake, glycogen synthesis, cell growth, cell cycle entry and cell survival.

No re-distribution of PDE4A11 expression was observed upon stimulation of PI-3K enzyme activity (Figures 3.6 and 3.7). However, the over-expression of recombinant proteins in cells is potentially misleading because of the likely saturation of anchor sites and the fact that different anchors are present in different cells. Moreover, the endogenous expression of PDE4A isoforms is relatively low compared to the PDE4B and PDE4D enzymes. Therefore, gross over-expression of PDE4A isoforms is in no way representative of the endogenous state. To assess the effect of the putative PIP3 binding PH domain and its potential role in the intra-cellular targeting of PDE4A11, cells with immunologically detectable levels of endogenous enzyme should be evaluated. Alternatively, the use of a low expression

construct, plus mutation of the putative PIP3 binding PH domain, will ascertain whether this domain does indeed participate in PDE4A11 intra-cellular targeting in transfected cells.

PDE4 enzymes can form distinct conformers as sensed by different sensitivities to inhibition by rolipram. As a general rule, in the absence of phosphorylation or specific interacting proteins, PDE4 enzymes exist in a low affinity rolipram binding state (LARBS). The interactions of PDE4A4B with the SH3 domains of Src tyrosyl kinases [McPhee et al., 1999] and PDE4A5 with the immunophilin XAP2 [Bolger et al., 2003] are interactions that are capable of increasing enzyme sensitivity for inhibition by rolipram, thus forming a high affinity rolipram binding state (HARBS). An analogous effect is not induced by PKA phosphorylation of either PDE4A4B or PDE4A5 [MacKenzie et al., 2002]. PDE4D3 is the only isoform to date where PKA phosphorylation confers both activation and the formation of HARBS, and these are proposed to occur via distinct mechanisms [Hoffmann et al., 1998]. Furthermore, chronic rolipram treatment of PDE4A4B induces the formation of accretion foci and it is currently proposed that this is caused by conformational switching to HARBS induced by rolipram and in the absence of cAMP [Terry et al., 2003]. Additionally, cytosolic and particulate forms of the same isoform display distinct thermal inactivation kinetics, providing further evidence for existence of altered catalytic conformations of the same protein [Rena et al., 2001 and Wallace et al., 2005].

It was hypothesised that the emetic side effects of PDE4 inhibition were a result of HARBS inhibition in the brain and that generating LARBS-specific inhibitors could overcome these effects; LARBS predominates in inflammatory cells [Richter and Conti, 2004 and Houslay et al., 2005]. Although this theory is now considered obsolete the mechanisms that underlie such conformational switching are still being pursued and resolution of the full-length PDE4 crystal structure will greatly advance our understanding of this phenomenon.

The particulate targeting of PDE4A4B, but not PDE4A10, is sufficient to induce enhanced sensitivity to inhibition by rolipram (Table 3.2) [Huston et al., 1996 and Rena et al., 2001]. PDE4A11 was also detected in the particulate fraction and although some alteration of conformation was indicated from thermal stability analysis (Figure 3.10) no conformational change in the catalytic unit was measured in response to rolipram (Figure 3.9 and Table 3.2). PDE4A10 and PDE4A11 both interact with the SH3 domain of Lyn, but to a lesser degree than that observed for PDE4A4B (Figure 3.15) [McPhee et al., 1999, Rena et al., 2001 and Wallace et al., 2005]. It was perceived that the lack of PDE4A10 and PDE4A11 N-terminal SH3 binding domains, given that this is the only point of primary sequence divergence, was responsible for the reduced interaction [Rena et al., 2001 and Wallace et al., 2005]. This theory does not explain the absence of conformational switching from LARBS to HARBS, as this effect is clearly mediated through the PDE4A conserved LR2 [McPhee et al., 1999]. However, analysis of the SH3 domain interactions using the peptide array approach has mapped N-terminal SH3 binding domains to both PDE4A10 and PDE4A11, but displayed limited interaction with the N-terminal of PDE4A4B (Figure 3.15). Therefore, it is my belief that the conformational switching occurs in PDE4A4B through preferential SH3 domain interactions with LR2, and conversely the N-terminal regions of PDE4A10 and PDE4A11 provide the preferential SH3 domain interaction sites within these isoforms. The properties of the unique N-terminal regions must confer a masking effect on the LR2 binding site and/or have higher affinity N-terminal SH3 binding, thus preventing the formation of high affinity conformers. Higher affinity for the N-terminal binding site over LR2 is unlikely given the reduced interaction in fusion protein pull-down assays (Figure 3.15) [Rena et al., 2001 and Wallace et al., 2005].

In agreement, long-term challenge of cells transfected with PDE4A4B causes the formation of accretion foci, an effect not observed with PDE4A10 or PDE4A11 [Terry et al., 2003 and Wallace et al., 2005].

The specific interaction of PDE4A5 with XAP2 also results in an increase in the sensitivity with which rolipram inhibits PDE4A5 [Bolger et al.,

2003]. However, data here shows that PDE4A11 is also capable of interacting with XAP2, with equal magnitude to PDE4A4B (Figure 3.17). One would advocate characterisation of this interaction to assess whether it confers similar inhibitory effects on PDE4A11 catalytic activity and alters the rolipram inhibition profile.

One potential mechanism for conformational switching that has not been addressed here is the suggestion that PDE4 enzymes form homo-dimers through inter-molecular UCR1-UCR2 interactions [Richter and Conti, 2004]. Dimerisation appears to be essential for PDE4 function and serves to stabilise PDE4 enzymes in HARBS. The use of alternatively tagged constructs of PDE4A11 would allow one to elucidate whether PDE4A11 is able to form dimers and whether this is essential for the modulation of both catalytic activity and inhibitor sensitivity.

The PKA phosphorylation of PDE4A11 at Ser-119 within the UCR1 regulatory module confers the expected activation of catalytic activity and enhanced degradation of localised cAMP concentrations (Figure 3.11) [Wallace et al., 2005]. The current consensus of opinion is that only PKA phosphorylation of PDE4D3 is able to activate and induce conformation switching [Sette and Conti, 1996, Hoffmann et al., 1998 and MacKenzie et al., 2002]. This effect is a likely consequence of the unique properties of the PDE4D3 N-terminal region. Therefore, although all long form PDE4A isoforms to date have not shown altered rolipram inhibition following PKA phosphorylation, it would be remiss to discount PDE4A11 at this stage.

Finally, I have concluded that the PDE4A4B/PDE4A5 and PDE4A11 isoforms can interact directly with β-arrestin (Figures 3.16 and 4.20), an effect that is likely to be mediated through the conserved catalytic binding domains [Bolger et al., 2003 and Bolger et al., 2006]. As such, PDE4A isoforms have the potential to form complexes with the β-arrestin scaffold proteins and therefore, participate in critical events such a β_2-adrenoceptor G_s to G_i switching, desensitisation and internalisation, and the activation of the T-cell receptor [Perry et al., 2002, Baillie et al., 2003 and Abrahamsen et al., 2004].

Our current knowledge of the other PDE4A isoforms indicates that PDE4A11, over PDE4A4B and PDE4A10, may represent an attractive target for therapeutic intervention for disease states characterised by excessive immune and inflammatory responses, such as asthma, COPD and rheumatoid arthritis. From these data, the promotion of PDE4A11 for selective inhibition stems from its low transcript levels in the adult brain, reduced interaction with SH3 domain-containing proteins, and prevention of accretion foci formation upon chronic rolipram treatment, underlying its inability to form HARBS. PDE4A11 can also interact with β-arrestin indicating a potential role in β_2-adrenoceptor function and full T-cell receptor activation. Furthermore, its specific recruitment to membrane ruffles, perhaps utilising a PIP3 binding PH domain, may indicate a potential role in cell migration. Only in cells where endogenous expression of PDE4A11 is detected and available for siRNA knockdown can we truly define the physiological significance of PDE4A11 expression.

The expression and action of inflammatory cytokines is fundamental in the onset of the immune and inflammatory response against infection and tissue injury. The activation of the p38 MAPK cascade initiates pro-inflammatory cytokine expression, including TNFα, IFNγ and IL-1, and appropriately, inhibition prevents such gene transcription [Lee et al., 1994]. p38 MAPK is widely appreciated to play a key role in the regulation of various stages of the inflammatory response, including cell adhesion, diapedisis, O_2^- and ROS production, and release of elastase and metalloproteinase enzymes [Herlaar and Brown, 1999]. p38 MAPK inhibitors and inhibitors of their downstream substrates, specifically MAPKAPK2, are also being pursued as potential drugs for inflammatory disease states [Saklatvala, 2004].

A point of convergence of cAMP and p38 MAPK signalling pathways has been established in monocytes, where IFNγ activation of p38 MAPK was attenuated by PDE4 inhibition by rolipram [MacKenzie and Houslay, 2000]. This indicates intra-cellular cAMP is involved in controlling the activation state of p38 MAPK, although the authors do not address the mechanism of such regulation. IFNγ activation of p38 MAPK occurs through activation of the IFN

Type I receptor signalling cascade involving GEF activation, stimulation of Rac GDP/GTP exchange, and activation of the MAPK signalling cascade, as indicated in Figure 4.1 [Platanias, 2003].

The aim of the fourth chapter of this thesis was to probe a point of cross talk between these signalling cascades, by firstly exploring the possibility that p38 MAPK-dependent protein kinases could phosphorylate PDE4 isoforms, and secondly, identifying any functional effects this may bestow. Chapter 4 described the MAPKAPK2 phosphorylation of PDE4A5.

Cell over-expression of PDE4A5 and activation of the p38 MAPK phosphorylation cascade facilitated its phosphorylation by MAPKAPK2 (Figures 4.8 – 4.13). Phosphorylation occurring in the whole cell, in the presence of other p38 MAPK integrated signalling systems, indicates that PDE4A5 is an authentic substrate for MAPKAPK2. Functionally, MAPKAPK2 phosphorylation of PDE4A5 attenuates its ability to be activated by PKA phosphorylation and reduces its ability to interact with XAP2.

PDE4A5 is activated by PKA (Figure 4.14) [MacKenzie et al., 2002 and Bolger et al., 2003]. Phosphorylation of PDE4A5 by MAPKAPK2 exerts negligible effect upon catalytic activity (Figure 4.15), but activity changes consequent upon MAPKAPK2 phosphorylation of PDE4 long isoforms from the other gene families, in view of the fact that UCR1 is conserved, should not be discounted. However, if phosphorylation by MAPKAPK2 is allowed to occur before PKA phosphorylation is induced, then the onset and amplitude of PKA activation is attenuated (Figure 4.15). Indeed, if all long isoforms can be phosphorylated by MAPKAPK2 then it may attenuate the PKA-induced conformational switching of PDE4D3 to HARBS. Therefore, in cells where these signalling pathways are present, the timing of pathway activation will be crucial in the regulation of intra-cellular cAMP concentrations. But how does phosphorylation at Ser-147 confer such an effect? A similar effect has been observed with XAP2 and the authors proposed that XAP2 binding could either hamper the ability of the active catalytic units of PKA to access the UCR1 site, or that it disrupts the conformation of the intra-molecular interactions between

UCR1 and UCR2 [Bolger et al., 2003]. The true mechanism of both PKA activation and such attenuation of activation will only be explicitly understood on resolution of the crystal structure of a full-length PDE4 isoform.

One should consider the effect of potential AKAP interactions with PDE4A5. Recent studies have shown that AKAP1, AKAP3 (specific for PDE4A5 in spermatozoa [Bajpai et al., 2005]) and AKAP8 can interact with PDE4A isoforms in T-lymphocytes [Asirvatham et al., 2004]. The dissociation of an AKAP interaction from PDE4A5 upon MAPKAPK2 phosphorylation may spatially re-locate PKA to a distant compartment of the cell and attenuate PKA-mediated activation.

WAVE-1 has been assigned AKAP function and is involved in the regulation of the actin cytoskeleton [Westphal et al., 2000]. It is found in a complex with both WRP and Rac1, where WRP, a GAF protein, negatively regulates Rac1 function [Soderling and Scott, 2006]. WAVE-1 binds Arp2/3, a substrate for MAPKAPK2 [Singh et al., 2003], which catalyses the formation of actin resulting in cell cytoskeletal rearrangements. Such modifications will alter cell motility and cell migration. Evidence also exists for the regulation of Rac1 function by intra-cellular cAMP in many cells, including CHO cells, myocardial endothelial cells, and vascular smooth muscle [Pomerance et al., 2000, Waschke et al., 2005 and Pelletier et al., 2005]. However, there is no clear consensus across cell types whether cAMP positively or negatively regulates Rac1 function. WAVE-1 can also bind the Abl tyrosyl kinase, known to interact with MAPKAPK2 but poorly with PDE4A isoforms through SH3 domain interactions [Ben-Levy et al., 1995 and McPhee et al., 1999]. Therefore, given the multitude of proteins involved in this complex, it would be fascinating to explore the possibility that a PDE4A isoform could also be recruited and participate in the function and regulation of the actin cytoskeleton. This may then have functional consequences for cell migration and underlie some mechanism through which cAMP inhibits Rac1 function and attenuates actin modifications that enhance cell motility. Furthermore, the formation of PIP3 is key in the regulation of Rac1 function, and therefore PDE4A11, given its intra-cellular localisation in membrane ruffles (Figure 3.5),

may be appropriately positioned to control the activation state of Rac1 and influence cell motility.

Furthermore, the PDE4A1, PDE4A5 and PDE4A10 isoforms are endogenously expressed in similar brain regions to WAVE-1 [McPhee et al., 2001 and Taskén and Aandahl, 2004]. Targeted knock out of WAVE-1 in mice, the central molecule in this complex, or the associated Abi2 or WRP proteins, gives rise to mice with reduced motor function and a cognitive deficient phenotype [Soderling and Scott, 2006]. The PDE4 inhibitor rolipram has shown clinical benefit in a variety of CNS defects including depression, Parkinson's, Alzheimer's and cognitive enhancement [O'Donnell and Zhang, 2004 and Houslay et al., 2005]. Therefore, PDE4 inhibition and the disruption of cAMP signalling through the WAVE-1 signalling cassette may underlie some of the beneficial CNS effects.

XAP2 induces conformational switching upon interaction with PDE4A5, as indicated by differential rolipram inhibition [Bolger et al., 2003]. Utilising the Ser-147-Asp phospho-mimetic conferred no alteration in rolipram inhibition (Figure 4.17). Foci formation is hypothesised to be indicative of PDE4A4B conformational changes and is dependent upon protein synthesis [Terry et al., 2003]. Anisomycin has been shown to reduce foci formation but this effect should be confirmed on reversal with a p38 MAPK inhibitor, such as SB203580, because anisomycin can also act as a protein synthesis inhibitor as well as a p38 MAPK activator [S. Vadrevu and M.D. Houslay, unpublished observation]. Taken together, the above data suggests that the phosphorylation of PDE4A5 by MAPKAPK2 has a role to play in the stabilisation of PDE4A5 conformation.

Moreover, PDE4 enzymes have the ability to form homo-dimers through inter-molecular interactions spanning the C-terminal of UCR1 and the N-terminal of UCR2 [Richter and Conti, 2002]. Dimerisation is not affected by PDE4 phosphorylation by PKA, but is in fact a pre-requisite for activation to occur. Furthermore, disruption of dimerisation shifts affinity of PDE4D3 to LARBS and the authors postulated that dimerisation stabilised PDE4D3 in

HARBS. It would be interesting to elucidate if PDE4A5 can form homo-dimers and if the interaction was subject to modification upon MAPKAPK2 phosphorylation. If phosphorylation of PDE4A5 by MAPKAPK2 served to disrupt dimerisation, and it is appropriately positioned to do so given its location at the dimerisation interface, then this would provide yet further evidence for PDE4 conformation stabilisation. Indeed, MAPKAPK2 phosphorylation of HSP27 serves to disrupt HSP27 oligomers [Gaestel, 2006].

The outcome of these experiments may provide a compelling argument that the functional effect of MAPKAPK2 phosphorylation of PDE4 isoforms is to protect them from conformational change, which results in an increase in sensitivity to inhibition by rolipram. Subsequently, this would provide the first evidence, to my knowledge, of a PDE4 modification that stabilises the enzyme in LARBS. This would be of therapeutic benefit given that the formation of LARBS is proposed to underlie the beneficial effects of PDE4 inhibition with the formation of HARBS associated with the undesirable side effects.

Further experiments should be undertaken in T-cells to assess the physiological significance of MAPKAPK2 activation and PDE4A5 phosphorylation. T-cells are known contain all the relevant components to assess potential endogenous signalling cassettes, with which PDE4A4B/PDE4A5 may participate including Src tyrosyl kinases, AKAPs and β-arrestin [Abrahamsen et al., 2004 and Asirvatham et al., 2004]. PDE4 inhibition is known to regulate the function of the T-cell receptor in a PKA-dependent manner [Abrahamsen et al., 2004]. Activation of the TCR-CD3 induces an increase in intra-cellular cAMP concentrations and stimulation of PKA. Active PKA targets the Src tyrosyl kinase Csk, which negatively regulates Lck tyrosyl kinase activity, and attenuates T-cell activation. This is controlled by CD28-dependent recruitment of PDE4 through β-arrestin, which functions to lower cAMP and activate Lck tyrosyl kinase activity for full T-cell activation. One can then appreciate how PDE4 inhibition serves to down-regulate T-cell activation through enhancing the inhibitory Csk phosphorylation of Lck.

Furthermore, inhibition of PDE4 in T-cells has also been shown to suppress TNFα, IFNγ, IL-2, IL-4 and IL-5 expression, which are responsible for p38 MAPK activation and Th1-Th2 cell differentiation [Houslay et al., 2005]. Significant mRNA transcripts are detected for all PDE4A long isoforms with transcript levels in Th2 cells predominating over the corresponding Th1 cell transcripts [Wallace et al., 2005]. Potentially, this suggests that PDE4A expression may have a role in T-cell function, regulating the immune and inflammatory response [Bertrand, 2000 and Hart, 2001]. Therefore, this would be an intriguing system to assess any physiological role of MAPKAPK2 phosphorylation upon T-cell function. MAPKAPK2 phosphorylation does not affect the PDE4A5 interaction with β-arrestin (Figure 4.19) but whether this is consistent with PDE4D5 remains to be ascertained.

XAP2 is known to confer a partial, non-competitive, inhibitory effect upon PDE4A5, with maximal inhibition of approximately 60% and an IC_{50} of 120nM [Bolger et al., 2003]. Phosphorylation of PDE4A5 reduces the interaction by approximately 50% (Figure 4.20), and therefore one is tempted to suggest that inhibition of PDE4A5 would be relieved and returned to some 70% of its native activity.

In the context of the inflammation, where p38 MAPK is active and controlling several stages of the response, relief of PDE4A5 inhibition by XAP2 and the concomitant lowering of cAMP levels will function to exacerbate the inflammatory reaction.

The AhR and PPARα are both ligand-activated intra-cellular receptors that directly bind to DNA and influence gene transcription. The endogenous expression of both receptors occurs in lung epithelial cells [Patel et al., 2003 and Teske et al., 2005]. The major risk factor in the development of COPD, defined as an irreversible and progressive restriction of airflow coupled with an abnormal lung inflammatory response, is exposure to noxious gases and particles, and in particular, cigarette smoke [Anderson and Bozinovski, 2003]. Lung AhRs are activated by dioxin and poly-aromatic hydrocarbons and results in increased neutrophil recruitment and the onset of an excessive

inflammatory response [Martinez et al., 2002 and Teske et al., 2005]. Activation of PPARα attenuates inflammatory mediator release, e.g. GM-CSF, IL-6, and adhesion molecule expression, and PPARα$^{(-/-)}$ mice develop an excessive inflammatory reaction phenotype [Staels et al., 1998 and Delerive et al., 1999]. XAP2 is an important component of both receptors and serves to confer both cytoplasmic stability and repression of gene transcription [Meyer and Perdew, 1999 and Sumamasekera et al., 2003]. Therefore, one can appreciate the beneficial role of such effects in the onset of the inflammatory response in COPD. Given the established ability of cAMP to attenuate the inflammatory response by a variety of mechanisms the partial inhibitory effect of XAP2 upon PDE4A5 activity further promotes the beneficial effects of XAP2 expression [Bolger et al., 2003]. Furthermore, PDE4A4B expression is up-regulated in smokers irrespective of their COPD status [Barber et al., 2004]. XAP2 inhibition of PDE4A4B may provide some protective or compensatory mechanism to the increased expression.

In the context of cancer cell proliferation there is a growing body of evidence to suggest that XAP2 is an important tumour suppressor protein. Very recently the role of XAP2 as a tumour suppressor has been identified in a study population from Finland, where mutations in XAP2 conferred susceptibility to pituitary adenomas [Vierimaa et al., 2006]. PPARα activation causes hypertrophy of the liver and hepatocyte proliferation, but interaction with XAP2 represses PPARα-mediated gene transcription [Sumamasekera et al., 2003].

MAPKAPK2 participates in the control of cell cycle regulation at both G_1/S phase and G_2/M phase [Gaestel, 2006]. At G_1/S phase, ubiquitin-mediated degradation of the p53 tumour suppressor occurs via MAPKAPK2 activation of HDM2 E3 ubiquitin ligase [Weber et al., 2006]. Phosphorylation and activation of the Cdc25B phosphatase, which is a critical checkpoint for G_2/M phase, is also mediated by MAPKAPK2. In prostate cancer, activation of MAPKAPK2, the phosphorylation of HSP27 and activation of matrix metalloproteinase 2 are necessary for cell invasion and metastasis [Xu et al., 2006].

Consistent with these observations of XAP2 as a tumour suppressor, the activation of MAPKAPK2 in the control of the cell cycle and the maintenance intra-cellular cAMP inducing cell cycle arrest and apoptosis, is the inhibitory effect of XAP2 on PDE4A5 activity [Houslay et al., 2005].

PDE4A5 is phosphorylated by MAPKAPK2 and here I have proposed that the integration of the cAMP and p38 MAPK signalling pathways has potential physiological significance in the control of PDE4 activity. Of interest for follow-up experiments is the hypotheses that (1) phosphorylation may confer stability of PDE4 conformation in LARBS, (2) experiments in T-cells may provide novel insight into the physiological significance of PDE4A5 phosphorylation and the interaction with AKAPs and (3) that PDE4 isoforms may be part of the WAVE-1 AKAP complex, where this scaffold protein controls the recruitment of PDE4A5 to MAPKAPK2 and the rearrangement of the actin cytoskeleton.

The production of O_2^- and ROS is a key factor in the innate immune response, and when this response is impaired, e.g. CGD, the host has increased susceptibility to infection [Vignais, 2000]. The characterisation of the oxidative or respiratory burst process has focussed upon phagocytic cells, where these cells engulf and subsequently destroy, through ROS production and protease release, invading micro-organisms, and also scavenge damaged and senescent cells. However, it is now widely appreciated that similar systems for the production of ROS are present in non-phagocytic cells, including the lung and the heart [Bokoch and Knaus, 2003]. The generation of O_2^- and ROS is generally a controlled process, but when this control is compromised excessive O_2^- and ROS can underlie the pathogenesis of a variety of disease states, including COPD and cardiac hypertrophy [Anderson and Bovinovski, 2003 and Murdoch et al., 2006].

Cardiac myocyte hypertrophy is an adaptive response of the heart to excessive exertion in an attempt to maintain optimal function. However, coupled with this response is the increased likelihood of arrhythmia and congestive heart failure. In cardiac myocytes, angiotensin II treatment

increases the production of O_2^- and induces the onset of cardiac hypertrophy [Nakamura, et al., 1998 and Nakagami et al., 2003]. These effects are dependent upon O_2^- production and can be diminished with anti-oxidant treatment.

PDE4 inhibition attenuates the production of O_2^- in many phagocytic cells, but how this is achieved and whether it translates to non-phagocytic cells is poorly understood [Hatzelmann and Schudt, 2001, Bokoch and Knaus, 2003 and Jacob et al., 2004]. What is appreciated though is that part of the inhibitory mechanism in phagocytic cells is PKA-dependent [Bengis-Garber and Gruener, 1996 and Lin et al., 2004].

The membrane translocation of p47-*phox* is a pre-requisite for NADPH oxidase activation and represents the rate-limiting step in enzyme assembly. In CGD, where p47-*phox* is deficient, the remaining cytosolic components are unable to translocate to the membrane [Sheppard et al., 2005]. p47-*phox* exists in an auto-inhibited state at rest and the inhibitory constraint is relieved upon multiple, preferential and sequential phosphorylation by an extensive array of protein kinases [Johnson et al., 1998, Inanami et al., 1998, Babior, 1999, Hoyal et al., 2003, Massenet et al., 2005 and Mitzuki et al., 2005]. The p47-*phox* structural rearrangement conferred following phosphorylation exposes the appropriate domains for p40-*phox* and p67-*phox*/Rac2-GTP recruitment and membrane association [Groemping and Rittinger, 2005].

The work presented in Chapter 5 proposed that a possible mechanism exists in cardiac myocytes, where increasing intra-cellular cAMP concentrations may serve to attenuate the production of O_2^- and ROS via a PKA-dependent mechanism. This hypothesis is based upon the observations that p47-*phox* was directly phosphorylated by PKA within the C-terminal SH3 domain-containing regions responsible for promoting p47-*phox* translocation (Figure 5.3), and that p47-*phox* expression at the membrane of cardiac myocytes was increased with angiotensin II, ablated with co-incubation of forskolin and rolipram, and partially rescued with the PKA inhibitor, H89 (Figure 5.6). Furthermore, the direct interaction of p47-*phox* with both

PDE4A4B and PDE4A10, and p67-*phox* specifically with PDE4A4B, indicated that PDE4 could play a critical role in controlling the PKA phosphorylation state of *phox* proteins (Figure 5.4).

From this preliminary work to address how PDE4 inhibition attenuates O_2^- and ROS production in cardiac myocytes, there are fundamental experiments required to elucidate the precise mechanism.

Site-directed mutagenesis of the putative PKA phosphorylation sites identified from the peptide array experiments should be generated and used to confirm the target site(s) in vitro. However, given the promiscuous nature of in vitro phosphorylation assays, the phosphorylation, and subsequent attenuation of phosphorylation, should also be confirmed in vivo, in a similar manner to the MAPKAPK2 phosphorylation of PDE4A5.

Future experiments should also confirm the PDE4 specificity of the p47-*phox* interaction by co-immuno-precipitation. Experiments should also extend the use of peptide array technology utilising the alanine scanning technique to identify the critical residues involved in each protein [Bolger et al., 2006]. Although from these initial experiments the use of SH3 domain interactions is excluded, it will be intriguing to determine whether p47-*phox* competes with other proteins for interaction with PDE4 isoforms, e.g. XAP2 or PDE4 dimerisation, and whether the interactions confer any functional effect upon PDE4 catalytic activity.

Initial experiments indicated that p67-*phox* showed interaction specificity with PDE4A4B, perhaps through TPR-mediated interactions, and the relevance of this interaction should not be overlooked. If the interaction between p67-*phox* and PDE4A4B was mediated through TPR domains, in an analogous manner to XAP2, then one could hypothesise p67-*phox* to confer inhibition of PDE4 activity, maintaining intra-cellular cAMP concentrations and preventing *phox* protein translocation. On activation of p38 MAPK-MAPKAPK2 signalling, a known activator of NADPH oxidase, MAPKAPK2 phosphorylation of PDE4A4B may promote the dissociation of p67-*phox* and

up-regulation of PDE4A4B activity to attenuate PKA activation, preventing inhibition of NADPH oxidase complex formation at the plasma membrane.

Given the attenuation of p47-*phox* translocation upon PDE4 inhibition, siRNA knockdown of endogenous PDE4 expression will facilitate the identification of the functionally relevant PDE4 isoform [Lynch et al., 2005].

Finally, experiments are certainly required to confirm the attenuation of p47-*phox* translocation following increases in intra-cellular cAMP concentrations does indeed translate to a reduction in O_2^- and ROS generation, perhaps using 2', 7'-dichlorofluorescein diacetate [Nakamura et al., 1998 and Nakagami et al., 2003]. As an indicator of cardiac hypertrophy, the measurement of cardiac myocyte surface area or incorporation of [^{3}H]-leucine experiments could be undertaken.

The work in this thesis forms three distinct chapters, (1) the characterisation of the novel PDE4A11 isoform, (2) the phosphorylation of PDE4A5 by MAPKAPK2, and (3) the participation of the cAMP-PKA-PDE4 signalling module in the control of NADPH oxidase function. However, it is entirely possible that PDE4A11, possibly the most abundantly expressed PDE4A isoform, is also a target for MAPKAPK2 phosphorylation and that the activation of p38 MAPK signalling may connect, regulate and allow interplay between these signalling pathways.

Chapter 7 References

Abrahamsen, H., Baillie, G., Ngai, J., Vang, T., Nika, K., Ruppelt, A., Mustelin, T., Zaccolo, M., Houslay, M. and Taskén, K. TCR- and CD28-Mediated Recruitment of Phosphodiesterase 4 to Lipid rafts Potentiates TCR Signaling. *J. Immunol.* 2004; **173:** 4847-4858.

Ahn, S., Shenoy, S.K., Wei, H. and Lefkowitz, R.J. Differential Kinetic and Spatial Patterns of β-Arrestin and G Protein-mediated ERK Activation by the Angiotensin II Receptor. *J. Biol. Chem.* 2004; **279:** 35518-35525.

Alexander, R.P., Warrellow, G.J., Eaton, M.A.W., Boyd, E.C., Head, J.C., Porter, J.R., Brown, J.A., Reuberson, J.T., Hutchison, B., Turner, P., Boyce, B., Barnes, D., Mason, B., Cannell, A., Taylor, R.J., Zomaya, A., Millican, A., Leonard, J., Morphy, R., Wales, M., Perry, M., Allen, R.A., Gozzard, N., Hughes, B. and Higgs, G. CDP840. A Prototype of a Novel Class of Orally Active Anti-Inflammatory Phosphodiesterase 4 Inhibitors. *Bioorg. Med. Chem.* 2002; **12:** 1451-1456.

Anderson, G.P. and Bozinovski, S. Acquired somatic mutations in the molecular pathogenesis of COPD. *Trends. Pharmacol. Sci.* 2003; **24:** 71-76.

Ariga, M., Neitzert, B., Nakae, S., Mottin, G., Bertrand, C., Pruniaux, M.P., Jin, S.L. and Conti, M. Nonredundant Function of Phosphodiesterases 4D and 4B in Neutrophil Recruitment to the Site of Inflammation. *J. Immunol.* 2004; **173:** 7531-7538.

Asirvatham, A.L., Galligan, S.G., Schillace, R.V., Davey, M.P., Vasta, V., Beavo, J.A. and Carr, D.W. A-Kinase Anchoring Proteins Interact with Phosphodiesterases in T Lymphocyte Cell Lines. *J. Immunol.* 2004; **173:** 4806-4814.

Babior, B.M. NADPH Oxidase: An Update. *Blood.* 1999; **93:** 1464-1476.

Badger, A.M., Bradbeer, J.N., Votta, B., Lee, J.C., Adams, J.C. and Griswold, D.E. Pharmacological profile of SB203580, a selective cytokine suppressive binding protein/p38kinase, in animal models of arthritis, bone resorption, endotoxin shock and immune function. *J. Pharmacol. Exp. Ther.* 1996; **279:** 1453-1461.

Baillie, G.S. and Houslay, M.D. Arrestin times for compartmentalised cAMP signalling and phosphodiesterase-4 enzymes. *Curr. Opin. Cell Biol.* 2005; **17:** 129-134.

Baillie, G.S., Huston, E., Scotland, G., Hodgkin, M., Gall, I., Peden, A.H., MacKenzie, C., Houslay, E.S., Currie, R., Pettitt, T.R., Walmsley, A.R., Wakelam, M.J.O., Warwicker, J. and Houslay, M.D. TAPAS-1, a Novel Microdomain within the Unique N-terminal Region of the PDE4A1 cAMP-specific Phosphodiesterase That allows Rapid Ca^{2+}-triggered Membrane Association with Selectivity for Interaction with Phosphatidic Acid. *J. Biol. Chem.* 2002; **277:** 28298-28309.

Baillie, G.S., MacKenzie, S.J. and Houslay, M.D. Phorbal 12-myristate 13-acetate Triggers the Protein Kinase A-Mediated Phosphorylation and Activation of the PDE4D5 cAMP Phosphodiesterase in Human Aortic Smooth Muscle Cells through a Route Involving Extracellular Signal Regulated Kinase (ERK). *Mol. Pharmacol.* 2001; **60:** 1100-1111.

Baillie, G.S., MacKenzie, S.J., McPhee, I. and Houslay, M.D. Sub-family selective actions of Erk2 MAP kinase to phosphorylate and regulate the activity of PDE4 cyclic AMP-specific phosphodiesterases. *Br. J. Pharmacol.* 2000; **131:** 811-819.

Baillie, G.S., Scott, J.D. and Houslay, M.D. Compartmentalisation of phosphodiesterases and protein kinase A: opposites attract. *FEBS Lett.* 2005; **579:** 3264-3270.

Baillie, G.S., Sood, A., McPhee, I., Gall, I., Perry, S.J., Lefkowitz, R.J. and Houslay, M.D. β-Arrestin-mediated PDE4 cAMP phosphodiesterase recruitment regulates β-adrenoceptor switching from G_s to G_i. *Proc. Natl. Acad. Sci.* 2003; **100:** 940-945.

Bajpai, M., Fiedler, S.E., Huang, Z., Vijayaraghavan, S., Olson, G.E., Livera, G., Conti, M. and Carr, D.W. AKAP3 Selectively Binds PDE4A Isoforms in Bovine Spermatozoa. *Biol. Reprod.* 2006; **74:** 109-118.

Balmanno, K., Millar, T., McMahon, M. and Cook, S.J. ΔRaf-1:ER Bypasses the Cyclic AMP Block of Extracellular Signal-Regulated Kinase 1 and 2 Activation but Not CDK2 Activation or Cell Cycle Reentry. *Mol. Cell. Biol.* 2003; **23:** 9303-9317.

Banan, M. and Puri, N. The Ins and Outs of RNAi in Mammalian Cells. *Curr. Pharm. Biotechnol.* 2004; **5:** 441-450.

Barber, R., Baillie, G.S., Bergmann, R., Shepherd, M.C., Sepper, R., Houslay, M.D. and Van Heeke, G. Differential expression of PDE4 cAMP phosphodiesterase isoforms in inflammatory cells of smokers with COPD, smokers without COPD, and nonsmokers. *Am. J. Physiol. Lung Cell Mol. Physiol.* 2004; **287:** L332-L343.

Barros, J.C. and Marshall, C.J. Activation of either ERK1/2 or ERK5 MAP kinase pathways can lead to disruption of the actin cytoskeleton. *J. Cell Sci.* 2005; **118:** 1663-1671.

Beard, M.B., Huston, E., Campbell, L., Gall, I., McPhee, I., Yarwood, S., Scotland, G. and Houslay, M.D. In addition to the SH3 binding region, multiple regions within the N-terminal noncatalytic portion of the cAMP-specific phosphodiesterase, PDE4A5, contribute to its intracellular targeting. *Cell. Signal.* 2002; **14:** 453-465.

Beard, M.B., O'Connell, J.C., Bolger, G.B. and Houslay, M.D. The unique N-terminal domain of the cAMP-specific phosphodiesterase PDE4D4 allows for interaction with specific SH3 domains. *FEBS Lett.* 1999; **460:** 173-177.

Beard, M.B., Olsen, A.E., Jones, R.E., Erdogan, S., Houslay, M.D. and Bolger, G.B. UCR1 and UCR2 Domains Unique to the cAMP-specific Phosphodiesterase Family Form a Discrete Module via Electrostatic Interactions. *J. Biol. Chem.* 2000; **275:** 10349-10358.

Beavo, J.A. and Brunton, L.L. Cyclic nucleotide research – still expanding after half a century. *Nature Rev. Mol. Cell Biol.* 2002; **3:** 710-718.

Beazely, M.A. and Watts, V.J. Regulatory properties of adenylate cyclases type 5 and 6: A progress report. *Eur. J. Pharmamcol.* 2006; **535:** 1-12.

Bengis-Garber, C. and Gruener, N. Protein Kinase A Downregulates the Phosphorylation of p47 Phox in Human Neutrophils: A Possible Pathway for Inhibition of the Respiratory Burst. *Cell. Signal.* 1996; **8:** 291-296.

Ben-Levy, R., Hooper, S., Wilson, R., Paterson, H.F. and Marshall, C.J. Nuclear export of the stress-activated protein kinase p38 mediated by its substrate MAPKAP kinase-2. *Curr. Biol.* 1998; **8:** 1049-1057.

Ben-Levy, R., Leighton, I.A., Doza, Y.N., Attwood, P., Morrice, N., Marshall, C.J. and Cohen, P. Identification of novel phosphorylation sites required for activation of MAPKAP kinase-2. *EMBO J.* 1995; **14:** 5920-5930.

Bertrand, C.P. Asthma: where beyond steroids? *Curr. Opin. Chem. Biol.* 2000; **4:** 407-411.

Berwick, D.C. and Tavaré, J.M. Identifying protein kinase substrates: hunting for the organ-grinder's monkey. *Trends Biochem. Sci.* 2004; **29:** 227-232.

Biondi, R.M. and Nebreda, A.R. Signalling specificity of Ser/Thr protein kinases through docking-site-mediated interactions. *Biochem. J.* 2003; **372:** 1-13.

Bokoch, G.M. and Knaus, U.G. NADPH oxidases: not just for leukocytes anymore! *Trends Biochem. Sci.* 2003; **28:** 502-508.

Bolger, G.B., Baillie, G.S., Li, X., Lynch, M.J., Herzyk, P., Mohamed, A., Mitchell, L.H., McCahill, A., Hundsrucker, C., Klussmann, E., Adams, D.R. and Houslay M.D. Scanning peptide array analyses identify overlapping binding sites for the signaling scaffold proteins, β-arrestin and RACK1 in the cAMP-specific phosphodiesterase PDE4D5. *Biochem. J.* 2006; **398:** 23-36.

Bolger, G.B., Erdogan, S., Jones, R.E., Loughney, K., Scotland, G., Hoffmann, R., Wilkinson, I., Farrell, C. and Houslay, M.D. Characterization of five different proteins produced by alternatively spliced mRNAs from the human cAMP-specific phosphodiesterase PDE4D gene. *Biochem. J.* 1997; **328:** 539-548.

Bolger, G.B., McCahill, A., Huston, E., Cheung, Y.F., McSorley, T., Baillie, G.S. and Houslay, M.D. The Unique Amino-terminal of the PDE4D5 cAMP Phosphodiesterase Isoform Confers Preferential Interaction with β-Arrestins. *J. Biol. Chem.* 2003; **278:** 49230-49238.

Bolger, G.B., McPhee, I. and Houslay, M.D. Alternative Splicing of cAMP-specific Phosphodiesterase mRNA Transcripts. *J. Biol. Chem.* 1996; **2:** 1065-1071.

Bolger, G.B., Michaeli, T., Martins, T., St. John, T., Steiner, B., Rodgers, L., Riggs, M., Wigler, M. and Ferguson, K. A Family of Human Phosphodiesterases Homologous to the *dunce* Learning and Memory Gene Product of *Drosophila melanogaster* Are Potential targets for Antidepressant Drugs. *Mol. Cell Biol.* 1993; **13:** 6558-6571.

Bolger, G.B., Peden, A.H., Steele, M.R., MacKenzie, C., McEwan, D.G., Wallace, D.A., Huston, E., Baillie, G.S. and Houslay, M.D. Attenuation of the Activity of the cAMP-specific Phosphodiesterase PDE4A5 by Interaction with the Immunophilin XAP2. *J. Biol. Chem.* 2003; **278:** 33351-33363.

Bolger, G.B., Rodgers, L. and Riggs, M. Differential CNS expression of alternative mRNA isoforms of the mammalian genes encoding cAMP-specific phosphodiesterases. *Gene.* 1994; **149**: 237-244.

Bos, J.L. Epac: a new cAMP target and new avenues in cAMP research. *Nat. Rev. Mol. Cell Biol.* 2003; **4:** 733-738.

Bradford, M.M. A rapid and sensitive method for the quantification of microgram quantities of protein utilizing the principle of protein-dye binding. *Anal. Biochem.* 1976; **72:** 248-254.

Bradley, J., Reisert, J. and Frings, S. Regulation of cyclic nucleotide-gated channels. *Curr. Opin. Neurobiol.* 2005; **15:** 343-349.

Breitwieser, G.E. G Protein-Coupled Receptor Oligomerization: Implications for G Protein Activation and Cell Signaling. *Circ. Res.* 2004; **94:** 17-27.

Brown, G.E., Stewart, M.Q., Bissonnette, S.A., Elia, A.E.H., Wilker, E. and Yaffe, M.B. Distinct Ligand-dependent Roles for p38 MAPK in Priming and Activation of the Neutrophil NADPH Oxidase. *J. Biol. Chem.* 2004; **279:** 27059-27068.

Brunton, L.L. PDE4: Arrested at the Border. Sci. STKE. 2003; pe44.

Bundey, R.A. and Insel, P.A. Discrete Intracellular Signaling Domains of Soluble Adenylyl Cyclase: Camps of cAMP? *Sci. STKE.* 2004; **19:** 1-3.

Bundschuh, D.S., Eltze, M., Barsig, J., Wollin, L., Hatzelmann, A. and Beume, R. In Vivo Efficacy in Airway Disease Models of Roflumilast, a Novel Orally Active PDE4 Inhibitor. *J. Pharmacol. Exp. Ther.* 2001; **297:** 280-290.

Burnouf, C. and Pruniaux, M.P. Recent Advances in PDE4 Inhibitors as Immunoregulators and Anti-Inflammatory Drugs. *Curr. Pharm. Design.* 2002; **8:** 1255-1296.

Cahill, M.A., Janknecht, R. and Nordheim, A. Signalling pathways: Jack of all cascades. *Curr. Biol.* 1996; **6:** 16-19.

Carlisle Michel, J.J., Dodge, K.L., Wong, W., Mayer, N.C., Langeberg, L.K. and Scott, J.D. PKA-phosphorylation of PDE4D3 facilitates the recruitment of the mAKAP signalling complex. *Biochem. J.* 2004; **381:** 587-592.

Chen, L., Janetopoulos, C., Huang, Y.E., Iijima, M., Borleis, J. and Devreotes, P.N. Two Phases of Actin Polymerisation Display Different Dependencies on PI(3,4,5)P3 Accumulation and Have Unique Roles during Chemotaxis. *Mol. Biol. Cell.* 2003; **14:** 5028-5037.

Chen, L. and Kass, R.S. A-kinase anchoring proteins: different partners, different dance. *Nature Cell Biol.* 2005; **7:** 1050-1051.

Chowdhury, A.K., Watkins, T., Parinandi, N.L., Saatian, B., Kleinberg, M.E., Usatyuk, P.V. and Natarajan, V. Src-mediated Tyrosine Phosphorylation of $p47^{phox}$ in Hyperoxia-induced Activation of NADPH Oxidase and Generation of Reactive Oxygen Species in Lung Endothelial Cells. *J. Biol. Chem.* 2005; **280:** 20700-20711.

Christensen, A.E., Selheim, F., de Rooij, J., Dremier, S., Schwede, F., Dao, K.K., Martinez, A., Maenhaut, C., Bos, J.L., Genieser, H.G. and Døskeland, S.O. cAMP Analog Mapping of Epac1 and cAMP Kinase. *J. Biol. Chem.* 2003; **278:** 35394-35402.

Colledge, M. and Scott, J.D. AKAPs: from structure to function. *Trends Cell Biol.* 1999; **9:** 216-221.

Conti, M., Richter, W., Méhats, C., Livera, G., Park, J.Y. and Jin, C. Cyclic AMP-specific PDE4 Phosphodiesterases as Critical Components of Cyclic AMP Signaling. *J. Biol. Chem.* 2003; **278:** 5493-5496.

Cooper, D.M.F. Regulation and organization of adenylyl cyclases and cAMP. *Biochem. J.* 2003; **375:** 517-529.

Corbin, J.D. and Francis, S.H. Cyclic GMP Phosphodiesterase-5: Target for Sildenafil. *J. Biol. Chem.* 1999; **274:** 13729-13732.

Cowan, K.J. and Storey, K.B. Mitogen-activated protein kinases: new signaling pathways functioning in cellular responses to environmental stress. *J. Exp. Biol.* 2003; **206:** 1107-1115.

Cuenda, A., Rouse, J., Doza, Y.N., Meier, R., Cohen, P., Gallagher, T.F., Young, P.R. and Lee, J.C. SB 203580 is a specific inhibitor of a MAP kinase homologue which is stimulated by cellular stresses and interleukin-1. *FEBS Lett.* 1995; **364;** 229-233.

Dang, P.M.C., Stensballe, A., Boussetta, T., Raad, H., Dewas, C., Kroviarski, Y., Hayem, G., Jensen, O.N., Gougerot-Pocidalo, M.A. and El-Benna, J. A specific $p47^{phox}$-serine phosphorylated by convergent MAPKs mediates neutrophil NADPH oxidase priming at inflammatory sites. *J. Clin. Invest.* 2006; **116:** 2033-2043.

Daniel, P.B., Walker, W.H. and Habener, J.F. Cyclic AMP Signaling and Gene Regulation. *Annu. Rev. Nutr.* 1998; **18:** 353-383.

Daum, G., Eisenmann-Tappe, I., Fries, H.W., Troppmair, J. and Rapp, U.R. The ins and outs of Raf kinases. *Trends. Biochem. Sci.* 1994; **19:** 474-479.

Davies, S.P., Reddy, H., Caivano, M. and Cohen, P. Specificity and mechanism of action of some commonly used protein kinase inhibitors. *Biochem. J.* 2000; **351:** 95-105.

Davis, R.L., Takayasu, H., Eberwine, M. and Myres, J. Cloning and characterization of mammalian homologs of the *Drosophila* dunce^{+} gene. *Proc. Natl. Acad. Sci.* 1989; **86:** 3604-3608.

Deak, M., Clifton, A.D., Lucocq, J. and Alessi, D.R. Mitogen- and stress-activated protein kinase-1 (MSK1) is directly activated by MAPK and SAPK2/p38, and may mediate activation of CREB. *EMBO J.* 1998; **17:** 4426-4441.

Delerive, P., De Bosscher, K., Besnard, S., Vanden Berge, W., Peters, J.M., Gonzalez, F.J., Fruchart, J.C., Tedgui, A., Haegeman, G. and Staels, B. Peroxisome Proliferators-activated Receptor α Negatively Regulates the Vascular Inflammatory Gene Response by Negative Cross-talk with Transcription Factors NF-κB and AP-1. *J. Biol. Chem.* 1999; **274:** 32048-32054.

Delghandi, M.P., Johannessen, M. and Moens, U. The cAMP signalling pathway activates CREB through PKA, p38 and MSK1 in NIH 3T3 cells. *Cell. Signal.* 2005; **17:** 1343-1351.

Dent, P., Yacoub, A., Fisher, P.M., Hagan, M.P. and Grant, S. MAPK pathways in radiation responses. *Oncogene.* 2003; **22:** 5885-5896.

de Rooij, J., Rehmann, H., van Triest, M., Cool, R.H., Wittinghofer, A. and Bos, J.L. Mechanism of Regulation of the Epac Family of cAMP-dependent RapGEFs. *J. Biol. Chem.* 2000; **275:** 20829-20836.

de Rooij, J., Zwartkruis, F.J.T., Verheijen, M.H.G., Cool, R.H., Nijman, S.M.B., Wittinghofer, A. and Bos, J.L. Epac is a Rap1 guanine-nucleotide-exchange factor directly activated by cAMP. *Nature.* 1998; **396:** 474-477.

Ding, Q., Gros, R., Gray, I.D., Taussig, R., Ferguson, S.S.G. and Feldman, R.D. Raf Kinase Activation of Adenylyl Cyclases: Isoform-Selective Regulation. *Mol. Pharmacol.* 2004; **66:** 921-928.

Doble, B.W. and Woodgett, J.R. GSK-3: tricks of the trade for a multi-tasking kinase. *J. Cell. Sci.* 2003; **116:** 1175-1186.

Dodeller, F. and Schulze-Koops, H. The p38 mitogen-activated protein kinase signaling cascade in CD4 T cells. *Arthritis Res. Ther.* 2006; **8:** 205-215.

Dodge, K.L., Khouangsathiene, S., Kapiloff, M.S., Mouton, R., Hill, E.V., Houslay, M.D., Langeberg, L.K. and Scott, J.D. mAKAP assembles a protein kinase A/PDE4 phosphodiesterase cAMP signaling module. *EMBO J.* 2001; **20:** 1921-1930.

Dodge-Kafka, K.L., Soughayer, J., Pare, G.C., Carlisle Michel, J.C., Langeberg, L.K., Kapiloff, M.S. and Scott, J.D. The protein kinase A anchoring protein mAKAP coordinates two integrated cAMP effector pathways. *Nature.* 2005; **437:** 574-578.

Dong, C., Davis, R.J. and Flavell, R.A. MAP Kinases in the Immune Response. *Annu. Rev. Immunol.* 2002; **20:** 55-72.

Dostal, D.E., Rothblum, K.N., Conrad, K.M., Cooper, G.R. and Baker, K.M. Detection of angiotensin I and II in cultured rate cardiac myocytes and fibroblasts. *Am. J. Physiol.* 1992; **263:** C851-C863.

Doughman, R.L., Firestone, A.J., Wojtasiak, M.L., Bunce, M.W. and Anderson, R.A. Membrane Ruffling Requires Coordination between Type Iα Phosphatidylinositol Phosphate Kinase and Rac Signaling. *J. Biol. Chem.* 2003; **278:** 23036-23045.

Dransfield, D.T., Bradford, A.J., Smith, J., Martin, M., Roy, C., Mangeat, P.H. and Goldenring, J.R. Ezrin is a cyclic AMP-dependent protein kinase anchoring protein. *EMBO J.* 1997; **16:** 35-43.

D'Sa, C., Eisch, A.J., Bolger, G.B. and Duman, R.S. Differential expression and regulation of the cAMP-selective phosphodiesterase type 4A splice variants in rat brain by chronic antidepressant administration. *Eur. J. Neurosci.* 2005; **22:** 1463-1475.

Durand, D., Cannella, D., Dubosclard, V., Pebay-Peyroula, E., Vachette, P. and Fieschi, F. Small-Angle X-ray Scattering Reveals an Extended Organization for the Autoinhibitory Resting State of the $p47^{phox}$ Modular protein. *Biochemistry.* 2006; **45:** 7185-7193.

El Benna, J., Han, J., Park, J.W., Schmid, E., Ulevitch, R.J. and Babior, B.M. Activation of p38 in Stimulated Human Neutrophils: Phosphorylation of the Oxidase Component p47phox by p38 and ERK but Not by JNK. *Arch. Biochem. Biophys.* 1996; **334:** 395-400.

Engels, P., Abdel'Al, S., Hulley, P. and Lubbert, H. Brain distribution of four rat homologues of the Drosophila dunce cAMP phosphodiesterase. *J. Neurosci. Res.* 1995; **41:** 169-178.

Erdogen, S. and Houslay, M.D. Challenge of human Jurkat T-cells with the adenylate cyclase activator forskolin elicits major changes in cAMP phosphodiesterase (PDE) expression by up-regulating PDE3 and inducing PDE4D1 and PDE4D2 splice variants as well as down-regulating a novel PDE4A splice variant. *Biochem. J.* 1997; **321:** 165-175.

Espanel, X. and Hooft van Huijsduijnen, R. Applying the SPOT peptide synthesis procedure to the study of protein tyrosine phosphatase substrate specificity: probing for the heavenly match in vitro. *Methods.* 2005; **35:** 64-72.

Esteban, J.A. AMPA Receptor Trafficking: A Road Map for Synaptic Plasticity. *Mol. Interventions.* 2003; **3:** 375-385.

Esteban, J.A., Shi, S.H., Wilson, C., Nuriya, M., Huganir, R.L. and Malinow, R. PKA phosphorylation of AMPA receptor subunits controls synaptic trafficking underlying plasticity. *Nat. Neurosci.* 2003; **6:** 136-143.

Fang, X., Yu, S.X., Lu, Y., Bast Jr, R.C., Woodgett, J.R. and Mills, G.B. Phosphorylation and inactivation of glycogen synthase 3 by protein kinase A. *Proc. Natl. Acad. Sci.* 2000; **97:** 11960-11965.

Fleming, Y.M., Frame, M.C. and Houslay, M.D. PDE4-regulated cAMP degradation controls the assembly of integrin-dependent actin adhesion structures and REF52 cell migration. *J. Cell Sci.* 2004; **117:** 2377-2388.

Francis, S.H., Turko, I.V. and Corbin, J.D. Cyclic Nucleotide Phosphodiesterases: Relating Structure and Function. *Prog. Nucleic Acid Res. Mol. Biol.* 2001; **69:** 1-52.

Frank, R. The SPOT-synthesis technique. Synthetic peptide arrays on membrane supports – principles and applications. *J. Immunol. Methods* 2002; **267:** 13-26.

Fraser, I.D.C, Cong, M., Kim, J., Rollins, E.N., Daaka, Y., Lefkowitz, R.J. and Scott, J.D. Assembly of an A kinase-anchoring protein-β_2-adrenergic receptor complex facilitates receptor phosphorylation and signaling. *Curr. Biol.* 2000; **10:** 409-412.

Freshney, N.W., Rawlinson, L., Guesdon, F., Jones, E., Cowley, S., Hsuan, J. and Saklatvala, J. Interleukin-1 activates a novel protein kinase cascade that results in the phosphorylation of Hsp27. *Cell.* 1994; **78:** 1039-1049.

Fukunaga, R. and Hunter, T. MNK1, a new MAP kinase-activated protein kinase, isolated by a novel expression screening method for identifying protein kinase substrates. *EMBO J.* 1997; **16:** 1921-1933.

Gaestel, M. MAPKAP kinases – MKs – two's company, three's a crowd. *Nat. Rev. Mol. Cell Biol.* 2006; **7:** 120-130.

Giembycz, M.A. Development status of second generation PDE4 inhibitors for asthma and COPD: the story so far. *Monaldi. Arch. Chest. Dis.* 2002; **57:** 48-64.

Giembycz, M.A. Life after PDE4: overcoming adverse events with dual-specificity phosphodiesterase inhibitors. *Curr. Opin. Pharmacol.* 2005; **5:** 238-244.

Giembycz, M.A. Phosphodiesterase 4 Inhibitors and the Treatment of Asthma. *Drugs.* 2000; **59:** 193-212.

Grange, M., Sette, C., Cuomo, M., Conti, M., Lagarde, M., Prigent, A. and Némoz, G. The cAMP-specific Phosphodiesterase PDE4D3 Is Regulated by Phosphatidic Acid Binding. *J. Biol. Chem.* 2000; **43:** 33379-33387.

Gretarsdottir, S., Thorleifsson, G., Reynisdottir, S.T., Manolescu, A., Jonsdottir, S., Jonsdottir, T., Gudmundsdottir, T., Bjarnadottir, S.M., Einarsson, O.B., Gudjonsdottir, H.M., Hawkins, M., Gudmundsson, G., Gudmundsdottir, H., Andrason, H., Gudmundsdottir, A.S., Sigurdardottir, M., Chou, T.T., Nahmias, J., Goss, S., Sveinbjörnsdottir, S., Valdimarsson, E.M., Jakobsson, F., Agnarsson, U., Gudnason, V., Thorgeirsson, G., Fingerle, J., Gurney, M., Gudbjartsson, D., Frigge, M.L., Kong, A., Stefansson, K. and Gulcher, J.R. The gene encoding phosphodiesterase 4D confers risk of ischemic stroke. *Nat. Genet.* 2003; **35:** 131-138.

Groemping, Y., Lapouge, K., Smerdon, S.J. and Rittinger, K. Molecular Basis of Phosphorylation-Induced Activation of the NADPH Oxidase. *Cell.* 2003; **113:** 343-355.

Groemping, Y. and Rittinger, K. Activation and assembly of the NADPH oxidase: a structural perspective. *Biochem. J.* 2005; **386:** 401-416.

Guay, D., Hamel, P., Blouin, M., Brideau, C., Chan, C.C., Chauret, N., Ducharme, Y., Huang, Z., Girard, M., Jones, T.R., Laliberté, F., Masson, P., McAuliffe, M., Piechuta, H., Silva, J., Young, R.N. and Girard, Y. Discovery of L-791,943: A Potent, Selective, Non Emetic and Orally Active Phosphodiesterase-4 Inhibitor. *Bioorg. Med. Chem.* 2002; **12:** 1457-1461.

Guay, J., Lambert, H., Gingras-Breton, G., Lavoie, J.N., Huot, J. and Landry, J. Regulation of actin filament dynamics by p38 map kinase-mediated phosphorylation of heat shock protein 27. *J. Cell Sci.* 1997; **110:** 357-368.

Guo, X., Gerl, R.E. and Schradar, J.W. Defining the Involvement of p38α MAPK in the Production of Anti and Proinflammatory Cytokines Using an SB 203580-resistant Form of the Kinase. *J. Biol. Chem.* 2003; **278:** 22237-22242.

Gupta, M. and Yarwood, S.J. MAP1A Light Chain 2 Interacts with Exchange Protein Activated by Cyclic AMP 1 (EPAC1) to Enhance Rap1 GTPase Activity and Cell Adhesion. *J. Biol. Chem.* 2005; **280:** 8109-8116.

Han, H., Stessin, A., Roberts, J., Hess, K., Gautam, N., Kamenetsky, M., Lou, O., Hyde, E., Nathan, N., Muller, W.A., Buck, J., Levin, L.R. and Nathan, C. Calcium-sensing soluble adenylyl cyclase mediates TNF signal transduction in human neutrophils. *J. Exp. Med.* 2005; **202:** 353-361.

Hansen, G., Jin, S.L., Umetsu, D.T. and Conti, M. Absence of muscarinic cholinergic airway responses in mice deficient in the cyclic nucleotide phosphodiesterase PDE4D. *Proc. Natl. Acad. Sci.* 2000; **97:** 6751-6756.

Härndahl, L., Jing, X.J., Ivarsson, R., Degerman, E., Ahrén, B., Manganiello, V.C., Renström, E. and Holst, L.S. Important Role of Phosphodiesterase 3B for the Stimulatory Action of cAMP on Pancreatic β-Cell Exocytosis and Release of Insulin. *J. Biol. Chem.* 2002; **277:** 37446-37455.

Hart, P.H. Regulation of the inflammatory response in asthma by mast cell products. *Immunol. Cell. Biol.* 2001; **79:** 149-153.

Hatzelmann, A. and Schudt, C. Anti-Inflammatory and Immunomodulatory Potential of the Novel PDE4 Inhibitor Roflumilast in Vitro. *J. Pharmacol. Exp. Ther.* 2001; **297:** 267-279.

Hayes, J.D. and McLellan, L.I. Glutathione and glutathione-dependent enzymes represent a co-ordinately regulated defence against oxidative stress. *Free Radic. Res.* 1999; **31:** 273-300.

Heidenreich, O., Neininger, A., Schratt, G., Zinck, R., Cahill, M.A., Engel, K., Kotlyarov, A., Kraft, R., Kostka, S., Gaestel, M. and Nordheim, A. MAPKAP Kinase 2 Phosphorylates Serum Response Factor *in Vitro* and *in Vivo*. *J. Biol. Chem.* 1999; **274:** 14434-14443.

Henn, V., Edemir, B., Stefan, E., Wiesner, B., Lorenz, D., Theilig, F., Schmitt, R., Vossebein, L., Tamma, G., Beyermann, M., Krause, E., Herberg, F.W., Valenti, G., Bachmann, S., Rosenthal, W. and Klussmann, E. Identification of a Novel A-kinase Anchoring Protein 18 Isoform and Evidence for Its Role in the Vasopressin-induced Aquaporin-2 Shuttle in Renal Principal Cells. *J. Biol. Chem.* 2004; **279:** 26654-26665.

Herlaar, E. and Brown, Z. p38 MAPK signalling cascades in inflammatory disease. *Mol. Med. Today.* 1999; **5:** 439-447.

Herman, S.B., Juilfs, D.M., Fauman, E.B., Juneau, P. and Menetski, J.P. Analysis of a Mutation in Phosphodiesterase Type 4 that Alters Both Inhibitor Activity and Nucleotide Selectivity. *Mol. Pharmacol.* 2000; **57:** 991-999.

Ho, D.T., Bardwell, A.J., Abdollahi, M. and Bardwell, L. A Docking Site in MKK4 Mediates High Affinity Binding to JNK MAPKs and Competes with Similar Docking Sites in JNK Substrates. *J. Biol. Chem.* 2003; **278:** 32662-32672.

Hoffmann, R., Baillie, G.S., MacKenzie, S.J., Yarwood, S.J. and Houslay, M.D. The MAP kinase ERK2 inhibits the cyclic AMP-specific phosphodiesterase HSPDE4D3 by phosphorylating it at Ser579. *EMBO J.* 1999; **18:** 893-903.

Hoffmann, R., Wilkinson, I.R., McCallum, J.F., Engels, P. and Houslay, M.D. cAMP-specific phosphodiesterase HSPDE4D3 mutants which mimic activation and changes in rolipram inhibition triggered by protein kinase A phosphorylation of Ser-54: generation of a molecular model. *Biochem. J.* 1998; **333:** 139-149.

Hollmann, M.W., Strumper, D., Herroeder, S. and Durieux, M.E. Receptors, G Proteins and Their Interactions. *Anesthesiology.* 2005; **103:** 1066-1078.

Hommes, D.W., Peppelenbosch, M.P and van Deventer, S.J.H. Mitogen activated protein (MAP) kinase signal transduction pathways and novel anti-inflammatory targets. *Gut.* 2003; **52:** 144-151.

Horton, Y.M., Sullivan, M. and Houslay, M.D. Molecular cloning of a novel splice variant of human type IV_A (PDE-IV_A) cyclic AMP phosphodiesterase and localization of the gene to the p13.1-q12 region of the human chromosome 19. *Biochem. J.* 1995; **308:** 683-691.

Hoshi, N., Langeberg, L.K. and Scott, J.D. Distinct enzyme combinations in AKAP signalling complexes permit functional diversity. *Nature Cell Biol.* 2005; **7:** 1066-1073.

Houslay, M.D. PDE4 cAMP-Specific Phosphodiesterases. *Prog. Nucleic Acid Res. Mol. Biol.* 2001; **69:** 249-315.

Houslay, M.D. The long and short of vascular smooth muscle phosphodiesterase-4 as a putative therapeutic target. *Mol. Pharmacol.* 2005; **68:** 563-567.

Houslay, M.D. and Adams, D.R. PDE4 cAMP phosphodiesterases: modular enzymes that orchestrate signalling cross-talk, desensitization and compartmentalization. *Biochem. J.* 2003; **370:** 1-18.

Houslay, M.D. and Kolch, W. Cell-Type Specific Integration of Cross-Talk between Extracellular Signal-Regulated Kinase and cAMP Signaling. *Mol. Pharmacol.* 2000; **58:** 659-668.

Houslay, M.D. and Milligan, G. Tailoring cAMP-signalling responses through isoform multiplicity. *Trends. Biochem. Sci.* 1997; **22:** 217-224.

Houslay, M.D., Schafer, P. and Zhang, K.Y.J. Phosphodiesterase-4 as a therapeutic target. *Drug Discov. Today.* 2005; **10:** 1503-1519.

Houslay, M.D., Sullivan, M. and Bolger, G.B. The multienzyme PDE4 cyclic AMP-specific phosphodiesterase family: Intracellular targeting, regulation, and selective inhibition by compounds exerting anti-inflammatory and anti-depressant actions. *Adv. Pharmacol.* 1998; **44:** 225-342.

Hoyal, C.R., Gutierrez, A., Young, B.M., Catz, S.D., Lin, J.H., Tsichlis, P.N. and Babior, B.M. Modulation of $p47^{PHOX}$ activity by site-specific phosphorylation: Akt-dependent activation of the NADPH oxidase. *Proc. Natl. Acad. Sci.* 2003; **100:** 5130-5135.

Huang, Z., Ducharme, Y., Macdonald, D. and Robichaud, A. The next generation of PDE4 inhibitors. *Curr. Opin. Chem. Biol.* 2001; **5:** 432-438.

Hurley, J.H. Structure, Mechanism, and Regulation of Mammalian Adenylyl Cyclase. *J. Biol. Chem.* 1999; **274:** 7599-7602.

Huston, E., Beard, M., McCallum, F., Pyne, N.J., Vandenabeele, P., Scotland, G. and Houslay, M.D. The cAMP-specific Phosphodiesterase PDE4A5 Is Cleaved Downstream of Its SH3 Interaction Domain by Caspase-3. *J. Biol. Chem.* 2000; **275:** 28063-28074.

Huston, E., Lumb, S., Russell, A., Catterall, C., Ross, A., Steele, M.R., Bolger, G.B., Perry, M.J., Owens, R.J. and Houslay, M.D. Molecular cloning and transient expression in COS cells of a novel human PDE4B cyclic AMP phosphodiesterase, HSPDE4B3. *Biochem. J.* 1997; **328:** 549-556.

Huston, E., Pooley, L., Julien, P., Scotland, G., McPhee, I., Sullivan, M., Bolger, G. and Houslay, M.D. The Human Cyclic AMP-specific Phosphodiesterase PDE-46 (HSPDE4A4B) Expressed in Transfected COS7 Cells Occurs as Both Particulate and Cytosolic Species That Exhibit Distinct Kinetics of Inhibition by the Anti-depressant Rolipram. *J. Biol. Chem.* 1996; **271:** 31334-31344.

Ibarra, N., Pollitt, A. and Insall, R.H. Regulation of actin assembly by SCAR/WAVE proteins. *Biochem. Soc. Trans.* 2005; **33:** 1243-1246.

Ichijo, H., Nishida, E., Irie, K., ten Dijke, P., Saitoh, M., Moriguchi, T., Takagi, M., Matsumoto, K., Miyazono, K. and Gotoh, Y. Induction of apoptosis by ASK1 a mammalian MAPKKK that activates SAPK/JNK and p38 signaling pathways. *Science.* 1997; **275:** 90-94.

Inanami, O., Johnson, J.L., McAdara, J.K., El Benna, J., Faust, L.R.P., Newburger, P.E. and Babior, B.M. Activation of the Leukocyte NADPH Oxidase by Phorbol Ester Requires the Phosphorylation of $p47^{PHOX}$ on Serine 303 or 304. *J. Biol. Chem.* 1998; **273:** 9539-9543.

Jacob, C., Szilagyi, C., Allen, J.A., Bertrand, C. and Lagente, V. Role of PDE4 in superoxide generation through p44/p42^{MAPK} regulation: a cAMP and a PKA-independent mechanism. *Br. J. Pharmacol.* 2004; **143:** 257-268.

Jaffe, A.R. and Hall, A. Rho GTPases: Biochemistry and Biology. *Annu. Rev. Cell Dev. Biol.* 2005; **21:** 247-269.

Javitch, J.A. The Ants Go Marching Two by Two: Oligomeric Structure of G-Protein-Coupled Receptors. *Mol. Pharmacol.* 2004; **66:** 1077-1082.

Jia, Y.H., Nie, J., Wu, C., Li, C. and Li, S.C. Novel Src Homology 3 Domain-binding Motifs Identified from proteomic Screen of a Pro-rich region. *Mol. Cell Proteomics.* 2005; **4:** 1155-1166.

Jin, S.L. and Conti, M. Induction of the cyclic nucleotide phosphodiesterase PDE4B is essential for LPS-activated TNF-α responses. *Proc. Natl. Acad. Sci.* 2002; **99:** 7628-7633.

Johnson, J.L., Park, J.W., El Benna, J., Faust, L.P., Inanami, O. and Babior, B.M. Activation of p47^{PHOX}, a Cytosolic Subunit of the Leukocyte NADPH Oxidase. *J. Biol. Chem.* 1998; **273:** 35147-35152.

Johnston, L.A., Erdogan, S., Cheung, Y.F., Sullivan, M., Barber, R., Lynch, M.J., Baillie, G.S., Van Heeke, G., Adams, D.R., Huston, E. and Houslay, M.D. Expression, intracellular distribution and basis for lack of catalytic activity of the PDE4A7 isoform encoded by the human PDE4A cAMP-specific phosphodiesterase gene. *Biochem. J.* 2004; **380:** 371-384.

Jones, N.A., Boswell-Smith, V., Lever, R. and Page C.P. The effect of selective phosphodiesterase isoenzyme inhibition on neutrophil function in vitro. *Pulm. Pharmacol. Ther.* 2005; **18:** 93-101.

Jones, S.W., de Souza, P.M. and Lindsay, M.A. siRNA for gene silencing: a route to drug target discovery. *Curr. Opin. Pharmacol.* 2004; **4:** 522-527.

Juilfs, D.M., Fülle, H.J., Zhao, A.Z., Houslay, M.D., Garbers, D.L. and Beavo, J.A. A subset of olfactory neurons that selectively express cGMP-stimulated phosphodiesterase (PDE2) and guanylyl cyclase-D define a unique olfactory signal transduction pathway. *Proc. Natl. Acad. Sci.* 1997; **94:** 3388-3395.

Kang, B.H. and Altieri, D.C. Regulation of Survivin Stability by the Aryl Hydrocarbon Receptor-interacting Protein. *J. Biol. Chem.* 2006; **281:** 24721-24727.

Kashuba, E., Kashuba, V., Pokrovskaja, K., Klein, G. and Szekely, L. Epstein-Barr virus encoded nuclear protein EBNA-3 binds XAP2, a protein associated with Hepatitis B virus X antigen. *Oncogene.* 2000; **19:** 1801-1806.

Kaupp, U.B. and Seifert, R. Cyclic Nucleotide-gated Ion Channels. *Physiol. Rev.* 2002; **82:** 769-824.

Kervinen, J., Ma, H., Bayoumy, S., Schubert, C., Milligan, C., Lewandowski, F., Moriarty, K., DesJarlais, R.L., Ramachandren, K., Wang, H., Harris, C.A., Grasberger, B., Todd, M., Springer, B.A. and Deckman, I. Effect of construct design on MAPKAP kinase-2 activity, thermodynamic stability and ligand-binding affinity. *Arch. Biochem. Biophys.* 2006; **449:** 47-56.

Klussmann, E., Edemir, B., Pepperle, B., Tamma, G., Henn, V., Klauschenz, E., Hundsrucker, C., Maric, K. and Rosenthal, W. Ht31: the first protein kinase A anchoring protein to integrate protein kinase A and Rho signaling. *FEBS Lett.* 2001; **507:** 264-268.

Kohout, T.A. and Lefkowitz, R.J. Regulation of G Protein-Coupled Receptor Kinases and Arrestins During Receptor Desensitization. *Mol. Pharmacol.* 2003; **63:** 9-18.

Kohyama, T., Liu, X., Wen, F.Q., Zhu, Y.K., Wang, H., Kim, H.J., Takizawa, H., Cieslinski, L.B., Barnette, M.S. and Rennard, S.I. PDE4 Inhibitors Attenuate Fibroblast Chemotaxsis and Contraction of Native Collagen Gels. *Am. J. Respir. Cell Mol. Biol.* 2002; **26:** 694-701.

Kolch, W. Coordinating ERK/MAPK Signalling Through Scaffolds and Inhibitors. *Nat. Rev. Mol. Cell Biol.* 2005; **6:** 827-837.

Kostic, M.M., Erdogen, S., Rena, G., Borchert, G., Hoch, B., Bartel, S., Scotland, G., Huston, E., Houslay, M.D. and Krause, E.G. Altered Expression of PDE1 and PDE4 Cyclic Nucleotide Phosphodiesterase Isoforms in 7-oxo-prostacyclin-preconditioned Rat Heart. *J. Mol. Cell. Cardiol.* 1997; **29:** 3135-3146.

Kotera, J., Sasaki, T., Kobayashi, T., Fujishige, K., Yamashita, Y. and Omori, K. Subcellular Localization of Cyclic Nucleotide Phosphodiesterase Type 10A Variants, and Alteration of the Localization by cAMP-dependent Protein Kinase-dependent Phosphorylation. *J. Biol. Chem.* 2004; **279:** 4366-4375.

Kotlyarov, A., Neininger, A., Schubert, C., Eckert, R., Birchmeier, C., Volk, H.D. and Gaestel, M. MAPKAP kinase 2 is essential for LPS-induced TNF-alpha biosynthesis. *Nat. Cell. Biol.* 1999; **1:** 94-97.

Kraemer, A., Rehmann, H.R., Cool, R.H., Theiss, C., de Rooij, J., Bos, J.L. and Wittinghofer, A. Dynamic Interaction of cAMP with the Rap Guanine-nucleotide Exchange Factor Epac1. *J. Mol. Biol.* 2001; **306:** 1167-1177.

Kuribayashi, F., Nunoi, H., Wakamatsu, K., Tsunawaki, S., Sato, K., Ito, T. and Sumimoto, H. The adaptor protein $p40^{phox}$ as a positive regulator of the superoxide-producing phagocyte oxidase. *EMBO J.* 2002; **21:** 6312-6320.

Kuzhandaivelu, N., Cong, Y.S., Inouye, C., Yang, W.M. and Seto, E. XAP2, a novel hepatitis B virus X-associated protein that inhibits X transactivation. *Nucleic Acids Res.* 1996; **24:** 4741-4750.

Kyriakis, J.M. and Avruch, J. Mammalian Mitogen-Activated Protein Kinase Signal Transduction Pathways Activated by Stress and Inflammation. *Physiol. Rev.* 2001; **81:** 807-869.

Laliberté, F., Han, Y., Govindarajan, A., Giroux, A., Liu, S., Bobechko, B., Lario, P., Bartlett, A., Gorseth, E., Gresser, M. and Huang, Z. Conformational Difference between PDE4 Apoenzyme and Holoenzyme. *Biochemistry.* 2000; **39:** 6449-6485.

Laliberté, F., Liu, S., Gorseth, E., Bobechko, B., Bartlett, A., Lario, P., Gresser, M.J. and Huang, Z. In vitro PKA phosphorylation-mediated human PDE4A4 activation. *FEBS Lett.* 2002; **512:** 205-208.

Langeberg, L.K. and Scott, J.D. A-kinase-anchoring proteins. *J. Cell Sci.* 2005; **118:** 3217-3220.

Lapouge, K., Smith, S.J.M., Walker, P.A., Gamblin, S.J., Smerdon, S.J. and Rittinger, K. Structure of the TPR Domain of $p67^{phox}$ in Complex with Rac·GTP. *Mol. Cell.* 2000; **6:** 899-907.

Larsen, J.K., Yamboliev, I.A., Weber, L.A. and Gerthoffer, W.T. Phosphorylation of the 27-kDa heat shock protein via p38 MAP kinase and MAPKAP kinase in smooth muscle. *Am. J. Physiol.* 1997; **273:** L930-L940.

Larson, D.R., Gosse, J.A., Holowka, D.A., Baird, B.A. and Webb, W.W. Temporally resolved interactions between antigen-stimulated IgE receptors and Lyn kinase on living cells. *J. Cell Biol.* 2005; **171:** 527-536.

Lawler, O.A., Miggin, S.M. and Kinsella, B.T. Protein Kinase A-mediated Phosphorylation of Serine 357 of the Mouse Prostacyclin Receptor Regulates Its Coupling to G_s-, to G_i-, and to G_q-coupled Effector Signaling. *J. Biol. Chem.* 2001; **276:** 33596-33607.

Lee, J.C., Laydon, J.T., McDonnell, P.C., Gallagher, T.F., Kumar, S., Green, D., McNulty, D., Blumenthal, M.J., Heys, J.R., Landvatter, S.W., Strickler, J.E., McLaughlin, M.M., Siemens, I.R., Fisher, S.M., Livi, G.P., White, J.R., Adams, J.L. and Young, P. A protein kinase involved in the regulation of inflammatory cytokine biosynthesis. *Nature.* 1994; **372:** 739-746.

Lee, M.E., Markowitz, J., Lee, J.O. and Lee, H. Crystal structure of phosphodiesterase 4D and inhibitor complex. *FEBS Lett.* 2002; **530:** 53-58.

Leemhuis, J., Boutillier, S., Barth, H., Feuerstein, T.J., Brock, C., Nürnberg, B., Aktories, K. and Meyer, D.K. Rho GTPases and Phosphoinositide 3-Kinase Organize Formation of Branched Dendrites. *J. Biol. Chem.* 2004; **279:** 585-596.

Lees, M.J., Peet, D.J. and Whitelaw, M.L. Defining the Role for XAP2 in Stabilization of the Dioxin Receptor. *J. Biol. Chem.* 2003; **278:** 35878-35888.

Lefkowitz, R.J., Pierce, K.L. and Luttrell, L.M. Dancing with Different Partners: Protein Kinase A Phosphorylation of Seven Membrane-Spanning Receptors Regulates Their G protein-Coupling Specificity. *Mol. Pharmacol.* 2002; **62:** 971-974.

Lefkowitz, R.J. and Shenoy, S.K. Transduction of Receptor Signals by β-Arrestins. *Science.* 2005; **308:** 512-517.

Le Jeune, I.R., Shepherd, M., Van Heeke, G., Houslay, M.D. and Hall, I.P. Cyclic AMP-dependent Transcriptional Up-regulation of Phosphodiesterase 4D5 in Human Airway Smooth Muscle Cells. *J. Biol. Chem.* 2002; **39:** 35980-35989.

Lenhard, J.M., Kassel, D.B., Rocque, W.J., Hamacher, L., Holmes, W.D., Patel, I., Hoffman, C. and Luther, M. Phosphorylation of a cAMP-specific phosphodiesterase (HSPDE4B2B) by mitogen-activated protein kinase. *Biochem. J.* 1996; **316:** 751-758.

Li, H., Adamik, R., Pacheco-Rodriguez, G., Moss, J. and Vaughan, M. Protein kinase-anchoring (AKAP) domains in brefeldin A-inhibited guanine nucleotide-exchange protein 2 (BIG2). *Proc. Natl. Acad. Sci.* 2003; **100:** 1627-1632.

Li, J.M., Gall, N.P., Grieve, D.J., Chen, M. and Shah, A.M. Activation of NADPH Oxidase During Progression of Cardiac Hypertrophy to Failure. *Hypertension.* 2002; **40:** 477-484.

Li, S.C. Specificity and versatility of SH3 and other proline-recognition domains: structural basis and implications for cellular signal transduction. *Biochem. J.* 2005; **390:** 641-653.

Li, X., Huston, E., Lynch, M.J., Houslay, M.D. and Baillie, G.S. Phosphodiesterase-4 influences the PKA phosphorylation status and membrane translocation of G-protein receptor kinase 2 (GRK2) in HEK-293β2 cells and cardiac myocytes. *Biochem. J.* 2006; **394:** 427-435.

Liebmann, C. Regulation of MAP kinase activity by peptide receptor signalling pathway: Paradigms of multiplicity. *Cell. Signal.* 2001; **13:** 777-785.

Lim, J., Pahlke, G. and Conti, M. Activation of the cAMP-specific Phosphodiesterase PDE4D3 by Phosphorylation. *J. Biol. Chem.* 1999; **28:** 19677-19685.

Lin, P., Welch, E.J., Gao, X.P., Malik, A.B. and Ye, R.D. Lysophosphatidylcholine Modulates Neutrophil Oxidant Production through Elevation of Cyclic AMP. *J. Immunol.* 2005; **174:** 2981-2989.

Lipworth, B.J. Phosphodiestaerase-4 inhibitors for asthma and chronic obstructive pulmonary disease. *Lancet.* 2005; **365:** 167-175.

Liu, S., Laliberté, F., Bobechko, B., Bartlett, A., Lario, P., Gorseth, E., Van Hamme, J., Gresser, M.J. and Huang, Z. Dissecting the Cofactor-Dependent and Independent Bindings of PDE4 Inhibitors. *Biochemistry.* 2001; **40:** 10179-10186.

Lobban, M., Shakur, Y., Beattie, J. and Houslay, M.D. Identification of two splice variant forms of type-IV_B cyclic AMP, DPD (rPDE-IVB1) and PDE-4 (rPDEIVB2) in brain: selective localization in membrane and cytosolic compartments and differential expression in various brain regions. *Biochem. J.* 1994; **304:** 399-406.

Lobbert, R.W., Winterpacht, A., Seipel, B. and Zabel, B.U. Molecular cloning and chromosomal assignment of the human homologue of the rat cGMP-inhibited phosphodiesterase 1 (PDE3A) -- a gene involved in fat metabolism located at 11p15.1. *Genomics.* 1996; **37:** 211-218.

Lopes, L.R., Hoyal, C.R., Knaus, U.G. and Babior, B.M. Activation of the Leukocyte NADPH Oxidase by Protein Kinase C in a Partially Recombinant Cell-free System. *J. Biol. Chem.* 1999; **274:** 15533-15537.

Lugnier, C. Cyclic nucleotide phosphodiesterase (PDE) superfamily: A new target for the development of specific therapeutic agents. *Pharmacol. Ther.* 2006; **109:** 366-398.

Luttrell, L.M. and Lefkowitz, R.J. The role of β-arrestins in the termination and transduction of G-protein-coupled receptor signals. *J. Cell Sci.* 2002; **115:** 455-465.

Lynch, M.J., Baillie, G.S., Mohamed, A., Li, X., Maisonneuve, C., Klussmann, E., van Heeke, G. and Houslay, M.D. RNA Silencing Identifies PDE4D5 as the Functionally Relevant cAMP Phosphodiesterase Interacting with βArrestin to Control the Protein Kinase A/AKAP79-mediated Switching of the β_2-Adrenergic Receptor to Activation of ERK in HEK293 Cells. *J. Biol. Chem.* 2005; **280:** 33178-33189.

MacDonald, D., Perrier, H., Liu, S., Laliberté, F., Rasori, R., Robichaud, A., Masson, P. and Huang, Z. Hunting the Emesis and Efficacy Targets of PDE4 Inhibitors: Identification of the Photoaffinity Probe 8-(3-Azidophenyl)-6-[(4-iodo-1*H*-1-imidazolyl)methyl]quinoline (APIIMQ). *J. Med. Chem.* 2000; **43:** 3820-3823.

MacKenzie, S.J., Baillie, G.S., McPhee, I., Bolger, G.B. and Houslay, M.D. ERK2 Mitogen-activated Protein Kinase Binding, Phosphorylation, and Regulation of the PDE4D cAMP-specific Phosphodiesterases. *J. Biol. Chem.* 2000; **275:** 16609-16617.

MacKenzie, S.J., Baillie, G.S., McPhee, I., MacKenzie, C., Seamons, R., McSorley, T., Millen, J., Beard, M.B., Van Heeke, G. and Houslay, M.D. Long PDE4 cAMP specific phosphodiesterases are activated by protein kinase A-mediated phosphorylation of a single serine residue in Upstream Conserved Region 1 (UCR1). *Br. J. Pharmacol.* 2002; **136:** 421-433.

MacKenzie, S.J. and Houslay, M.D. Action of rolipram on specific PDE4 cAMP phosphodiesterase isoforms and on the phosphorylation of cAMP-response-element-binding protein (CREB) and p38 mitogen-activated protein (MAP) kinase in U937 monocytic cells. *Biochem. J.* 2000; **347:** 571-578.

MacKenzie, S.J., Yarwood, S.J., Peden, A.H., Bolger, G.B., Vernon, R.G. and Houslay, M.D. Stimulation of p70S6 kinase via a growth hormone-controlled phosphatidylinositol 3-kinase pathway leads to the activation of a PDE4A cyclic AMP-specific phosphodiesterase in 3T3-F442A preadipocytes. *Proc. Natl. Acad. Sci.* 1998; **95:** 3549-3554.

MacLean, M.R., Johnston, E.D., McCulloch, K.M., Pooley, L., Houslay, M.D. and Sweeney, G. Phosphodiesterase Isoforms in the Pulmonary Arterial Circulation of the Rat: Changes in Pulmonary Hypertension. *J. Pharmacol. Exp. Ther.* 1997; **283:** 619-624.

Magiera, M.M., Gupta, M., Rundell, C.J., Satish, N., Ernens, I. and Yarwood, S.J. Exchange protein directly activated by cAMP (EPAC) interacts with the light chain (LC) 2 of MAP1A. *Biochem. J.* 2004; **382:** 803-810.

Malarkey, K., Belham, C.M., Paul, A., Graham, A., McLees, A., Scott, P.H. and Plevin, R. The regulation of tyrosine kinase signalling pathways by growth factor and G-protein –coupled receptors. *Biochem. J.* 1995; **309:** 361-375.

Manganiello, V. Short-term regulation of PDE4 activity. *Br. J. Pharmacol.* 2002; **136:** 339-340.

Manning, C.D., Burman, M., Christensen, S.B., Cieslinski, L.B., Essayan, D.M., Grous, M., Torphy, T.J. and Barnette, M.S. Suppression of human inflammatory cell function by subtype-selective PDE4 inhibitors correlates with inhibition of PDE4A and PDE4B. *Br. J. Pharmacol.* 1999; **128:** 1393-1398.

Marchmont, R.J. and Houslay, M.D. A Peripheral and an Intrinsic Enzyme Constitute the Cyclic AMP Phosphodiesterase Activity of Rat Liver Plasma Membranes. *Biochem. J.* 1980; **187:** 381-392.

Martinez, J.M., Afshari, C.A., Bushel, P.R., Matsuda, A., Takahashi, T. and Walker, N.J. Differential toxicogenomic responses to 2,3,7,8-tetrachlorodibenzo-p-dioxin in malignant and nonmalignant human airway epithelial cells. *Toxicol. Sci.* 2002; **69:** 409-423.

Martyn, K.D., Kim, M.J., Quinn, M.T., Dinauer, M.C. and Knaus, U.G. p21-activated kinase (Pak) regulates NADPH oxidase activation in human neutrophils. *Blood.* 2005; **106:** 3962-3969.

Massenet, C., Chenavas, S., Cohen-Addad, C., Dagher, M.C., Brandolin, G., Pebay-Peyroula, E. and Fieschi, F. Effects of $p47^{phox}$ C Terminus Phosphorylations on Binding Interactions with $p40^{phox}$ and $p67^{phox}$. *J. Biol. Chem.* 2005; **280:** 13752-13761.

Matsumoto, T., Kobayashi, T. and Kamata, K. Alterations in EDHF-type relaxation and phosphodiesterase activity in mesenteric arteries from diabetic rats. *Am. J. Physiol. Heart Circ. Physiol.* 2003; **285:** H283-H291.

Maurice, D.H., Palmer, D., Tilley, D.G., Dunkerley, H.A., Netherton, S.J., Raymond, D.R., Elabatarny, H.S. and Jimmo, S.L. Cyclic Nucleotide Phosphodiesterase Activity, Expression, and Targeting in Cells of the Cardiovascular System. *Mol. Pharmacol.* 2003; **64:** 533-546.

Mayer, B.J. SH3 domains: complexity in moderation. *J. Cell. Sci.* 2001; **114:** 1253-1263.

Mayr, B. and Montminy, M. Transcriptional regulation by the phosphorylation-dependent factor CREB. *Nat. Rev. Mol. Cell Biol.* 2001; **2:** 599-609.

McCahill, A., McSorley, T., Huston, E., Hill, E.V., Lynch, M.J., Gall, I., Keryer, G., Lygren, B., Taskén, K., van Heeke, G. and Houslay, M.D. In resting COS1 cells a dominant negative approach shows that specific, anchored PDE4 cAMP phosphodiesterase isoforms gate the activation, by basal cyclic AMP production, of AKAP-tethered protein kinase A type II located at the centrosomal region. *Cell Signal.* 2005; **17:** 1158-1173.

McCahill, A., Warwicker, J., Bolger, G.B., Houslay, M.D. and Yarwood, S.J. The RACK1 Scaffold Protein: A Dynamic Cog in Cell Response Mechanisms. *Mol. Pharmacol.* 2002; **62:** 1261-1273.

McConnachie, G., Langeberg, L.K. and Scott, J.D. AKAP signaling complexes: getting to the heart of the matter. *Trends Mol. Med.* 2006; **12:** 317-313.

McLaughlin, M.M., Kumar, S., McDonnell, P.C., Van Horn, S., Lee, J.C., Livi, G.P. and Young, P.R. Identification of mitogen-activated protein (MAP) kinase-activated protein kinase-3, a novel substrate of CSBP p38 MAP kinase. *J. Biol. Chem.* 1996; **271:** 8488-8492.

McPhee, I., Cochran, S. and Houslay, M.D. The novel long PDE4A10 cyclic AMP phosphodiesterase shows a pattern of expression within brain that is distinct from the long PDE4A5 and short PDE4A1 isoforms. *Cell. Signal.* 2001; **13:** 911-918.

McPhee, I., Pooley, L., Lobban, M., Bolger, G. and Houslay, M.D. Identification, characterization and regional distribution in brain of RPDE-6 (RNPDE4A5), a novel splice variant of the PDE4A cyclic AMP phosphodiesterase family. *Biochem. J.* 1995; **310:** 965-974.

McPhee, I., Yarwood, S.J., Scotland, G., Huston, E., Beard, M.B., Ross, A.H., Houslay, E.S. and Houslay, M.D. Association with SRC Family Tyrosyl Kinase LYN Triggers a Conformational Change in the Catalytic Region of Human cAMP-specific Phosphodiesterase HSPDE4A4B. *J. Biol. Chem.* 1999; **274:** 11796-11810.

McSorley, T., Stefan, E., Henn, V., Wiesner, B., Baillie, G.S., Houslay, M.D., Rosenthal, W. and Klussmann, E. Spatial organisation of AKAP18 and PDE4 isoforms in renal collecting duct principal cells. *Eur. J. Cell Biol.* 2006; **85:** 673-678.

Meacci, E., Taira, M., Moos Jr., M., Smith, C.J., Movsesian, M.A., Degerman, E., Belfrage, P. and Manganiello, V. Molecular cloning and expression of human myocardial cGMP-inhibited cAMP phosphodiesterase. *Proc. Nat. Acad. Sci.* 1992; **89:** 3721-3725.

Méhats, C., Jin, S.L., Wahlstrom, J., Law, E., Umetsu, D.T. and Conti, M. PDE4D plays a critical role in the control of smooth muscle contraction. *FASEB J.* 2003; **17:** 1831-1841.

Méhats, C., Tanguy, G., Dallot, E., Robert, B., Rebourcet, R., Ferré F. and Leroy, M.J. Selective Up-Regulation of Phosphodiesterase-4 Cyclic Adenosine 3', 5'-Monophosphate (cAMP)-Specific Phosphodiesterase Variants by Elevated cAMP Content in Human Myometrial Cells in Culture. *Endocrinology.* 1999; **140:** 3228-3237.

Meng, W., Swenson, L.L., Fitzgibbon, M.J., Hayakawa, K., ter Haar, E., Behrens, A.E., Fulghum, J.R. and Lippke, J.A. Structure of Mitogen-activated Protein Kinase-activated Protein (MAPKAP) Kinase 2 Suggests a Bifunctional Switch That Couples Kinase Activation with Nuclear Export. *J. Biol. Chem.* 2002; **277:** 37401-37405.

Mercier, J.F., Salahpour, A., Angers, S., Breit, A. and Bouvier, M. Quantitative Assessment of β1- and β2-Adrenergic Receptor Homo- and Heterodimerization by Bioluminescence Resonance Energy Transfer. *J. Biol. Chem.* 2002; **277:** 44925-44931.

Meyer, B.K. and Perdew, G.H. Characterization of the AhR-hsp90-XAP2 core complex and the role of the immunophilin-related protein XAP2 in AhR stabilization. *Biochemistry.* 1999; **38:** 8907-8917.

Michie, A.M., Lobban, M., Müller, T., Harnett, M.M. and Houslay, M.D. Rapid Regulation of PDE-2 and PDE-4 Cyclic AMP Phosphodiesterase Activity Following Ligation of the T Cell Antigen Receptor on Thymocytes: Analysis Using the Selective Inhibitors erythro-9-(2-hydroxy-3-nonyl)-adenine (EHNA) and Rolipram. *Cell. Signal.* 1995; **8:** 97-110.

Miki, T., Taira, M., Hockman, S., Shimada, F., Lieman, J., Napolitano, M., Ward, D., Taira, M., Makino, H. and Manganiello, V.C. Characterization of the cDNA and gene encoding human PDE3B, the cGIP1 isoform of the human cyclic GMP-inhibited cyclic nucleotide phosphodiesterase family. *Genomics* 1996; **36:** 476-485.

Milatovich, A., Bolger, G., Michaeli, T. and Francke, U. Chromosome localizations of genes for five cAMP-specific phosphodiesterases in man and mouse. *Somat. Cell Molec. Genet.* 1994; **20:** 75-86.

Millar, J.K., Pickard, B.S., Mackie, S., James, R., Christie, S., Buchanan, S.R., Malloy, M.P., Chubb, J.E., Huston, E., Baillie, G.S., Thomson, P.A., Hill, E.V., Brandon, N.J., Rain, J.C., Camargo, L.M., Whiting, P.J., Houslay, M.D., Blackwood, D.H.R, Muir, W.J. and Porteous, D.J. DISC1 and PDE4B Are Interacting Genetic Factors in Schizophrenia That Regulate cAMP Signaling. *Science.* 2005; **310:** 1187-1191.

Millen, J., MacLean, M.R. and Houslay, M.D. Hypoxia-induced remodelling of PDE4 isoform expression and cAMP handling in human pulmonary artery smooth muscle cells. *Eur. J. Cell Biol.* 2006; **85:** 679-691.

Milligan, G. G Protein-Coupled Receptor Dimerization: Function and Ligand Pharmacology. *Mol. Pharmacol.* 2004; **66:** 1-7.

Mitzuki, K., Takeya, R., Kuribayashi, F., Nobuhisa, I., Kohda, D., Nunoi, H., Takeshige, K. and Sumimoto, H. A region C-terminal to the proline-rich core of $p47^{phox}$ regulates activation of the phagocyte NADPH oxidase by interacting with the C-terminal SH3 domain of $p67^{phox}$. *Arch. Biochem. Biophys.* 2005; **444:** 185-194.

Mongillo, M., McSorley, T., Evellin, S., Sood, A., Lissandron, V., Terrin, A., Huston, E., Hannawacker, A., Lohse, M.J., Pozzan, T., Houslay, M.D. and Zaccolo, M. Fluorescence Resonance Energy Transfer-Based Analysis of cAMP Dynamics in Live Neonatal Rat Cardiac Myocytes Reveals Distinct Functions of Compartmentalized Phosphodiesterases. *Circ. Res.* 2004; **95:** 67-75.

Montminy, M. Transcriptional Regulation by Cyclic AMP. *Annu. Rev. Biochem.* 1997; **66:** 807-822.

Muise, E.S., Chute, I.C., Claveau, D., Masson, P., Boulet, L., Tkalec, L., Pon, D.J., Girard, Y., Frenette, R. and Mancini, J.A. Comparison of inhibition of ovalbumin-induced bronchoconstriction in guinea pigs and *in vitro* inhibition of tumor necrosis factor-α formation with phosphodiesterase 4 (PDE4) selective inhibitors. *Biochem. Pharmacol.* 2002; **63:** 1527-1535.

Murdoch, C.E., Grieve, D.J. Cave, A.C., Looi, Y.H. and Shah, A.M. NADPH Oxidase and heart failure. *Curr. Opin. Pharmacol.* 2006; **6:** 148-153.

Murphy, B.J. and Scott, J.D. Functional Anchoring of the cAMP-Dependent Protein Kinase. *Trends Cardiovasc. Med.* 1998; **8:** 89-95.

Nahas, N., Molski, T.F.P., Fernandez, G.A. and Sha'afi, R.I. Tyrosine phosphorylation and activation of a new mitogen-activated protein (MAP)-kinase cascade in human neutrophils stimulated with various agonists. *Biochem. J.* 1996; **318:** 247-253.

Nakagami, H., Takemoto, M. and Liao, J.K. NADPH oxidase-derived superoxide anion mediates Angiotensin II-induced cardiac hypertrophy. *J. Mol. Cell. Cardiol.* 2003; **35:** 851-859.

Nakamura, K. Fushimi, K., Kouchi, H., Mihara, K., Miyazaki, M. Ohe, T. and Namba, M. Inhibitory Effects of Antioxidants on Neonatal Rat Cardiac Myocyte Hypertrophy Induced by Tumor Necrosis Factor-α and Angiotensin II. *Circulation.* 1998; **98:** 794-799.

Némoz, G., Sette, C. and Conti, M. Selective Activation of Rolipram-Sensitive, cAMP-Specific Phosphodiesterase Isoforms by Phosphatidic Acid. *Mol. Pharmacol.* 1997; **51:** 242-249.

Némoz, G., Zhang, R., Sette, C. and Conti, M. Identification of cyclic AMP-phosphodiesterase variants from the PDE4D gene expressed in human peripheral mononuclear cells. *FEBS Lett.* 1996; **384:** 97-102.

New, L., Jiang, Y., Zhao, M., Liu, K., Zhu, W., Flood, L.J., Kato, Y., Parry, G.C.N. and Han, J. PRAK, a novel protein kinase regulated by the p38 MAP kinase. *EMBO J.* 1998; **17:** 3372-3384.

Newlon, M.G., Roy, M., Morikis, D., Carr, D.W., Westphal, R., Scott, J.D. and Jennings, P.A. A novel mechanism of PKA anchoring revealed by solution structures of anchoring complexes. *EMBO J.* 2001; **20:** 1651-1662.

Newlon, M.G., Roy, M., Morikis, D., Hausken, Z.E., Coghlan, V., Scott, J.D. and Jennings, P.A. The molecular basis for protein kinase A anchoring revealed by solution NMR. *Nat. Struct. Biol.* 1999; **6:** 222-227.

Nishitoh, H., Saitoh, M., Mochida, Y., Takeda, K., Nakana, H., Rothe, M., Miyazono, K. and Ichijo, H. ASK1 is essential for JNK/SAPK activation by TRAF2. *Mol. Cell.* 1998; **2:** 389-395.

Oakley, R.H., Laporte, S.A., Holt, J.A., Barak, L.S. and Caron, M.G. Association of β-arrestin with G Protein-coupled Receptors during Clathrin-mediated Endocytosis Dictates the Profile of Receptor Resensitization. *J. Biol. Chem.* 1999; **274:** 32248-32257.

O'Connell, J.C., McCallum, J.F., McPhee, I., Wakefield, J., Houslay, E.S., Wishart, W., Bolger, G., Frame, M. and Houslay, M.D. The SH3 domain of Src tyrosyl kinase interacts with the N-terminal splice region of the PDE4A cAMP-specific phosphodiesterase RPDE-6 (RNPDE4A5). *Biochem. J.* 1996; **318:** 255-262.

O' Donnell, J.M. and Zhang, H.T. Antidepressant effects of inhibitors of cAMP phosphodiesterase (PDE4). *Trends Pharmacol. Sci.* 2004; **25:** 158-163.

Oger, S., Méhats, C., Dallot, E., Ferré, F. and Leroy, M.J. Interleukin-1β Induces Phosphodiesterase 4B2 Expression in Human Myometrial Cells through a Prostaglandin E2- and Cyclic Adenosine 3' 5'-Monophosphate-Dependent Pathway. *J. Clin. Endocrinol. Metab.* 2002; **87:** 5524-5531.

Oliveria, S.F., Gomez, L.L. and Dell'Acqua, M.L. Imaging kinase-AKAP79-phosphatase scaffold complexes at the plasma membrane in living cells using FRET microscopy. *J. Cell Biol.* 2003; **160:** 101-112.

Onuma, H., Osawa, H., Yamada, K., Ogura, T., Tanabe, F., Granner, D.K. and Makino, H. Identification of the Insulin-Regulated Interaction of Phosphodiesterase 3B With 14-3-3β Protein. *Diabetes.* 2002; **51:** 3362-3367.

Patel, H.J., Belvisi, M.G., Bishop-Bailey, D., Yacoub, M.H. and Mitchell, J.A. Activation of Peroxisome Proliferator-Activated Receptors in Human Airway Smooth Muscle Cells Has a Superior Anti-inflammatory Profile to Corticosteroids: Relevance for Chronic Obstructive Pulmonary Disease Therapy. *J. Immunol.* 2003; **170:** 2663-2669.

Pearson, G., Robinson, F., Beers-Gibson, T., Xu, B.E., Karandikar, M., Berman, K. and Cobb, M.H. Mitogen-Activated protein (MAP) Kinase Pathways: Regulation and Physiological Functions. *Endocrine Reviews.* 2001; **22:** 153-183.

Pelletier, S., Julien, C., Popoff, M.R., Lamarche-Vane, N. and Meloche, S. Cyclic AMP Induces Morphological Changes of Vascular Smooth Muscle Cells by Inhibiting a Rac-Dependent Signaling Pathway. *J. Cell. Physiol.* 2005; **204:** 412-422.

Penela, P., Ribas, C. and Mayor Jr., F. Mechanisms of regulation of the expression and function of G protein receptor kinases. *Cell Signal.* 2003; **15:** 973-981.

Percival, M.D., Yeh, B. and Falgueyret, J.P. Zinc Dependent Activation of cAMP-Specific Phosphodiesterase (PDE4A). *Biochem. Biophys. Res. Comm.* 1997; **241:** 175-180.

Perry, S.J., Baillie, G.S., Kohout, T.A., McPhee, I., Magiera, M., Ang, K.L., Miller, W.E., McLean, A.J., Conti, M., Houslay, M.D. and Lefkowitz, R.J. Targeting of Cyclic AMP Degradation to β_2-Adrenergic Receptors by β-Arrestins. *Science.* 2002; **298:** 834-836.

Platanias, L.C. The p38 mitogen-activated protein kinase pathway and its role in interferon signaling. *Pharmacol. Ther.* 2003; **98:** 129-142.

Pollenz, R.S. and Dougherty, E.J. Redefining the Role of the Endogenous XAP2 and C-terminal hsp70-interacting Protein on the Endogenous Ah Receptors Expressed in Mouse and Rat Cell Lines. *J. Biol. Chem.* 2005; **280:** 33346-33356.

Pomerance, M., Abdullah, H.B., Kamerji, S., Corréze, C. and Blondeau, J.P. Thyroid-stimulating Hormone and Cyclic AMP Activate p38 Mitogen-activated Protein Kinase Cascade. *J. Biol. Chem.* 2000; **275:** 40539-40546.

Ponsioen, B., Zhao, J., Riedl, J., Zwartkruis, F., van der Krogt, G., Zaccolo, M., Moolenaar, W.H., Bos, J.L. and Jalink, K. Detecting cAMP-induced Epac activation by fluorescence resonance energy transfer: Epac as a novel cAMP indicator. *EMBO reports.* 2004; **5:** 1176-1180.

Pryzwansky, K.B. and Madden, V.J. Type 4A cAMP-specific phosphodiesterase is stored in granules of human neutrophils and eosinophils. *Cell Tissue Res.* 2003; **312:** 301-311.

Ramadoss, P., Petrulis, J.R., Hollingshead, B.D., Kusnadi, A. and Perdew, G.H. Divergent roles of hepatitis B virus X-associated protein 2 (XAP2) in human versus mouse Ah receptor complexes. *Biochemistry.* 2004; **43:** 700-709.

Rangarajan, S., Enserink, J.M., Kuiperij, H.B., de Rooij, J., Price, L.S., Schwede, F. and Bos, J.L. Cyclic AMP induces integrin-mediated cell adhesion through Epac and Rap1 upon stimulation of the β_2-adrenergic receptor. *J. Cell Biol.* 2003; **160:** 487-493.

Rapacciuolo, A., Suvarna, S., Barki-Harrington, L., Luttrell, L.M., Cong, M., Lefkowitz, R.J. and Rockman, H.A. Protein Kinase A and G protein-coupled Receptor Kinase Phosphorylation Mediates β-1 Adrenergic Receptor Endocytosis through Different Pathways. *J. Biol. Chem.* 2003; **278:** 35403-35411.

Rashid, A.J., O'Dowd, B.F. and George, S.R. Minireview: Diversity and Complexity of Signaling through Peptidergic G Protein-Coupled Receptors. *Endocrinology.* 2004; **145:** 2645-2652.

Rehmann, H., Das, J., Knipscheer, P., Wittinghofer, A. and Bos, J.L. Structure of the cyclic-AMP-responsive exchange factor Epac2 in its auto-inhibited state. *Nature.* 2006; **439:** 625-628.

Rehmann, H., Prakash, B., Wolf, E., Rueppel, A, de Rooij, J., Bos, J.L. and Wittinghofer, A. Structure and regulation of the cAMP-binding domains of Epac2. *Nat. Struct. Biol.* 2003; **10:** 26-32.

Reineke, U., Volkmer-Engert, R. and Schneider-Mergener, J. Applications of peptide arrays prepared by SPOT-technology. *Curr. Opin. Biotechnol.* 2001; **12:** 59-64.

Rena, G., Begg, F., Ross, A., MacKenzie, C., McPhee, I., Campbell, L., Huston, E., Sullivan, M. and Houslay, M.D. Molecular Cloning, Genomic Positioning, Promoter Identification, and Characterization of the Novel Cyclic AMP-Specific Phosphodiesterase PDE4A10. *Mol. Pharmacol.* 2001; **59:** 996-1011.

Richter, W. and Conti, M. Dimerization of the Type 4 cAMP-specific Phosphodiesterases Is Mediated by the Upstream Conserved Regions (UCRs). *J. Biol. Chem.* 2002; **277:** 40212-40221.

Richter, W. and Conti, M. The Oligomerization State Determines Regulatory Properties and Inhibitor Sensitivity of Type 4 cAMP-specific Phosphodiesterases. *J. Biol. Chem.* 2004; **279:** 30338-30348.

Richter, W., Hermsdorf, T., Lilie, H., Egerland, U., Rudolph, R., Kronbach, T. and Dettmer, D. Refolding, Purification, and Characterization of Human Recombinant PDE4A Constructs Expressed in Escherichia coli. *Protein Expr. Purif.* 2000; **19:** 375-383.

Richter, W., Jin, S.L. and Conti, M. Splice variants of the cyclic nucleotide phosphodiesterase PDE4D are differentially expressed and regulated in rat tissue. *Biochem. J.* 2005; **388:** 803-811.

Richter, W., Unciuleac, L., Hermsdorf, T., Kronbach, T. and Dettmer, D. Identification of substrate specificity determinants in human cAMP-specific phosphodiesterase 4A by single-point mutagenesis. *Cell. Signal.* 2001; **13:** 159-167.

Rincon, M., Enslen, H., Raingeaud, J., Recht, M., Zapton, T., Su, M.S., Penix, L.A., Davis, S.J. and Flavell, R.A. Interferon-gamma expression by Th1 effector T cells mediated by p38 MAP kinase signalling pathway. *EMBO J.* 1998; **17:** 2817-2829.

Rochais, F., Vandecasteele, G., Lefebvre, F., Lugnier, C., Lum, H., Mazet, J.L., Cooper, D.M.F. and Fischmeister, R. Negative Feedback Exerted by cAMP-dependent Protein Kinase and cAMP Phosphodiesterase on Subsarcolemmal cAMP Signals in Intact Cardiac Myocytes. *J. Biol. Chem.* 2004; **279:** 52095-52105.

Rocque, W.J., Holmes, W.D., Patel, I.R., Dougherty, R.W., Ittoop, O., Overton, L., Hoffman, C.R., Wisely, G.B., Willard, D.H. and Luther, M.A. Detailed Characterization of a purified Type 4 Phosphodiesterase, HSPDE4B2B: Differentiation of High- and Low-Affinity (R)-Rolipram Binding. *Protein Expr. Purif.* 1997; **9:** 191-202.

Rocque, W.J., Tian, G., Wiseman, J.S., Holmes, W.D., Zajac-Thompson, I., Willard, D.H., Patel, I.R., Wisely, G.B., Clay, W.C., Kadwell, S.H., Hoffman, C.R. and Luther, M.A. Human Recombinant Phosphodiesterase 4B2B Binds (R)-Rolipram at a Single Site with Two Affinities. *Biochemistry.* 1997; **36:** 14250-14261.

Ron, D. Signaling Cascades Regulating NMDA Receptor Sensitivity to Ethanol. *Neuroscientist.* 2004; **10:** 325-336.

Rondinone, C.M., Carvalho, E., Rahn, T., Manganiello, V.C., Degerman, E. and Smith, U.P. Phosphorylation of PDE3B by Phosphatidyl 3-Kinase Associated with the Insulin Receptor. *J. Biol. Chem.* 2000; **275:** 10093-10098.

Rouse, J., Cohen, P., Trigon, S., Morange, M., Alonso-Llamazares, A., Zamanillo, D., Hunt, T. and Nebreda, A. A novel kinase cascade triggered by stress and heat shock that stimulates MAPKAP kinase-2 and phosphorylation of heat shock proteins. *Cell.* 1994; **78:** 1027-1037.

Rousseau, S., Morrice, N., Peggie, M., Campbell, D.G., Gaestel, M. and Cohen, P. Inhibition of SAPK2a/p38 prevents hnRNP A0 phosphorylation by MAPKAP-K2 and its interaction with cytokine mRNAs. *EMBO J.* 2002; **21:** 6505-6514.

Rousseau, S., Peggie, M., Campbell, D.G., Nebreda, A.R. and Cohen, P. Nogo-B is a new physiological substrate for MAPKAP-K2. *Biochem. J.* 2005; **391:** 433-440.

Saklatvala, J. The p38 MAPK kinase pathway as a therapeutic target in inflammatory disease. *Curr. Opin. Pharmacol.* 2004; **4:** 372-377.

San Miguel, S.M., Namdar-Attar, M., Noh, T., Frenkel, B. and Bab, I. ERK1/2-actiavted de Novo Mapkapk2 Synthesis Is Essential for Osteogenic Growth Peptide Mitogenic Signaling in Osteoblastic Cells. *J. Biol. Chem.* 2005: **280:** 37495-37502.

Schmitt, J.M. and Stork, P.J. Cyclic AMP-mediated Inhibition of Cell Growth Requires the Small G Protein Rap1. *Mol. Cell. Biol.* 2001; **21:** 3671-3683.

Scotland, G. and Houslay, M.D. Chimeric constructs show that the unique N-terminal domain of the cyclic AMP phosphodiesterase RD1 (RNPDE4A_{1A}; rPDE-IVA1) can confer membrane association upon the normally cytosolic protein chloramphenicol acetyltransferase. *Biochem. J.* 1995; **308:** 673-681.

Sette, C. and Conti, M. Phosphorylation and Activation of a cAMP-specific Phosphodiesterase by the cAMP-dependent Protein Kinase. *J. Biol. Chem.* 1996; **28:** 16526-16534.

Sette, C., Iona, S. and Conti, M. The Short-term Activation of a Rolipram-sensitive, cAMP-specific Phosphodiesterase by Thyroid-stimulating Hormone in Thyroid FRTL-5 Cells is Mediated by a cAMP-dependent Phosphorylation. *J. Biol. Chem.* 1994; **12:** 9245-9252.

Shakur, Y., Takeda, K., Kenan, Y., Yu, Z.X., Rena, G., Barndt, D., Houslay, M.D., Degerman, E., Ferrans, V. and Manganiello, V.C. Membrane Localization of Cyclic Nucleotide Phosphodiesterase 3 (PDE3). *J. Biol. Chem.* 2000; **275:** 38749-38761.

Shakur, Y., Wilson, M., Pooley, L., Lobban, M., Griffiths, S.L., Campbell, A.M., Beattie, J., Daly, C. and Houslay, M.D. Identification and characterization of the type-IVA cyclic AMP-specific phosphodiesterase RD1 as a membrane-bound protein expressed in cerebellum. *Biochem. J.* 1995; **306:** 801-809.

Sharrocks, A.D., Yang, S.H. and Galanis, A. Docking domains and substrate-specificity determination for MAP kinases. *Trends Biochem. Sci.* 2000; **25:** 448-453.

Shaywitz, A.J. and Greenberg, M.E. CREB: A stimulus-induced transcription factor activated by diverse array of extracellular signals. *Annu. Rev. Biochem.* 1999; **68:** 821-861.

Shenoy, S.K., Drake, M.T., Nelson, C.D., Houtz, D.A., Xiao, K., Madabushi, S., Reiter, E., Premont, R.T., Lichtarge, O. and Lefkowitz, R.J. β-arrestin-dependent, G Protein-independent ERK1/2 Activation by the β_2-adrenergic Receptor. *J. Biol. Chem.* 2006; **281:** 1261-1273.

Shepherd, M., McSorley, T., Olsen, A.E., Johnston, L.A., Thomson, N.C., Baillie, G.S., Houslay, M.D. and Bolger, G.B. Molecular cloning and subcellular distribution of the novel PDE4B4 cAMP-specific phosphodiesterase isoform. *Biochem. J.* 2003; **370:** 429-438.

Shepherd, M.C., Baillie, G.S., Stirling, D.I. and Houslay, M.D. Remodelling of the PDE4 cAMP phosphodiesterase isoform profile upon monocyte-macrophage differentiation of human U937 cells. *Br. J. Pharmacol.* 2004; **142:** 339-351.

Sheppard, F.R., Kelher, M.R., Moore, E.E., McLaughlin, N.J.D., Banerjee, A. and Silliman, C.C. Structural organization of the neutrophil NADPH oxidase: phosphorylation and translocation during priming and activation. *J. Leukoc. Biol.* 2005; **78:** 1025-1042.

Shmelzer, Z., Haddad, N., Admon, E., Pessach, I., Leto, T.L., Eitan-Hazan, Z., Hershfinkel, M. and Levy, R. Unique targeting of cytosolic phospholipase A_2 to plasma membranes mediated by the NADPH oxidase in phagocytes. *J. Cell Biol.* 2003; **162:** 683-692.

Simaan, M., Bédard-Goulet, S., Fessart, D., Gratton, J.P. and Laporte, S.A. Dissociation of β-arrestin from internalized bradykinin B2 receptor is necessary for receptor recycling and resensitization. *Cell Signal.* 2005; **17:** 1074-1083.

Singh, S., Powell, D.W., Rane, M.J., Millard, T.H., Trent, J.O., Pierce, W.M., Klein, J.B., Machesky, L.M. and McLeish, K.R. Identification of the p16-Arc subunit of the Arp2/3 complex as a substrate of MAPK-activated protein kinase 2 by proteomics analysis. *J. Biol. Chem.* 2003; **278:** 36410-36417.

Smith, K.J., Scotland, G., Beattie, J., Trayer, I.P. and Houslay, M.D. Determination of the Structure of the N-terminal Splice Region of the Cyclic AMP-specific Phosphodiesterase RD1 (RNPDE4A1) by ^{1}H NMR and Identification of the Membrane Association Domain Using Chimeric Constructs. *J. Biol. Chem.* 1996; **271:** 16703-16711.

Smith, P.G., Wang, F., Wilkinson, K.N., Savage, K.J., Klein, U., Neuberg, D.S., Bollag, G., Shipp., M.A. and Aguiar, R.C.T. The phosphodiesterase PDE4B limits cAMP-associated PI3K/AKT-dependent apoptosis in diffuse large B-cell lymphoma. *Blood.* 2005; **105:** 308-316.

Snyder, P.B., Florio, V.A., Ferguson, K. and Loughney, K. Isolation, Expression and Analysis of Splice Variants of a Human Ca^{2+}/Calmodulin-Stimulated Phosphodiesterase (PDE1A). *Cell. Signal.* 1999; **11:** 535-544.

Soderling, S.H. and Beavo, J.A. Regulation of cAMP and cGMP signaling: new phosphodiesterases and new functions. *Curr. Opin. Cell Biol.* 2000; **12:** 174-179.

Soderling, S.H. and Scott, J.D. WAVE signalling: from biochemistry to biology. *Biochem. Soc. Trans.* 2006; **34:** 73-76.

Song, G., Ouyang, G. and Bao, S. The activation of Akt/PKB signaling pathway and cell survival. *J. Cell. Mol. Med.* 2005; **9:** 59-71.

Souness, J.E., Aldous, D. and Sargent, C. Immunosuppressive and anti-inflammatory effects of cyclic AMP phosphodiesterase (PDE) type 4 inhibitors. *Immunopharmacology.* 2000; **47:** 127-162.

Spence, S., Rena, G., Sweeney, G. and Houslay, M.D. Induction of Ca^{2+}/calmodulin-stimulated cyclic AMP phosphodiesterase (PDE1) activity in Chinese hamster ovary (CHO) by phorbal 12-myristate 13-acetate and by the selective overexpression of protein kinase C isoforms. *Biochem. J.* 1995; **310:** 975-982.

Staels, B., Koenig, W., Habib, A., Merval, R., Lebret, M., Torra, I.P., Delerive, P., Fadel, A., Chinetti, G., Fruchart, J.C., Najib, J., Maclouf, J. and Tedgui, A. Activation of human aortic smooth-muscle cells is inhibited by PPARα but not PPARγ activators. *Nature.* 1998; **393:** 790-793.

Staples, K.J., Bergmann, M., Tomita, K., Houslay, M.D., McPhee, I., Barnes, P.J., Giembycz, M.A. and Newton, R. Adenosine 3',5'-Cyclic Monophosphate (cAMP)-Dependent Inhibition of IL-5 from Human T Lymphocytes Is Not Mediated by the cAMP-Dependent Protein Kinase A. *J. Immunol.* 2001; **167:** 2074-2080.

Steele, M.R., McCahill, A., Thompson, D.S., MacKenzie, C., Isaacs, N.W., Houslay, M.D. and Bolger, G.B. Identification of a surface on the β-propeller protein RACK1 that interacts with the cAMP-specific phosphodiesterase PDE4D5. *Cell. Signal.* 2001; **13:** 507-513.

Stokoe, D., Campbell, D.G., Nakielny, S., Hidaka, H., Leevers, S.J., Marshall, C. and Cohen, P. MAPKAP kinase-2; a novel protein kinase activated by mitogen-activated protein kinase. *EMBO J.* 1992; **11:** 3985-3994.

Stokoe, D., Caudwell, B., Cohen, P.T.W and Cohen, P. The substrate specificity and structure of mitogen-activated protein (MAP) kinase-activated protein kinase-2. *Biochem. J.* 1993; **296:** 843-849.

Strock, J. and Diversé-Pierluissi, M.A. Ca^{2+} Channels As Integrators of G Protein-Mediated Signalling in Neurons. *Mol. Pharmacol.* 2004; **66:** 1071-1076.

Sudo, T., Kawai, K., Matsuzaki, H. and Osada, H. p38 mitogen-activated protein kinase plays a key role in regulating MAPKAPK2 expression. *Biochem. Biophys. Res. Commun.* 2005; **337:** 415-421.

Sullivan, M., Olsen, A.S. and Houslay, M.D. Genomic Organisation of the Human Cyclic AMP-Specific Phosphodiesterase PDE4C Gene and Its Chromosomal Localisation to 19p13.1, Between RAB3A and JUND. *Cell. Signal.* 1999; **11:** 735-742.

Sullivan, M., Rena, G., Begg, F., Gordon, L., Olsen, A.S. and Houslay M.D. Identification and characterization of the human homologue of the short PDE4A cAMP-specific phosphodiesterase RD1 (PDE4A1) by analysis of the human HPDE4A gene locus located at chromosome 19p13.2. *Biochem. J.* 1998; **333:** 693-703.

Sumamasekera, W.K., Tien, E.S., Turpey, R., Vanden Heuvel, J.P. and Perdew, G.H. Evidence That Peroxisome Proliferator-activated Receptor α Is Complexed with the 90-kDa Heat Shock Protein and the Hepatitis Virus B X-associated Protein 2. *J. Biol. Chem.* 2003; **278:** 4467-4473.

Sun, F., Hug, M.J., Bradbury, N.A. and Frizzell, R.A. Protein Kinase A Associates with Cystic Fibrosis Transmembrane Conductance Regulator via an Interaction with Ezrin. *J. Biol. Chem.* 2000; **275:** 14360-14366.

Sun, X.C., Zhai, C.B., Cui, M., Chen, Y., Levin, L.R., Buck, J. and Bonanno, J.A. HCO_3^--dependent soluble adenylyl cyclase activates cystic fibrosis transmembrane conductance regulator in corneal endothelium. *Am. J. Physiol. Cell Physiol.* 2003; **284:** C1114-C1122.

Sunahara, R.K. and Taussig, R. Isoforms of Mammalian Adenylyl Cyclase: Multiplicities of Signaling. *Mol. Interventions.* 2002; **2:** 168-184.

Sung, B.J., Hwang, K.Y., Jeon, Y.H., Lee, J.I., Heo, Y.S., Kim, J.H., Moon, J., Yoon, J.M., Hyun, Y.L., Kim, E., Eum, S.J., Park, S.Y., Lee, J.O., Lee, T.G., Ro, S. and Cho, J.M. Structure of the catalytic domain of human phosphodiesterase 5 with bound drug molecules. *Nature.* 2003; **425:** 98-102.

Sutherland, E.W. and Rall, T.W. Fractionation and Characterization of a cyclic adenine ribonucleotide formed by tissue particles. *J. Biol. Chem.* 1958; **232:** 1077-1091.

Swinnen, J.V., Joseph, D.R. and Conti, M. Molecular cloning of rat homologues of the *Drosophila melanogaster* dunce cAMP phosphodiesterase: Evidence for a family of genes. *Proc. Natl. Acad. Sci.* 1989; **86:** 5325-5329.

Szpirer, C., Szpirer, J., Riviere, M., Swinnen, J., Vicini, E. and Conti, M. Chromosomal localization of the human and rat genes (PDE4D and PDE4B) encoding the cAMP-specific phosphodiesterases 3 and 4. *Cytogenet. Cell Genet.* 1995; **69:** 11-14.

Tan, Y., Rouse, J., Zhang, A., Cariati, S., Cohen, P. and Comb, M. FGF and stress regulate CREB and ATF1 via a pathway involving p38 MAP kinase and MAPKAP kinase-2. *EMBO J.* 1996; **15:** 4629-4642.

Tanoue, T., Adachi, M., Moriguchi, T. and Nishida, E. A conserved docking motif in MAP kinases common to substrates, activators and regulators. *Nat. Cell Biol.* 2000; **2:** 110-116.

Tanoue, T. and Nishida, E. Molecular recognitions in the MAP kinase cascades. *Cell. Signal.* 2003; **15:** 455-462.

Tao, J., Wang, H. and Malbon, C.C. Protein Kinase A regulates AKAP250 (gravin) scaffold binding to the β2-adrenergic receptor. *EMBO J.* 2003; **22:** 6419-6429.

Taskén, K. and Aandahl, E.M. Localized Effects of cAMP Mediated by Distinct Routes of Protein Kinase A. *Physiol. Rev.* 2004; **84:** 137-167.

Taskén, K.A., Collas, P., Kemmner, W.A., Witczak, O., Conti, M. and Taskén, K. Phosphodiesterase 4D and protein kinase A type II constitute a signaling unit in the centrosomal area. *J. Biol. Chem.* 2001; **276:** 21999-22002.

Teixeira, M.M., Gristwood, R.W., Cooper, N. and Hellewell, P.G. Phosphodiesterase (PDE)4 inhibitors: anti-inflammatory drugs of the future? *Trends Pharmacol. Sci.* 1997; **18:** 164-170.

Terry, R., Cheung, Y.F., Praestegaard, M., Baillie, G.S., Huston, E., Gall, I., Adams, D.R. and Houslay M.D. Occupancy of the catalytic site of PDE4A4 cyclic AMP phosphodiesterase by rolipram triggers the dynamic redistribution of this specific isoform in living cells through a cyclic AMP independent process. *Cell Signal.* 2003; **15:** 955-971.

Teske, S., Bohn, A.A., Regal, J.F., Neumiller, J.J. and Lawrence, B.P. Activation of the aryl hydrocarbon receptor increases pulmonary neutrophilia and diminishes host resistance to influenza A virus. *Am. J. Physiol. Lung Cell Mol. Physiol.* 2005; **289:** L111-L124.

Thompson, W.J. and Appleman, M.M. Multiple Cyclic Nucleotide Phosphodiesterase Activities from Rat Brain. *Biochemistry.* 1971; **10:** 311-316.

Tibbles, L.A. and Woodgett, J.R. The stress-activated protein kinase pathways. *Cell. Mol. Life Sci.* 1999; **55:** 1230-1254.

Tilley, D.G. and Maurice, D.H. Vascular Smooth Muscle Cell Phenotype-Dependent Phosphodiesterase 4D Short Form Expression: Role of Differential Histone Acetylation on cAMP-Regulated Function. *Mol. Pharmacol.* 2005; **68:** 596-605.

Uhlik, M.T., Abell, A.N., Johnson, N.L., Sun, W., Cuevas, B.D., Lobel-Rice, K.E., Home, E.A., Dell'Acqua, M.L. and Johnson, G.L. Rac-MEKK3-MKK3 scaffolding for p38 MAPK activation during hyperosmotic shock. *Nat. Cell. Biol.* 2003; **5:** 1104-1110.

Vaughan, D.J., Millman, E.E., Godines, V., Friedman, J., Tran, T.M., Dai, W., Knoll, B.J., Clark, R.B. and Moore, R.H. Role of the G Protein-coupled Receptor Kinase Site Serine Cluster in β_2-Adrenergic Receptor Internalization, Desensitization, and β-Arrestin Translocation. *J. Biol. Chem.* 2006; **281:** 7684-7692.

Verde, I., Pahlke, G., Salanova, M., Zhang, G., Wang, S., Coletti, D., Onuffer, J., Jin, S.L. and Conti, M. Myomegalin Is a Novel Protein of the Golgi/Centrosome That Interacts with a Cyclic Nucleotide Phosphodiesterase. *J. Biol. Chem.* 2001; **276:** 11189-11198.

Vicini, E. and Conti, M. Characterization of an Intronic Promoter of a Cyclic Adenosine 3',5'-Monophosphate (cAMP)-Specific Phosphodiesterase Gene that Confers Hormone and cAMP Inducibility. *Mol. Endocrinol.* 1997; **11:** 839-850.

Vierimaa, O., Georgitsi, M., Lehtonen, R., Vahteristo, P., Kokko, A., Raitila, A., Tuppurainen, K., Ebeling, T.M.L., Salmela, P.I., Paschke, R., Gündogdu, S., De Menis, E., Mäkinen, M.J., Launonen, V., Karhu, A. and Aaltonen, L.A. Pituitary Adenoma Predisposition Caused by Germline Mutations in the *AIP* Gene. *Science.* 2006; **312:** 1228-1230.

Vignais, P.V. The super-oxide-generating NADPH oxidase: structural aspects and activation mechanism. *Cell. Mol. Life Sci.* 2002; **59:** 1428-1459.

Wallace, D.A., Johnston, L.A., Huston, E., MacMaster, D., Houslay, T.M., Cheung, Y.F., Campbell, L., Millen, J.E., Smith, R.A., Gall, I.G., Knowles, R.G., Sullivan, M. and Houslay, M.D. Identification and Characterization of PDE4A11, a Novel, Widely Expressed Long Isoform Encoded by the Human PDE4A cAMP Phosphodiesterase Gene. *Mol. Pharmacol.* 2005; **67:** 1920-1934.

Wang, D., Deng, C., Bugaj-Gaweda, B., Kwan, M., Gunwaldsen, C., Leonard, C., Xin, X., Hu, Y., Unterbeck, A. and De Vivo, M. Cloning and characterization of novel PDE4D isoforms PDE4D6 and PDE4D7. *Cell. Signal.* 2003; **15:** 883-891.

Wang, Z., Dillon, T.J., Pokala, V., Mishra, S., Labudda, K., Hunter, B. and Stork, P.J.S. Rap1-Mediated Activation of Extracellular Signal-Regulated Kinases by Cyclic AMP Is Dependent on the Mode of Rap1 Activation. *Mol. Cell. Biol.* 2006; **26:** 2130-2145.

Waschke, J., Drenckhahn, D., Adamson, R.H., Barth, H. and Curry, F.E. cAMP protects endothelial barrier functions by preventing Rac-1 inhibition. *Am. J. Physiol. Heart Circ. Physiol.* 2004; **287:** 2427-2433.

Waskiewicz, A.J., Flynn, A., Proud, C.G. and Cooper, J.A. Mitogen-activated protein kinases activate the serine/threonine kinases Mnk1 and Mnk2. *EMBO J.* 1997; **16:** 1909-1920.

Waskiewicz, A.J., Johnson, J.C., Penn, B., Mahalingam, M., Kimball. S.R. and Cooper, J.A. Phosphorylation of the cap-binding protein eukaryotic translation initiation factor 4E by protein kinase Mnk1 in vivo. *Mol. Cell Biol.* 1999; **19:** 1871-1880.

Weber, H.O., Ludwig, R.L., Morrison, D., Kotlyarov, A., Gaestel, M. and Vousden, K.H. HDM2 phosphorylation by MAPKAP kinase 2. *Oncogene.* 2005; **24:** 1965-1972.

Werz, O., Klemm, J., Samuelsson, B. and Rådmark, O. 5-Lipoxygenase is phosphorylated by p38 kinase-dependent MAPKAP kinases. *Proc. Natl. Acad. Sci.* 2000; **97:** 5261-5266.

Werz, O., Szellas, D., Steinhilber, D. and Rådmark, O. Arachadonic Acid Promotes Phosphorylation of 5-Lipoxygenase at Ser-271 by MAPK-activated Protein Kinase 2 (MK2). *J. Biol. Chem.* 2002; **277:** 14793-14800.

Westphal, R.S., Soderling, S.H., Alto, N.M., Langeberg, L.K. and Scott, J.D. Scar/WAVE-1, a Wiskott-Aldrich syndrome protein, assembles an actin-associated multi-kinase scaffold. *EMBO J.* 2000; **19:** 4589-4600.

Wientjes, F.B., Reeves, E.P., Soskic, V., Furthmayr, H. and Segal, A.W. The NADPH Oxidase Components $p47^{phox}$ and $p40^{phox}$ Bind to Moesin through Their PX Domain. *Biochem. Biophys. Res. Commun.* 2001; **289:** 382-388.

Willoughby, D. and Cooper, D.M.F. Ca^{2+} stimulation of adenylyl cyclase generates dynamic oscillations in cyclic AMP. *J. Cell Sci.* 2005; **119:** 828-836.

Willoughby, D., Wong, W., Schaack, J., Scott, J.D. and Cooper, D.M.F. An anchored PKA and PDE4 complex regulates subplasmalemmal cAMP dynamics. *EMBO J.* 2006; **25:** 2051-2061.

Winzen, R., Kracht, M., Ritter, B., Wilhelm, A., Chen, C.Y., Shyu, A.B., Muller, M., Gaestel, M., Resch, K. and Holtmann, H. The p38 MAP kinase pathway signals for cytokine-induced stabilization via MAP kinase-activated protein kinase 2 and an AU-rich region targeted mechanism. *EMBO J.* 1999; **18:** 4969-4980.

Wong, W. and Scott, J.D. AKAP Signalling Complexes: Focal Points in Space and Time. *Nat. Rev. Mol. Cell Biol.* 2004; **5:** 959-970.

Wong, W.S.F. and Koh, D.S.K. Advances in Immunopharmacology of Asthma. *Biochem. Pharmacol.* 2000; **59:** 1323-1355.

Wu, R.F., Gu, Y., Xu, Y.C., Nwariaku, F.E. and Terada, L.S. Vascular Endothelial Growth Factor Causes Translocation of $p47^{phox}$ to Membrane Ruffles through WAVE1. *J. Biol. Chem.* 2003; **278:** 36830-36840.

Xiang, Y., Naro, F., Zoudilova, M., Jin, S.L., Conti, M. and Kobilka, B. Phosphodiesterase 4D is required for β_2-adrenoceptor subtype-specific signaling in cardiac myocytes. *Proc. Natl. Acad. Sci.* 2005; **102:** 909-914.

Xu, L., Chen, S. and Bergan, R.C. MAPKAPK2 and HSP27 are downstream effectors of p38 MAP kinase-mediated matrix metalloproteinase type 2 activation and cell invasion in human prostate cancer. *Oncogene.* 2006; **25:** 2987-2998.

Xu, R.X., Hassell, A.M., Vanderwall, D., Lambert, M.H., Holmes, W.D., Luther, M.A., Rocque, W.J., Milburn, M.V., Zhao, Y., Ke, H. and Nolte, R.T. Atomic Structure of PDE4: Insights into Phosphodiesterase Mechanism and Specificity. *Science.* 2000; **288:** 1822-1825.

Xu, R.X., Rocque, W.J., Lambert, M.H., Vanderwall, D.E., Luther, M.A. and Nolte, R.T. Crystal Structures of the Catalytic Domain of Phosphodiesterase 4B Complexed with AMP, 8-Br-AMP, and Rolipram. *J. Mol. Biol.* 2004; **337:** 355-365.

Yarwood, S.J. Microtubule-associated proteins (MAPs) regulate cAMP signalling through exchange protein directly activated by cAMP (EPAC). *Biochem. Soc. Trans.* 2005; **33:** 1327-1329.

Yarwood, S.J., Sale, E.M., Sale, G.J., Houslay, M.D., Kilgour, K. and Anderson, N.G. Growth Hormone-dependent Differentiation of 3T3-F442A Preadipocytes Requires Janus Kinase/Signal Transducer and Activator of Transcription but Not Mitogen-activated Protein Kinase or p70 S6 Kinase Signaling. *J. Biol. Chem.* 1999; **274:** 8662-8668.

Yarwood, S.J., Steele, M.R., Scotland, G., Houslay, M.D. and Bolger, G.B. The RACK1 Signaling Scaffold Protein Selectively Interacts with the cAMP-specific Phosphodiesterase PDE4D5 Isoform. *J. Biol. Chem.* 1999; **21:** 14909-14917.

Yin, D., Gavi, S., Wang, H. and Malbon, C.C. Probing Receptor Structure/Function with Chimeric G-Protein-Coupled Receptors. *Mol. Pharmacol.* 2004; **65:** 1323-1335.

Young, E.C. and Krougliak, N. Distinct Structural Determinants of Efficacy and Sensitivity in the Ligand-binding Domain of Cyclic Nucleotide-gated Channels. *J. Biol. Chem.* 2004; **279:** 3553-3562.

Young, P.R., McLaughlin, M.M., Kumar, S., Kassis, S., Doyle, M.L., McNulty, D., Gallagher, T.F., Fisher, S., McDonnell, P.C., Carr, S.A., Huddleson, M.J., Seibel, G., Porter, T.G., Livi, G.P., Adams, J.L. and Lee, J.C. Pyridinyl Imidazole Inhibitors of p38 Mitogen-activated Protein Kinase Bind in the ATP Site. *J. Biol. Chem.* 1997; **272:** 12116-12121.

Yuasa, T., Ohno, S., Kehri, J.H. and Kyriakis, J.M. Tumor Necrosis Factor Signalling to Stress-activated Protein Kinase (SAPK)/Jun NH2-terminal Kinase (JNK) and p38. *J. Biol. Chem.* 1998; **273:** 22681-22692.

Yuzawa, S., Ogura, K., Horiuchi, M., Suzuki, N.N., Fujioka, Y., Kataoka, M., Sumimoto, H. and Inagaki, F. Solution Structure of the Tandem Src Homology 3 Domains of p47phox in an Autoinhibited Form. *J. Biol. Chem.* 2004; **279:** 29752-29760.

Zaccolo, M. Phosphodiesterases and compartmentalized cAMP signalling in the heart. *Eur. J. Cell Biol.* 2006; **85:** 693-697.

Zaccolo, M. and Pozzan, T. Discrete Microdomains with High Concentration of cAMP in Stimulated Rat Neonatal Cardiac Myocytes. *Science.* 2002; **295:** 1711-1715.

Zambon, A.C., Zhang, L., Minovitsky, S., Kanter, J.R., Prabhakar, S., Salomonis, N., Vranizan, K., Dubchak, I., Conklin, B.R. and Insel, P.A. Gene expression patterns define key transcriptional events in cell-cycle regulation by cAMP and protein kinase A. *Proc. Natl. Acad. Sci.* 2005; **102:** 8561-8566.

Zhan, Y., He, D., Newburger, P.E. and Zhou, G.W. $p47^{phox}$ PX Domain of NADPH Oxidase Targets Cell Membrane Via Moesin-Mediated Association With the Actin Cytoskeleton. *J. Cell. Biochem.* 2004; **92:** 795-809.

Zhang, K.Y.J., Ibrahim, P.N., Gillette, S. and Bollag, G. Phosphodiesterase-4 as a potential drug target. *Expert Opin. Ther. Targets.* 2005; **9:** 1283-1305.

Zmuda-Trzebiatowska, E., Oknianska, A., Manganiello, V.C. and Degerman, E. Role of PDE3B in insulin-induced glucose uptake, GLUT-4 translocation and lipogenesis in primary rat adipocytes. *Cell. Signal.* 2006; **18:** 382-390.

Zou, Y., Komuro, I., Yamazaki, T., Kudoh, S., Uozumi, H., Kadowaki, T. and Yazaki, Y. Both Gs and Gi Proteins Are Critically Involved in Isoproternol-induced Cardiomyocyte Hypertrophy. *J. Biol. Chem.* 1999; **274:** 9760-9770.

Zwartkruis, F.J.T. and Bos, J.L. Ras and Rap1: Two Highly Related Small GTPases with Distinct Function. *Exp. Cell Res.* 1999; **253:** 157-165.

Chapter 8 Peer Reviewed Publications

- **Wallace, D.A.,** Johnston, L.A., Huston, E., MacMaster, D., Houslay, T.M., Cheung, Y.F., Campbell, L., Millen, J.E., Smith, R.A., Gall, I.G., Knowles, R.G., Sullivan, M. and Houslay, M.D. Identification and Characterization of PDE4A11, a Novel, Widely Expressed Long Isoform Encoded by the Human PDE4A cAMP Phosphodiesterase Gene. *Mol. Pharmacol.* 2005; **67:** 1920-1934.

- Bolger, G.B., Peden, A.H., Steele, M.R., MacKenzie, C., McEwan, D.G., **Wallace, D.A.,** Huston, E., Baillie, G.S. and Houslay, M.D. Attenuation of the Activity of the cAMP-specific Phosphodiesterase PDE4A5 by Interaction with the Immunophilin XAP2. *J. Biol. Chem.* 2003; **278:** 33351-33363.